Multimerization and Membrane Distribution of the Gag Structural Polyprotein During HIV-1 Assembly

by

Ian Barclay Hogue

A dissertation submitted in partial fulfillment
of the requirements for the degree of
Doctor of Philosophy
(Microbiology & Immunology)
in The University of Michigan
2010

Doctoral Committee:

Assistant Professor Akira Ono, Chair
Professor Michael J. Imperiale
Professor Jennifer J. Linderman
Professor Joel A. Swanson
Associate Professor Alice Telesnitsky

ACKNOWLEDGEMENTS

I would like to thank the people who have had a great impact on my life and career, without whom this achievement would have been impossible. Thank you to my wife, Maritza Garza-Hogue, for her patience and support during these years of long hours and hard work. Thank you to my parents, Henry and Brenda Hogue, both scientists, for setting me on this trajectory. In particular, thank you to my Mom for being my career role model, and opening many doors for me as I was getting started in my career. Thank you to all of the PIs who allowed me to learn so much working in their labs. In particular, thank you to David Margolis, Ginger Lehrman, and other members of the Margolis lab for preparing me for graduate school by treating me like I was already a graduate student. I would like to especially thank Kathy Spindler, my first lab rotation mentor, for helping me off to a good start in graduate school and serving as an informal mentor when I needed advice. Thank you to my thesis committee for all of their advice and constructive criticism. Finally, thank you to Akira Ono. I cannot imagine a better mentor or lab for me. Thank you.

The examples presented in Chapter II were created with assistance of many collaborators. The BiFC assay was optimized and extensively tested by Jingga Inlora in the course of her undergraduate honors thesis work in the Ono lab. The TIRF assays were performed with the assistance of Arun Anantharam in collaboration with the Ron Holz lab. The immunogold backscatter SEM assay was performed with the technical assistance

of Dotty Sorenson, Bruce Donohoe, and Chris Edwards at the U of M Microscopy and Image-analysis Laboratory, and helpful discussions with Albert Liu of the Ben Margolis lab.

The work presented in Chapter III was previously published:

Hogue, I. B., A. Hoppe, and A. Ono. Quantitative fluorescence resonance energy transfer microscopy analysis of the human immunodeficicency virus type 1 Gag-Gag interaction: relative contributions of the CA and NC domains and membrane binding. Journal of Virology, 2009. 83(14): 7322-36.

I would like to acknowledge the contributions of my co-author, Adam Hoppe, who assisted with technical expertise, interpretation of data, and editing the manuscript. I would like to also acknowledge members of the Ono lab, my thesis committee, Eric Freed, and Simeone Marino for helpful discussions, those listed in the Materials and Methods section who provided reagents and equipment, and Jingga Inlora and Seung Oh for technical assistance.

The work in Chapter IV was performed with technical advice from Shelley Almburg and Chris Edwards at the U of M Microscopy and Image-analysis Laboratory. I would like to acknowledge my thesis committee and members of the Ono lab for helpful discussions, especially Nick Llewellyn and Jonathan Grover who helped optimize antibody co-patching, microscopy, and image analysis methods. I would also like to acknowledge Jingga Inlora and Maddy Nye for technical assistance, and those listed in the Materials and Methods section who provided reagents.

The example presented in Chapter V was created in collaboration with Nick Llewellyn.

With regard to the computational biology work presented in the appendices, I would like to acknowledge my co-authors and members of the Denise Kirschner lab for

their contributions and assistance. In particular, thank you to Simeone Marino for teaching me so much about computational biology.

TABLE OF CONTENTS

Acknowledgements ..... **ii**

List of Figures ..... **viii**

List of Appendices ..... **x**

Chapter I **Introduction** **1**
- The HIV-1 Pandemic 1
- The Molecular Virology of HIV-1 1
  - Attachment and Entry 1
  - Post-Entry Events 2
  - Transcription, Splicing, and RNA Export 4
  - Assembly 6
  - Site of Assembly 7
  - Membrane Binding 7
  - Multimerization 8
  - Microdomain Distribution of Gag 9
  - Lipid Rafts 10
  - Tetraspanin Enriched Microdomains 11
  - Budding, Release, and Maturation 13
- Interrelationships between Steps of HIV-1 Assembly 14

Chapter II **Review of Microscopy-based Methods to Study Protein Complexes on the Plasma Membrane** **29**
- Introduction 29
- Fluorescence Microscopy Techniques 29
  - Wide-Field and Confocal Fluorescence Microscopy 29
  - Total Internal Reflection Fluorescence Microscopy 32
  - Polarized TIRF Microscopy 33
  - Co-patching Assay 34
  - Bimolecular Fluorescence Complementation 35
  - Fluorescence Resonance Energy Transfer 37
- Electron Microscopy Techniques 37
  - Scanning Electron Microscopy 37

Backscattered Electron Detection of Immunogold 38
Correlative Fluorescence and Scanning Electron Microscopy 39

Chapter III **Relative Contributions of the CA and NC Domains and Membrane Binding to Gag-Gag Interaction During HIV-1 Assembly 48**
Abstract 48
Introduction 49
Materials and Methods 53
Results 60
Validation of chimeric Gag constructs 60
FRET assay for Gag multimerization 61
CA-CTD can form a "half-interface" which is only partially defective, but fully disrupting the CA-CTD dimerization interface abolishes FRET 63
The NC mutant is only partially defective in the context of native myristoylation 64
Mutations in both the CA-CTD and NC reduce steady-state Gag membrane binding 65
In the absence of myristoylation, both CA-CTD and NC mutations cause a complete loss of interactions with Gag molecules 66
Constitutive and enhanced membrane binding can rescue the interaction of the NC mutant, but not the CA-CTD mutant, with WT Gag 67
Discussion 69

Chapter IV **Gag Reorganizes Plasma Membrane Microdomains During HIV-1 Assembly 93**
Abstract 93
Introduction 94
HIV-1 Assembly 94
Lipid Rafts 95
Tetraspanin-Enriched Microdomains 96
Lipid Rafts and TEMs are Distinct Microdomains 97
Co-patching Assay 98
Materials and Methods 99
Results 103

Without antibody-mediated patching, microdomain markers appear widely distributed on the PM 103
Antibody-mediated co-patching assay can distinguish lipid rafts and TEMs 104
Gag co-patches with both lipid raft and TEM markers 105
Gag induces the coalescence of lipid rafts and TEMs, but non-membrane bound Gag cannot 106
Gag membrane binding motif substitutions have no effect on association with, and coalescence of, lipid rafts and TEMs 107
Discussion 109
Chapter V **Discussion 136**
Summary of Results 136
Future Directions 139
Microdomains and Gag Multimerization 139
Microdomains and Budding 140
Microdomains and Cytoskeleton 141
Microdomains and the Cellular Restiction Factor Tetherin 142
Microdomains and Cell-to-Cell Transmission 143
High-Throughput Screening to Develop Antiretroviral Drugs 144

Appendices **..... 150**

LIST OF FIGURES

Figure		
1.1	Schematic of HIV-1 genome organization and Gag structural polyprotein	16
1.2	Schematic of the HIV-1 replication cycle	17
1.3	HIV-1 assembly on the plasma membrane	18
2.1	Schematic of pTIRF and example pTIRF data	41
2.2	Bimolecular Fluorescence Complementation is not useful as an assay for Gag multimerization	42
2.3	Backscattered electron detection of an immunogold-labeled lipid raft marker	43
2.4	Correlative fluorescence/FRET/SEM	44
3.1	Gag derivatives, expression, and VLP release	73
3.2	FRET microscopy of control constructs	75
3.3	FRET microscopy of mutant Gag constructs	76
3.4	Gag membrane binding	78
3.5	FRET microscopy of N-terminal myristoylation-deficient constructs	80
3.6	FRET microscopy of constructs with constitutively enhanced membrane binding	82
4.1	Distribution of microdomain markers without antibody-mediated patching	115
4.2	Antibody-mediated co-patching assay can distinguish lipid rafts and TEMs	117
4.3	Gag co-patches with both lipid raft and TEM markers	119

4.4 Gag induces the coalescence of lipid rafts and TEMs, but non-membrane bound Gag cannot 121

4.5 Gag membrane binding motif substitutions have no effect on association with, and coalescence of, lipid rafts and TEMs 124

5.1 Model of assembly at the polarized T cell uropod, and potential role of microdomains 146

LIST OF APPENDICES

Appendix

Preface to the Appendices 150

A Uncertainty and Sensitivity Analysis Methods 152

B The Dual Role of Dendritic Cells in the Immune Response to HIV-1 Infection 191

CHAPTER I

Introduction

The HIV-1 Pandemic

Human Immunodeficiency Virus Type 1 (HIV-1) is a pandemic human pathogen, and the causative agent of Acquired Immune Deficiency Syndrome (AIDS). HIV-1 is descended from a simian immunodeficiency virus that is endemic to chimpanzees in West Africa, and appears to have entered the human population on three independent occasions (1). Based on homology and diversity of HIV-1 sequences detected in preserved tissue samples from the 1950s-1960s, the HIV-1 pandemic likely began between 1902 and 1921 (2); however, the pandemic was not appreciated until 1981 (3), and the causative virus was not identified until 1983 (4). In the decades since, HIV-1 prevalence has increased to approximately 33.4 million people worldwide, with approximately 2 million AIDS-related deaths per year (5).

The Molecular Virology of HIV-1

Attachment and Entry

The HIV-1 genome, Gag structural polyprotein, and viral replication cycle are depicted in Figures 1.1 and 1.2.

Virus particles contain Env, the envelope glycoprotein, within their lipid

envelope. Env is a trimeric complex of heterodimers, composed of surface subunit gp120 and transmembrane subunit gp41, both of which are derived from the *env* gene product by proteolysis. Particles bind to cell surface receptor CD4 and co-receptors CCR5 or CXCR4 via their Env glycoproteins. This receptor specificity is the primary determinant of the virus tropism for CD4+ T lymphocytes and macrophages; however, it has been suggested that other cell types, such as hematopoietic progenitor cells, are susceptible as well (6). Co-receptor usage correlates with disease progression, with CCR5-tropic viruses predominating early and CXCR4-tropic viruses predominating late in disease progression; however, the mechanisms that underlie this correlation remain controversial (7). Upon receptor binding, a conformational change in Env promotes membrane fusion, leading to entry of the viral core into the cytoplasm. It is thought that fusion and entry occur primarily at the cell surface. However, fusion and entry from an endocytic compartment has been recently observed (8). There are currently two approved antiretroviral drugs targeting HIV-1 entry: a fusion inhibitor that stabilizes gp41 in a non-fusogenic conformation, and a CCR5 antagonist that blocks binding to this co-receptor (9).

Post-Entry Events

The viral core is composed primarily of the viral structural proteins p24 (capsid, CA) and p7 (nucleocapsid, NC), viral enzymes reverse transcriptase (RT) and integrase (IN), and two copies of the RNA genome. After entry, the viral core traffics through the cytoplasm and the CA protein dissociates to uncoat the complex. This uncoating process can be disrupted by the intrinsic cellular defense factor TRIM5α, leading to premature

uncoating and proteasomal degradation, which is one major factor governing the species tropism of retroviruses (10, 11). HIV-1 is restricted by TRIM5α (or homologues) in many other primate species, and human TRIM5α restricts many primate and non-primate retroviruses; but importantly, human TRIM5α does not strongly restrict HIV-1.

During trafficking and uncoating, the viral enzyme RT mediates reverse transcription of the RNA genome into DNA, and the viral complex (now called the pre-integration complex, or PIC) is imported into the nucleus. This reverse transcription step can be disrupted by the intrinsic cellular defense factor APOBEC3G, if it is incorporated to the virion during assembly. APOBEC3G is a cytidine deaminase that causes deoxycytidine to deoxyuridine hypermutation in the negative strand of the viral genome during reverse transcription. However, the HIV-1 accessory protein Vif prevents APOBEC3G encapsidation and mediates its degradation in virus-producing cells (12). A wide variety of reverse transcriptase inhibitors have been developed, but resistance to these drugs remains a problem.

In contrast to other retroviruses that depend on nuclear envelope breakdown during the cell cycle to access the nucleus, the HIV-1 PIC can be imported to the nucleus even in non-cycling cells. It has been suggested that nuclear import of the PIC is mediated by the viral structural proteins p17 (matrix, MA) and CA, accessory protein Vpr, viral integrase, and cis-acting sequences on the viral DNA, as well as a variety of host nuclear transport factors (13). Once inside the nucleus, the viral integrase, within the pre-integration complex, mediates the recombination of viral DNA into the host genome, forming a provirus. It has been shown that HIV-1 proviruses are preferentially integrated into or near actively transcribed host genes, often into introns (14). There is currently one

approved antiretroviral drug that inhibits the viral integrase.

Transcription, Splicing, and RNA Export

The long terminal repeat (LTR) on the 5' end of the HIV-1 provirus contains host transcription factor binding sites and enhancer elements, and thus functions as a promoter for proviral gene transcription. However, in the absence of the HIV-1 accessory protein Tat, transcription elongation is inefficient. Tat is a *trans* factor that binds the *cis*-acting TAR element (*Trans*-Activating Response element) near the 5' end of the nascent viral RNA. Tat recruits the positive transcription elongation factor complex P-TEFb, which phosphorylates RNA polymerase II, promoting transcript elongation. Thus, small amounts of Tat produced by inefficient transcription positively feedback to promote robust transcription of proviral genes (15).

HIV-1 transcriptional control may have important implications for the course of disease in patients undergoing antiretroviral therapy. Despite antiretroviral therapy reducing viremia to undetectable levels, the virus persists indefinitely in latent reservoirs, and viral loads rebound upon termination of therapy. Long-term reservoirs are thought to consist primarily of long-lived cell types, like quiescent resting CD4+ T-cells or bone marrow hematopoietic progenitor cells (6), containing transcriptionally-silent provirus. The complex molecular mechanisms that contribute to proviral transcriptional silencing are under active investigation. In general, transcriptional silencing is thought to be multifactorial, involving: (i) Disruption of proviral transcription by *cis*-elements and transcription complexes on nearby actively-transcribed host genes; (ii) Availability of transcription factors and co-factors that vary with cell cycle, cell signaling, and

immunological activation; (iii) Chromatin structure; (iv) Cellular microRNA and RNA interference systems (16).

HIV-1 takes advantage of host RNA splicing machinery to generate a diversity of alternatively spliced mRNAs encoding viral proteins. The structural polyprotein, Gag, and polyprotein containing the viral enzymes, Gag-Pol, are expressed from ~9kb full-length unspliced mRNAs. These mRNAs also serve as the viral genomic RNAs. There is one major 5' splice donor upstream of the Gag/Gag-Pol start codon and multiple 3' splice acceptors downstream from the *pol* gene. These splicing events give rise to several ~4kb mRNAs that encode the envelope glycoprotein, Env, or accessory proteins Vif, Vpr, or Vpu. Another pair of splice sites remove most of the *env* gene, generating several ~2kb mRNAs that encode accessory proteins Tat, Rev, and Nef (17-19).

The accessory protein Rev is necessary for the nuclear export of the incompletely spliced ~9kb and ~4kb viral RNA species. Rev monomers bind and then cooperatively multimerize on a *cis*-acting RNA structure element, the Rev Responsive Element (RRE), within the *env* gene of incompletely spliced transcripts. Rev contains a nuclear localization signal sequence that binds importin-β, and a nuclear export signal sequence that binds CRM1/exportin1. Thus, Rev cycles between the nucleus and cytoplasm, exporting incompletely spliced viral RNAs. In addition to the RRE, other *cis*-acting RNA elements are important: First, RNA structural elements are thought to make splicing of viral transcripts inefficient, providing a pool of incompletely spliced viral RNAs as substrates for Rev-mediated export. Second, *cis*-acting instability elements are necessary for Rev-dependence of viral transcripts, because silent mutations that disrupt these instability elements allow Rev-independent expression (17-19).

By analogy to the expression regulation of many other viruses, it has been suggested that this alternative splicing strategy loosely divides viral gene expression into an "early" Rev-independent phase, during which Tat, Rev, and Nef (which is involved in evasion of the immune response) are expressed, and a "late" Rev-dependent phase, during which everything necessary for virus assembly is expressed at high-levels due to the positive feedback of Tat and Rev (17-19).

Assembly

The viral structural polyprotein Gag is necessary and sufficient for the assembly of virus-like particles. Gag is a 55 kDa polyprotein composed of 4 major structural domains (and 2 spacer polypeptides), as defined by cleavage by the viral protease: matrix (MA), capsid (CA), nucleocapsid (NC), and p6. However, proteolytic cleavage occurs largely after virion assembly and release; thus, its constituents must work together in the context of the full-length Gag polyprotein to drive particle assembly. After its synthesis in the cytosol, Gag traffics to the site of assembly, binds cellular membranes, multimerizes, partitions into membrane microdomains, buds through the membrane, and recruits host factors that mediate membrane scission, releasing an immature particle (20, 21). It is increasingly apparent that many of these molecular functions do not occur in any particular order, but rather occur in a coordinated, interdependent fashion (discussed in "Interrelationships between steps of HIV-1 assembly" below, and Chapter V). Importantly, there are currently no antiretroviral drugs targeting HIV-1 assembly. A more detailed view of assembly on the plasma membrane is depicted in Figure 1.3.

Site of Assembly

Gag traffics to its site of assembly by largely unknown mechanisms. It is not known whether Gag traffics to the site of assembly as a soluble monomer, or if Gag membrane binding and multimerization play a role in trafficking. Until recently it was thought that the site of virus assembly varied by host cell type. HIV-1 appears to assemble on the plasma membrane in T cells and some laboratory cell lines. It was thought that late endosomes/multivesicular bodies (LE/MVB) were the site of assembly in macrophages, based on the apparently intracellular location of assembling Gag and presence of LE/MVB markers, such as the tetraspanin protein CD63 and ESCRT (Endosomal Sorting Complexes Required for Transport) (22, 23). However, it was recently demonstrated that the site of assembly in macrophages are actually deep invaginations of the plasma membrane (24, 25), and that markers like CD63 strongly co-localize with Gag, even at assembly sites that are unambiguously on the plasma membrane (24-33).

Membrane Binding

Gag membrane binding is mediated by its N-terminal MA domain, containing bipartite membrane binding motifs. The MA domain is co-translationally myristoylated, and contains a patch of basic residues that bind the phospholipid phosphatidylinositol-(4,5)-bisphosphate [$PI(4,5)P_2$] (34-41). Prior to membrane binding, the myristoyl moiety is sequestered in a hydrophobic pocket of the MA domain. It is thought that the myristoyl group switches to an exposed conformation to promote membrane binding upon Gag multimerization (mediated by CA or NC, as described below), or upon $PI(4,5)P_2$ binding

(38, 42-45).

Studies from our laboratory and others have demonstrated, using a liposome binding assay *in vitro*, that the basic residues in MA bind $PI(4,5)P_2$ (41, 46, 47), which is predominantly on the plasma membrane of cells. Moreover, the basic residues also appear to inhibit non-specific membrane binding, possibly by regulating myristoyl exposure and competitively binding RNA (46). Thus, $PI(4,5)P_2$ binding, coupled with inhibition of non-specific membrane binding, may cause assembly to be targeted to the plasma membrane.

Interestingly, an NMR study using soluble $PI(4,5)P_2$ (with short acyl chains, allowing it to remain dissolved) showed that, after myristoyl exposure, the hydrophobic pocket of the MA domain becomes occupied by the typically unsaturated 2' acyl chain of $PI(4,5)P_2$ – effectively exchanging an unsaturated acyl chain for the saturated myristoyl chain (38). It remains to be seen if this acyl chain exchange occurs in the more authentic case of Gag binding a lipid bilayer, as opposed to dissolved lipids. If so, this sequestration of the unsaturated 2' acyl chain of $PI(4,5)P_2$ has been predicted to facilitate Gag association with lipid rafts (see below).

Multimerization

Previous studies have identified two major functional regions that contribute to Gag multimerization (20, 21, 33, 48-62). Biochemical, genetic, and structural studies have shown that the C-terminal region of the CA domain (CA-CTD) forms an interface that mediates Gag homodimerization (33, 53, 63-65). In additon to the CA-CTD, the NC domain also contributes to Gag multimerization via fifteen basic residues. It is thought

that the contribution of NC to assembly is due to its ability to bind RNA, since the addition of RNA promotes the formation of Gag particles *in vitro*, and RNase treatment disrupts Gag-Gag interactions (50, 58, 64, 66-68). However, RNA is not necessary *per se*, since leucine zipper dimerization motifs can substitute for NC (69-73). This suggests a model in which RNA serves a structural role, such as a scaffold, to promote Gag-Gag interactions through NC. Because RNA is a large polymer that could conceivably accommodate the binding of many Gag molecules, it has been suggested that RNA facilitates long-range Gag-Gag interactions to form higher-order multimers. However, based on studies *in vitro* using short oligonucleotides, and the fact that protein-protein dimerization motifs can substitute for NC, it has instead been suggested that this RNA scaffolding interaction is only necessary for low-order Gag multimerization (69-77). Importantly, most studies of CA- and NC-mediated Gag multimerization have used purified *in vitro* systems that may not accurately reflect the behavior of Gag in cells – for example, by neglecting the influence of cellular membranes on Gag multimerization. The work presented in Chapter III addreses this gap in knowledge.

Microdomain Distribution of Gag

The plasma membrane is heterogeneous, consisting of diverse microdomains. This partitioning of membrane components is regulated by lipid-lipid, protein-protein, and protein-lipid interactions in order to compartmentalize cellular processes (78, 79). As with many diverse enveloped viruses, HIV-1 was initially proposed to assemble at lipid rafts, based on sensitivity to cellular cholesterol depletion and co-fractionation of viral components with detergent-resistant membranes.

Lipid Rafts

Spontaneous partitioning – or equilibration – of lipids into an ordered phase and a disordered phase has been observed in chemically-defined model membranes, and model membranes reconstituted from cellular membrane components (78, 79). The ordered phase is enriched in cholesterol and saturated lipids, and the disordered phase is enriched in unsaturated lipids. This biophysical phenomenon of lipid phase separation in model membranes has been hypothesized to underlie the phenomenon of lipid rafts in cells; thus, assays that are thought to measure ordered/disordered phase separation have been widely used as an empirical definition of lipid rafts in cells. Assays that are thought to measure this biophysical ordered/disordered phase separation in cellular membranes include: (i) Sensitivity to cellular cholesterol depletion; (ii) Resistance to non-ionic detergents; and, (iii) Spectral shift of the lipophilic fluorescent dye laurdan, which is thought to measure the degree to which laurdan is desolvated by dense ordered packing of its surrounding lipids (80, 81). Results from each of these assays have been taken as evidence for lipid raft involvement in HIV-1 assembly (64, 82-94).

However, cellular membranes contain a greater diversity of lipids and proteins, the partitioning of which is governed by a much greater complexity of lipid-lipid, protein-lipid, and protein-protein interactions. Thus, the phenomenon of lipid rafts in cellular membranes is not reducible to the preferential association of lipids seen in simple model membranes. The current concept of lipid rafts in cellular membranes places a greater emphasis on molecular characterization of lipid rafts, by identifying both lipids and proteins that have tendencies to preferentially associate (78, 79). The current consensus is

that lipid rafts are highly dynamic, sub-microscopic membrane domains enriched in sterols, sphingolipids, glycosylphosphatidylinositol-anchored (GPI-anchored) proteins, and proteins modified with saturated acyl chains (78, 79). Biochemical, proteomics, and lipidomics studies have shown that the HIV-1 envelope is enriched in many of these lipids and proteins that are also enriched in lipid rafts (95-102), and in cells, Gag co-localizes or co-patches with raft markers, such as the glycosphingolipid GM1, and GPI-anchored proteins (82, 88, 103).

Tetraspanin Enriched Microdomains

As discussed above (see "Site of Assembly"), the first evidence of association between tetraspanin proteins and HIV-1 assembly were early studies that found the tetraspanin protein CD63 enriched in the envelopes of HIV-1 particles. This was taken as evidence that Gag traffics through, or assembles at, an endosomal compartment, such as the LE/MVB. However, it was later shown that Gag associates with CD63 and other tetraspanin proteins at discrete microdomains on the plasma membrane.

Tetraspanin Enriched Microdomains (TEMs) are plasma membrane microdomains organized by the homo- and hetero-oligomerization of tetraspanins, a family of homologous proteins with four transmembrane domains. Proteomics studies have identified a wide variety of proteins associated with TEMs. Most notably, tetraspanins interact with cell adhesion molecules, integrins, and cell signaling proteins, suggesting that TEMs serve as a platform to spatially organize cell-cell and cell-extracellular matrix adhesion and signaling (104-106). Tetraspanins CD63 and CD81 have been shown to associate with phosphatidylinositol 4-kinase, a critical enzyme in

creating $PI(4,5)P_2$ (107), the lipid to which Gag binds. In addition, tetraspanins have been reported to positively and negatively regulate cell-cell fusion in the development of muscle fibers, multinucleated phagocytes, and sperm-oocyte fusion (104-106). Importantly, different tetraspanins appear to be at least partially redundant in the cell functions measured in some of these studies.

A variety of studies have suggested roles for tetraspanins and TEMs in different phases of the HIV-1 replication cycle: Tetraspanins at the surface of uninfected target cells may promote (108, 109) or inhibit (110) viral entry, and tetraspanins incorporated into virus particles inhibit entry (111-113). CD63 may indirectly reduce susceptibility of uninfected target cells by diverting HIV-1 co-receptor CXCR4 from the cell surface (114). CD81 may promote signal transduction leading to increased proviral transcription in infected cells (115). TEMs may play important roles in mediating direct cell-to-cell transmission of HIV-1 via virological synapses (30, 113, 116), which is thought to be the most efficient mode of virus spread within an infected host (discussed in Chapter V). The role of tetraspanins and TEMs in Gag assembly is, however, currently unclear. The gross effects on assembly of perturbing tetraspanins by siRNA knockdown or over-expression are so far contradictory: some studies report perturbation reduces particle production (112, 117), while others report no effect (111, 113, 118).

Tetraspanins, including CD9, CD63, and CD81, are incorporated into virus particles (26, 100, 111, 119-125), co-immunoprecipitate with Gag-laden cellular membranes (112), and strongly co-localize/co-patch with Gag by immunofluorescence and electron microscopy assays (24, 25, 27-33). Because tetraspanins are at least partially functionally redundant, and have pleiotropic effects on the HIV-1 replication cycle, to

more directly test the functional relevance of tetraspanins, it is essential to first determine the molecular mechanisms that govern Gag association with TEMs. The work presented in Chapter IV addresses this goal.

Budding, Release and Maturation

The p6 domain of Gag contains two protein-protein interaction motifs that recruit components of the cellular ESCRT complexes: PTAP that recruits Tsg101, and LxxLF that recruits AIP-1/ALIX. These proteins then recruit additional ESCRT components, which mediate membrane scission, releasing virus particles from the plasma membrane (126). It has also been suggested that sequences within NC contribute to, but are not required for, AIP-1/ALIX recruitment (127, 128). In uninfected cells, the ESCRT complexes mediate both the membrane budding and membrane scission that produces intraluminal vesicles within the LE/MVB. Gag mutants that are unable to recruit ESCRT, and Gag in cells expressing dominant-negative ESCRT proteins, still produce structures on the plasma membrane that appear to be immature virions. These structures appear tethered to the plasma membrane due to failure of membrane scission. Based on these observations, it was thought that ESCRT complexes only mediate membrane scission, and that Gag alone was sufficient to cause membrane budding.

However, a recent study of HIV-1 budding using high-resolution cryo-electron tomography has suggested a greater role for ESCRT in virion morphogenesis. This study compared the three-dimensional structures of released immature virions to tethered particles produced by Gag deficient in ESCRT recruitment. In released immature virions, multimerized Gag formed a partial-sphere lining only ~70% of the inner membrane

surface. In contrast, in cell-tethered particles deficient in ESCRT recruitment, Gag formed a nearly complete sphere lining nearly 100% of the particle inner membrane surface. These observations suggest that Gag is sufficient to begin budding, but that ESCRT complexes play an earlier and more active role in completing the budding process (129).

The release of virus particles can be inhibited by incorporation of the host restriction factor, tetherin (BST2/CD317). Tetherin localizes at interface between nascent virus particles and the host plasma membrane, and is thought to physically tether particles to the cell surface, eventually promoting their internalization and destruction. Interestingly, several unrelated enveloped viruses have been shown to be restricted by tetherin, suggesting that some common feature or mechanism of enveloped virus assembly governs tetherin incorporation. In the case of HIV-1, tetherin is down-regulated from the cell surface by the viral accessory protein Vpu (130).

Finally, during and after particle budding and release, the viral protease within the Gag-Pol polyprotein cleaves both Gag and Gag-Pol polyproteins. These cleavage events cause a structural rearrangement during which CA, NC, viral enzymes, and viral RNAs condense into a cone-shaped core, producing a mature, infectious virion. Protease inhibitor antiretroviral drugs target this final step in the replication cycle.

Interrelationships between Steps of HIV-1 Assembly

As with any complex system, one recurring theme in molecular studies of HIV-1 is that necessary steps in the replication cycle are often interrelated, and cannot be easily spatiotemporally or genetically separated. For example, the early events in the replication

cycle, uncoating, reverse transcription, and nuclear entry, all appear to be interdependent (131).

Importantly, this also appears to be the case with late events in the replication cycle leading to HIV-1 assembly. Gag intracellular trafficking, membrane binding, RNA binding, multimerization, microdomain distribution, budding, and release are likely all interrelated. Other work in our laboratory has found functional interrelationships between different modes of membrane binding and RNA binding (46), membrane binding and intracellular trafficking (41, 46), and multimerization and subcellular localization (132).

The work presented in Chapters III and IV of this dissertation represents an effort to unravel these interrelationships spatially and quantitatively using microscopy methods (discussed in Chapter II), and mechanistically, using careful molecular genetics approaches. In the study presented in Chapter III, I analyzed how Gag multimerization and membrane binding appear to be functionally interrelated, and suggested that membrane and RNA may play functionally similar roles as scaffolds. In Chapter IV, I studied the microdomain distribution of Gag, focusing on the relationships between different modes of Gag membrane binding and association with lipid rafts and TEMs.

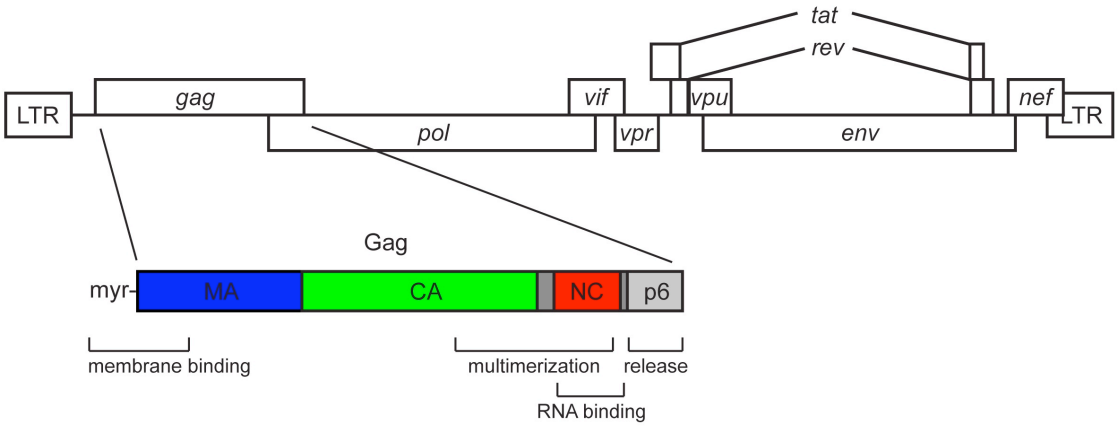

Figure 1.1. Schematic of HIV-1 genome organization and Gag structural polyprotein. The HIV-1 genome expresses nine major proteins. Gag, Vif, Vpr, Tat, Rev, Vpu, Env, and Nef are produced by alternative RNA splicing. The Gag-Pol polyprotein is produced by ribosomal frameshift between the *gag* and *pol* reading frames. Gag is N-terminally myrisotylated (myr), and is composed of four major structural domains, matrix (MA), capsid (CA), nucleocapsid (NC), and p6. Major functional domains of the polyprotein are indicated.

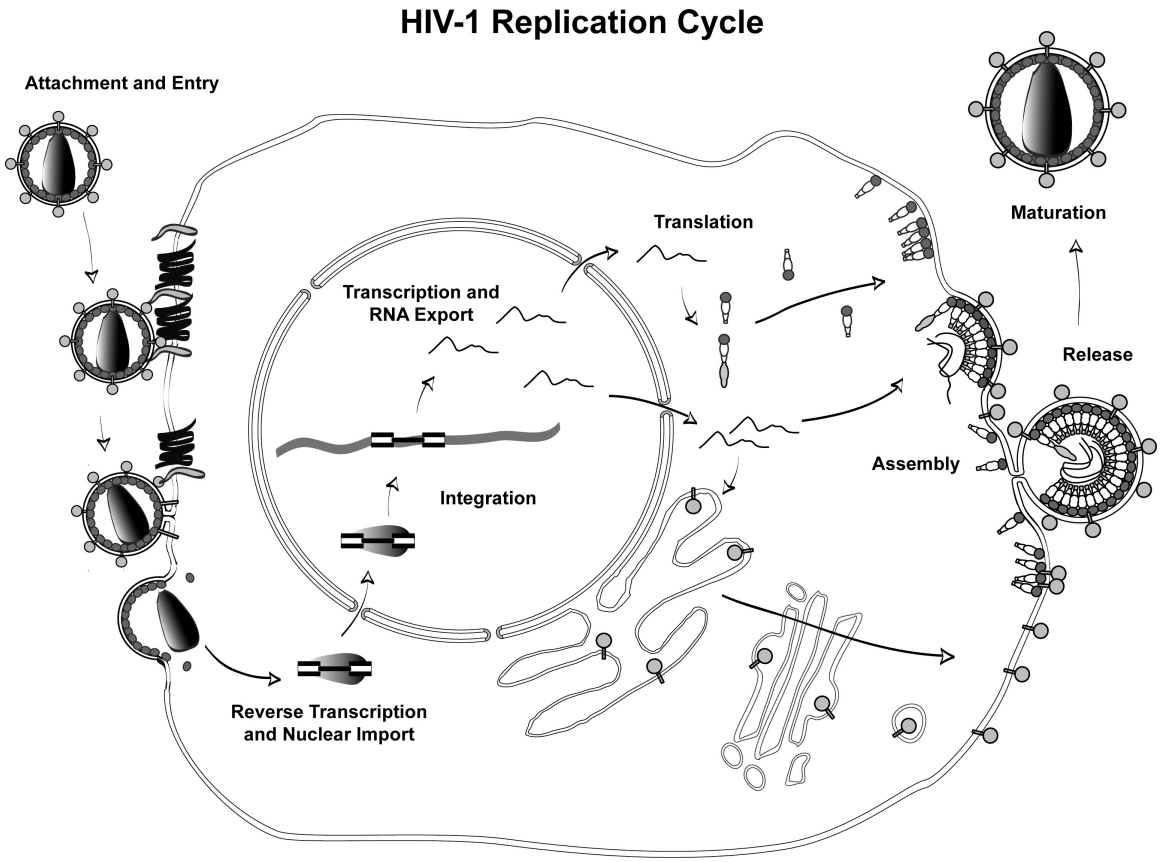

Figure 1.2. Schematic of the HIV-1 replication cycle. Virus particles attach to cell surface receptors. The viral lipid envelope fuses with the cell plasma membrane, and the viral core enters the cell. The core traffics to the nucleus, uncoats, reverse transcribes viral RNA into DNA, and enters the nucleus. Viral DNA is integrated into the host genome, forming a provirus. Viral RNAs are transcribed and exported from the nucleus. Viral proteins are translated and traffic to the plasma membrane. Gag and Gag-Pol are depicted in the cytoplasm and on the plasma membrane. Env is depicted trafficking through the secretory pathway. On the plasma membrane, Gag drives the assembly of nascent immature virus particles. During and after release, the virus particle matures into its infectious form, completing the replication cycle.

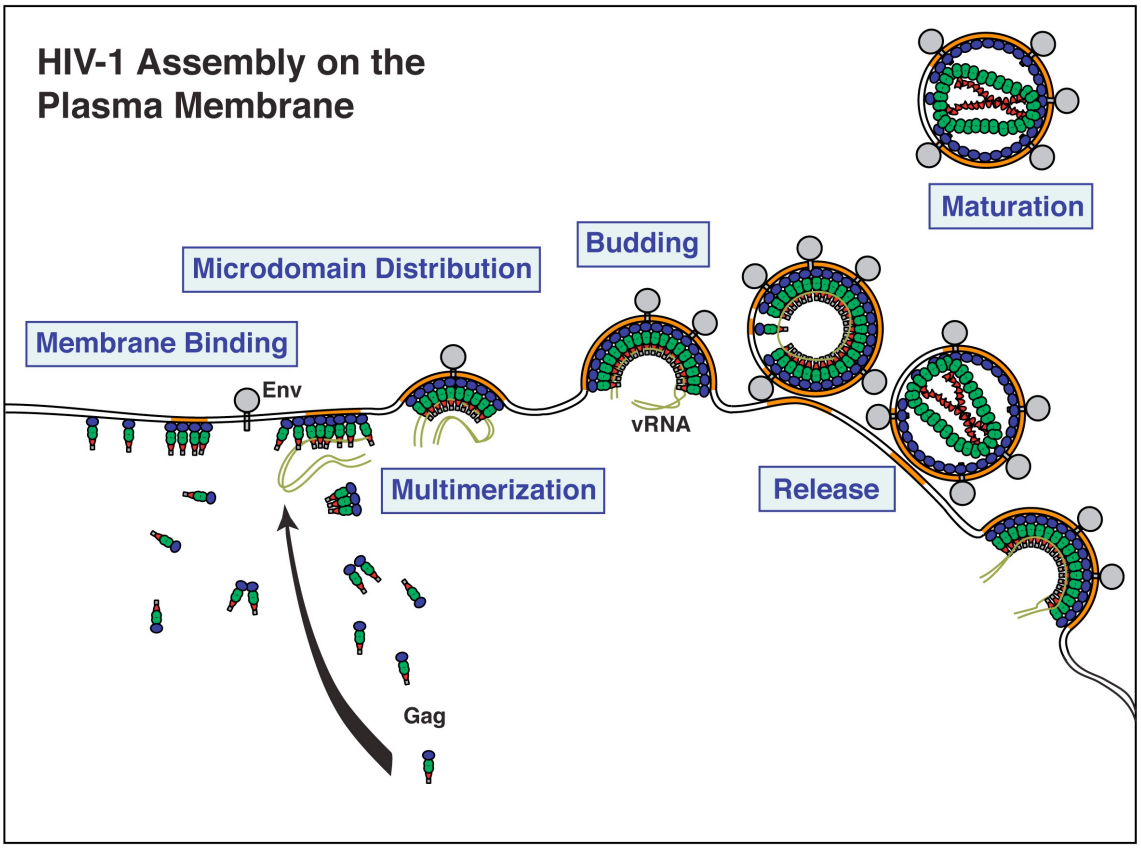

Figure 1.3. HIV-1 assembly on the plasma membrane. Gag binds the plasma membrane and recruits Env via its matrix domain. Gag binds viral genomic RNA via its nucleocapsid domain. Gag multimerizes via its capsid and nucleocapsid domains, and buds through the plasma membrane. Gag recruits components of the host ESCRT complexes via its p6 domain, which mediate release.

REFERENCES

1. Keele, B.F., et al., *Chimpanzee reservoirs of pandemic and nonpandemic HIV-1*. Science, 2006. **313**(5786): p. 523-6.

2. Worobey, M., et al., *Direct evidence of extensive diversity of HIV-1 in Kinshasa by 1960.* Nature, 2008. **455**(7213): p. 661-4.

3. CDC, *Kaposi's sarcoma and Pneumocystis pneumonia among homosexual men--New York City and California.* MMWR Morb Mortal Wkly Rep, 1981. **30**(25): p. 305-8.

4. Barre-Sinoussi, F., et al., *Isolation of a T-lymphotropic retrovirus from a patient at risk for acquired immune deficiency syndrome (AIDS).* Science, 1983. **220**(4599): p. 868-71.

5. UNAIDS, *AIDS epidemic update December 2009*. 2009, Geneva: UNAIDS.

6. Carter, C.C., et al., *HIV-1 infects multipotent progenitor cells causing cell death and establishing latent cellular reservoirs.* Nat Med, 2010.

7. Mosier, D.E., *How HIV changes its tropism: evolution and adaptation?* Curr Opin HIV AIDS, 2009. **4**(2): p. 125-30.

8. Miyauchi, K., et al., *HIV enters cells via endocytosis and dynamin-dependent fusion with endosomes.* Cell, 2009. **137**(3): p. 433-44.

9. Kuritzkes, D.R., *HIV-1 entry inhibitors: an overview.* Curr Opin HIV AIDS, 2009. **4**(2): p. 82-7.

10. Stremlau, M., et al., *Specific recognition and accelerated uncoating of retroviral capsids by the TRIM5alpha restriction factor.* Proc Natl Acad Sci U S A, 2006. **103**(14): p. 5514-9.

11. Mascarenhas, A.P. and K. Musier-Forsyth, *The capsid protein of human immunodeficiency virus: interactions of HIV-1 capsid with host protein factors.* Febs J, 2009. **276**(21): p. 6118-27.

12. Goila-Gaur, R. and K. Strebel, *HIV-1 Vif, APOBEC, and intrinsic immunity.* Retrovirology, 2008. **5**: p. 51.

13. Riviere, L., J.L. Darlix, and A. Cimarelli, *Analysis of the viral elements required in the nuclear import of HIV-1 DNA.* J Virol. **84**(2): p. 729-39.

14. Bushman, F.D., *Integration site selection by lentiviruses: biology and possible control.* Curr Top Microbiol Immunol, 2002. **261**: p. 165-77.

15. Garber, M.E. and K.A. Jones, *HIV-1 Tat: coping with negative elongation factors.* Curr Opin Immunol, 1999. **11**(4): p. 460-5.

16. Colin, L. and C. Van Lint, *Molecular control of HIV-1 postintegration latency: implications for the development of new therapeutic strategies.* Retrovirology, 2009. **6**: p. 111.

17. Pollard, V.W. and M.H. Malim, *The HIV-1 Rev protein.* Annu Rev Microbiol, 1998. **52**: p. 491-532.

18. Suhasini, M. and T.R. Reddy, *Cellular proteins and HIV-1 Rev function.* Curr HIV Res, 2009. **7**(1): p. 91-100.

19. Nekhai, S. and K.T. Jeang, *Transcriptional and post-transcriptional regulation of HIV-1 gene expression: role of cellular factors for Tat and Rev.* Future Microbiol, 2006. **1**: p. 417-26.

20. Adamson, C.S. and I.M. Jones, *The molecular basis of HIV capsid assembly--five years of progress.* Rev Med Virol, 2004. **14**(2): p. 107-21.

21. Freed, E.O., *HIV-1 gag proteins: diverse functions in the virus life cycle.* Virology, 1998. **251**(1): p. 1-15.

22. Pelchen-Matthews, A., B. Kramer, and M. Marsh, *Infectious HIV-1 assembles in late endosomes in primary macrophages.* J Cell Biol, 2003. **162**(3): p. 443-55.

23. Raposo, G., et al., *Human macrophages accumulate HIV-1 particles in MHC II compartments.* Traffic, 2002. **3**(10): p. 718-29.

24. Deneka, M., et al., *In macrophages, HIV-1 assembles into an intracellular plasma membrane domain containing the tetraspanins CD81, CD9, and CD53.* J Cell Biol, 2007. **177**(2): p. 329-41.

25. Welsch, S., et al., *HIV-1 Buds Predominantly at the Plasma Membrane of Primary Human Macrophages.* PLoS Pathog, 2007. **3**(3): p. e36.

26. Nydegger, S., et al., *HIV-1 egress is gated through late endosomal membranes.* Traffic, 2003. **4**(12): p. 902-10.

27. Booth, A.M., et al., *Exosomes and HIV Gag bud from endosome-like domains of the T cell plasma membrane.* J Cell Biol, 2006. **172**(6): p. 923-35.

28. Grigorov, B., et al., *Assembly of infectious HIV-1 in human epithelial and T-lymphoblastic cell lines.* J Mol Biol, 2006. **359**(4): p. 848-62.

29. Nydegger, S., et al., *Mapping of tetraspanin-enriched microdomains that can function as gateways for HIV-1.* J Cell Biol, 2006. **173**(5): p. 795-807.

30. Jolly, C. and Q.J. Sattentau, *Human immunodeficiency virus type 1 assembly, budding, and cell-cell spread in T cells take place in tetraspanin-enriched plasma membrane domains.* J Virol, 2007. **81**(15): p. 7873-84.

31. Garcia, E., D.S. Nikolic, and V. Piguet, *HIV-1 replication in dendritic cells occurs through a tetraspanin-containing compartment enriched in AP-3.* Traffic, 2008. **9**(2): p. 200-14.

32. Turville, S.G., et al., *Resolution of de novo HIV production and trafficking in immature dendritic cells.* Nat Methods, 2008. **5**(1): p. 75-85.

33. Hogue, I.B., A. Hoppe, and A. Ono, *Quantitative fluorescence resonance energy transfer microscopy analysis of the human immunodeficiency virus type 1 Gag-Gag interaction: relative contributions of the CA and NC domains and membrane binding.* J Virol, 2009. **83**(14): p. 7322-36.

34. Gottlinger, H.G., J.G. Sodroski, and W.A. Haseltine, *Role of capsid precursor processing and myristoylation in morphogenesis and infectivity of human immunodeficiency virus type 1.* Proc Natl Acad Sci U S A, 1989. **86**(15): p. 5781-5.

35. Bryant, M. and L. Ratner, *Myristoylation-dependent replication and assembly of human immunodeficiency virus 1.* Proc Natl Acad Sci U S A, 1990. **87**(2): p. 523-7.

36. Zhou, W., et al., *Identification of a membrane-binding domain within the amino-terminal region of human immunodeficiency virus type 1 Gag protein which interacts with acidic phospholipids.* J Virol, 1994. **68**(4): p. 2556-69.

37. Hill, C.P., et al., *Crystal structures of the trimeric human immunodeficiency virus type 1 matrix protein: implications for membrane association and assembly.* Proc Natl Acad Sci U S A, 1996. **93**(7): p. 3099-3104.

38. Saad, J.S., et al., *Structural basis for targeting HIV-1 Gag proteins to the plasma membrane for virus assembly.* Proc Natl Acad Sci U S A, 2006. **103**(30): p. 11364-9.

39. Shkriabai, N., et al., *Interactions of HIV-1 Gag with assembly cofactors.* Biochemistry, 2006. **45**(13): p. 4077-83.

40. Dalton, A.K., et al., *Electrostatic Interactions Drive Membrane Association of the Human Immunodeficiency Virus Type 1 Gag MA Domain.* J Virol, 2007. **81**(12): p. 6434-45.

41. Chukkapalli, V., et al., *Interaction between the human immunodeficiency virus type 1 Gag matrix domain and phosphatidylinositol-(4,5)-bisphosphate is essential for efficient gag membrane binding.* J Virol, 2008. **82**(5): p. 2405-17.

42. Saad, J.S., et al., *Point mutations in the HIV-1 matrix protein turn off the myristyl switch.* J Mol Biol, 2007. **366**(2): p. 574-85.

43. Spearman, P., et al., *Membrane binding of human immunodeficiency virus type 1 matrix protein in vivo supports a conformational myristyl switch mechanism.* J Virol, 1997. **71**(9): p. 6582-92.

44. Tang, C., et al., *Entropic switch regulates myristate exposure in the HIV-1 matrix protein.* Proc Natl Acad Sci U S A, 2004. **101**(2): p. 517-22.

45. Zhou, W. and M.D. Resh, *Differential membrane binding of the human immunodeficiency virus type 1 matrix protein.* J Virol, 1996. **70**(12): p. 8540-8.

46. Chukkapalli, V., S.J. Oh, and A. Ono, *Opposing mechanisms involving RNA and lipids regulate HIV-1 Gag membrane binding through the highly basic region of the matrix domain.* Proc Natl Acad Sci U S A, 2010. **107**(4): p. 1600-5.

47. Alfadhli, A., A. Still, and E. Barklis, *Analysis of human immunodeficiency virus type 1 matrix binding to membranes and nucleic acids.* J Virol, 2009. **83**(23): p. 12196-203.

48. Ehrlich, L.S., B.E. Agresta, and C.A. Carter, *Assembly of recombinant human immunodeficiency virus type 1 capsid protein in vitro.* J Virol, 1992. **66**(8): p. 4874-83.

49. Franke, E.K., et al., *Specificity and sequence requirements for interactions between various retroviral Gag proteins.* J Virol, 1994. **68**(8): p. 5300-5.

50. Campbell, S. and V.M. Vogt, *Self-assembly in vitro of purified CA-NC proteins from Rous sarcoma virus and human immunodeficiency virus type 1.* J Virol, 1995. **69**(10): p. 6487-97.

51. Momany, C., et al., *Crystal structure of dimeric HIV-1 capsid protein.* Nat Struct Biol, 1996. **3**(9): p. 763-70.

52. Zhang, W.H., et al., *Gag-Gag interactions in the C-terminal domain of human immunodeficiency virus type 1 p24 capsid antigen are essential for Gag particle assembly.* J Gen Virol, 1996. **77**(4): p. 743-51.

53. Gamble, T.R., et al., *Structure of the carboxyl-terminal dimerization domain of the HIV-1 capsid protein.* Science, 1997. **278**(5339): p. 849-53.

54. Swanstrom, R. and J.W. Wills, *Synthesis, Assembly, and Processing of Viral Proteins*, in *Retroviruses*, J.M. Coffin, S.H. Hughes, and H.E. Varmus, Editors. 1997, Cold Spring Harbor Laboratory Press: New York. p. 263-334.

55. Dawson, L. and X.F. Yu, *The role of nucleocapsid of HIV-1 in virus assembly.* Virology, 1998. **251**(1): p. 141-57.

56. Gross, I., et al., *N-Terminal extension of human immunodeficiency virus capsid protein converts the in vitro assembly phenotype from tubular to spherical particles.* J Virol, 1998. **72**(6): p. 4798-810.

57. Burniston, M.T., et al., *Human immunodeficiency virus type 1 Gag polyprotein multimerization requires the nucleocapsid domain and RNA and is promoted by the capsid-dimer interface and the basic region of matrix protein.* J Virol, 1999. **73**(10): p. 8527-40.

58. Campbell, S. and A. Rein, *In vitro assembly properties of human immunodeficiency virus type 1 Gag protein lacking the p6 domain.* J Virol, 1999. **73**(3): p. 2270-9.

59. Cimarelli, A. and J. Luban, *Human immunodeficiency virus type 1 virion density is not determined by nucleocapsid basic residues.* J Virol, 2000. **74**(15): p. 6734-40.

60. Sandefur, S., et al., *Mapping and characterization of the N-terminal I domain of human immunodeficiency virus type 1 Pr55(Gag).* J Virol, 2000. **74**(16): p. 7238-49.

61. Huseby, D., et al., *Assembly of human immunodeficiency virus precursor gag proteins.* J Biol Chem, 2005. **280**(18): p. 17664-70.

62. Li, H., et al., *Myristoylation is required for human immunodeficiency virus type 1 Gag-Gag multimerization in mammalian cells.* J Virol, 2007. **81**(23): p. 12899-910.

63. von Schwedler, U.K., et al., *Functional surfaces of the human immunodeficiency virus type 1 capsid protein.* J Virol, 2003. **77**(9): p. 5439-50.

64. Ono, A., et al., *Association of human immunodeficiency virus type 1 gag with membrane does not require highly basic sequences in the nucleocapsid: use of a novel Gag multimerization assay.* J Virol, 2005. **79**(22): p. 14131-40.

65. Joshi, A., K. Nagashima, and E.O. Freed, *Mutation of dileucine-like motifs in the human immunodeficiency virus type 1 capsid disrupts virus assembly, gag-gag interactions, gag-membrane binding, and virion maturation.* J Virol, 2006. **80**(16): p. 7939-51.

66. Cimarelli, A., et al., *Basic residues in human immunodeficiency virus type 1 nucleocapsid promote virion assembly via interaction with RNA.* J Virol, 2000. **74**(7): p. 3046-57.

67. Muriaux, D., et al., *RNA is a structural element in retrovirus particles.* Proc Natl Acad Sci U S A, 2001. **98**(9): p. 5246-51.

68. Khorchid, A., et al., *Role of RNA in facilitating Gag/Gag-Pol interaction.* J Virol, 2002. **76**(8): p. 4131-7.

69. Accola, M.A., B. Strack, and H.G. Gottlinger, *Efficient particle production by minimal Gag constructs which retain the carboxy-terminal domain of human immunodeficiency virus type 1 capsid-p2 and a late assembly domain.* J Virol, 2000. **74**(12): p. 5395-402.

70. Alfadhli, A., et al., *Analysis of human immunodeficiency virus type 1 Gag dimerization-induced assembly.* J Virol, 2005. **79**(23): p. 14498-506.

71. Crist, R.M., et al., *Assembly properties of human immunodeficiency virus type 1 Gag-leucine zipper chimeras: implications for retrovirus assembly.* J Virol, 2009. **83**(5): p. 2216-25.

72. Johnson, M.C., et al., *Nucleic acid-independent retrovirus assembly can be driven by dimerization.* J Virol, 2002. **76**(22): p. 11177-85.

73. Zhang, Y., et al., *Analysis of the assembly function of the human immunodeficiency virus type 1 gag protein nucleocapsid domain.* J Virol, 1998. **72**(3): p. 1782-9.

74. Gross, I., H. Hohenberg, and H.G. Krausslich, *In vitro assembly properties of purified bacterially expressed capsid proteins of human immunodeficiency virus.* Eur J Biochem, 1997. **249**(2): p. 592-600.

75. Ma, Y.M. and V.M. Vogt, *Rous sarcoma virus Gag protein-oligonucleotide interaction suggests a critical role for protein dimer formation in assembly.* J Virol, 2002. **76**(11): p. 5452-62.

76. Ma, Y.M. and V.M. Vogt, *Nucleic acid binding-induced Gag dimerization in the assembly of Rous sarcoma virus particles in vitro.* J Virol, 2004. **78**(1): p. 52-60.

77. Roldan, A., et al., *In vitro identification and characterization of an early complex linking HIV-1 genomic RNA recognition and Pr55Gag multimerization.* J Biol Chem, 2004. **279**(38): p. 39886-94.

78. Coskun, U. and K. Simons, *Membrane rafting: From apical sorting to phase segregation.* FEBS Lett, 2009.

79. Lingwood, D. and K. Simons, *Lipid rafts as a membrane-organizing principle.* Science, 2010. **327**(5961): p. 46-50.

80. Parasassi, T., et al., *Phase fluctuation in phospholipid membranes revealed by Laurdan fluorescence.* Biophys J, 1990. **57**(6): p. 1179-86.

81. Parasassi, T., et al., *Laurdan and Prodan as Polarity-Sensitive Fluorescent Membrane Probes.* Journal of Fluorescence, 1998. **8**(4): p. 365-373.

82. Nguyen, D.H. and J.E. Hildreth, *Evidence for budding of human immunodeficiency virus type 1 selectively from glycolipid-enriched membrane lipid rafts.* J Virol, 2000. **74**(7): p. 3264-72.

83. Lindwasser, O.W. and M.D. Resh, *Multimerization of human immunodeficiency virus type 1 Gag promotes its localization to barges, raft-like membrane microdomains.* J Virol, 2001. **75**(17): p. 7913-24.

84. Ono, A. and E.O. Freed, *Plasma membrane rafts play a critical role in HIV-1 assembly and release.* Proc Natl Acad Sci U S A, 2001. **98**(24): p. 13925-30.

85. Lindwasser, O.W. and M.D. Resh, *Myristoylation as a target for inhibiting HIV assembly: unsaturated fatty acids block viral budding.* Proc Natl Acad Sci U S A, 2002. **99**(20): p. 13037-42.

86. Ding, L., et al., *Independent segregation of human immunodeficiency virus type 1 Gag protein complexes and lipid rafts.* J Virol, 2003. **77**(3): p. 1916-26.

87. Halwani, R., et al., *Rapid localization of Gag/GagPol complexes to detergent-resistant membrane during the assembly of human immunodeficiency virus type 1.* J Virol, 2003. **77**(7): p. 3973-84.

88. Holm, K., et al., *Human immunodeficiency virus type 1 assembly and lipid rafts: Pr55(gag) associates with membrane domains that are largely resistant to Brij98 but sensitive to Triton X-100.* J Virol, 2003. **77**(8): p. 4805-17.

89. Bhattacharya, J., A. Repik, and P.R. Clapham, *Gag regulates association of human immunodeficiency virus type 1 envelope with detergent-resistant membranes.* J Virol, 2006. **80**(11): p. 5292-300.

90. Dou, J., et al., *Characterization of a myristoylated, monomeric HIV Gag protein.* Virology, 2009. **387**(2): p. 341-52.

91. Pickl, W.F., F.X. Pimentel-Muinos, and B. Seed, *Lipid rafts and pseudotyping.* J Virol, 2001. **75**(15): p. 7175-83.

92. Gomez, C.Y. and T.J. Hope, *Mobility of human immunodeficiency virus type 1 Pr55Gag in living cells.* J Virol, 2006. **80**(17): p. 8796-806.

93. Ono, A., A.A. Waheed, and E.O. Freed, *Depletion of cellular cholesterol inhibits membrane binding and higher-order multimerization of human immunodeficiency virus type 1 Gag.* Virology, 2007. **360**(1): p. 27-35.

94. Lorizate, M., et al., *Probing HIV-1 membrane liquid order by Laurdan staining reveals producer cell-dependent differences.* J Biol Chem, 2009. **284**(33): p. 22238-47.

95. Aloia, R.C., H. Tian, and F.C. Jensen, *Lipid composition and fluidity of the human immunodeficiency virus envelope and host cell plasma membranes.* Proc Natl Acad Sci U S A, 1993. **90**(11): p. 5181-5.

96. Saifuddin, M., et al., *Role of virion-associated glycosylphosphatidylinositol-linked proteins CD55 and CD59 in complement resistance of cell line-derived and primary isolates of HIV-1.* J Exp Med, 1995. **182**(2): p. 501-9.

97. Nakamura, M., et al., *Quantification of the CD55 and CD59, membrane inhibitors of complement on HIV-1 particles as a function of complement-mediated virolysis.* Microbiol Immunol, 1996. **40**(8): p. 561-7.

98. Graham, D.R., et al., *Cholesterol depletion of human immunodeficiency virus type 1 and simian immunodeficiency virus with beta-cyclodextrin inactivates and permeabilizes the virions: evidence for virion-associated lipid rafts.* J Virol, 2003. **77**(15): p. 8237-48.

99. Brugger, B., et al., *The HIV lipidome: a raft with an unusual composition.* Proc Natl Acad Sci U S A, 2006. **103**(8): p. 2641-6.

100. Chertova, E., et al., *Proteomic and biochemical analysis of purified human immunodeficiency virus type 1 produced from infected monocyte-derived macrophages.* J Virol, 2006. **80**(18): p. 9039-52.

101. Chan, R., et al., *Retroviruses human immunodeficiency virus and murine leukemia virus are enriched in phosphoinositides.* J Virol, 2008. **82**(22): p. 11228-38.

102. Ott, D.E., *Cellular proteins detected in HIV-1.* Rev Med Virol, 2008. **18**(3): p. 159-75.

103. Ono, A. and E.O. Freed, *Role of lipid rafts in virus replication.* Adv Virus Res, 2005. **64**: p. 311-58.

104. Charrin, S., et al., *Lateral organization of membrane proteins: tetraspanins spin their web.* Biochem J, 2009. **420**(2): p. 133-54.

105. Thali, M., *The Roles of Tetraspanins in HIV-1 Replication.* Curr Top Microbiol Immunol, 2009. **339**: p. 85-102.

106. Yanez-Mo, M., et al., *Tetraspanin-enriched microdomains: a functional unit in cell plasma membranes.* Trends Cell Biol, 2009. **19**(9): p. 434-46.

107. Berditchevski, F., et al., *A novel link between integrins, transmembrane-4 superfamily proteins (CD63 and CD81), and phosphatidylinositol 4-kinase.* J Biol Chem, 1997. **272**(5): p. 2595-8.

108. Ho, S.H., et al., *Recombinant extracellular domains of tetraspanin proteins are potent inhibitors of the infection of macrophages by human immunodeficiency virus type 1.* J Virol, 2006. **80**(13): p. 6487-96.

109. von Lindern, J.J., et al., *Potential role for CD63 in CCR5-mediated human immunodeficiency virus type 1 infection of macrophages.* J Virol, 2003. **77**(6): p. 3624-33.

110. Gordon-Alonso, M., et al., *Tetraspanins CD9 and CD81 modulate HIV-1-induced membrane fusion.* J Immunol, 2006. **177**(8): p. 5129-37.

111. Sato, K., et al., *Modulation of human immunodeficiency virus type 1 infectivity through incorporation of tetraspanin proteins.* J Virol, 2008. **82**(2): p. 1021-33.

112. Grigorov, B., et al., *A role for CD81 on the late steps of HIV-1 replication in a chronically infected T cell line.* Retrovirology, 2009. **6**: p. 28.

113. Krementsov, D.N., et al., *Tetraspanins regulate cell-to-cell transmission of HIV-1.* Retrovirology, 2009. **6**: p. 64.

114. Yoshida, T., et al., *A CD63 mutant inhibits T-cell tropic human immunodeficiency virus type 1 entry by disrupting CXCR4 trafficking to the plasma membrane.* Traffic, 2008. **9**(4): p. 540-58.

115. Tardif, M.R. and M.J. Tremblay, *Tetraspanin CD81 provides a costimulatory signal resulting in increased human immunodeficiency virus type 1 gene expression in primary CD4+ T lymphocytes through NF-kappaB, NFAT, and AP-1 transduction pathways.* J Virol, 2005. **79**(7): p. 4316-28.

116. Rudnicka, D., et al., *Simultaneous cell-to-cell transmission of human immunodeficiency virus to multiple targets through polysynapses.* J Virol, 2009. **83**(12): p. 6234-46.

117. Chen, H., et al., *A critical role for CD63 in HIV replication and infection of macrophages and cell lines.* Virology, 2008. **379**(2): p. 191-6.

118. Ruiz-Mateos, E., et al., *CD63 is not required for production of infectious human immunodeficiency virus type 1 in human macrophages.* J Virol, 2008. **82**(10): p. 4751-61.

119. Meerloo, T., et al., *Modulation of cell surface molecules during HIV-1 infection of H9 cells. An immunoelectron microscopic study.* AIDS, 1992. **6**(10): p. 1105-16.

120. Meerloo, T., et al., *Host cell membrane proteins on human immunodeficiency virus type 1 after in vitro infection of H9 cells and blood mononuclear cells. An immuno-electron microscopic study.* J Gen Virol, 1993. **74**(1): p. 129-35.

121. Orentas, R.J. and J.E. Hildreth, *Association of host cell surface adhesion receptors and other membrane proteins with HIV and SIV.* AIDS Res Hum Retroviruses, 1993. **9**(11): p. 1157-65.

122. Gluschankof, P., et al., *Cell membrane vesicles are a major contaminant of gradient-enriched human immunodeficiency virus type-1 preparations.* Virology, 1997. **230**(1): p. 125-33.

123. Nguyen, D.G., et al., *Evidence that HIV budding in primary macrophages occurs through the exosome release pathway.* J Biol Chem, 2003. **278**(52): p. 52347-52354.

124. Pelchen-Matthews, A., B. Kramer, and M. Marsh, *Infectious HIV-1 assembles in late endosomes in primary macrophages.* J Cell Biol, 2003. **162**(3): p. 443-455.

125. Khurana, S., et al., *Human immunodeficiency virus type 1 and influenza virus exit via different membrane microdomains.* J Virol, 2007. **81**(22): p. 12630-40.

126. Bieniasz, P.D., *Late budding domains and host proteins in enveloped virus release.* Virology, 2006. **344**(1): p. 55-63.

127. Dussupt, V., et al., *The nucleocapsid region of HIV-1 Gag cooperates with the PTAP and LYPXnL late domains to recruit the cellular machinery necessary for viral budding.* PLoS Pathog, 2009. **5**(3): p. e1000339.

128. Popov, S., et al., *Human immunodeficiency virus type 1 Gag engages the Bro1 domain of ALIX/AIP1 through the nucleocapsid.* J Virol, 2008. **82**(3): p. 1389-98.

129. Carlson, L.A., et al., *Three-dimensional analysis of budding sites and released virus suggests a revised model for HIV-1 morphogenesis.* Cell Host Microbe, 2008. **4**(6): p. 592-9.

130. Neil, S.J., T. Zang, and P.D. Bieniasz, *Tetherin inhibits retrovirus release and is antagonized by HIV-1 Vpu.* Nature, 2008. **451**(7177): p. 425-30.

131. Arhel, N.J., et al., *HIV-1 DNA Flap formation promotes uncoating of the pre-integration complex at the nuclear pore.* Embo J, 2007. **26**(12): p. 3025-37.

132. Llewellyn, G.N., et al., *Nucleocapsid-Dependent Localization of HIV-1 Gag to Uropods in Polarized T Cells Facilitates Cell-to-Cell Transmission.* Manuscript in preparation, 2010.

CHAPTER II

Review of Microscopy-based Methods to Study Protein Complexes on the Plasma Membrane

INTRODUCTION

The study of protein complexes on the plasma membrane presents many unique challenges. In the decades since the recognition of the HIV-1 pandemic in 1981, there have been many great advances in microscopy-based techniques for studying phenomena on the plasma membrane. Many of these methods have been used, or are currently being used to study HIV-1 and other viruses. In this chapter, I will review some of these methods, particularly those currently used in the HIV-1 assembly field, and those I investigated or established in the course of this dissertation work.

FLUORESCENCE MICROSCOPY TECHNIQUES

Wide-Field and Confocal Fluorescence Microscopy

One challenge to studying plasma membrane complexes is the need to separate fluorescent signals on the plasma membrane from those originating elsewhere in the cell.

The optics of wide-field fluorescence (i.e. epifluorescence) microscopes transmit all emission light collected by the objective to the detector. Thus, wide-field images contain sharp fluorescence signals from the sample focal plane, mixed with blurred out-of-focus fluorescence signals from above and below the focal plane. For qualitative imaging, this can be advantageous: The blurring of features encodes three-dimensional information, and can be intuitively interpreted by viewers as such. However, for quantitative imaging, where fluorescence intensities ideally are proportional to the concentration of fluorescent molecules at that cellular location, such blurring represents error or imprecision in concentration measurements. One example of this problem is apparent in my study of HIV-1 Gag multimerization using a wild-field fluorescence-based assay (i.e. Fluorescence Resonance Energy Transfer) presented in Chapter III and (1). To what extent Gag begins to multimerize in the cytoplasm prior to membrane binding is currently an open question in the HIV-1 assembly field. Although I observed Gag puncta producing high FRET predominately on the plasma membrane, it is impossible to know whether moderate FRET signals that appear to be in the cytosol are authentic, or blurred FRET signals from Gag puncta above or below the focal plane (Chapter III, Figure 3.2, A) and (1). I addressed this problem using a deconvolution method (see Chapter III, and below).

There are three commonly used methods to mitigate this blurring problem: (i) acquiring images at multiple focal planes and performing a maximum intensity projection; (ii) acquiring images at multiple focal planes and performing deconvolution; and (iii) confocal fluorescence microscopy.

First, because out-of-focus fluorescence signals tend to be of lower intensity than their in-focus counterparts, maximum intensity projection will tend to preserve in-focus features while discarding out-of-focus blur. This method was used to produce the images of T cells shown in Chapter V, Figure 5.1. However, this method must be used with care: by projecting different cellular regions onto one image, cellular features that are well separated on the z-axis can artifactually appear co-localized in projection.

Second, the blurring of out-of-focus features can be mathematically represented by the convolution of non-blurred fluorescence intensities with the point-spread function. The point spread function describes how an idealized point source will become blurred as it goes out of focus, and is dependent on the optics of the microscope. There is a variety of software to perform deconvolution to de-blur the fluorescence images. As mentioned above, I used this method in Chapter III (Figure 3.2, B). However the accuracy of deconvolution is limited by uncertainties: if the point spread function and other parameters are not estimated well, deconvolution can produce more artifacts than it corrects. For example, it is possible to over-correct for optical blurring, producing images that qualitatively look sharply in-focus, but do not authentically represent the distribution of fluorescent molecules.

Finally, confocal microscopy reduces the problem of optical blurring by using a pin-hole aperture within the microscope optical path to discard fluorescence that is not in-focus. One drawback to confocal microscopy in general is that, since the pinhole aperture discards much of the total fluorescence collected by the objective, higher illumination intensities or exposure times are necessary, leading to increased photobleaching of fluorophores, and phototoxicity in live cells. Specific implementations of confocal

microscopy may also have specific drawbacks, for example laser scanning confocal acquistition can be too slow for live-cell imaging. In the studies of plasma membrane microdomains presented in Chapter IV, I used laser scanning confocal microscopy to image HIV-1 Gag on the plasma membrane, largely excluding out-of-focus cytosolic or intracellular Gag fluorescence.

Both wide-field and confocal microscopy are widely used, and form the basis for many of the assays described below.

Total Internal Reflection Fluorescence Microscopy

Another method to selectively image phenomena on or near the plasma membrane is Total Internal Reflection Fluorescence Microscopy (TIRF), developed by Daniel Axelrod at the University of Michigan (2). TIRF takes advantage of high numerical aperture oil-immersion objectives to reflect a laser beam off of the interface between the glass coverslip and the aqueous media. Although the laser light is completely reflected, it establishes an evanescent electromagnetic field that exponentially decays, penetrating only ~100 nm into cells attached to the coverslip. This evanescent field thus selectively excites fluorophores on or near the ventral surface of the plasma membrane. TIRF has been used in single-particle tracking of Gag on cellular membranes (3), demonstrating that Gag assembles on the plasma membrane, (4) and measuring the kinetics and dynamics of HIV-1 assembly (5-7).

Polarized TIRF Microscopy

A variant of TIRF, polarized TIRF (pTIRF), has been developed to measure membrane orientation in small-scale plasma membrane topological features (8). The excitation of fluorescent molecules is dependent on the orientation of their transition dipole moment (and thus the orientation of the physical molecule) relative to the polarization of the excitation light. In general-purpose fluorescence microscopy, fluorescent molecules are assumed to be in random orientations due to diffusion of small molecules, or rotational and conformational freedoms within large complexes. Thus, the effect of excitation light polarization is typically assumed to be negligible. pTIRF microscopy takes advantage of a widely-used lipophilic membrane dye, DiI, which orients in the lipid bilayer non-randomly, such that its transition dipole moment is parallel to the plane of the membrane. By switching the polarization of the reflected laser light, the evanescent excitation field in TIRF can be switched between polarization parallel or perpendicular to the coverslip. In this system, DiI-labeled membrane that is perpendicular to the coverslip will be preferentially excited by perpendicular polarization, and excitation with parallel polarization serves as a control for staining intensity and other non-orientation effects (Figure 2.1, A).

It is currently unknown to what extent HIV-1 budding though the plasma membrane is driven by Gag multimerization, versus host factors like Endosomal Sorting Complexes Required for Transport (ESCRT). Optimizing pTIRF to directly assay membrane curvature at assembling Gag multimers would be useful to identify the molecular mechanisms of HIV-1 budding. Using a mathematical model of pTIRF (9), we estimated that the membrane curvature of a budding HIV-1 virion should be detectable in

this system (Ron Holz, personal communication). However, preliminary results have been inconclusive (Figure 2.1, B).

Co-patching Assay

It was first appreciated in the 1960s that treating cells with divalent antibodies causes the clustering of cell surface antigens into microscopically visible patches. Subsequently, this was also shown using multivalent lipid-binding toxins, such as cholera toxin B subunit (10-14). In some experimental systems, this effect has been considered an unwanted artifact. For example, clustering of GPI-anchored proteins when stained with divalent antibodies after paraformaldehyde (PFA) fixation was thought to be evidence for microscopically visible lipid rafts, until it was demonstrated that antibody-induced clustering of GPI-anchored proteins can occur even after PFA fixation (14). Other more stringent fixation methods, such as glutaraldehyde, or PFA in combination with glutaraldehyde or methanol have since been shown to prevent this artifact (15). For fluorescence microscopy studies of plasma membrane complexes, these alternative fixation methods are problematic because glutaraldehyde produces high nonspecific autofluorescence, and methanol permeablizes cellular membranes allowing both intracellular and extracellular antibody staining.

The well-established co-patching method to study plasma membrane microdomains takes advantage of this antibody- or toxin-mediated patching effect (15). When two microdomain markers are independently clustered using specific antibodies or toxins, these markers can co-localize within the same patch, or “co-patch”, indicating some shared affinity. Inversely, markers independently clustered into patches can

segregate, indicating a lack of shared affinity (14, 15). Whether markers co-patch is sensitive to cellular cholesterol depletion, and largely correlates with their co-fractionation in detergent-resistant membranes, suggesting that co-patching is reflective of the markers' native sub-microscopic microdomain affinities in the absence of experimental manipulation (15). It is thought that inducing multimerization of microdomain markers by multivalent antibody or toxin binding confers cooperativity on the association between markers and the microdomains in which they reside. This cooperativity may amplify otherwise weak associations to cluster microdomains into larger patches or stabilize dynamic microdomains by limiting their dissociation. I used this co-patching method to distinguish lipid rafts and tetraspanin enriched microdomains in Chapter IV.

The major caveat of this method, however, is that antibody- or toxin-induced clustering might induce membrane heterogeneity that is not reflective of the natural microdomain partitioning of non-cross-linked markers. To address this concern, other methods to study microdomains have been used, for example, measuring FRET between microdomain markers, or observing immunogold labeling of microdomain markers by electron microscopy, which do not require antibody treatment or use more stringent fixation to prevent patching, respectively.

Bimolecular Fluorescence Complementation

To study Gag on the plasma membrane, we initially established an assay for Gag multimerization based on Bimolecular Fluorescence Complementation (BiFC). BiFC was developed by Tom Kerppola at the University of Michigan (16, 17). In the BiFC method,

fluorescent protein derivatives of *Aequorea victoria* green fluorescent protein (GFP) are genetically divided into two fragments. Each fragment is genetically fused to potentially interacting proteins of interest. When the non-fluorescent fragments of GFP are brought together by protein-protein interactions between the proteins to which they are attached, the GFP fragments can refold to reconstitute a functional fluorescent protein. This refolding is thought to be irreversible, leading to the "kinetic trapping" of low-affinity and transient interactions (17). Thus, BiFC may be more sensitive than alternative methods, such as FRET (described in Chapter III), in which the complex is free to associate and dissociate at equilibrium.

To develop this method as an assay for Gag multimerization, we genetically fused fragments of the GFP derivative mVenus to the C-terminus of Gag. Using wild-type Gag that is known to multimerize, we found that BiFC signal is dependent on temperature, as a brief incubation at 4°C markedly increased BiFC. This effect is likely because fluorescent protein fluorophore maturation is rate limiting at 37°C (18). We found that PFA fixation, which does not severely affect whole fluorescent proteins, abolishes BiFC fluorescence nearly completely. We also found that BiFC signal was strongly dependent on expression level of Gag-BiFC constructs (unpublished data).

To determine whether BiFC signal is dependent on Gag multimerization, we introduced mutations in Gag multimerization motifs (mutation WM184,185AA that disrupts dimerization by Gag CA domain, and mutation 14A1G that disrupts multimerization mediated by Gag NC domain, see Chapter III). In all cases, strong BiFC signal was observed, regardless of multimerization motif mutations (Figure 2.2). Thus, the BiFC method is not useful as an assay for Gag multimerization.

Fluorescence Resonance Energy Transfer

Fluorescence Resconance Energy Transfer (FRET) is the non-radiative transfer of energy between spectrally-matched fluorescent molecules in nanometer-scale proximity. FRET has proven to be a strong method to study Gag multimerization, in our laboratory and others (1, 5, 19-22). Chapter III of this dissertation contains a discussion and examples of FRET used to assay Gag multimerization.

ELECTRON MICROSCOPY TECHNIQUES

Scanning Electron Microscopy

In scanning electron microscopy (SEM), an image is formed by detecting secondary electrons or backscattered electrons produced as an electron beam scans over a conductive surface. For biological samples, tissues and cells typically must be fixed, dehydrated, and coated with a conductive material, such as carbon or gold. A conductive surface is necessary to prevent the buildup of static charges that severely degrade imaging. Secondary electron detection forms an image that is primarily based on surface topology. Backscattered electron detection is sensitive to the atomic number of atoms in the cell surface, and thus produces image contrast based on composition (23).

SEM has several advantages compared to light microscopy. (i) SEM produces higher-resolution images. It can resolve features on the order of tens of nanometers, compared to ~200nm with light microscopy. (ii) SEM also has a much better depth of field, typically allowing the entire surface of the cell to appear in-focus. Thus, there are

no problems with out-of-focus signals, as described for epifluorescence microscopy (see above). (iii) SEM only images the cell surface. Thus, when studying phenomena on the plasma membrane, unwanted intracellular features cannot interfere, as with fluorescence microscopy.

However, one major drawback is that cells must be fixed, dehydrated, and coated with a conductive material. Thus, SEM cannot image live cells, as with fluorescence microscopy. Furthermore, dehydration causes structural changes on the cell surface, like shrinkage and cracking, which can obscure features of interest. The resolution of cell surface features is also limited by the need to coat the cell with a conductive material, which can obscure small features. There are two common methods to coat samples: sputter coating and vacuum evaporation. Sputter coating is easier to perform, but produces thicker and more uneven coatings. In our experience, HIV-1 particles budding on the cell surface are easily detected despite dehydration and sputter coating with gold.

Backscattered Electron Detection of Immunogold

Secondary electron detection is useful to visualize cell surface features, such as budding virus particles, but cannot resolve specific molecules. To overcome this limitation, methods to detect antibodies conjugated to colloidal gold particles (immunogold) have been developed (23). Briefly, before or after fixation, cells are incubated with primary antibodies to detect molecules of interest, and then incubated with immunogold secondary antibodies. Cells are then dehydrated, coated with carbon, and imaged with backscattered electron detection. As mentioned above, backscattered electron detection is sensitive to atomic number of atoms within the cell surface. Because

cells are primarily composed of elements with low atomic number, and cells are coated with low atomic number carbon, immunogold particles produce high atomic number contrast on the cell surface. This method produces high contrast images that can resolve individual immunogold particles (Figure 2.3).

Others have used this method to detect viral glycoproteins recruited to budding HIV-1 particles on the cell surface (24, 25). We are currently investigating this method to detect microdomain markers recruited to budding particles. Importantly, antibody staining can be performed after stringent fixation with glutaraldehyde, which prevents antibody-mediated clustering of microdomain markers (see "Copatching Assay", above).

Correlative Fluorescence and Scanning Electron Microscopy

Because of the limitations inherent to both fluorescence microscopy and SEM methods, as described above, there has been a great interest in combining these methods to take advantage of the strengths of each. Many different ways of combining fluorescence and electron microscopy have been used (26), but I will focus on those used in the HIV-1 assembly field, and the establishment and optimization of the multicolor/FRET/SEM method developed in our laboratory. In 2005, another group combined fluorescence detection of HIV-1 Gag with SEM detection of HIV-1 particles on the cell surface (27). This was the first direct demonstration that fluorescent puncta formed on cells by Gag represent virus particles. However, their method was limited to measuring a single fluorescence channel. Moreover, the cell shrinkage and cracking due to dehydration for SEM made it difficult perfectly align virus particles detected by SEM with their respective fluorescent Gag puncta.

I extended their method to be able to simultaneously visualize fluorescent Gag puncta, Gag multimerization by FRET, and a cell surface microdomain marker (Figure 2.4). Briefly, cells growing on photoetched gridded coverslips and expressing Gag-YFP and Gag-CFP (see Chapter III) were incubated with fluorescent antibodies to cluster microdomain markers (see Chapter IV, and "Copatching Assay", above). Cells were also incubated with a suspension of 520 nm silica microspheres, which nonspecifically attach to the cell surface. Cells were fixed with PFA and imaged by laser scanning confocal microscopy (see above). Gag-YFP, Gag-CFP, and microdomain markers were detected by fluorescence. Based on these fluorescence images, FRET between Gag-CFP and Gag-YFP was calculated (see Chapter III). Coverslip grid numbers and silica microspheres were detected by differential interference contrast. Cells were further fixed with glutaraldehyde, dehydrated, and sputter coated with gold. Cells were then imaged by SEM secondary electron detection to identify surface topological features, such as budding virus particles. Coverslip grid numbers visible by both light microscopy and SEM allow the same cell to be identified in both imaging methods. Silica microspheres were also visible on the cell surface by both imaging methods, allowing precise alignment of fluorescence and SEM images, despite cell shrinkage.

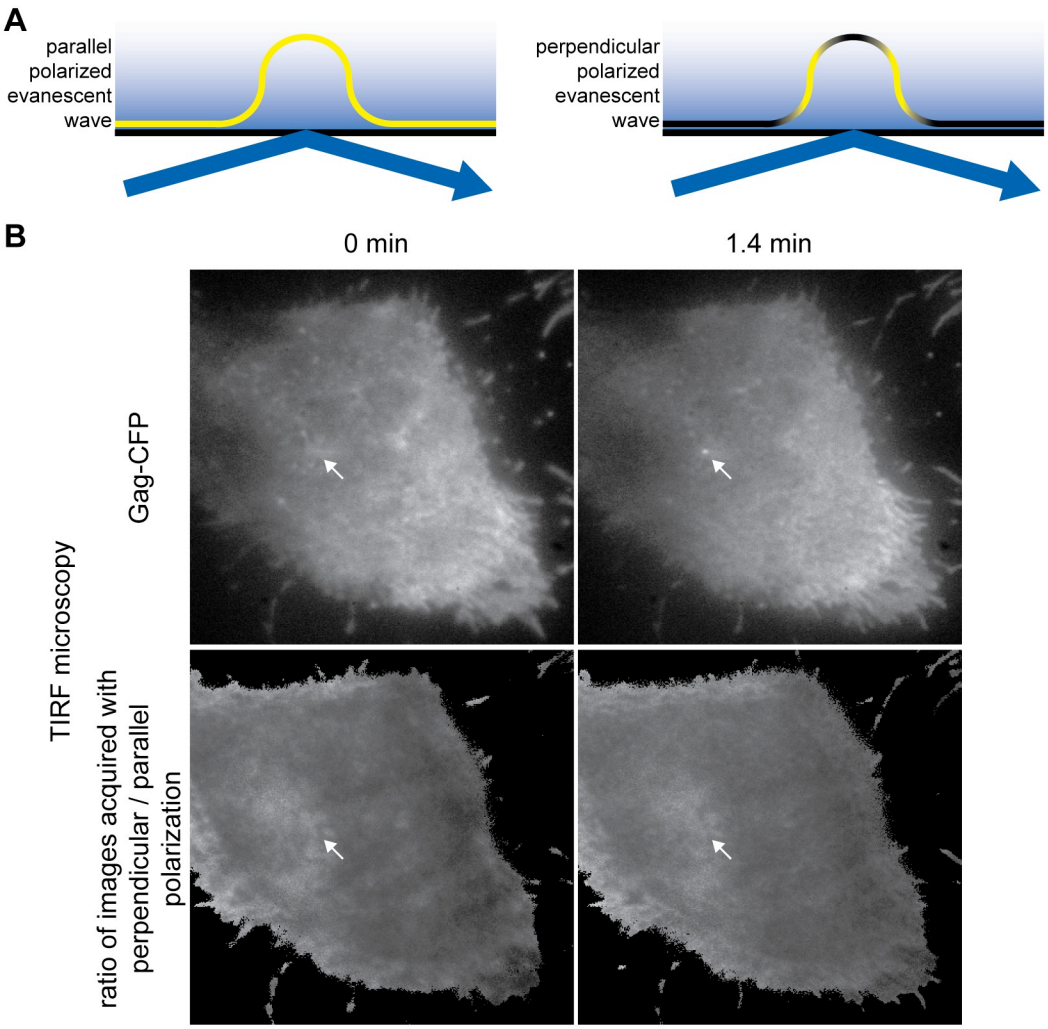

Figure 2.1. Schematic of pTIRF and example pTIRF data. **(A)** Evanescent wave (blue gradient) polarized perpendicular to the coverslip selectively excites DiI-stained membrane (yellow) that is perpendicular to the coverslip. Parallel polarized excitation excites all membrane. **(B)** TIRF microscopy reveals an increase in Gag-CFP signal (arrow) that may be assembling particles. However, no corresponding change in membrane curvature is apparent by pTIRF. Methods: HeLa cells expressing Gag-CFP were stained with DiI and imaged on a custom-built pTIRF microscope in collaboration with the Ron Holz lab, as previously described (9).

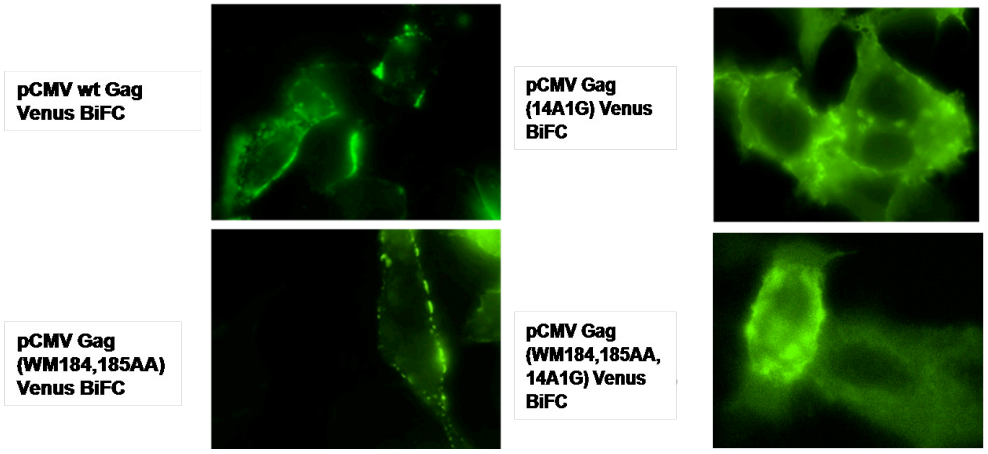

Figure 2.2. Bimolecular Fluorescence Complementation is not useful as an assay for Gag multimerization. HeLa cells were transfected with constructs expressing Gag fused to Venus fluorescent protein fragments. Derivatives containing mutations known to disrupt Gag multimerization (WM184,185AA and 14A1G) still produced strong BiFC fluorescence.

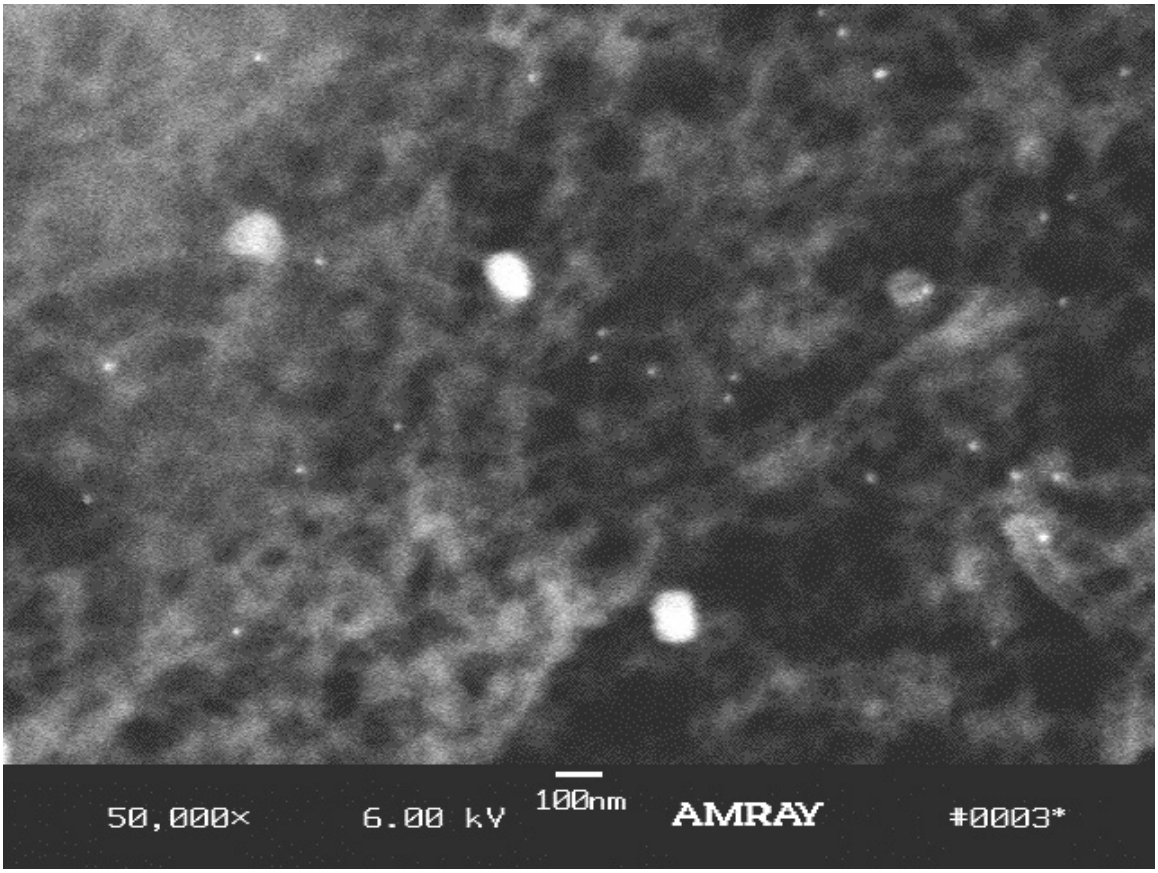

Figure 2.3. Backscattered electron detection of an immunogold-labeled lipid raft marker. Bright pin-point puncta are 12nm gold particles. Methods: HeLa cells were plated on indium-tin oxide-coated coverslips, transfected as described in Chapters III & IV to express raft marker YFP-HA-TMD, as described in Chapter IV. Cells were fixed in 4% PFA+0.2% glutaraldehyde, stained with mouse anti-GFP primary antibody and anti-mouse 12nm colloidal gold-conjugated secondary antibody, further fixed in 2% glutaraldehyde, dehydrated with EtOH and hexamethyldisilazane, coated with carbon by vacuum evaporation, and imaged on an Amray 1910FEG scanning electron microscope equipped with a Robinson BSE detector.

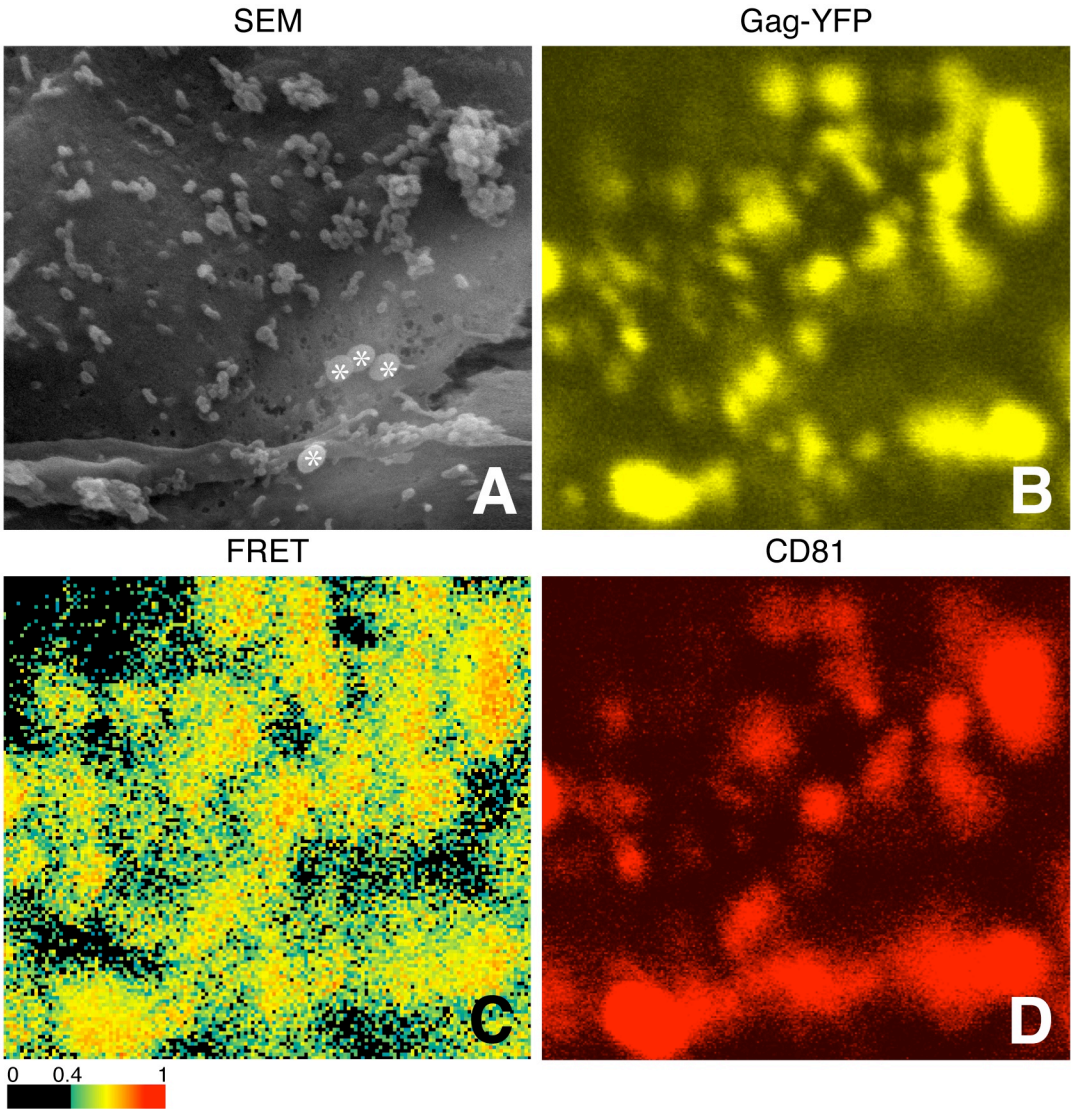

Figure 2.4. Correlative fluorescence/FRET/SEM. **(A)** Single virus particles and clusters of multiple virus particles are apparent by SEM secondary electron detection of cell surface topology. 520 nm silica microspheres that assisted in aligning SEM and fluorescence images are marked (*). **(B)** Gag-YFP **(C)** Gag multimerization measured by FRET (see Chapter III) **(D)** tetraspanin enriched microdomain marker CD81.

REFERENCES

1. Hogue, I.B., A. Hoppe, and A. Ono, *Quantitative fluorescence resonance energy transfer microscopy analysis of the human immunodeficiency virus type 1 Gag-Gag interaction: relative contributions of the CA and NC domains and membrane binding.* J Virol, 2009. **83**(14): p. 7322-36.

2. Axelrod, D., T.P. Burghardt, and N.L. Thompson, *Total internal reflection fluorescence.* Annu Rev Biophys Bioeng, 1984. **13**: p. 247-68.

3. Manley, S., et al., *High-density mapping of single-molecule trajectories with photoactivated localization microscopy.* Nat Methods, 2008. **5**(2): p. 155-7.

4. Jouvenet, N., et al., *Plasma membrane is the site of productive HIV-1 particle assembly.* PLoS Biol, 2006. **4**(12): p. e435.

5. Jouvenet, N., P.D. Bieniasz, and S.M. Simon, *Imaging the biogenesis of individual HIV-1 virions in live cells.* Nature, 2008. **454**(7201): p. 236-40.

6. Ivanchenko, S., et al., *Dynamics of HIV-1 assembly and release.* PLoS Pathog, 2009. **5**(11): p. e1000652.

7. Jouvenet, N., S.M. Simon, and P.D. Bieniasz, *Imaging the interaction of HIV-1 genomes and Gag during assembly of individual viral particles.* Proc Natl Acad Sci U S A, 2009. **106**(45): p. 19114-9.

8. Sund, S.E., J.A. Swanson, and D. Axelrod, *Cell membrane orientation visualized by polarized total internal reflection fluorescence.* Biophys J, 1999. **77**(4): p. 2266-83.

9. Anantharam, A., et al., *Localized topological changes of the plasma membrane upon exocytosis visualized by polarized TIRFM.* J Cell Biol, 2010. **188**(3): p. 415-28.

10. Cerottini, J.C. and K.T. Brunner, *Localization of mouse isoantigens on the cell surface as revealed by immunofluorescence.* Immunology, 1967. **13**(4): p. 395-403.

11. Taylor, R.B., et al., *Redistribution and pinocytosis of lymphocyte surface immunoglobulin molecules induced by anti-immunoglobulin antibody.* Nat New Biol, 1971. **233**: p. 225-9.

12. Revesz, T. and M. Greaves, *Ligand-induced redistribution of lymphocyte membrane ganglioside GM1.* Nature, 1975. **257**(5522): p. 103-6.

13. Spiegel, S., et al., *Direct visualization of redistribution and capping of fluorescent gangliosides on lymphocytes.* J Cell Biol, 1984. **99**(5): p. 1575-81.

14. Mayor, S., K.G. Rothberg, and F.R. Maxfield, *Sequestration of GPI-anchored proteins in caveolae triggered by cross-linking.* Science, 1994. **264**(5167): p. 1948-51.

15. Harder, T., et al., *Lipid domain structure of the plasma membrane revealed by patching of membrane components.* J Cell Biol, 1998. **141**(4): p. 929-42.

16. Hu, C.D., Y. Chinenov, and T.K. Kerppola, *Visualization of interactions among bZIP and Rel family proteins in living cells using bimolecular fluorescence complementation.* Mol Cell, 2002. **9**(4): p. 789-98.

17. Kerppola, T.K., *Bimolecular fluorescence complementation (BiFC) analysis as a probe of protein interactions in living cells.* Annu Rev Biophys, 2008. **37**: p. 465-87.

18. Nagai, T., et al., *A variant of yellow fluorescent protein with fast and efficient maturation for cell-biological applications.* Nat Biotechnol, 2002. **20**(1): p. 87-90.

19. Hubner, W., et al., *Sequence of human immunodeficiency virus type 1 (HIV-1) Gag localization and oligomerization monitored with live confocal imaging of a replication-competent, fluorescently tagged HIV-1.* J Virol, 2007. **81**(22): p. 12596-607.

20. Larson, D.R., et al., *Direct measurement of Gag-Gag interaction during retrovirus assembly with FRET and fluorescence correlation spectroscopy.* J Cell Biol, 2003. **162**(7): p. 1233-44.

21. Derdowski, A., L. Ding, and P. Spearman, *A novel fluorescence resonance energy transfer assay demonstrates that the human immunodeficiency virus type 1 Pr55Gag I domain mediates Gag-Gag interactions.* J Virol, 2004. **78**(3): p. 1230-42.

22. Llewellyn, G.N., et al., *Nucleocapsid-Dependent Localization of HIV-1 Gag to Uropods in Polarized T Cells Facilitates Cell-to-Cell Transmission.* Manuscript in preparation, 2010.

23. Hermann, R., P. Walther, and M. Muller, *Immunogold labeling in scanning electron microscopy.* Histochem Cell Biol, 1996. **106**(1): p. 31-9.

24. Jorgenson, R.L., V.M. Vogt, and M.C. Johnson, *Foreign glycoproteins can be actively recruited to virus assembly sites during pseudotyping.* J Virol, 2009. **83**(9): p. 4060-7.

25. Lucas, T.M., et al., *Pseudotyping incompatibility between HIV-1 and gibbon ape leukemia virus Env is modulated by Vpu.* J Virol, 2010. **84**(6): p. 2666-74.

26. Giepmans, B.N., *Bridging fluorescence microscopy and electron microscopy.* Histochem Cell Biol, 2008. **130**(2): p. 211-7.

27. Larson, D.R., et al., *Visualization of retrovirus budding with correlated light and electron microscopy.* Proc Natl Acad Sci U S A, 2005. **102**(43): p. 15453-8.

CHAPTER III

Relative Contributions of the CA and NC Domains and Membrane Binding to Gag-Gag Interaction During HIV-1 Assembly

ABSTRACT

The HIV-1 structural polyprotein $Pr55^{Gag}$ is necessary and sufficient for the assembly of virus-like particles on cellular membranes. Previous studies have demonstrated the importance of the capsid C-terminal domain (CA-CTD), nucleocapsid (NC), and membrane association in Gag-Gag interaction, but the relationships between these factors remain unclear. In this study, we systematically altered CA-CTD, NC, and the ability to bind membrane, to determine the relative contributions of, and interplay between these factors. To directly measure Gag-Gag interaction, we utilized chimeric Gag-fluorescent protein fusion constructs and a fluorescence resonance energy transfer (FRET) method. We found that the CA-CTD is essential for Gag-Gag interaction at the plasma membrane, as disruption of CA-CTD has severe impacts on FRET. Data from experiments in which wild type and CA-CTD mutant Gag molecules are coexpressed support the idea that the CA-CTD dimerization interface consists of two reciprocal interactions. Mutations in NC have less severe impacts on FRET between normally-myristoylated Gag proteins than CA-CTD mutations. Notably, when non-myristoylated Gag interacts with WT Gag, NC is

essential for FRET, despite the presence of CA-CTD. In contrast, constitutively enhanced membrane binding eliminates the need for NC to produce a WT level of FRET. These results, from cell-based experiments, suggest a model in which both membrane binding and NC-RNA interaction serve a similar scaffolding function, so that one can functionally compensate for a defect in the other.

INTRODUCTION

The HIV-1 structural precursor polyprotein $Pr55^{Gag}$ is necessary and sufficient for the assembly of virus-like particles (VLPs). Gag is composed of four major structural domains, matrix (MA), capsid (CA), nucleocapsid (NC), and p6; as well as two spacer peptides, SP1 and SP2 (1-3). Following particle assembly and release, cleavage by HIV-1 protease separates these domains. However, these domains must work together in the context of the full-length Gag polyprotein to drive particle assembly.

Previous studies have mapped two major functional domains involved in the early steps of assembly: first, Gag associates with cellular membranes via basic residues and N-terminal myristoylation of the MA domain (4-11); second, the Gag-Gag interaction domains that span the CA C-terminal domain (CA-CTD) and NC domain promote Gag multimerization (1-3, 12-25). Structural and genetic studies have identified two residues (W184 & M185) within a dimerization interface in the CA-CTD that are critical to CA-CA interaction (13, 26-28). Analytical ultracentrifugation of heterodimers formed between WT Gag and Gag mutants with changes at these residues suggests that the

dimerization interface consists of two reciprocal interactions, one of which can be disrupted to form a "half-interface" (29).

In addition to CA-CTD, NC contributes to assembly via 15 basic residues (18-21, 23, 26, 30-43), although some have suggested that NC instead contributes to stability of mature virions after assembly (44-46). It is thought that the contribution of NC to assembly is due to its ability to bind RNA, since addition of RNA promotes formation of particles *in vitro* (19, 22, 24, 47, 48), and RNase treatment disrupts Gag-Gag interaction (18) and immature viral cores (49). However, RNA is not necessary *per se*, since dimerization motifs can substitute for NC (42, 50-53). This suggests a model in which RNA serves a structural role, such as a scaffold, to promote Gag-Gag interaction through NC. Based on *in vitro* studies, it has been suggested that this RNA scaffolding interaction facilitates the low-order Gag multimerization mediated by CA-CTD dimerization (47, 51, 53-56). Despite a wealth of biochemical data, the relative contributions of the CA-CTD and NC to Gag multimerization leading to assembly are yet to be determined in cells.

Mutations in Gag interaction domains alter membrane binding, in addition to affecting Gag multimerization. In particular, mutations or truncations of CA reduce membrane binding (26, 57, 58), and others have reported that mutations or truncations of NC affect membrane binding (59-62). These findings are consistent with a myristoyl switch model of membrane binding, in which Gag can switch between high and low membrane affinity states (4, 60, 63-69). Many have proposed, and some have provided direct evidence (69), that Gag multimerization mediated by CA or NC interactions promotes exposure of the myristoyl moiety, to facilitate membrane association.

Gag membrane binding and multimerization appear to be interrelated steps of

virus assembly, since membrane binding also facilitates Gag multimerization. Unlike betaretroviruses that fully assemble prior to membrane targeting and envelopment (type B/D), lentiviruses, such as HIV, assemble only on cellular membranes at normal Gag expression levels (type C), although non-membrane bound Gag complexes exist (39, 70-73). Consistent with this, mutations that reduce Gag membrane association cause a defect in Gag multimerization (26, 74). Therefore, in addition to their primary effects on Gag-Gag interaction, mutations in Gag interaction domains cause a defect in membrane binding, which, in turn, causes a secondary multimerization defect. To determine the relative contributions of the CA-CTD and the NC domain to Gag-Gag interaction at the plasma membrane, it is essential to eliminate secondary effects due to modulation of membrane binding.

Except for studies using a His-tag-mediated membrane binding system (22, 75), biochemical studies of C-type Gag multimerization typically lack membranes. Therefore, these studies do not fully represent particle assembly, which occurs on biological membranes in cells. Furthermore, many biochemical and structural approaches are limited to isolated domains or truncated Gag constructs. Thus, some of these studies are perhaps more relevant to the behavior of protease-cleaved Gag in mature virions. With few exceptions (26, 76), cell-based studies of Gag multimerization have typically been limited to measuring how well mutant Gag is incorporated into VLPs when co-expressed with WT Gag. Since VLP production is a complex multi-step process, effects of mutations on other steps in the process can confound this indirect measure. For example, NC contributes to VLP production by both promoting multimerization and interacting with the host factor ALIX to promote VLP release (77, 78). To directly assay Gag

multimerization in cells, several groups (70, 79-81) have developed microscopy assays based on fluorescence resonance energy transfer (FRET). These assays measure the transfer of energy between donor and acceptor fluorescent molecules that are brought within ~5 nanometers by the association of the proteins to which they are attached (82-84). However, these microscopy-based Gag FRET assays have not been used to fully elucidate several fundamental aspects of HIV-1 Gag multimerization at the plasma membrane of cells, such as the relative contributions of CA-CTD and NC, and the effect of membrane binding on Gag-Gag interaction. In this study, we used a FRET method based on calibrated spectral analysis of fluorescence microscopy images (83). This algorithm measures FRET as a function of the fractions of both donor and acceptor fluorescent protein-tagged Gag molecules participating in FRET. For cells expressing Gag molecules tagged with donor (cyan fluorescent protein) and acceptor (yellow fluorescent protein) molecules, this method measures the apparent FRET efficiency, which is a function of the mole fraction of Gag constructs in complex. By measuring apparent FRET efficiencies, estimates of the mole fractions of interacting proteins can be obtained.

Using this FRET-based assay, we aim to answer two questions: 1. What are the relative contributions of CA-CTD and NC domains to Gag multimerization when secondary effects via membrane binding are held constant? 2. What is the effect of modulating membrane binding on the ability of Gag mutants to interact with WT Gag?

Our data demonstrate that the CA-CTD dimerization interface is essential for Gag multimerization at the plasma membrane, as fully disrupting the CA-CTD interaction abolishes FRET, whereas a modest level of FRET is still detected in the absence of NC.

We also present evidence that the CA-CTD dimerization interface consists of two reciprocal interactions, allowing the formation of a half-interface that can still contribute to Gag multimerization. Notably, when Gag derivatives with intact CA-CTD were coexpressed with WT Gag, either membrane binding ability or NC was required for the Gag mutants to interact with WT Gag, suggesting functional compensation between these factors.

MATERIALS and METHODS

Plasmids

The HIV-1 molecular clone pNL4-3 was described previously (85). The molecular clone encoding non-functional viral protease, pNL4-3/PR-, was described previously (86). The derivative pNL4-3/Gag-Venus, encoding Gag with a C-terminal mVenus-variant yellow fluorescent protein (YFP) fusion, was described previously (8). This construct contains extensive deletion of *pol*, and silent mutations to reduce ribosomal frameshift to the *pol* reading frame (8). This construct also does not express *vif* or *vpr* (87). The derivative pNL4-3/Gag-mCerulean, encoding Gag with a C-terminal mCerulean (88) cyan fluorescent protein (CFP) fusion, was generated by replacing mVenus of pNL4-3/Gag-Venus with mCerulean, PCR amplified from pmCerulean-N1 (obtained from S. Straight of the University of Michigan Center for Live-Cell Imaging). The plasmid pNL4-3/CA152xba220 was generated by PCR mutagenesis. The sequence coding for residues I153 through Q219 was replaced with an XbaI restriction site coding for the dipeptide SR. This mutant will be referred to as delCA-CTD for simplicity. The

derivative pNL4-3/WM184,185AA was described previously (26). The derivative pNL4-3/14A1G was generated by PCR mutagenesis. The amino acid substitutions are as previously described for the 15A NC mutant (20, 32), except residue R405 was mutated to Gly instead of Ala to preserve the ApaI restriction site, and mutagenesis was performed in a pNL4-3 genetic background. pNL4-3/delNC was a kind gift from D. Ott (44). Chimeric Gag constructs derived from pNL4-3/delNC do not contain silent mutations to reduce ribosomal frameshift to the *pol* reading frame, but do retain extensive deletion of *pol*. pNL4-3/1GA was described previously (89). The construct with the first 10 residues of Fyn kinase replacing the Gag start codon (pNL4-3/Fyn(10)fullMA/GagVenus) was described previously (8). The Gag derivatives used in FRET experiments (see Figure 3.1) were constructed from the aforementioned plasmids using standard molecular biology techniques. The mVenus expression plasmid, pmVenus-N1, was created by replacing mCerulean in pmCerulean-N1 with mVenus from pNL4-3/Gag-Venus. pFyn(10)-mVenus, which expresses mVenus with an N-terminal 10 residue Fyn kinase acylation signal, was created by PCR mutagenesis. pmCerulean-mVenus-linked was created by replacing mCitrine in pmCerulean-mCitrine (a gift from S. Straight of the University of Michigan Center for Live-Cell Imaging) with mVenus from pNL4-3/Gag-Venus. This construct expresses mCerulean and mVenus in tandem, separated by a 27 amino acid linker coded by the pmCerulean-N1 multiple cloning site.

Cells and Transfection

HeLa cells were cultured as described previously (90). For microscopy, $4.2x10^4$ cells were seeded in each well of 8-well chamber slides (Nalge Nunc, Rochester, NY),

grown for 24 hours, and transfected with Lipofectamine 2000 (Invitrogen) according to manufacturer's instructions. For VLP release assay, membrane flotation, myristoylation assay, and immunoblotting, $5.6x10^5$ cells were seeded in each well of 6-well plates (Corning), grown overnight, and transfected as above.

VLP Release Assay

Transfected HeLa cells and supernatants were harvested at 18 h post-transfection. VLPs were pelleted by ultracentrifugation from 0.45 μm-filtered cell supernatants, as previously described (91). Gag constructs in cell lysates and VLPs were detected by immunoblotting, using rabbit anti-p17 (AIDS Research and Reference Reagent Program, Division of AIDS, NIAID, NIH: Dr. Paul Spearman) and rabbit polyclonal anti-GFP (Clontech) as primary antibody and Alexa Fluor 594-conjugated anti-rabbit IgG as secondary antibody (Invitrogen). Secondary antibody fluorescence was quantified using a Typhoon Trio imager (GE Healthcare). VLP release efficiency was calculated as previously described (91).

Membrane Flotation Assay

Transfected HeLa cells were harvested at 18-20 h post-transfection. Cells were prepared for membrane flotation centrifugation as previously described (64). To measure steady-state membrane association, Gag constructs were detected by immunoblotting as described previously (92). Gag constructs were detected using rabbit polyclonal anti-GFP (Clontech), and Alexa Fluor 488-conjugated anti-rabbit IgG as secondary antibody (Invitrogen). Gag in each fraction was quantified using a Typhoon Trio imager (GE

Healthcare), and percent membrane binding was calculated by the sum of Gag in membrane fractions 1 and 2 divided by the sum total Gag in all five fractions.

Myristoylation Assay

Six hours post-transfection, HeLa cells were metabolically radiolabeled overnight with [^{3}H]myristic acid (Perkin-Elmer) as previously described (64). Chimeric Gag proteins were immunoprecipitated from cell lysates using HIV-Ig (AIDS Research and Reference Reagent Program, Division of AIDS, NIAID, NIH: NABI and NHLBI). Autoradiography was performed as previously described (64). Total Gag protein was detected by immunoblotting using rabbit polyclonal anti-GFP, as described above.

Fluorescence Microscopy

At 17 h post-transfection, the HeLa cells were rinsed once with PBS, fixed in 4% paraformaldehyde (EMS, Hatfield, PA) in PBS for 30 min, rinsed once with PBS, and mounted in Fluoromount-G (Southern Biotech) for 2D microscopy. Alternatively, for 3D microscopy, cells were incubated with anti-human CD81 (BD Pharmingen) for 15 min at 37 degrees C, without membrane permeablization to label only cell surface CD81 proteins. Cells were fixed in 4% paraformaldehyde in PBS for 30 min, and remaining paraformaldehyde was neutralized by adding 0.1 M glycine in PBS. Cells were then blocked in 3% BSA in PBS, and incubated with Alexa Fluor 594-conjugated anti-mouse IgG as secondary antibody (Invitrogen). Cells were then imaged immersed in PBS. All microscopy was performed at the University of Michigan Center for Live-Cell Imaging. 2D microscopy was performed on an Olympus IX70 inverted microscope (Olympus;

Center Valley PA), with X-Cite 120 metal halide light source (EXFO; Mississauga, ON, Canada), 100X (oil immersion; UPlan Fl, NA=1.30) objective, CFP/YFP/RFP-optimized filter set (86006-SPR, Chroma Technology Corp., Rockingham VT) mounted in a Lambda 10-3 automatic filter wheel (Sutter Instrument Co., Novato CA), CoolSNAP HQ2 14-bit CCD camera (Photometrics; Tucson AZ), controlled by Metamorph Premier v6.3 software (Molecular Devices, Downingtown PA). 3D microscopy was performed on a previously described custom-built fluorescence microscope (93). Images were collected using three filter combinations: YFP excitation/YFP emission (100 ms exposure), CFP excitation/CFP emission (200 ms exposure), and CFP excitation/YFP emission (150 ms exposure).

Image Analysis, Quantitation, and Statistics

FRET was calculated from 2D epifluorescence microscopy images using the method of Hoppe et al (83). FRET produces two changes in fluorescence signals: 1) a decrease in donor fluorescence, and 2) a proportional increase in acceptor fluorescence. The loss in donor fluorescence due to FRET can be measured by photobleaching the acceptor and recording the recovery of donor fluorescence. However, these measurements only observe the amount of donor bound by acceptor, which can be influenced by the local ratio of acceptor- and donor-tagged Gag molecules. For example, during heterotypic expression of mutant Gag-YFP and WT Gag-CFP, a minority of mutant Gag-YFP molecules is recruited into a multimer containing a majority of WT Gag-CFP, producing locally skewed ratios of molecules. Using a FRET method that measures only the degree that WT Gag-CFP is participating in FRET would produce a

low FRET efficiency simply because WT Gag-CFP is locally in excess, masking any mutant/WT interaction that may be present.

To overcome this limitation, the FRET algorithm used in this study converts the fluorescence signals from direct donor fluorescence, direct acceptor fluorescence, and acceptor fluorescence due to FRET, into measures of molecule concentration and FRET efficiency (83). Because FRET efficiency can be affected non-linearly by higher-order multimerization [e.g. multiple donors competing for multiple acceptors (94, 95)], the absolute mole fraction of molecules participating in FRET is underdetermined. Thus, FRET in this study is reported as average apparent FRET efficiency (E_{avg}), which is a function of (but not directly proportional to) the average mole fraction of fluorophores participating in FRET [$E_{avg} = (E_A + E_D)/2$ in the nomenclature of Hoppe, et al. (83)]. E_{avg} ranges from 0 – 1 and provides a measure of the strength of an interaction with reduced dependence on the relative expression of the donor and acceptor tagged molecules (96, 97).

For 3D epifluorescence microscopy, FRET was either calculated from single X,Y-planes as for 2D microscopy, or calculated using a method that reconstructs the 3D distribution of fluorescent molecules by deconvolution (93). These calculations were performed using custom FRET calculator software, implemented in MATLAB (R2008a; The Mathworks, Natick MA), and developed by the University of Michigan Center for Live-Cell Imaging (available for download at:
http://sitemaker.umich.edu/4dimagingcenter/).

To calculate FRET using this method, it is necessary to experimentally determine the constants α, β, γ, and ξ. The constants α and β describe the crosstalk of donor and

acceptor fluorophores into each other's detection channel. The constant γ is the ratio of the extinction coefficients of the two fluorophores, which is necessary to calculate the degree of acceptor fluorophore participation in FRET from the measured increase in acceptor fluorescence due to FRET. The constant ξ relates the increase in acceptor fluorescence due to FRET to the decrease in donor fluorescence due to FRET, which is necessary to calculate the degree of donor fluorophore participation in FRET (83). To experimentally determine the constants α, β, γ, and ξ, HeLa cells were transfected with pmCerulean-N1, pmVenus-N1, or pmCerulean-mVenus-linked. Cells were fixed, mounted, and images were collected as described above. Regions positive for fluorescence were manually selected surrounding approximately 40 fluorescent cells distributed over 10 microscopy fields. Constants α, β, γ, and ξ were calculated from these data as previously described (83).

After calculating FRET E_{avg} for entire microscopy fields using the FRET method described above, regions of interest were automatically selected around fluorescent puncta using the GranFilter plugin (98) in ImageJ (ver. 1.40g, NIH, Bethesda, MD; http://rsb.info.nih.gov/ij/). Plugin settings were as follows: circular structure element, 5 pixel radius, 1 pixel step size, image unmasked. With these settings, the GranFilter plugin serves as an image filter to identify regions of interest around fluorescent puncta in a consistent and reproducible manner. FRET E_{avg} values were then recorded at the regions of interest (for examples of how GranFilter selects puncta, see supplemental material, available online at: http://dx.doi.org/10.1128/JVI.02545-08). When multiple regions of interest were measured per cell, measurements were averaged on a cell-by-cell basis so that cells with more puncta identified by GranFilter are not over-represented in the

population statistics. Approximately 40-50 cells were measured for each experimental condition. Statistical significance was assessed by two-tailed Student's *t* test (Microsoft Excel).

Fluorescence images in this paper were prepared by scaling using the "auto-scale" function and converting to 8-bit pixel depth in Metamorph. FRET images were manually thresholded to mask regions where fluorescence signals were below approximately 4000 on a 0-16383 (14-bit) range, to avoid including cell-free regions where there is no fluorescence, and therefore no FRET. FRET images of E_{avg} were prepared by applying a pseudocolor map over the range of 0-1, as indicated on the figure color scale bars, and converting to 8-bit pixel depth in Metamorph. Text annotation was added in Adobe Illustrator (Adobe). Images were not otherwise altered.

RESULTS

Validation of chimeric Gag constructs

To assay Gag multimerization we created proviral molecular clones that express Gag with YFP (yellow fluorescent protein, mVenus variant) or CFP (cyan fluorescent protein, mCerulean variant) fused to its C-terminus (Figure 3.1, A). To test the relative contributions of CA-CTD and NC to Gag multimerization, we introduced deletions or point mutations (Figure 3.1, A). Mutations in CA-CTD were chosen to disrupt the dimerization interface in the C-terminal domain by deleting most of the C-terminal domain (delCA-CTD), or by altering critical residues (WM184,185AA). Mutations in NC were chosen to abolish RNA binding by deleting most of NC (delNC), or by replacing

fifteen basic residues with neutral residues (14A1G).

Previously, others have observed that C-terminal fluorescent protein fusions to HIV-1 Gag interfere with budding of particles (99). To characterize the performance of our chimeric constructs, we performed a VLP release assay, comparing a construct expressing non-chimeric WT Gag to our chimeric constructs expressing Gag-YFP. We found that Gag-YFP is not defective in VLP release relative to non-chimeric Gag. However, Gag-YFP constructs with mutations in CA-CTD or NC were completely defective in VLP release (Figure 3.1, B). To confirm that our chimeric Gag species are full-length, we probed parallel immunoblots with anti-p17 and anti-GFP antibodies, which recognize N- and C-termini, respectively (Figure 3.1, B). Based on the band intensity of proteins recognized by anti-GFP, greater than 97% of YFP-tagged proteins retain full-length Gag sequence.

FRET assay for Gag multimerization

When we co-expressed Gag-CFP and Gag-YFP, we detected robust FRET (Figure 3.2, A, third row, and Figure 3, B). In contrast, FRET was absent when Gag-CFP was co-expressed with cytosolic YFP (Figure 3.2, A, first row, and Figure 3.5, B). Moreover, FRET was also absent when Gag-CFP was co-expressed with membrane-targeted Fyn(10)-YFP (Figure 3.2, A, second row, and Figure 3.3, B). Therefore, our FRET method detected the specific interaction between Gag molecules, consistent with previous work (70, 79, 80, 100). The FRET values reported by our assay are a function of the mole fraction of fluorescent proteins participating in FRET (83). Thus, the contributions of Gag interaction domains can be assessed quantitatively. Throughout these studies, all

cells imaged expressed approximately equal levels of CFP- and YFP-tagged fluorescent proteins.

Consistent with previous FRET microscopy studies of Gag, the highest levels of FRET detected by our method appeared primarily associated with puncta on the plasma membrane (Figure 3.2, A, third row). However, moderate FRET appeared diffuse throughout the cell. To more precisely localize Gag FRET within the 3D cell volume, we performed 3D epifluorescence microscopy of cells expressing Gag-CFP/YFP, and immunostained without membrane permeablization to detect plasma membrane CD81, a tetraspanin protein that co-localizes with Gag (101-103). In all cases, Gag-CFP/YFP puncta appeared on the cell surface, and co-localized with CD81 immunofluorescence (Figure 3.2, B). To determine whether diffuse FRET throughout the cells is indicative of authentic intracellular/cytosolic Gag-Gag interaction, or is a result of out-of-focus light spilling over from Gag puncta on other focal planes, we calculated FRET from 3D microscopy with or without deconvolution. Without deconvolution, FRET was calculated from single X,Y-planes independently (identically to the 2D microscopy performed in Figure 3.2, A and throughout). As in Figure 3.2, A, third row, moderate FRET appeared diffuse throughout the cell (Figure 3.2, B). However, when deconvolution is used to remove the blurred out-of-focus light from other focal planes, the FRET signals outside Gag-CFP/YFP puncta and in the cell interior are largely removed (Figure 3.2, B). Therefore, the moderate FRET values outside of plasma membrane puncta with 2D FRET microscopy are likely predominately FRET signals from other focal planes, inclusion of which is inherent to epifluorescence microscopy. Throughout this study,

when FRET is quantified over multiple cells, only FRET values present at Gag puncta are included (see Methods).

To examine the effects of CA-CTD and NC mutations on Gag multimerization by FRET, we co-transfected HIV-1 molecular clones expressing CFP- and YFP-tagged, WT or mutant Gag. To fully examine the phenotype of these constructs, we tested both homotypic Gag interaction (i.e. both CFP- and YFP-tagged Gag molecules contain an identical change in CA-CTD or NC) and heterotypic interaction between WT Gag-CFP and mutant Gag-YFP (i.e. CFP-tagged Gag molecules are wild type, and YFP-tagged Gag molecules are mutant).

CA-CTD can form a "half-interface" which is only partially defective, but fully disrupting the CA-CTD dimerization interface abolishes FRET

We detected no FRET due to homotypic interactions between WM184,185AA Gag constructs or between delCA-CTD Gag constructs (not significantly different from Fyn(10)-YFP negative control $p>0.01$; Figure 3.3, A, second and fourth rows, and B), indicating that these mutations abolished close Gag-Gag interaction. Likewise, we detected no FRET due to heterotypic interactions between WT Gag-CFP and delCA-CTD Gag-YFP molecules (not significantly different from Fyn(10)-YFP negative control $p>0.01$; Figure 3.3, A, third row, and B). In these cases, the CA-CTD mutant constructs were primarily diffuse in the cytosol, suggesting that reduced membrane binding could contribute to the lack of FRET. However, some membrane lining and puncta were observed during homotypic WM184,185AA Gag-CFP/YFP expression (Figure 3.3, A, second row, arrows), yet these structures lacked significant FRET (Figure 3.3, B). We

tested whether reduced membrane binding contributes to lack of FRET below by introducing mutations that directly alter membrane association.

In contrast to the above experimental conditions that produced no significant Gag-Gag interaction, heterotypic interaction between WM184,185AA Gag-YFP and WT Gag-CFP produced moderately high FRET, approximately 86% of that produced by homotypic WT Gag-CFP/YFP interaction (Figure 3.3, A, first row, and B). As described below, this moderately high FRET phenotype is also apparent when WT Gag-CFP was co-expressed with WM184,185AA Gag-YFP containing additional mutations (1GA and Fyn[10]) that directly alter membrane association. As detailed in the discussion, these data suggest that the CA-CTD dimerization interface consists of two reciprocal interactions, and that disruption of one interaction still allows the formation of a half-interface.

NC mutant is only partially defective in the context of native myristoylation

As described above, fully disrupting the CA-CTD dimerization interface produced no FRET above negative control background. In contrast, all experimental conditions in which NC mutants were tested produced intermediate FRET values (greater than negative control $p<0.01$; Figure 3.3). For both the 14A1G basic residue mutant and the NC deletion mutant, heterotypic interaction between WT Gag-CFP and NC mutant Gag-YFP was greater than homotypic interactions between mutants ($p<0.01$). Homotypic interactions were indistinguishable between 14A1G Gag-CFP/YFP and delNC Gag-CFP/YFP ($p>0.01$). Altogether, these results suggest that, in contrast to CA-CTD, NC is not essential for Gag-Gag interaction as detected by FRET.

Mutations in both CA-CTD and NC reduce steady-state Gag membrane binding

It is possible that the mutant phenotypes observed in our FRET assay are not due to a primary effect of mutations on Gag-Gag interaction, but rather are due to a secondary effect via membrane binding. This stems from the previous findings that mutations that disrupt Gag multimerization also reduce Gag membrane binding, and conversely, membrane binding affects Gag multimerization (see Introduction).

Previous studies showed that the WM184,185AA mutation reduces Gag membrane binding, whereas changes in the NC basic residues do not (26). However, these experiments examined the initial rate of membrane association of newly synthesized Gag, but not the steady-state membrane binding levels that are more relevant to the interpretation of FRET microscopy data. To examine the effect of CA-CTD and NC mutations on steady-state membrane binding of Gag-YFP, we performed a membrane flotation assay and quantified the amount of membrane-associated Gag-YFP by immunoblotting. We found that more than half of WT Gag-YFP was membrane associated, whereas CA-CTD and NC mutations reduced membrane binding (Figure 3.4, A). Both CA-CTD mutations (delCA-CTD and WM184,185AA) and mutations in the basic residues of NC (14A1G) reduced membrane binding severely, whereas NC deletion (delNC) had a less severe effect. This membrane binding defect in mutant Gag derivatives is not due to a defect in myristoylation (Figure 3.4, B). Because these mutations alter membrane association to different degrees, to accurately assess the effect of these mutations on Gag-Gag interaction, it is necessary to control for this effect on membrane binding.

In the absence of myristoylation, both CA-CTD and NC mutations cause complete loss of interaction with WT Gag molecules

To control the effect of CA-CTD and NC mutations on membrane binding, and to determine how membrane binding modulates Gag multimerization, we impaired membrane binding by introducing a mutation that abolishes N-terminal myristoylation of Gag (1GA). We detected no homotypic interaction between 1GA Gag-CFP/YFP constructs, at either the plasma membrane or in the cytosol (Figure 3.4, C), in agreement with previous studies (74). In other experimental systems, Gag multimerization has been detected in the absence of membrane binding (19, 72, 104). In this experimental system, in which Gag is expressed from a proviral molecular clone, myristoylation is required for Gag-Gag interaction as detected by FRET.

However, it has been demonstrated that normally myristoylated Gag can interact with non-myristoylated Gag and rescue it into virus particles (18, 92, 105-107), and this interaction can be detected by FRET (74). We took advantage of this observation to examine the role of the NC and CA-CTD interactions by co-expressing non-myristoylated mutant Gag-YFP constructs with normally myristoylated WT Gag-CFP. In this system, interactions driven by the CA-CTD and NC domains can produce FRET, yet the secondary effects of CA-CTD and NC mutations via membrane binding are controlled because membrane binding is severely disrupted in the mutant constructs.

We detected FRET between WT Gag-CFP and 1GA Gag-YFP, associated with WT Gag-CFP plasma membrane puncta (statistically significantly greater than YFP negative control $p<0.01$; Figure 3.5, A, first row, and B). Consistent with the results in

Figure 3.3 that suggest a CA-CTD "half-interface", co-expression of WT Gag-CFP and 1GA/WM184,185AA Gag-YFP is only partially defective relative to WT Gag-CFP / 1GA Gag-YFP (significantly greater than YFP negative control $p<0.01$; Figure 3.5, A, second row, and B). Also consistent with the normally myristoylated constructs in Figure 3.3, we detected no FRET when the CA-CTD dimerization interface was fully abolished (WT Gag-CFP and 1GA/delCA-CTD Gag-YFP; not significantly different from YFP negative control $p>0.01$; Figure 3.5, A, third row, and B). Notably, in contrast to results in Figure 3.3, we detected no FRET when NC was disrupted, despite the presence of an intact CA-CTD (WT Gag-CFP and either 1GA/14A1G or 1GA/delNC Gag-YFP; not significantly different from YFP negative control $p>0.01$; Figure 3.5, A, fourth and fifth rows, and B). Thus, without myristoylation, NC function is necessary for Gag-Gag interaction detected by FRET. Together with the data shown in Figure 3.3, these results indicate that the CA-CTD dimerization interface alone is not sufficient - either myristoylation or NC is required for mutant Gag derivatives to interact with WT Gag.

Constitutive and enhanced membrane binding can rescue interaction of NC mutant, but not CA-CTD mutant, with WT Gag

As an alternative way of controlling the effect of CA-CTD and NC mutations on membrane binding, and additionally to determine the effect of membrane binding on the ability of Gag mutants to multimerize, we next examined constitutively membrane binding Gag derivatives. Membrane binding was enhanced by a ten-residue exogenous triple-acylation signal derived from Fyn kinase [Fyn(10)] at their N-terminus. This modification has been shown to confer cholesterol independence (108) and

phosphotidylinositol-(4,5)-bisphosphate independence (8) on Gag membrane binding. We performed a membrane flotation assay on these constructs to ensure that CA-CTD and NC mutations do not have an effect on membrane binding in the context of Fyn(10). We found that the Fyn(10) triple-acylation signal causes ~75% membrane binding in all constructs, regardless of CA-CTD or NC disruption (Figure 3.4, A). Thus, membrane binding in the context of Fyn(10) is likely unaltered by the multimerization ability of these derivatives.

When we co-expressed Fyn(10)-modified CA-CTD or NC mutant Gag-YFP with WT Gag-CFP (Figure 3.6), FRET results were mostly in agreement with those of normally myristoylated constructs (Figure 3.3). We detected strong interaction between WT Gag-CFP and Fyn(10) Gag-YFP (Figure 3.6, A, first row, and B). Consistent with formation of a "half-interface", we detected moderately high FRET between WT Gag-CFP and Fyn(10)/WM184,185AA Gag-YFP (significantly greater than Fyn(10)-YFP negative control $p<0.01$; Figure 3.6, A, second row, and B). However, we detected no FRET between WT Gag-CFP and Fyn(10)/delCA-CTD Gag-YFP (not significantly different from Fyn(10)-YFP negative control $p>0.01$; Figure 3.6, A, third row, and B). Though not directly comparable to the data from co-expression with WT Gag-CFP above, we also tested homotypic interactions between Fyn(10)/WM184,185AA Gag-CFP/YFP or Fyn(10)/delCA-CTD Gag-CFP/YFP. We found no significant difference ($p>0.01$; data not shown), which is consistent with a half-interface model in that homotypic expression of WM184,185AA mutants should be as defective as the delCA-CTD deletion mutant. Since CA-CTD mutant phenotypes were relatively unchanged by the addition of the Fyn(10) sequence, these results indicate that the Gag multimerization

defect seen in CA-CTD mutants is a direct consequence of defective Gag-Gag interaction, and not due to a secondary effect via membrane binding.

However, in contrast to results from normally myristoylated NC mutant constructs, we find near-WT levels of FRET between WT Gag-CFP and either Fyn(10)/14A1G or Fyn(10)/delNC Gag-YFP (not significantly different from WT Gag-CFP/Fyn(10) Gag-YFP $p>0.01$; Figure 3.6, A, fourth and fifth rows, and B). These data demonstrate that constitutive or enhanced membrane binding can rescue NC mutant interaction with WT Gag-CFP multimers, suggesting functional compensation between membrane binding and NC function.

DISCUSSION

Previous studies have demonstrated the importance of the CA-CTD, NC, and membrane association during HIV-1 assembly. In particular, Li, et al, measured the multimerization of Gag derivatives by analyzing total FRET in bulk cell suspensions. Their study demonstrated that protein-protein interactions mediated by CA and NC-RNA interactions are important, and that N-terminal myristoylation is necessary for Gag multimerization in cells (74), which our data confirmed. However, the relative contributions of, and interplay between CA, NC, and membrane binding during Gag assembly in cells have not been determined in previous studies. In this current study, we have addressed these points by systematically altering the CA-CTD, NC, and the ability to bind membrane, and comparing the resulting Gag derivatives in a microscopy-based FRET assay.

Overall, we found that the CA-CTD is more important for close Gag-Gag interaction than NC, as Gag with a CA-CTD deletion mutation was fully defective in all cases, whereas NC mutants were only partially defective in multimerization. In addition, our data is consistent with a model in which the CA-CTD dimerization interface consists of two reciprocal interactions, allowing the formation of a half-interface. Finally, we found that NC mutation phenotypes are affected by membrane binding, revealing functional compensation between NC function and Gag association with membrane.

To fully test the multimerization phenotypes of Gag CA-CTD and NC mutants, we compared homotypic expression (i.e. FRET measured between constructs which both contain identical mutations) with heterotypic expression (i.e. FRET measured between WT and mutant constructs), in the context of normally myristoylated Gag (Figure 3.3). The CA-CTD dimerization interface point mutant, WM184,185AA, and both NC deletion and amino acid substitution mutants showed significantly greater heterotypic interaction than homotypic interaction. This higher FRET due to heterotypic interaction is likely due to several causes:

First, FRET due to heterotypic interaction could be a more sensitive measure of Gag-Gag affinity, since weak interactions might be sufficient to recruit mutant Gag molecules into a multimer of WT Gag, but not sufficient for mutants to form multimers alone. By this rationale, the lack of difference between delCA-CTD homotypic and heterotypic interaction – both are completely defective - supports the importance of CA-CTD and relative unimportance of NC in Gag multimerization. Alternatively, higher heterotypic interaction could indicate that WT molecules can provide *in trans* a function that the mutant construct lacks, either to individual molecules or to the Gag multimer as a

whole, such as the ability to bind membrane. In light of our finding that NC mutation phenotypes are affected by membrane binding, this is a likely explanation of the higher heterotypic interaction seen with NC mutants. This possibility is more directly addressed by the experiments in which we alter membrane binding of mutant constructs *in cis*, as discussed below. Finally, in the case of the CA-CTD dimerization interface mutant WM184,185AA, the great difference between homotypic (WM184,185AA Gag-CFP/YFP) and heterotypic (WM184,185AA Gag-YFP co-expressed with WT Gag-CFP) interaction could indicate that the CA-CTD dimerization interface is actually composed of two reciprocal interactions, one of which can be abolished to form a "half-interface". The possibility of a half-interface can be inferred from structural studies of isolated CA domain fragments: the CA appears to dimerize by the burial and hydrophobic packing of critical residues W184 and M185 of one CA-CTD fragment into a mostly hydrophobic pocket on the second CA-CTD fragment (109), and *vice versa*. During heterodimerization of WT and WM184,185AA mutant molecules, the WT molecule can interact with the mutant, but the mutant cannot perform the reciprocal interaction, leading to a partial interface. Others have presented *in vitro* evidence for the existence of a CA-CTD "half-interface" using non-myristoylated, truncated Gag derivatives (29). Our data provide evidence of the same phenomenon using full-length Gag derivatives in a cell-based assay, and support the possibility that the Gag-Gag interface mediated by CA-CTD is the same or similar to the interface previously observed between isolated, mature CA proteins.

As described in the introduction, Gag membrane binding and multimerization are interrelated phenomena. An important caveat to the interpretation of CA-CTD and NC

mutant phenotypes is that multimerization defects imposed by these mutations affect Gag membrane association (Figure 3.4, A), which could, in turn, have a secondary effect on Gag multimerization. Therefore, we genetically separated the *primary* effect of mutations (i.e. the effect on protein-protein or protein-RNA scaffolding interactions) from the *secondary* effect on multimerization via membrane binding by altering the N-terminal acylation of Gag. Comparing CA-CTD mutation constructs to their WT counterparts in each membrane binding condition, we found the relative phenotypes of CA-CTD mutants to be consistent regardless of membrane binding changes. Therefore, we conclude that the CA-CTD mutations directly affect Gag-Gag interaction, rather than via a secondary effect on membrane binding. Comparing NC mutation constructs to their WT counterparts in each membrane binding condition reveals discordant results: The defect in interaction between NC mutant and WT Gag is exacerbated by abolished membrane binding, but rescued to WT levels by constitutive and enhanced membrane binding.

Previous biochemical studies have given rise to a model in which RNA serves as a scaffold for a growing Gag multimer (18, 19, 22, 24, 47-49). It has also been postulated that cellular membranes, particularly membrane microdomains, could serve as platforms for Gag multimerization (110). Our results provide evidence, using full-length Gag constructs in the biologically relevant milieu of the cell, to link these two models: the ability to bind at least one of either membrane or RNA is required for a Gag derivative with an intact CA-CTD to be rescued into multimers of WT Gag. Furthermore, our observation of functional compensation between membrane binding and NC function suggests that the two play complementary mechanistic roles, such as a scaffold, during Gag multimerization.

Figure 3.1. Gag derivatives, expression, and VLP release. **(A)** Gag derivatives used in this study. HIV-1 molecular clones that express chimeric Gag-fluorescent protein fusions (WT Gag-CFP/YFP) were generated. Deletions or amino acid substitutions were created in the capsid (CA) domain (delCA-CTD and WM184,185AA, respectively), and the nucleocapsid (NC) domain (delNC and 14A1G, respectively). This panel of mutants was additionally altered to reduce membrane binding by abolishing N-terminal myristoylation (1GA), or enhance membrane binding by adding a triple-acylation signal [Fyn(10)]. Sites of N-terminal myristoylation (myr) and palmitoylation (palm) are indicated. **(B)** Expression and virus-like particle (VLP) release. VLP release of chimeric Gag-YFP and mutant constructs was compared to that of non-chimeric Gag. Immunoblots were probed to detect the matrix domain of Gag (αMA) or the YFP tag (αGFP) to ensure that chimeric Gag proteins are full-length. Data are representative of four independent experiments.

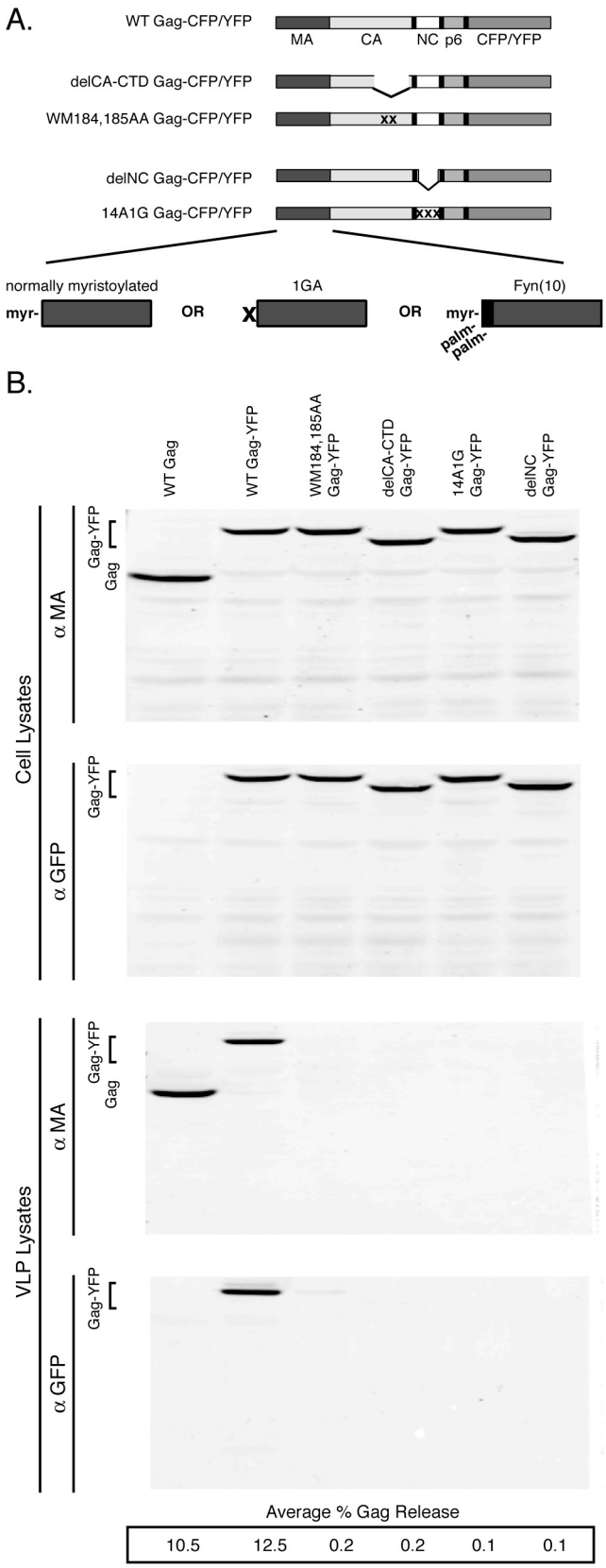

Figure 3.1. Gag derivatives, expression, and VLP release.

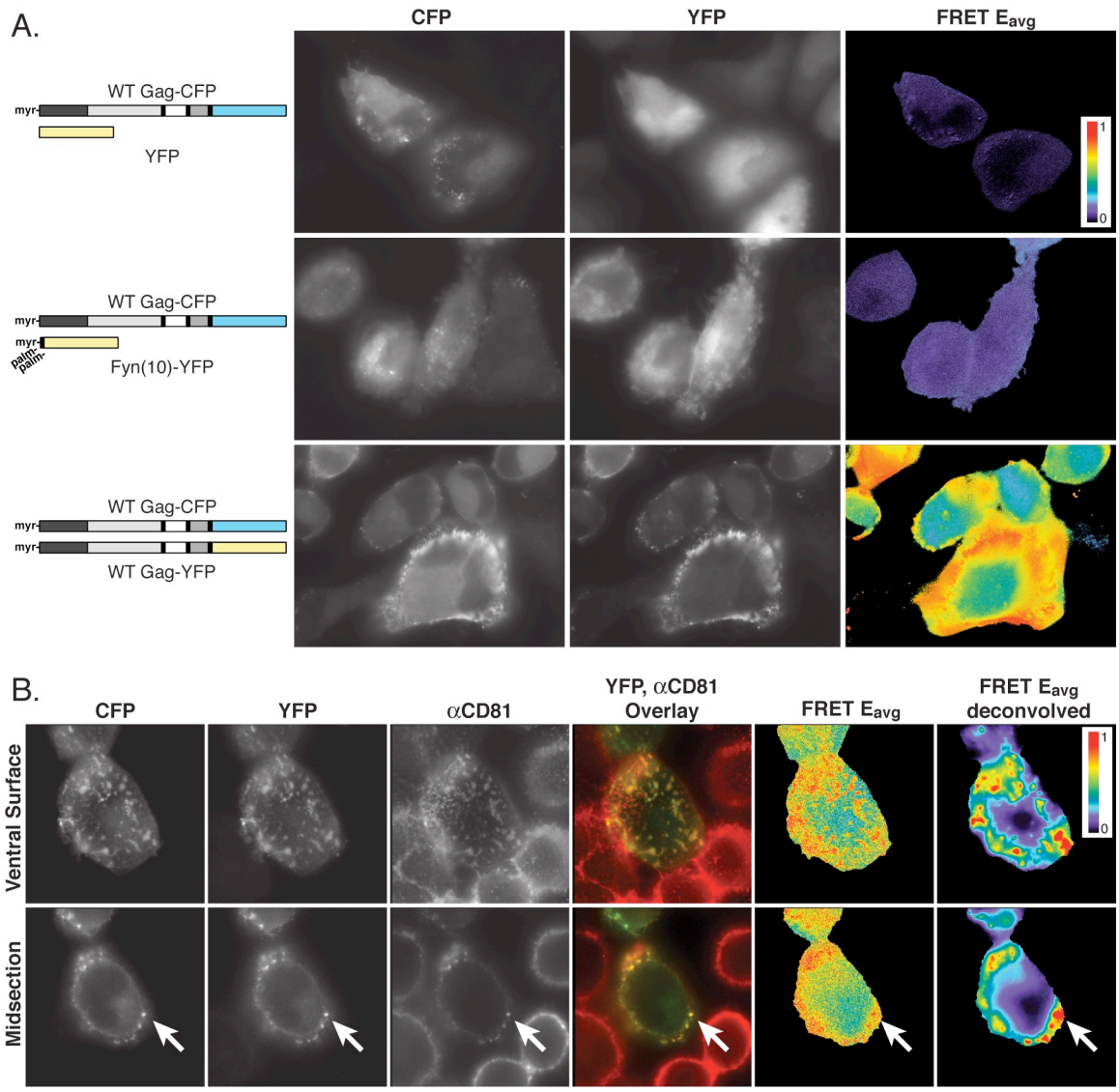

Figure 3.2. FRET microscopy of control constructs **(A)** Negative control constructs, YFP (not fused to Gag or any other membrane-association signal) and Fyn(10)-YFP (fused to a triple-acylation signal), were co-expressed with WT Gag-CFP. Note that Fyn(10)-YFP fluorescence intensity appears uneven or punctate, which is likely due to presence of membrane ruffles and blebs. As a positive control, WT Gag-CFP/YFP were co-expressed. Images of FRET E_{avg} were calculated from images taken with three filter combinations: CFP excitation/CFP emission (CFP), YFP excitation/YFP emission (YFP), and CFP excitation/YFP emission (not shown). FRET E_{avg} values are color-coded according to the scale bar on the top panel. **(B)** Gag FRET is predominately associated with plasma membrane puncta. WT Gag-CFP/YFP were co-expressed, and cells were immunostained without membrane permeablization to detect cell-surface CD81. Images of WT Gag-YFP (green) and anti-CD81 (red) were overlaid to illustrate co-localization (yellow). Images of FRET E_{avg} were calculated as above, or with deconvolution of 3D image to reduce the contribution of out-of-focus light from other focal planes.

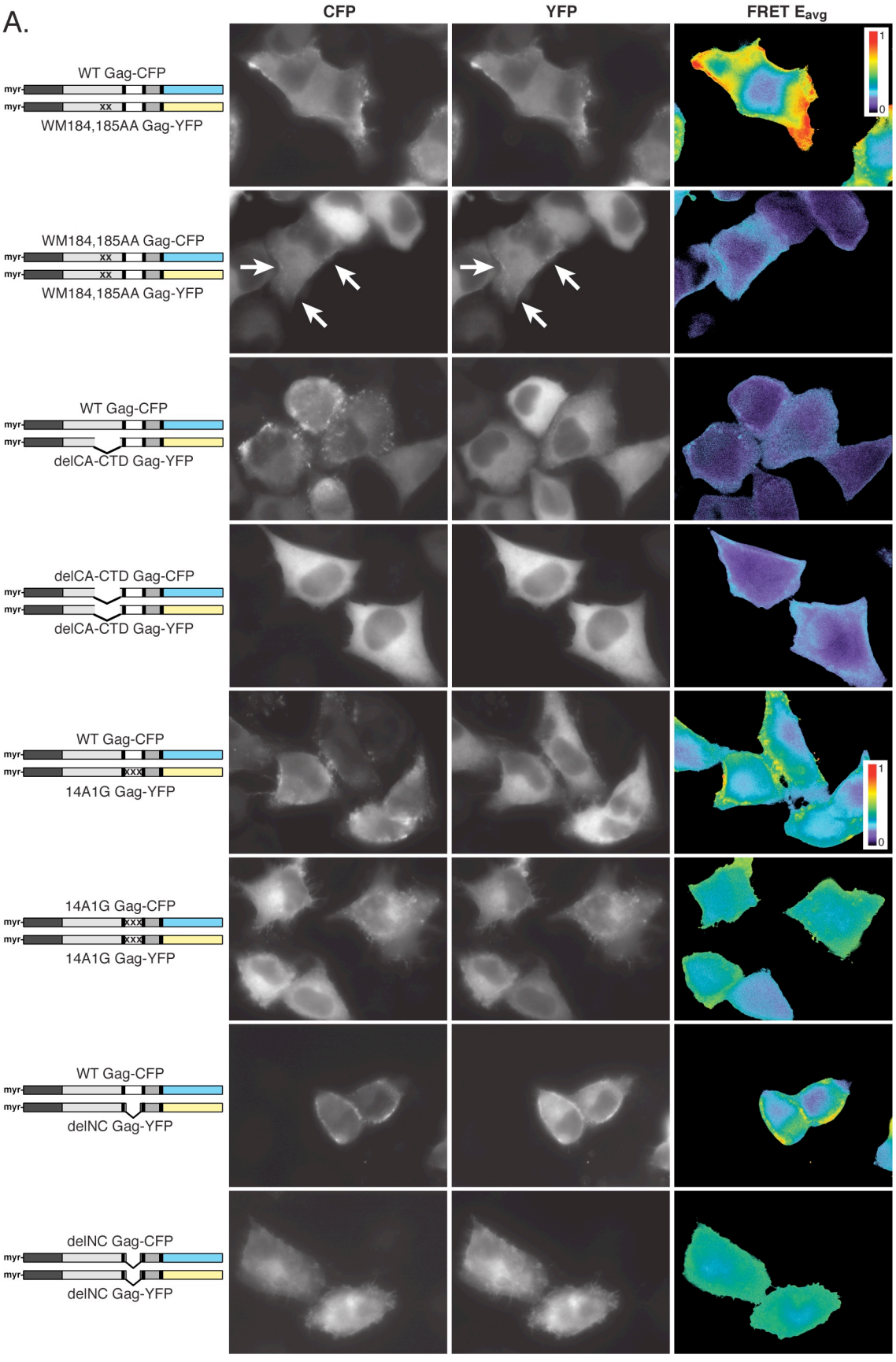
A.
CFP
YFP
FRET Eavg
1
0
WT Gag-CFP
myr-
myr-
xx
WM184,185AA Gag-YFP
WM184,185AA Gag-CFP
WM184,185AA Gag-YFP
WT Gag-CFP
delCA-CTD Gag-YFP
delCA-CTD Gag-CFP
delCA-CTD Gag-YFP
WT Gag-CFP
xxx
14A1G Gag-YFP
14A1G Gag-CFP
14A1G Gag-YFP
WT Gag-CFP
delNC Gag-YFP
delNC Gag-CFP
delNC Gag-YFP

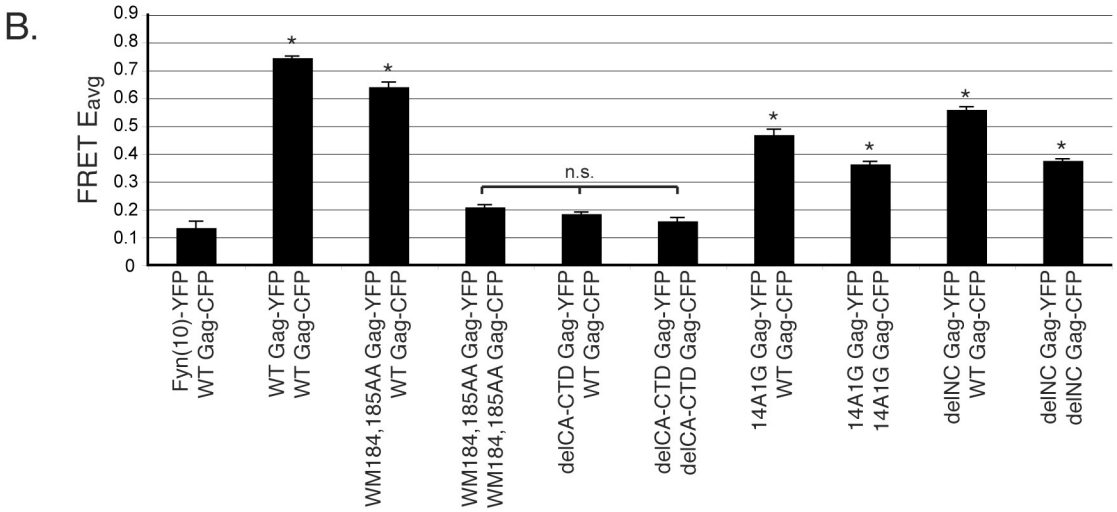

Figure 3.3. FRET microscopy of mutant Gag constructs **(A)** Gag-CFP/YFP constructs containing CA mutations (WM184,185AA or delCA-CTD) or NC mutations (14A1G or delNC) were co-expressed homotypically (i.e. both Gag-CFP and Gag-YFP constructs contain the same mutation), or heterotypically (i.e. the Gag-YFP construct contains a mutation but the Gag-CFP construct does not). Images of FRET E_{avg} were calculated from images taken with three filter combinations: CFP excitation/CFP emission (CFP), YFP excitation/YFP emission (YFP), and CFP excitation/YFP emission (not shown). FRET E_{avg} values are color-coded according to the scale bar on the top panel. In the case of WM184,185AA Gag-CFP/YFP homotypic expression, plasma membrane puncta are indicated (arrows). **(B)** E_{avg} in fluorescent puncta were quantified over approximately 50 cells. Similar results were obtained in >4 independent experiments. ∗ = significantly greater than Fyn(10)-YFP negative control, $p<0.01$. n.s. = no statistical difference, $p>0.01$. Error bars represent standard error of the mean.

Figure 3.4. Gag membrane binding **(A)** Membrane binding analysis of Gag derivatives. Fluorescent protein constructs (YFP and Fyn[10]-YFP) or chimeric Gag constructs (see Figure 3.1A) were expressed in HeLa cells and then subjected to membrane flotation centrifugation, divided into five equal-volume fractions, and detected by immunoblotting with HIV-Ig. The left two fractions include membrane-associated material (M) whereas the right two fractions include non-membrane associated material (NM). The percentage of membrane binding was calculated by the ratio of membrane-associated signal to total signal. Data are representative of three independent experiments in the case of normally myristoylated constructs, and two independent experiments in the case of Fyn(10) constructs. **(B)** Gag derivatives are myristoylated. Cells expressing chimeric Gag constructs were metabolically labeled with [^{3}H]myristic acid, and analyzed by autoradiography to detected myrisotylated Gag (top panel), or immunoblotting with anti-GFP antibody to detect total Gag-YFP proteins (bottom panel). **(C)** Myristoylation of Gag is necessary to detect FRET. Myristoylation-defective (1GA) Gag-CFP/YFP constructs were co-expressed. The image containing FRET E_{avg} values was calculated as in Figure 3.2. FRET E_{avg} values are color-coded according to the scale bar. Average FRET values were quantified over 10 cells, and compared with negative control and WT Gag-CFP/YFP conditions from Figure 3.2 (bar graph). $*$ = significantly greater than YFP negative control, $p<0.01$. n.s. = not significantly different from YFP negative control, $p>0.05$. Error bars represent standard error of the mean.

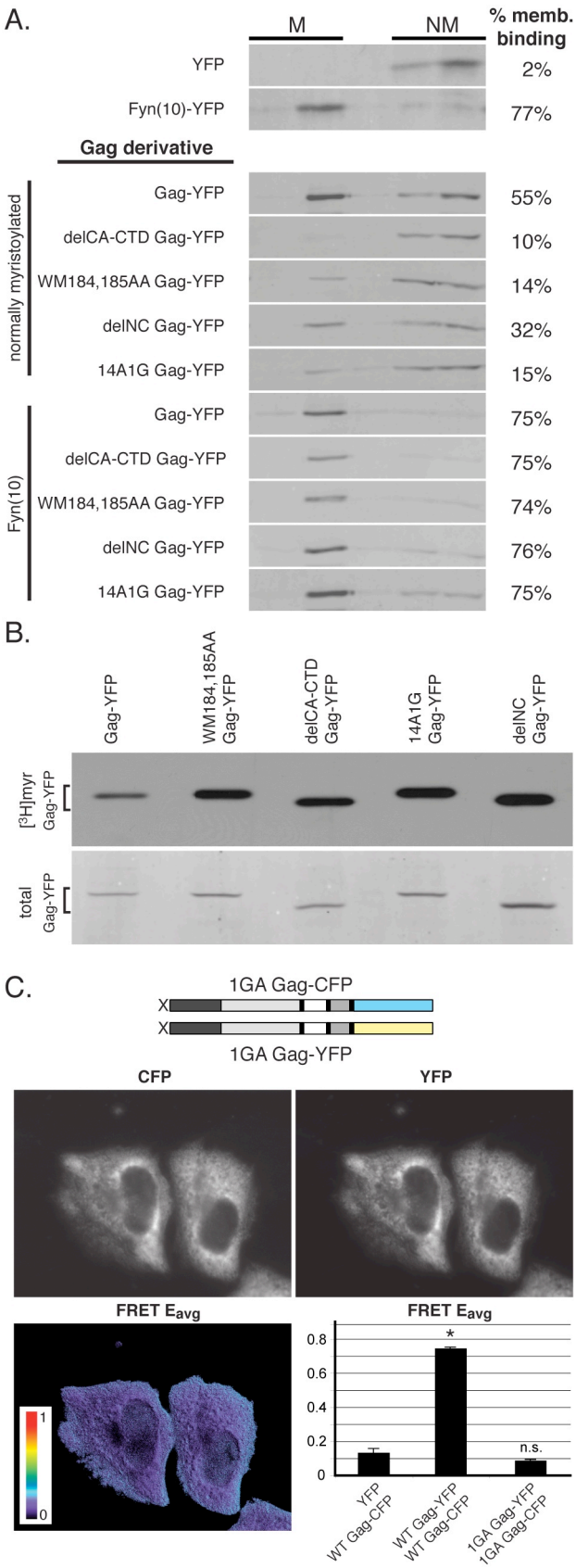

Figure 3.4. Gag membrane binding.

Figure 3.5. FRET microscopy of N-terminal myristoylation-deficient constructs **(A)** Myristoylation-defective (1GA) Gag-YFP constructs containing CA mutations (WM184,185AA or delCA-CTD) or NC mutations (14A1G or delNC) were co-expressed with WT Gag-CFP. Images of FRET E_{avg} were calculated as in Figure 3.2. FRET E_{avg} values are color-coded according to the scale bar on the top panel. Puncta with higher FRET efficiencies are indicated (arrows). **(B)** E_{avg} in fluorescent puncta were quantified over approximately 50 cells, and are representative of 3 independent experiments. Note that the impacts of CA mutations on 1GA Gag-YFP interacting with WT Gag-CFP are similar to those on Gag-YFP interacting with WT Gag-CFP (Figure 3.3); however, NC mutant Gag constructs are completely defective, unlike their normally myristoylated counterparts (Figure 3.3). $*$ = significantly greater than YFP negative control, $p<0.01$. Error bars represent standard error of the mean.

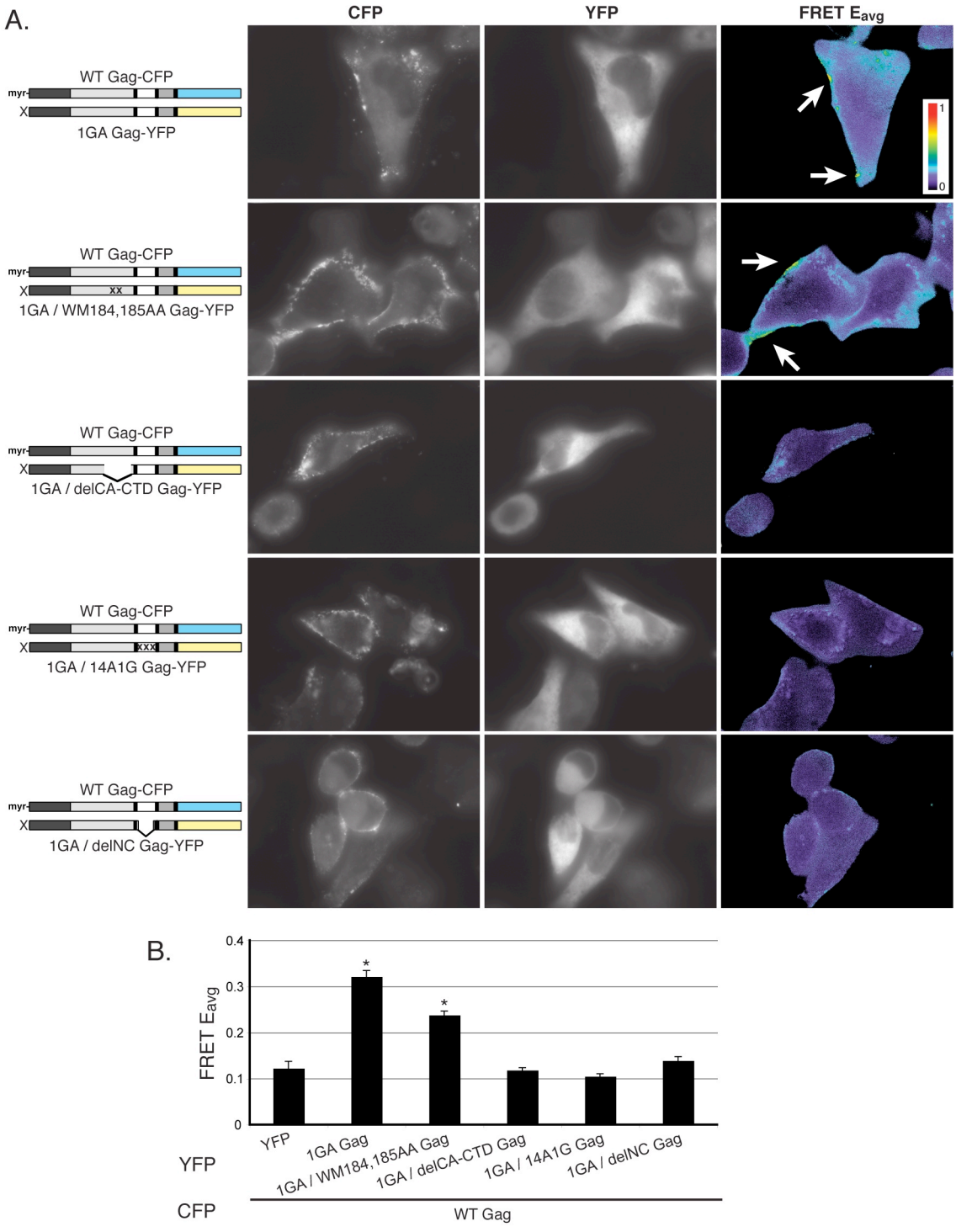

Figure 3.5. FRET microscopy of N-terminal myristoylation-deficient constructs.

Figure 3.6. FRET microscopy of constructs with constitutively enhanced membrane binding **(A)** Gag-YFP constructs modified with a triple-acylation signal [Fyn(10)], additionally containing CA mutations (WM184,185AA or delCA-CTD) or NC mutations (14A1G or delNC), were co-expressed with WT Gag-CFP. Images of FRET E_{avg} were calculated as in Figure 3.2. FRET E_{avg} values are color-coded according to the scale bar on the top panel. **(B)** E_{avg} in fluorescent puncta were quantified over approximately 50 cells, and are representative of 4 independent experiments. Note that the impacts of CA mutations on Fyn(10) Gag-YFP interacting with WT Gag-CFP are similar to those on Gag-YFP interacting with WT Gag-CFP (Figure 3.3); however, NC mutant Gag constructs are rescued into WT Gag-CFP puncta at near WT levels, unlike their normally myristoylated or myristoylation-deficient counterparts (Figures 3 & 5). ∗ = significantly greater than Fyn(10)-YFP negative control, $p<0.01$. n.s. = no statistical difference, $p>0.01$. Error bars represent standard error of the mean.

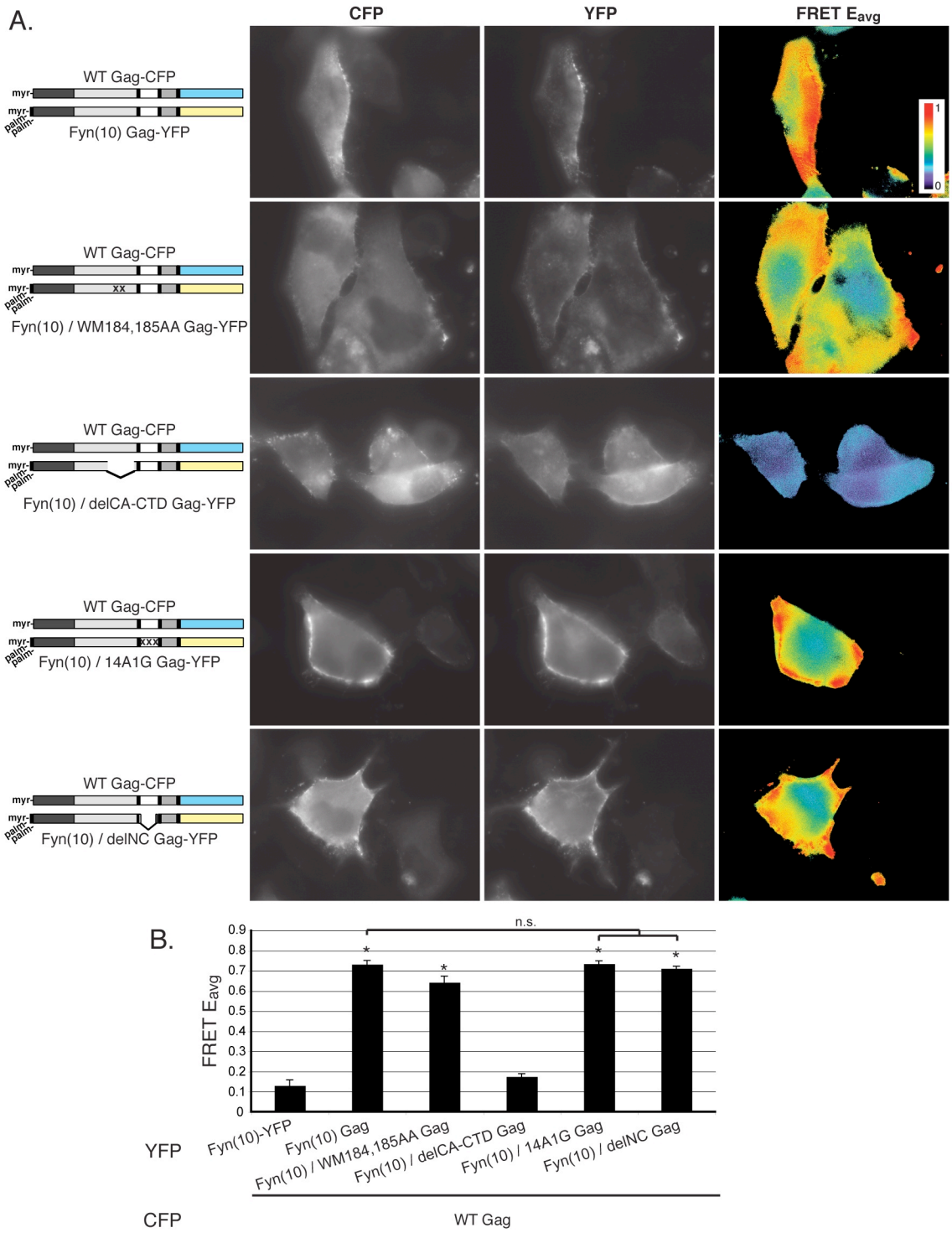

Figure 3.6. FRET microscopy of constructs with constitutively enhanced membrane binding.

REFERENCES

1. Adamson, C.S. and I.M. Jones, *The molecular basis of HIV capsid assembly--five years of progress*. Rev Med Virol, 2004. **14**(2): p. 107-21.

2. Freed, E.O., *HIV-1 gag proteins: diverse functions in the virus life cycle*. Virology, 1998. **251**(1): p. 1-15.

3. Swanstrom, R. and J.W. Wills, *Synthesis, Assembly, and Processing of Viral Proteins*, in *Retroviruses*, J.M. Coffin, S.H. Hughes, and H.E. Varmus, Editors. 1997, Cold Spring Harbor Laboratory Press: New York. p. 263-334.

4. Saad, J.S., et al., *Structural basis for targeting HIV-1 Gag proteins to the plasma membrane for virus assembly*. Proc Natl Acad Sci U S A, 2006. **103**(30): p. 11364-9.

5. Bryant, M. and L. Ratner, *Myristoylation-dependent replication and assembly of human immunodeficiency virus 1*. Proc Natl Acad Sci U S A, 1990. **87**(2): p. 523-7.

6. Gottlinger, H.G., J.G. Sodroski, and W.A. Haseltine, *Role of capsid precursor processing and myristoylation in morphogenesis and infectivity of human immunodeficiency virus type 1*. Proc Natl Acad Sci U S A, 1989. **86**(15): p. 5781-5.

7. Zhou, W., et al., *Identification of a membrane-binding domain within the amino-terminal region of human immunodeficiency virus type 1 Gag protein which interacts with acidic phospholipids*. J Virol, 1994. **68**(4): p. 2556-69.

8. Chukkapalli, V., et al., *Interaction between the human immunodeficiency virus type 1 Gag matrix domain and phosphatidylinositol-(4,5)-bisphosphate is essential for efficient gag membrane binding*. J Virol, 2008. **82**(5): p. 2405-17.

9. Hill, C.P., et al., *Crystal structures of the trimeric human immunodeficiency virus type 1 matrix protein: implications for membrane association and assembly*. Proc Natl Acad Sci U S A, 1996. **93**(7): p. 3099-3104.

10. Shkriabai, N., et al., *Interactions of HIV-1 Gag with assembly cofactors*. Biochemistry, 2006. **45**(13): p. 4077-83.

11. Dalton, A.K., et al., *Electrostatic Interactions Drive Membrane Association of the Human Immunodeficiency Virus Type 1 Gag MA Domain*. J Virol, 2007. **81**(12): p. 6434-45.

12. Zhang, W.H., et al., *Gag-Gag interactions in the C-terminal domain of human immunodeficiency virus type 1 p24 capsid antigen are essential for Gag particle assembly*. J Gen Virol, 1996. **77 (Pt 4)**: p. 743-51.

13. Gamble, T.R., et al., *Structure of the carboxyl-terminal dimerization domain of the HIV-1 capsid protein*. Science, 1997. **278**(5339): p. 849-53.

14. Franke, E.K., et al., *Specificity and sequence requirements for interactions between various retroviral Gag proteins*. J Virol, 1994. **68**(8): p. 5300-5.

15. Ehrlich, L.S., B.E. Agresta, and C.A. Carter, *Assembly of recombinant human immunodeficiency virus type 1 capsid protein in vitro*. J Virol, 1992. **66**(8): p. 4874-83.

16. Gross, I., et al., *N-Terminal extension of human immunodeficiency virus capsid protein converts the in vitro assembly phenotype from tubular to spherical particles*. J Virol, 1998. **72**(6): p. 4798-810.

17. Momany, C., et al., *Crystal structure of dimeric HIV-1 capsid protein*. Nat Struct Biol, 1996. **3**(9): p. 763-70.

18. Burniston, M.T., et al., *Human immunodeficiency virus type 1 Gag polyprotein multimerization requires the nucleocapsid domain and RNA and is promoted by the capsid-dimer interface and the basic region of matrix protein*. J Virol, 1999. **73**(10): p. 8527-40.

19. Campbell, S. and A. Rein, *In vitro assembly properties of human immunodeficiency virus type 1 Gag protein lacking the p6 domain*. J Virol, 1999. **73**(3): p. 2270-9.

20. Cimarelli, A. and J. Luban, *Human immunodeficiency virus type 1 virion density is not determined by nucleocapsid basic residues*. J Virol, 2000. **74**(15): p. 6734-40.

21. Dawson, L. and X.F. Yu, *The role of nucleocapsid of HIV-1 in virus assembly*. Virology, 1998. **251**(1): p. 141-57.

22. Huseby, D., et al., *Assembly of human immunodeficiency virus precursor gag proteins*. J Biol Chem, 2005. **280**(18): p. 17664-70.

23. Sandefur, S., et al., *Mapping and characterization of the N-terminal I domain of human immunodeficiency virus type 1 Pr55(Gag)*. J Virol, 2000. **74**(16): p. 7238-49.

24. Campbell, S. and V.M. Vogt, *Self-assembly in vitro of purified CA-NC proteins from Rous sarcoma virus and human immunodeficiency virus type 1*. J Virol, 1995. **69**(10): p. 6487-97.

25. Zabransky, A., E. Hunter, and M. Sakalian, *Identification of a minimal HIV-1 gag domain sufficient for self-association*. Virology, 2002. **294**(1): p. 141-50.

26. Ono, A., et al., *Association of human immunodeficiency virus type 1 gag with membrane does not require highly basic sequences in the nucleocapsid: use of a novel Gag multimerization assay*. J Virol, 2005. **79**(22): p. 14131-40.

27. von Schwedler, U.K., et al., *Functional surfaces of the human immunodeficiency virus type 1 capsid protein*. J Virol, 2003. **77**(9): p. 5439-50.

28. Joshi, A., K. Nagashima, and E.O. Freed, *Mutation of dileucine-like motifs in the human immunodeficiency virus type 1 capsid disrupts virus assembly, gag-gag interactions, gag-membrane binding, and virion maturation*. J Virol, 2006. **80**(16): p. 7939-51.

29. Datta, S.A., et al., *Interactions between HIV-1 Gag molecules in solution: an inositol phosphate-mediated switch*. J Mol Biol, 2007. **365**(3): p. 799-811.

30. Dorfman, T., et al., *Mapping of functionally important residues of a cysteine-histidine box in the human immunodeficiency virus type 1 nucleocapsid protein*. J Virol, 1993. **67**(10): p. 6159-69.

31. Lee, E.G. and M.L. Linial, *Basic residues of the retroviral nucleocapsid play different roles in gag-gag and Gag-Psi RNA interactions*. J Virol, 2004. **78**(16): p. 8486-95.

32. Poon, D.T., J. Wu, and A. Aldovini, *Charged amino acid residues of human immunodeficiency virus type 1 nucleocapsid p7 protein involved in RNA packaging and infectivity*. J Virol, 1996. **70**(10): p. 6607-16.

33. Borsetti, A., A. Ohagen, and H.G. Gottlinger, *The C-terminal half of the human immunodeficiency virus type 1 Gag precursor is sufficient for efficient particle assembly*. J Virol, 1998. **72**(11): p. 9313-7.

34. Feng, Y.X., et al., *Reversible binding of recombinant human immunodeficiency virus type 1 gag protein to nucleic acids in virus-like particle assembly in vitro*. J Virol, 2002. **76**(22): p. 11757-62.

35. Gheysen, D., et al., *Assembly and release of HIV-1 precursor Pr55gag virus-like particles from recombinant baculovirus-infected insect cells*. Cell, 1989. **59**(1): p. 103-12.

36. Hockley, D.J., et al., *Comparative morphology of Gag protein structures produced by mutants of the gag gene of human immunodeficiency virus type 1*. J Gen Virol, 1994. **75 (Pt 11)**: p. 2985-97.

37. Hoshikawa, N., et al., *Role of the gag and pol genes of human immunodeficiency virus in the morphogenesis and maturation of retrovirus-like particles expressed*

by recombinant vaccinia virus: an ultrastructural study. J Gen Virol, 1991. **72 (Pt 10)**: p. 2509-17.

38. Khorchid, A., et al., *Role of RNA in facilitating Gag/Gag-Pol interaction*. J Virol, 2002. **76**(8): p. 4131-7.

39. Lee, Y.M., B. Liu, and X.F. Yu, *Formation of virus assembly intermediate complexes in the cytoplasm by wild-type and assembly-defective mutant human immunodeficiency virus type 1 and their association with membranes*. J Virol, 1999. **73**(7): p. 5654-62.

40. Wang, C.T., H.Y. Lai, and J.J. Li, *Analysis of minimal human immunodeficiency virus type 1 gag coding sequences capable of virus-like particle assembly and release*. J Virol, 1998. **72**(10): p. 7950-9.

41. Zhang, Y. and E. Barklis, *Effects of nucleocapsid mutations on human immunodeficiency virus assembly and RNA encapsidation*. J Virol, 1997. **71**(9): p. 6765-76.

42. Zhang, Y., et al., *Analysis of the assembly function of the human immunodeficiency virus type 1 gag protein nucleocapsid domain*. J Virol, 1998. **72**(3): p. 1782-9.

43. Bowzard, J.B., et al., *Importance of basic residues in the nucleocapsid sequence for retrovirus Gag assembly and complementation rescue*. J Virol, 1998. **72**(11): p. 9034-44.

44. Ott, D.E., et al., *Elimination of protease activity restores efficient virion production to a human immunodeficiency virus type 1 nucleocapsid deletion mutant*. J Virol, 2003. **77**(10): p. 5547-56.

45. Wang, S.W., K. Noonan, and A. Aldovini, *Nucleocapsid-RNA interactions are essential to structural stability but not to assembly of retroviruses*. J Virol, 2004. **78**(2): p. 716-23.

46. Wang, S.W. and A. Aldovini, *RNA incorporation is critical for retroviral particle integrity after cell membrane assembly of Gag complexes*. J Virol, 2002. **76**(23): p. 11853-65.

47. Gross, I., H. Hohenberg, and H.G. Krausslich, *In vitro assembly properties of purified bacterially expressed capsid proteins of human immunodeficiency virus*. Eur J Biochem, 1997. **249**(2): p. 592-600.

48. Campbell, S. and V.M. Vogt, *In vitro assembly of virus-like particles with Rous sarcoma virus Gag deletion mutants: identification of the p10 domain as a morphological determinant in the formation of spherical particles*. J Virol, 1997. **71**(6): p. 4425-35.

49. Muriaux, D., et al., *RNA is a structural element in retrovirus particles*. Proc Natl Acad Sci U S A, 2001. **98**(9): p. 5246-51.

50. Accola, M.A., B. Strack, and H.G. Gottlinger, *Efficient particle production by minimal Gag constructs which retain the carboxy-terminal domain of human immunodeficiency virus type 1 capsid-p2 and a late assembly domain*. J Virol, 2000. **74**(12): p. 5395-402.

51. Johnson, M.C., et al., *Nucleic acid-independent retrovirus assembly can be driven by dimerization*. J Virol, 2002. **76**(22): p. 11177-85.

52. Crist, R.M., et al., *Assembly properties of human immunodeficiency virus type 1 Gag-leucine zipper chimeras: implications for retrovirus assembly*. J Virol, 2009. **83**(5): p. 2216-25.

53. Alfadhli, A., et al., *Analysis of human immunodeficiency virus type 1 Gag dimerization-induced assembly*. J Virol, 2005. **79**(23): p. 14498-506.

54. Ma, Y.M. and V.M. Vogt, *Rous sarcoma virus Gag protein-oligonucleotide interaction suggests a critical role for protein dimer formation in assembly*. J Virol, 2002. **76**(11): p. 5452-62.

55. Ma, Y.M. and V.M. Vogt, *Nucleic acid binding-induced Gag dimerization in the assembly of Rous sarcoma virus particles in vitro*. J Virol, 2004. **78**(1): p. 52-60.

56. Roldan, A., et al., *In vitro identification and characterization of an early complex linking HIV-1 genomic RNA recognition and Pr55Gag multimerization*. J Biol Chem, 2004. **279**(38): p. 39886-94.

57. Dalton, A.K., et al., *Biochemical characterization of rous sarcoma virus MA protein interaction with membranes*. J Virol, 2005. **79**(10): p. 6227-38.

58. Provitera, P., et al., *Role of the major homology region in assembly of HIV-1 Gag*. Biochemistry, 2001. **40**(18): p. 5565-72.

59. Sandefur, S., V. Varthakavi, and P. Spearman, *The I domain is required for efficient plasma membrane binding of human immunodeficiency virus type 1 Pr55Gag*. J Virol, 1998. **72**(4): p. 2723-32.

60. Zhou, W. and M.D. Resh, *Differential membrane binding of the human immunodeficiency virus type 1 matrix protein*. J Virol, 1996. **70**(12): p. 8540-8.

61. Perez-Caballero, D., et al., *Human immunodeficiency virus type 1 matrix inhibits and confers cooperativity on gag precursor-membrane interactions*. J Virol, 2004. **78**(17): p. 9560-3.

62. Callahan, E.M. and J.W. Wills, *Link between genome packaging and rate of budding for Rous sarcoma virus*. J Virol, 2003. **77**(17): p. 9388-98.

63. Hermida-Matsumoto, L. and M.D. Resh, *Human immunodeficiency virus type 1 protease triggers a myristoyl switch that modulates membrane binding of Pr55(gag) and p17MA*. J Virol, 1999. **73**(3): p. 1902-8.

64. Ono, A. and E.O. Freed, *Binding of human immunodeficiency virus type 1 Gag to membrane: role of the matrix amino terminus*. J Virol, 1999. **73**(5): p. 4136-4144.

65. Paillart, J.C. and H.G. Gottlinger, *Opposing effects of human immunodeficiency virus type 1 matrix mutations support a myristyl switch model of gag membrane targeting*. J Virol, 1999. **73**(4): p. 2604-12.

66. Resh, M.D., *A myristoyl switch regulates membrane binding of HIV-1 Gag*. Proc Natl Acad Sci U S A, 2004. **101**(2): p. 417-8.

67. Saad, J.S., et al., *Point mutations in the HIV-1 matrix protein turn off the myristyl switch*. J Mol Biol, 2007. **366**(2): p. 574-85.

68. Spearman, P., et al., *Membrane binding of human immunodeficiency virus type 1 matrix protein in vivo supports a conformational myristyl switch mechanism*. J Virol, 1997. **71**(9): p. 6582-92.

69. Tang, C., et al., *Entropic switch regulates myristate exposure in the HIV-1 matrix protein*. Proc Natl Acad Sci U S A, 2004. **101**(2): p. 517-22.

70. Hubner, W., et al., *Sequence of human immunodeficiency virus type 1 (HIV-1) Gag localization and oligomerization monitored with live confocal imaging of a replication-competent, fluorescently tagged HIV-1*. J Virol, 2007. **81**(22): p. 12596-607.

71. Lingappa, J.R., et al., *Basic residues in the nucleocapsid domain of Gag are required for interaction of HIV-1 gag with ABCE1 (HP68), a cellular protein important for HIV-1 capsid assembly*. J Biol Chem, 2006. **281**(7): p. 3773-84.

72. Lingappa, J.R., et al., *A multistep, ATP-dependent pathway for assembly of human immunodeficiency virus capsids in a cell-free system*. J Cell Biol, 1997. **136**(3): p. 567-81.

73. Morikawa, Y., T. Goto, and F. Momose, *Human immunodeficiency virus type 1 Gag assembly through assembly intermediates*. J Biol Chem, 2004. **279**(30): p. 31964-72.

74. Li, H., et al., *Myristoylation is required for human immunodeficiency virus type 1 Gag-Gag multimerization in mammalian cells*. J Virol, 2007. **81**(23): p. 12899-910.

75. Barklis, E., et al., *Structural analysis of membrane-bound retrovirus capsid proteins*. EMBO J, 1997. **16**(6): p. 1199-213.

76. Jager, S., E. Gottwein, and H.G. Krausslich, *Ubiquitination of human immunodeficiency virus type 1 Gag is highly dependent on Gag membrane association*. J Virol, 2007. **81**(17): p. 9193-201.

77. Popov, S., et al., *Human immunodeficiency virus type 1 Gag engages the Bro1 domain of ALIX/AIP1 through the nucleocapsid*. J Virol, 2008. **82**(3): p. 1389-98.

78. Dussupt, V., et al., *The nucleocapsid region of HIV-1 Gag cooperates with the PTAP and LYPXnL late domains to recruit the cellular machinery necessary for viral budding*. PLoS Pathog, 2009. **5**(3): p. e1000339.

79. Larson, D.R., et al., *Direct measurement of Gag-Gag interaction during retrovirus assembly with FRET and fluorescence correlation spectroscopy*. J Cell Biol, 2003. **162**(7): p. 1233-44.

80. Derdowski, A., L. Ding, and P. Spearman, *A novel fluorescence resonance energy transfer assay demonstrates that the human immunodeficiency virus type 1 Pr55Gag I domain mediates Gag-Gag interactions*. J Virol, 2004. **78**(3): p. 1230-42.

81. Jouvenet, N., P.D. Bieniasz, and S.M. Simon, *Imaging the biogenesis of individual HIV-1 virions in live cells*. Nature, 2008. **454**(7201): p. 236-40.

82. Sekar, R.B. and A. Periasamy, *Fluorescence resonance energy transfer (FRET) microscopy imaging of live cell protein localizations*. J Cell Biol, 2003. **160**(5): p. 629-33.

83. Hoppe, A., K. Christensen, and J.A. Swanson, *Fluorescence resonance energy transfer-based stoichiometry in living cells*. Biophys J, 2002. **83**(6): p. 3652-64.

84. Jares-Erijman, E.A. and T.M. Jovin, *FRET imaging*. Nat Biotechnol, 2003. **21**(11): p. 1387-95.

85. Adachi, A., et al., *Production of acquired immunodeficiency syndrome-associated retrovirus in human and nonhuman cells transfected with an infectious molecular clone*. J Virol, 1986. **59**(2): p. 284-91.

86. Huang, M., et al., *p6Gag is required for particle production from full-length human immunodeficiency virus type 1 molecular clones expressing protease*. J Virol, 1995. **69**(11): p. 6810-8.

87. Sutton, R.E., et al., *Human immunodeficiency virus type 1 vectors efficiently transduce human hematopoietic stem cells*. J Virol, 1998. **72**(7): p. 5781-8.

88. Rizzo, M.A., et al., *An improved cyan fluorescent protein variant useful for FRET*. Nat Biotechnol, 2004. **22**(4): p. 445-9.

89. Freed, E.O., et al., *Single amino acid changes in the human immunodeficiency virus type 1 matrix protein block virus particle production*. J Virol, 1994. **68**(8): p. 5311-5320.

90. Freed, E.O. and M.A. Martin, *Evidence for a functional interaction between the V1/V2 and C4 domains of human immunodeficiency virus type 1 envelope glycoprotein gp120*. J Virol, 1994. **68**(4): p. 2503-12.

91. Ono, A., et al., *Phosphatidylinositol (4,5) bisphosphate regulates HIV-1 Gag targeting to the plasma membrane*. Proc Natl Acad Sci U S A, 2004. **101**(41): p. 14889-14894.

92. Ono, A., D. Demirov, and E.O. Freed, *Relationship between human immunodeficiency virus type 1 Gag multimerization and membrane binding*. J Virol, 2000. **74**(11): p. 5142-50.

93. Hoppe, A.D., et al., *Three-dimensional FRET reconstruction microscopy for analysis of dynamic molecular interactions in live cells*. Biophys J, 2008. **95**(1): p. 400-18.

94. Berney, C. and G. Danuser, *FRET or no FRET: a quantitative comparison*. Biophys J, 2003. **84**(6): p. 3992-4010.

95. Kiskowski, M.A. and A.K. Kenworthy, *In silico characterization of resonance energy transfer for disk-shaped membrane domains*. Biophys J, 2007. **92**(9): p. 3040-51.

96. Beemiller, P., A.D. Hoppe, and J.A. Swanson, *A phosphatidylinositol-3-kinase-dependent signal transition regulates ARF1 and ARF6 during Fcgamma receptor-mediated phagocytosis*. PLoS Biol, 2006. **4**(6): p. e162.

97. Cai, D., et al., *Kinesin-1 structural organization and conformational changes revealed by FRET stoichiometry in live cells*. J Cell Biol, 2007. **176**(1): p. 51-63.

98. Prodanov, D., J. Heeroma, and E. Marani, *Automatic morphometry of synaptic boutons of cultured cells using granulometric analysis of digital images*. J Neurosci Methods, 2006. **151**(2): p. 168-77.

99. Larson, D.R., et al., *Visualization of retrovirus budding with correlated light and electron microscopy*. Proc Natl Acad Sci U S A, 2005. **102**(43): p. 15453-8.

100. Jouvenet, N., P.D. Bieniasz, and S.M. Simon, *Imaging the biogenesis of individual HIV-1 virions in live cells*. Nature, 2008.

101. Nydegger, S., et al., *Mapping of tetraspanin-enriched microdomains that can function as gateways for HIV-1*. J Cell Biol, 2006. **173**(5): p. 795-807.

102. Jolly, C. and Q.J. Sattentau, *Human immunodeficiency virus type 1 assembly, budding, and cell-cell spread in T cells take place in tetraspanin-enriched plasma membrane domains*. J Virol, 2007. **81**(15): p. 7873-84.

103. Booth, A.M., et al., *Exosomes and HIV Gag bud from endosome-like domains of the T cell plasma membrane*. J Cell Biol, 2006. **172**(6): p. 923-35.

104. Yu, F., et al., *Characterization of Rous sarcoma virus Gag particles assembled in vitro*. J Virol, 2001. **75**(6): p. 2753-64.

105. Park, J. and C.D. Morrow, *The nonmyristylated Pr160gag-pol polyprotein of human immunodeficiency virus type 1 interacts with Pr55gag and is incorporated into viruslike particles*. J Virol, 1992. **66**(11): p. 6304-13.

106. Morikawa, Y., et al., *Complete inhibition of human immunodeficiency virus Gag myristoylation is necessary for inhibition of particle budding*. J Biol Chem, 1996. **271**(5): p. 2868-73.

107. Kawada, S., et al., *Dominant negative inhibition of human immunodeficiency virus particle production by the nonmyristoylated form of gag*. J Virol, 2008. **82**(9): p. 4384-99.

108. Ono, A., A.A. Waheed, and E.O. Freed, *Depletion of cellular cholesterol inhibits membrane binding and higher-order multimerization of human immunodeficiency virus type 1 Gag*. Virology, 2007. **360**(1): p. 27-35.

109. Worthylake, D.K., et al., *Structures of the HIV-1 capsid protein dimerization domain at 2.6 A resolution*. Acta Crystallogr D Biol Crystallogr, 1999. **55**(Pt 1): p. 85-92.

110. Ono, A. and E.O. Freed, *Role of lipid rafts in virus replication*. Adv Virus Res, 2005. **64**: p. 311-58.

CHAPTER IV

Gag Reorganizes Plasma Membrane Microdomains During HIV-1 Assembly

ABSTRACT

The nature of biological membranes is fundamental to the study of assembly and egress of enveloped viruses. Two types of plasma membrane microdomains, lipid rafts and tetraspanin-enriched microdomains (TEMs), are currently proposed to be platforms for HIV-1 assembly. However, a variety of studies have demonstrated that lipid rafts and TEMs are distinct microdomains. Yet, Gag appears to associate with both lipid rafts and TEMs, raising the question of whether lipid raft and TEMs are coalesced by Gag, or if they remain segregated and constitute distinct assembly sites. To assay the association between Gag and microdomain markers, we took advantage of a well-established antibody-mediated co-patching assay to stabilize microdomains into microscopically visible membrane patches. We found that various combinations of lipid raft and TEM markers co-patched to a greater extent in the presence of membrane-bound Gag, suggesting that Gag induces the coalescence of lipid rafts and TEMs. To determine whether the mode of Gag membrane binding plays a role in microdomain association and coalescence, we measured the co-patching of microdomain markers in the presence of Gag derivatives with various membrane binding motif substitutions. While Gag

membrane binding is necessary to induce coalescence of lipid rafts and TEMs, either acylation of Gag or ability to bind $PI(4,5)P_2$ are sufficient.

INTRODUCTION

The nature of biological membranes is fundamental to the study of assembly and egress of enveloped viruses. Based on decades of cell biological, biochemical, and biophysical research, the current consensus is that the plasma membrane (PM) is heterogeneous, consisting of diverse microdomains. This partitioning of membrane components is regulated by lipid-lipid, protein-protein, and protein-lipid interactions in order to compartmentalize cellular processes (1, 2). As viruses interact intimately with their host cells, it would not be surprising for viruses to take advantage of pre-existing host membrane microdomains to compartmentalize their own viral processes. Additionally or alternatively, viruses might hijack membrane organization, restructuring microdomains to facilitate viral processes, or modulate cellular processes for their benefit.

HIV-1 Assembly

Human immunodeficiency virus type 1 (HIV-1) assembly occurs on the PM (3), and is driven by the structural polyprotein Gag, which is necessary and sufficient for the formation of virus-like particles (VLPs). Gag binding to the PM is mediated by its N-terminal matrix (MA) domain, which is myristoylated and contains basic residues that bind the PM phospholipid phosphatidylinositol-(4,5)-bisphosphate [$PI(4,5)P_2$] (4-11).

Prior to membrane binding, the myristoyl moiety is sequestered in a hydrophobic patch on the MA domain, and its exposure may be regulated by $PI(4,5)P_2$ binding (8). The capsid (CA) and nucleocapsid (NC) domains within Gag, and the ability of Gag to bind cellular membranes, each promote Gag multimerization (12-29). The CA domain forms an interface that mediates Gag homo-dimerization (17, 29-32). The NC domain binds RNA, which is thought to serve as a scaffold promoting higher-order Gag multimerization (14, 23, 31, 33-35). Likewise, the ability of Gag to bind membrane may allow Gag to similarly use the PM as a scaffold for multimerization (29) – particularly if membrane-bound Gag molecules are laterally concentrated by their affinity for particular membrane microdomains. Two types of microdomains, lipid rafts and tetraspanin-enriched microdomains (TEMs), are currently proposed to be platforms for HIV-1 assembly (36-39).

Lipid Rafts

Lipid rafts are dynamic, sub-microscopic domains enriched in sterols, sphingolipids, glycosylphosphatidylinositol-anchored (GPI-anchored) proteins, and proteins modified with saturated acyl chains (1, 2). Proteomics, lipidomics, and biochemical studies have shown that the HIV-1 envelope is enriched in lipids and proteins that are also enriched in lipid rafts (40-47). In cells, Gag co-localizes/co-patches with lipid raft markers by immunofluorescence (48-50), and co-fractionates with lipid raft markers in detergent resistant membranes (DRMs) (31, 48, 49, 51-57). Depletion of cellular cholesterol, which disrupts lipid rafts, reduces virus particle production and disrupts the behavior of Gag in cells measured by a variety of assays (52, 58-60).

Importantly, one study loaded cells with an unsaturated myristate analogue, which blocked Gag fractionation into DRMs and reduced virus production, suggesting that N-terminal saturated acylation is a necessary molecular determinant of lipid raft association and assembly of Gag (53). Alternatively, an NMR study showed that, upon $PI(4,5)P_2$ binding and myristoyl exposure, MA sequesters the typically unsaturated 2' acyl chain of $PI(4,5)P_2$ in the hydrophobic patch vacated by the myristoyl moiety. If this unique mode of $PI(4,5)P_2$ binding occurs on cellular membranes, it is predicted to facilitate Gag association with lipid rafts (8). However, chimeric Gag constructs that bind membrane via non-acylated phosphatidylinositide-binding domains [e.g. pleckstrin homology (PH) domains], which are not thought to sequester the 2' acyl chain of $PI(4,5)P_2$, can still produce VLPs (3, 61, 62). This suggests that neither acylation, nor sequestration of $PI(4,5)P_2$ acyl chains, are necessary for assembly. Overall, the precise determinants of Gag's lipid raft association remain to be elucidated.

Tetraspanin-Enriched Microdomains

TEMs are membrane microdomains organized by homo- and hetero-oligomerization of tetraspanins, a family of homologous proteins with four transmembrane domains (38, 63, 64). A variety of studies have suggested roles for tetraspanins and TEMs in other phases of the retroviral replication cycle, but research into whether TEMs affect virus assembly and release remains contradictory (38). Tetraspanins, including CD9, CD63, and CD81, are incorporated into virus particles (45, 65-73), co-immunoprecipitate with Gag-laden cellular membranes (74), and strongly co-localize/co-patch with Gag by immunofluorescence and electron microscopy assays (29,

75-82). Tetraspanins CD63 and CD81 have been shown to associate with phosphatidylinositol 4-kinase, a critical enzyme in creating $PI(4,5)P_2$ (83). Thus $PI(4,5)P_2$ might recruit Gag to TEMs; however, this hypothesis has not been tested. The molecular determinants of Gag association with TEMs are currently unknown.

Lipid Rafts and TEMs are Distinct Microdomains

Lipid rafts and TEMs can be biochemically distinguished as they have distinct detergent sensitivities, TEMs are relatively less sensitive to cholesterol depletion, and have distinct constituents by proteomic analysis (84-90). Furthermore, many microscopy-based studies have observed segregation or distinct behaviors of lipid raft and TEM markers (77, 91, 92). Yet, as described above, Gag appears to associate with both lipid rafts and TEMs, raising the question of whether lipid raft and TEMs are coalesced by Gag, or if they remain segregated and constitute distinct assembly sites.

One study comparing the assembly sites of HIV-1 Gag and influenza showed that Gag associates with TEMs, but fails to recruit the canonical raft marker influenza hemagglutinin (HA), suggesting that Gag does not coalesce lipid rafts and TEMs (72). However, as HA was expressed with other influenza proteins, it is possible that HA was sequestered at assembling influenza virions and could not freely associate with lipid rafts or Gag. Therefore, it remains unclear whether Gag induces the coalescence of lipid rafts and TEMs.

Co-patching Assay

Oligomeric or multivalent proteins that interact with membrane constituents can alter microdomain structure and dynamics, by stabilizing or coalescing microdomains into larger structures, and concentrating or segregating membrane components (1, 2). For example, flotillin/reggie proteins are thought to be organizers of lipid rafts (93), and tetraspanins organize TEMs. Similarly, it has long been appreciated that binding of exogenous multivalent proteins, such as antibodies or lipid-binding toxins, can induce the clustering of membrane components into microscopically visible patches on the cell surface (94-98). When two microdomain markers are independently clustered using specific antibodies, these markers can co-localize within the same patch, or "co-patch", possibly indicating shared microdomain affinity. Inversely, markers independently clustered into patches can segregate, indicating a lack of shared affinity (98, 99). It is thought that this shared affinity (or lack thereof) during antibody co-patching is representative of the markers' native sub-microscopic microdomain affinities in the absence of experimental manipulation.

Using these methods, we aim to answer two questions: (i) does Gag reorganize cellular microdomains, inducing the coalescence of lipid rafts and TEMs; and, (ii) what are the molecular determinants of Gag microdomain reorganization?

Our data demonstrate that Gag does induce the coalescence of lipid rafts and TEMs. Lipid raft and TEM markers co-patch to a greater degree in the presence of wild-type (WT) Gag than in the presence of a derivative that is completely deficient in membrane binding, indicating that Gag membrane binding is necessary to induce lipid

raft/TEM coalescence. Gag derivatives that are either acylated or PI(4,5)P_2-binding are sufficient to induce coalescence, suggesting that the mode of Gag membrane binding does not affect microdomain association.

MATERIALS and METHODS

Plasmids

Derivatives of the HIV-1 molecular clone pNL4-3 encoding Gag with a C-terminal fluorescent protein fusion [either mVenus yellow fluorescent protein (YFP) or mRFP red fluorescent protein (RFP)] were described previously (11, 29). These chimeric derivatives do not express *pol*, *vif*, or *vpr*. A derivative expressing Gag that is completely defective in membrane binding was constructed by combining two previously described mutations, 1GA and 6A2T. This construct contains amino acid substitutions within the MA domain, replacing eight basic residues that bind acidic phospholipids, and abolishing the N-terminal myristoylation signal (100, 101). Derivatives in which the start codon or entire MA sequence were replaced with the sequence encoding the ten residue myristoylation and dual-palmitoylation signal of Fyn kinase [Fyn(10)fullMA or Fyn(10)ΔMA, respectively] were described previously (11). Derivative $PH_{PLC\delta1}$delMA was created by replacing the sequence encoding the MA globular head (codons 1-114) with the sequence encoding the first 170 amino acids, containing the PH domain, of phospholipase Cδ1, isoform 2 ($PH_{PLC\delta1}$). The junctions between pNL4-3 and $PH_{PLC\delta1}$ DNA sequences are as follows (bold type represents pNL4-3 sequence, italic type represents $PH_{PLC\delta1}$ sequence, and the start codon is underlined):

GAGGCTAGAAGGAGAGAG*ATG**GACTCGGGCCGGGAC* (upstream junction);

*GAGCTGCAGAACTTCCTG***AAGGCACAGCAAGCAGCA** (downstream junction).

The cloned $PH_{PLC\delta1}$ sequence was a kind gift from T. Balla and J. Swanson (102, 103). $PH_{PLC\delta1}$delMA Gag derivatives did not express well (data not shown), but normal expression levels were rescued by co-transfecting pCMV-Rev (a kind gift from S. Venkatesan, National Institutes of Health) and pcDNA3.1-HIVTat101 [a kind gift from D. Markovitz, University of Michigan, originally from E. Verdin (104)], expressing HIV-1 *rev* and *tat* genes respectively.

Expression vectors encoding monomeric mVenus (YFP) were described previously (29). mNonFP, a non-fluorescent derivative of mCitrine (105), containing a mutation (Y67C) that abolishes fluorophore formation (106), was a kind gift from S. Straight at the University of Michigan Center for Live-Cell Imaging. All fluorescent protein constructs contain the mutation A206K to suppress fluorescent protein dimerization (107).

We generated constructs expressing GPI-anchored mVenus (YFP-GPI) or mNonFP (NonFP-GPI) based on a previously described GPI-anchored fluorescent protein construct [a kind gift from J. Silver, National Institutes of Health, originally from K. Simons (108)]. We generated constructs expressing mVenus, or mNonFP fused to the transmembrane domain of influenza hemagglutinin (YFP-HA-TMD or NonFP-HA-TMD) based on previously described constructs, a kind gift from A. Herrmann (109).

CD63 fused to mVenus (CD63-YFP) was created based on pCD63-EGFP-bos [a kind gift from G. Griffiths (110)]. CD81 and CD9 fused to mVenus (CD81-YFP and

CD9-YFP) were created based on CD81-GFP and CD9-GFP [a kind gift from F. Sánchez-Madrid (111)].

Cells and Transfection

HeLa cells were cultured as described previously (100). For confocal microscopy, $4.2x10^4$ cells were seeded in each well of 8-well chamber slides (Lab-Tek, Thermo Fisher). Cells were grown for 24 hours, and transfected with 0.6 ug/well of pNL4-3-based plasmid using Lipofectamine 2000 (Invitrogen) according to manufacturer's instructions. When co-expressing pNL4-3-based plasmid with any other plasmids, cells were transfected with 0.6 ug/well of pNL4-3-based plasmid plus 0.06 ug/well of each other plasmid, as above.

Co-patching Assay and Confocal Fluorescence Microscopy

At 16-18 hours post-transfection, chamber slides were brought to room temperature for 10 min, then incubated 10 min with primary antibodies detecting CD46, CD59, CD81 (mouse monoclonal, BD Biosciences), CD9 (mouse monoclonal, AbD Serotec), CD63 (mouse monoclonal, Santa Cruz Biotechnology), or GFP derivative NonFP (rabbit polyclonal, Clontech), diluted 1:100 in cell culture media. Then, slides were rinsed 3 times in phosphate buffered saline (PBS), then incubated for 10 min with fluorescent secondary antibodies (Invitrogen) diluted 1:200 in cell culture media. Alternatively, cells were stained with Vybrant DiD (Invitrogen) diluted 1:200 in PBS for 10 min. Slides were then rinsed 3 times in PBS, immediately fixed in 4% paraformaldehyde (Electron Microscopy Sciences) in PBS for 1 hr, rinsed in PBS once,

and mounted in Fluoromount-G (Southern Biotech). Slides were imaged using a Leica TCS SP5 X laser scanning confocal microscope equipped with a multi-line argon laser, and a tunable, broad spectrum pulsed-source (i.e. "white-light") laser. Confocal pinhole was set to 1 Airy unit, and focal plane was selected to image the dorsal surface of each cell. We used a 100X oil-immersion 1.40 numerical aperture PL APO objective with 6X scanning zoom, producing an image resolution of 25x25 nm per pixel, 1024x1024 pixels per image. YFP was measured using 514nm excitation and 525-575nm emission. Alexa594 or RFP were measured using 590nm excitation and 600-640nm emission. Alexa647 was measured using 650nm excitation and 660-750nm emission. Samples were imaged with each excitation wavelength sequentially, and excitation and emission wavelengths were chosen to minimize crosstalk between fluorescence channels.

Image Analysis, Quantitation, and Statistics

The degree of co-patching between microdomain markers was quantified using ImageJ (version 1.43o; NIH [http://rsb.info.nih.gov/ij/]). Images were first cropped, retaining the dorsal surface where the PM is nearly parallel to the focal plane. To avoid spuriously colocalized signals, the lateral surface, where the PM is not parallel to the focal plane and largely out of focus, was discarded.

The Pearson's correlation coefficient between fluorescence channels was calculated using the JACoP plugin of ImageJ (112). This correlation coefficient ranges from -1 to 1, where 1 represents perfect co-localization, zero represents random distributions of fluorescence intensities that can spuriously co-localize by chance, and -1 represents perfect segregation of fluorescence signals. In practice, without performing

additional image manipulations, such as deconvolution or background subtraction, correlation coefficients calculated from fluorescence micrographs are always greater than zero due to spurious co-localization of out-of-focus fluorescence background (data not shown).

Ten to thirty cells were measured for each experimental condition. Statistical significance was assessed using a nonparametric Mann-Whitney U test (implemented in Microsoft Excel). Fluorescence images were prepared for publication by auto-scaling brightness and contrast in ImageJ.

RESULTS

Without antibody-mediated patching, microdomain markers appear widely distributed on the PM

Lipid rafts are too small and dynamic to be resolved by light microscopy. Likewise, TEMs are small, and individual tetraspanin molecules are dynamically exchanged between TEMs and a population not associated with TEMs (92). Because of this small size and dynamic behavior, previous studies have reported that, in the absence of antibody-mediated patching, microdomain markers appear widely distributed on the PM. To characterize the behavior of microdomain markers in our experimental system, in the presence of HIV-1 Gag, we first visualized the distribution of microdomain markers on the dorsal surface of cells without antibody-mediated patching. To detect microdomain markers without using antibodies, we used fluorescent protein fusions: Lipid raft markers GPI-anchored YFP (YFP-GPI) and YFP-tagged influenza HA

transmembrane domain (YFP-HA-TMD); and TEM markers markers YFP-CD81, YFP-CD9, and YFP-CD63 (see Table 4.1 for a comparison of microdomain markers used in these experiments). Similar to the general membrane dye, DiD (Figure 4.1, bottom row), each micrdomain marker appeared widely distributed on the cell surface, and were preferentially detected in cell-surface structures resembling ruffles or filopodia (Figure 4.1).

In many cases, both lipid raft and TEM markers appeared enriched at Gag puncta, suggesting that these markers have a preference for Gag puncta even in the absence of antibody-mediated patching. Critically, the membrane dye DiD did not appear enriched at Gag puncta. This indicates that the apparent enrichment of microdomain markers at Gag puncta is not due to preferential detection or local abundance of membranous structures, like ruffles, filopodia, or clusters of virus particles on cell surface. However, due to the broad distribution of microdomain markers, it is difficult to distinguish authentic co-localization/co-enrichment at Gag puncta relative to the high background of markers not associated with Gag puncta. To overcome this limitation, in subsequent experiments, we took advantage of the well-established antibody-mediated co-patching method (99).

Antibody-mediated co-patching assay can distinguish lipid rafts and TEMs

Antibody-induced microdomain marker patches are thought to reflect the native sub-microscopic microdomain affinities of markers in the absence of experimental manipulation. To validate that this assay can distinguish different classes of microdomains in the absence of Gag, we performed a co-patching assay detecting markers within or between classes of markers. Microdomain markers used in these

experiments are summarized in Table 4.1. Previous studies have reported that TEMs are not homogenous with regard to tetraspanin composition: TEMs contain varying ratios of different tetraspanins, including some in which only a single type of tetraspanin protein was detected (77). Consistent with these observations, we detected a high degree of colocalization between independently patched CD81 and CD9, but we also detected CD81-containing TEMs that do contain detectable amounts of CD9 (Figure 4.2, top row). In agreement with previous co-patching studies (99), different lipid raft markers, CD59, NonFP-GPI, and NonFP-HA-TMD, co-patched strongly on a punctum-by-punctum basis (Figure 4.2, rows 2-3). Consistent with previous reports showing that lipid rafts and TEMs are distinct microdomains (see Introduction), lipid raft marker CD59 and TEM marker CD81 segregated in this co-patching assay (Figure 4.2, fourth row). TEM marker CD81 and lipid raft marker NonFP-GPI also segregated from the control non-TEM/non-raft marker, CD46 (Figure 4.2, rows 5-6). These results confirm that this assay can distinguish different classes of microdomain markers.

Gag co-patches with both lipid raft and TEM markers

As described in the Introduction, studies using a wide variety of methods have shown that Gag associates with lipid rafts, and that Gag associates with TEMs. To validate this co-patching assay in the presence of Gag, microdomain markers were antibody-patched on Gag-YFP-expressing cells. Antibody-mediated patching is not necessary to visualize Gag patches, as Gag naturally forms distinct puncta on the PM. In each case, Gag co-patched strongly with both TEM and lipid raft markers (Figure 4.3,

rows 1-6), but segregated from non-TEM/non-raft control, CD46 (Figure 4.3, bottom row).

Gag induces the coalescence of lipid rafts and TEMs, but non-membrane bound Gag cannot

Because Gag associates with each of lipid rafts and TEMs, we next tested whether Gag induces the coalescence of lipid raft and TEM markers in a co-patching assay. Importantly, other HIV-1 proteins, including Env, Nef, Vpu, and Tat, may interact with membrane microdomains. In particular, Nef has been proposed to alter lipid rafts and their constituent lipids and proteins (113-117). In addition, transfection of plasmids by lipofection has been shown to disrupt coxsackievirus entry in a cholesterol-dependent manner (118), and the permissiveness of cells to lipofection correlates with cell surface density of GM1 (119), circumstantial evidence suggesting that cationic liposomes may interact with or disrupt lipid rafts in an unknown manner. To control for the effects of lipofection and expression of other HIV-1 proteins on microdomains, we first measured the co-patching of microdomain markers when cells are transfected with an HIV-1 molecular clone containing multiple mutations that completely abolish Gag membrane binding (1GA/6A2T). This Gag derivative is diffuse in the cytosol and does not form PM puncta, although when performing confocal microscopy focusing on the dorsal surface of cells, the fluorescence signal has a mottled appearance likely due to membrane ruffles and blebs (Figure 4.4, A). In the presence of non-membrane-bound Gag, antibody-patched lipid raft and TEM markers remain largely segregated (Figure 4.4, A). This finding indicates that the effects of other HIV-1 proteins, and effects of lipofection and

other experimental manipulations, are not sufficient to induce lipid raft and TEM coalescence. However, in the presence of Gag with WT membrane binding motifs (WT Gag-YFP), antibody-patched lipid raft and TEM markers are strongly coalesced at Gag puncta (Figure 4.4, B). Importantly, this coalescence of microdomain markers by WT Gag-YFP appears to be specific to lipid raft and TEM markers, because WT Gag-YFP does not appear to coalesce TEMs with a negative control non-raft/non-TEM marker, CD46 (Figure 4.4, C).

To quantify the degree of co-patching, we calculated the correlation between fluorescence intensities of lipid raft and TEM markers over many cells, for each experimental condition (see Methods). In all combinations of lipid raft and TEM markers tested, the correlation between fluorescence intensities of different markers were significantly greater in the presence of WT Gag-YFP than non-membrane bound 1GA/6A2T Gag-YFP (Figure 4.4, D). However, there was no significant difference in correlation between TEM marker CD81 and negative control marker CD46 in the presence of either 1GA/6A2T or WT Gag-YFP (Figure 4.4, D). Altogether, these results indicate that Gag reproducibly induces the coalescence of lipid rafts and TEMs, that other HIV-1 proteins are not sufficient to induce this coalescence, and that Gag membrane binding is necessary for this coalescence.

Gag membrane binding motif substitutions have no effect on association with, and coalescence of, lipid rafts and TEMs

It has been suggested that Gag acylation, or a potential unique mode of $PI(4,5)P_2$ binding involving MA sequestering the saturated 2' acyl chain of $PI(4,5)P_2$, determine

Gag association with lipid rafts (see Introduction). However, this is supported only by indirect evidence. The molecular determinants of Gag association with TEMs are also unknown. To test whether acylation, PI(4,5)P_2 binding, or other functions within the MA domain are molecular determinants of microdomain interaction, we generated a panel of Gag derivatives containing functional substitutions of MA membrane binding motifs.

Fyn(10)fullMA Gag-YFP is acylated, but retains PI(4,5)P_2-binding MA basic residues. This construct is less dependent on PI(4,5)P_2 for membrane binding (11). Fyn(10)ΔMA Gag-YFP is acylated, but has its entire MA domain deleted. This construct does not have any detectable affinity for PI(4,5)P_2 (11). $PH_{PLC\delta1}$delMA Gag-YFP contains a PI(4,5)P_2-binding PH domain, and a substantial deletion removing most of MA. This construct contains no acylation signals. Although each of these constructs have very different modes of membrane binding, each are capable of forming VLPs (unpublished data, 3, 11, 61, 62).

In each experimental condition tested, Gag-YFP with membrane binding motif substitutions induced the coalescence of lipid rafts and TEMs (Figure 4.5, A), similarly to WT Gag-YFP (Figure 4.4). Correlations between microdomain marker fluorescence intensities were measured over many cells, and compared to WT Gag-YFP and negative control 1GA/6A2T Gag-YFP from Figure 4.4 (see Figure 4.5, B). Because co-expressing Tat and Rev *in trans* was necessary to rescue $PH_{PLC\delta1}$delMA Gag-YFP expression (see Methods), we controlled for this difference by also co-expressing WT Gag-YFP with Tat and Rev. Co-expressing Tat and Rev appeared to have no effect on microdomain marker correlations (Figure 4.5, B). Each Gag derivative with membrane binding motif substitutions appeared to coalesce lipid rafts and TEMs similarly to WT Gag-YFP, and

significantly more than non-membrane binding 1GA/6A2T Gag-YFP (Figure 4.5, B). These results indicate that, while Gag membrane binding is necessary (Figure 4.4), the particular mode of membrane binding has no effect on interaction with, and coalescence of lipid rafts and TEMs. Either acylation or $PI(4,5)P_2$ binding are sufficient. Moreover, these results show that other functions within the MA domain, such as acyl chain sequestration or unknown interactions with other host factors, are not necessary, as the entire MA sequence is dispensable.

DISCUSSION

Using a wide variety of methods, previous studies have demonstrated that Gag associates with lipid rafts, and that Gag associates with TEMs, each of which have been proposed to be platforms for HIV-1 assembly. However, other studies have shown that, in the absence of HIV-1, lipid rafts and TEMs are distinct microdomains. Two possible, but not mutually exclusive, models can explain this contradiction:

First, it is possible that individual Gag multimers interact with distinct microdomains bimodally or quantally – interacting with one or another, but not both simultaneously. This "quantal" model is supported by a study that co-expressed HIV-1 Gag, HIV-1 Env glycoprotein, and Ebola glycoprotein (120). The two viral glycoproteins were observed to segregate into distinct microscopic-scale domains in the presence or absence of Gag, and individual VLPs produced by Gag were found to have incorporated either HIV-1 Env glycoprotein or Ebola glycoprotein, but not a mixture of both.

Alternatively, our data support a "coalescence" model in which Gag actively reorganizes the membrane by inducing the coalescence of otherwise distinct microdomain constituents, lipid raft markers and tetraspanin proteins. Thus, rather than taking advantage of pre-existing microdomains organized by cellular factors, Gag itself may function as a microdomain-organizing factor to create a possibly virus-specific class of microdomain.

Recently, Gould *et al* proposed that HIV-1 takes advantage of a pre-existing exosome biogenesis and release pathway for the production of infectious virions (121). Exosomes are small membranous vesicles either produced by budding directly through specialized "endosome-like" microdomains of the PM, or initially generated as intralumenal vesicles of late endosomes/multivesicular bodies (LE/MVB) and then released into the extracellular space by fusion of the LE/MVB with the PM. Virus particles and exosomes share many characteristics, including similar size, involvement of the cellular ESCRT complexes in their biogenesis, and similar lipid and cellular protein constituents. Based on these similarities, Gould *et al* proposed a strong link between retrovirus assembly and exosome biogenesis (122). Using a variety of approaches, including antibody-mediated patching of cell surface proteins, the authors showed that membrane binding plus higher-order multimerization are sufficient for proteins to be targeted to endosome-like PM microdomains and become exosome cargo (121). In light of these findings, Gould *et al* proposed a model in which Gag, as a membrane binding and multimerizing protein, is cargo for the pre-existing exosome pathway, and that virions are exosomes containing infectious viral components (121, 122).

A critical question raised by this "Trojan exosome" model is to what degree do viral components actively hijack and alter cellular machinery for viral purposes, versus passively masquerading as substrate of pre-existing host processes. Though not directly precluded, this model does not require any more complex role for Gag in virion assembly than as a passive substrate. In contrast, we observed differences in membrane microdomain organization in the presence and absence of membrane-bound Gag. Thus, our data favor a more active role for Gag interacting with and altering host membrane systems.

To date, the biophysical underpinnings that govern Gag's association with, and coalescence of lipid rafts and TEMs are not known. It has been suggested that lipid raft formation is at least partially driven by preferential associations between planar cholesterol molecules and saturated acyl chains (2). Thus, it has been suggested that Gag N-terminal myristoylation (a saturated acylation) causes Gag's partitioning into lipid rafts. However, our observation that $PH_{PLC\delta1}$delMA Gag co-patches and coalesces lipid rafts and TEMs as efficiently as wild type Gag shows that myristoylation of Gag is dispensable. Additionally, the ability of Gag to bind $PI(4,5)P_2$ is also dispensable, as Fyn(10)ΔMA Gag, which contains no known $PI(4,5)P_2$-binding motifs, co-patches and coalesces lipid rafts and TEMs as well as wild type Gag.

It is difficult to envision how Gag derivatives using very different molecular interactions with the membrane can all cause the same lipid raft/TEM coalescence. It is intriguing to speculate that a more general membrane phenomenon underlies this coalescence of microdomains – a property or function of the membrane that Gag derivatives can affect regardless of membrane binding mode. It has been proposed that

cellular membranes exist in a metastable state: affinities between membrane components provide a latent propensity or potential for membrane components to partition or compartmentalize (2). Thus, relatively small effects on local membrane dynamics by microdomain organizing proteins may trigger this underlying predisposition for partitioning, amplifying small protein-based signals into larger-scale membrane reorganization. If this model of membrane microdomain function is true, different Gag derivatives may be able to trigger similar membrane reorganization regardless of their mode of membrane binding. In this case, we might predict that many unrelated viruses that assemble on the plasma membrane could induce similar microdomain reorganization.

The ability of Gag to reorganize host membranes may have many important implications for viral fitness: (i) If small Gag multimers induce specialized membrane microdomains that attract subsequent Gag monomers, this cooperative binding could promote Gag multimerization and virion assembly; (ii) Since biophysical studies of artificial membranes have shown relationships between lipid composition and membrane curvature (123), it is conceivable that changes in microdomain composition induced by Gag may contribute to membrane curvature during virus budding; (iii) Gag interaction with membrane microdomains may recruit the HIV-1 envelope glycoproteins, and may underlie the phenomenon of viral pseudotyping by recruiting heterologous viral envelope glycoproteins; (iv) By altering host microdomains, Gag may influence the incorporation of host factors that may directly or indirectly affect viral fitness. For example, it is thought that tetraspanin proteins modulate virus infectivity (73, 74, 124), and lipid rafts may mediate targeting of the antiviral restriction factor tetherin to assembling virions, preventing their release (125, 126); (v) Finally, microdomains appear to be involved in

the formation of cell synapses that mediate direct cell-to-cell virus transmission, which is thought to be the primary mode of virus spread within an infected host. Current work in our laboratory suggests that the rearward flow of PM microdomains may be responsible for the localization of virus assembly to the uropod of polarized T-cells, which is the site of frequent cell-cell contact (127).

In light of these potentially critical roles for microdomains in HIV-1 replication, further investigation is necessary to better define cellular microdomains, identify the molecular determinants by which Gag interacts with these microdomains, and elucidate what impacts these membrane phenomena have on the virus replication cycle.

Table 4.1. Microdomain markers used in this study.

Name	Expression	Membrane Association	Detection Method
Raft Markers			
CD59	Endogenous	GPI anchor	Antibody Patching
NonFP-GPI	Transgene	GPI anchor	Antibody Patching
NonFP-HA-TMD	Transgene	Transmembrane	Antibody Patching
YFP-GPI	Transgene	GPI anchor	Intrinsic Fluorescence
YFP-HA-TMD	Transgene	Transmembrane	Intrinsic Fluorescence
TEM Markers			
CD81	Endogenous	Transmembrane	Antibody Patching
CD9	Endogenous	Transmembrane	Antibody Patching
CD63	Endogenous	Transmembrane	Antibody Patching
YFP-CD81	Transgene	Transmembrane	Intrinsic Fluorescence
YFP-CD9	Transgene	Transmembrane	Intrinsic Fluorescence
YFP-CD63	Transgene	Transmembrane	Intrinsic Fluorescence
Non-TEM / Non-raft Controls			
CD46	Endogenous	Transmembrane	Antibody Patching
DiD		2 octadecyl acyl chains	Intrinsic Fluorescence

Figure 4.1. Distribution of microdomain markers without antibody-mediated patching. YFP-tagged lipid raft markers and TEM markers were each co-expressed with Gag-RFP (see Table 4.1 for a summary of microdomain markers used). In each case, microdomain markers appear widely distributed on the dorsal surface of the cell. In the case of YFP-GPI, YFP-HA-TMD, and YFP-CD81, markers appear to be enriched at Gag-RFP puncta. As a control, cells expressing Gag-YFP were stained with the general membrane dye DiD. DiD does not appear enriched at Gag-YFP puncta. Each image is 12μm x 12μm.

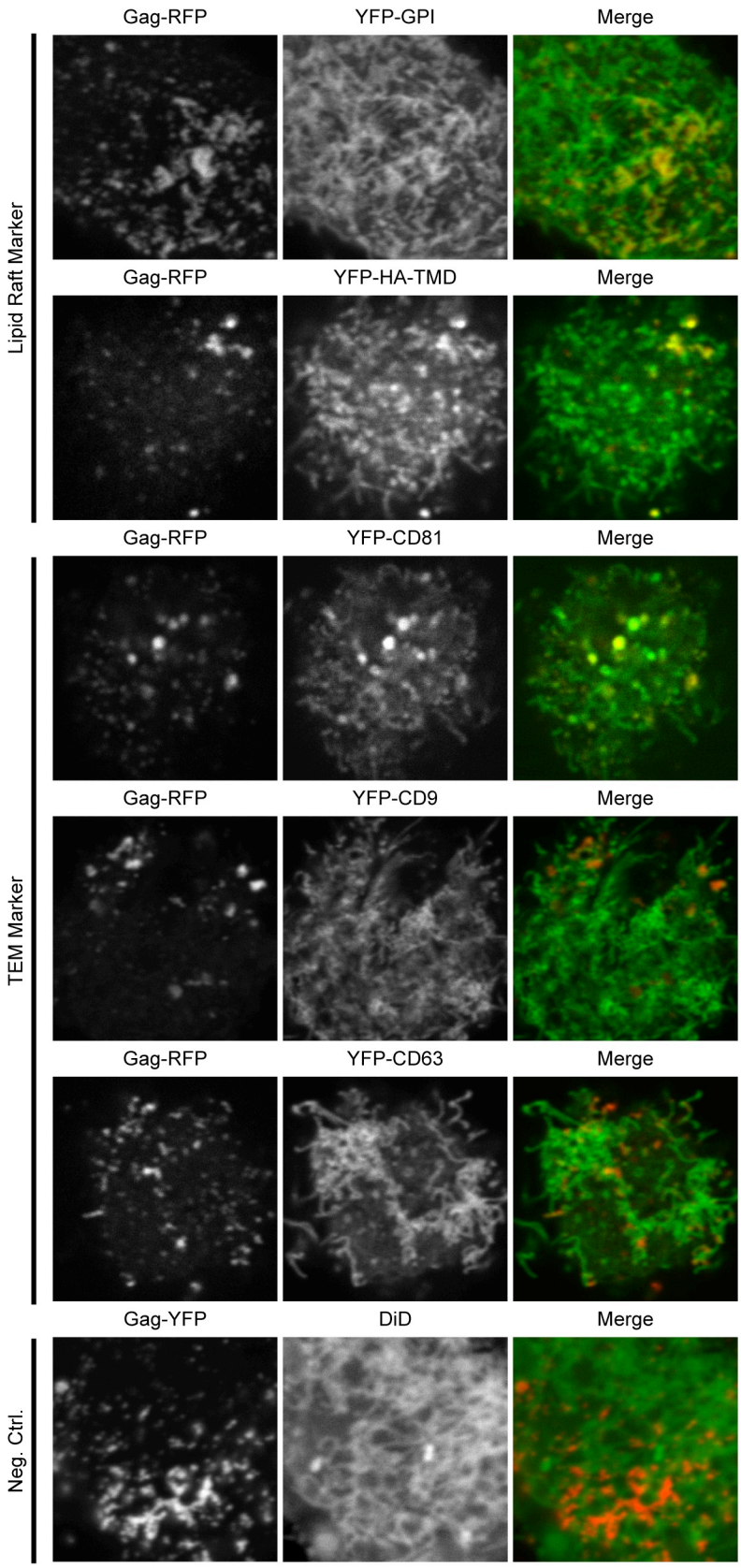

Figure 4.1. Distribution of microdomain markers without antibody-mediated patching

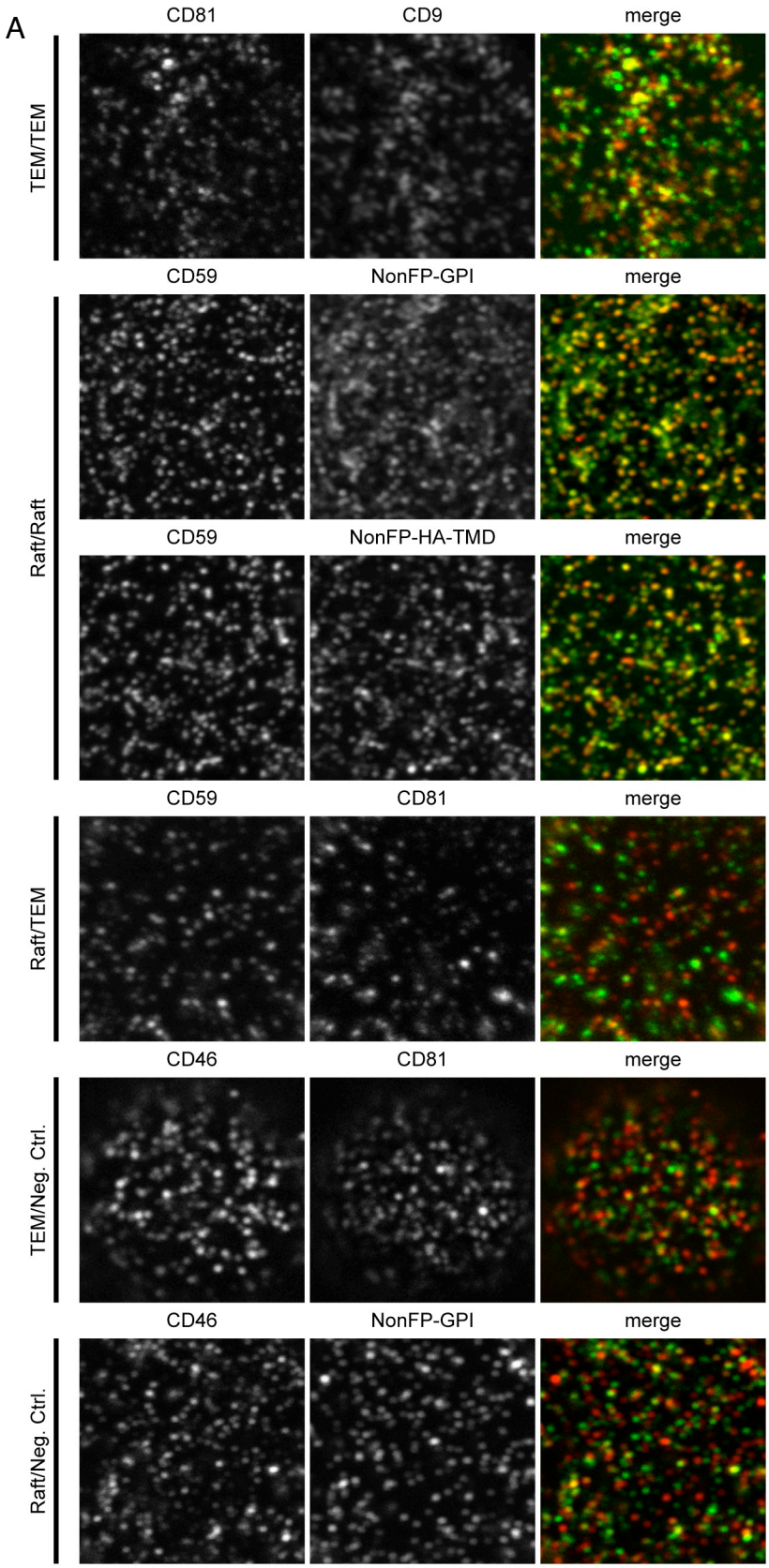
A
CD81
CD9
merge
TEM/TEM
CD59
NonFP-GPI
merge
CD59
NonFP-HA-TMD
merge
Raft/Raft
CD59
CD81
merge
Raft/TEM
CD46
CD81
merge
TEM/Neg. Ctrl.
CD46
NonFP-GPI
merge
Raft/Neg. Ctrl.

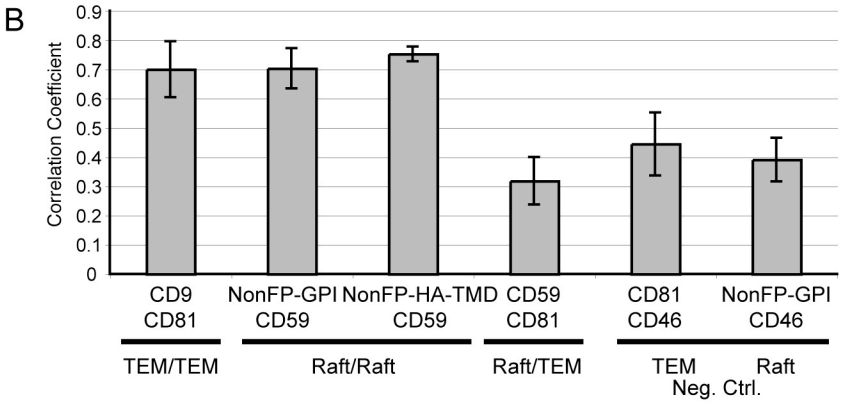

Figure 4.2. Antibody-mediated co-patching assay can distinguish lipid rafts and TEMs. Cells were treated with antibodies to independently induce patching of microdomain markers (see Table 4.1 for a summary of microdomain markers used), and the dorsal surfaces of cells were imaged. **(A)** TEM markers co-patched (first row), lipid raft markers co-patched (rows 2-3), but a lipid raft marker did not co-patch with a TEM marker (row 4). TEM and lipid raft markers also did not co-patch with a negative control non-TEM/non-raft marker (bottom row). **(B)** The correlation between lipid raft and TEM fluorescence intensities were calculated and averaged from 5 cells per condition. Error bars represent ± 1 S.D. Each image is 12μm x 12μm.

Figure 4.3. Gag co-patches with both lipid raft and TEM markers. Cells expressing Gag-YFP and microdomain markers were treated with antibodies to independently induce patching of the microdomain markers (see Table 4.1 for a summary of microdomain markers used). Gag-YFP co-patches with TEM markers (rows 1-3), and lipid raft markers (rows 4-6), but not with a negative control non-TEM/non-raft marker (bottom row). Each image is 12μm x 12μm.

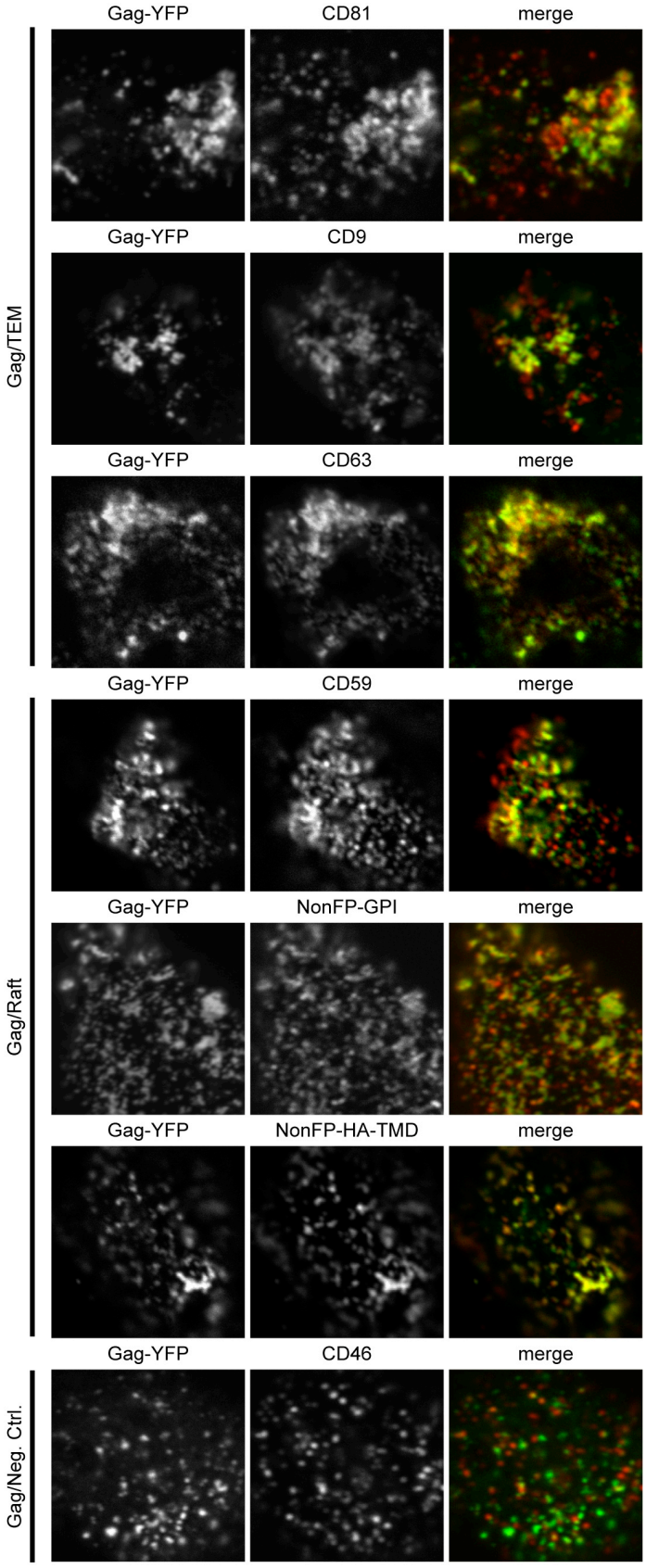

Figure 4.3. Gag co-patches with both lipid raft and TEM markers.

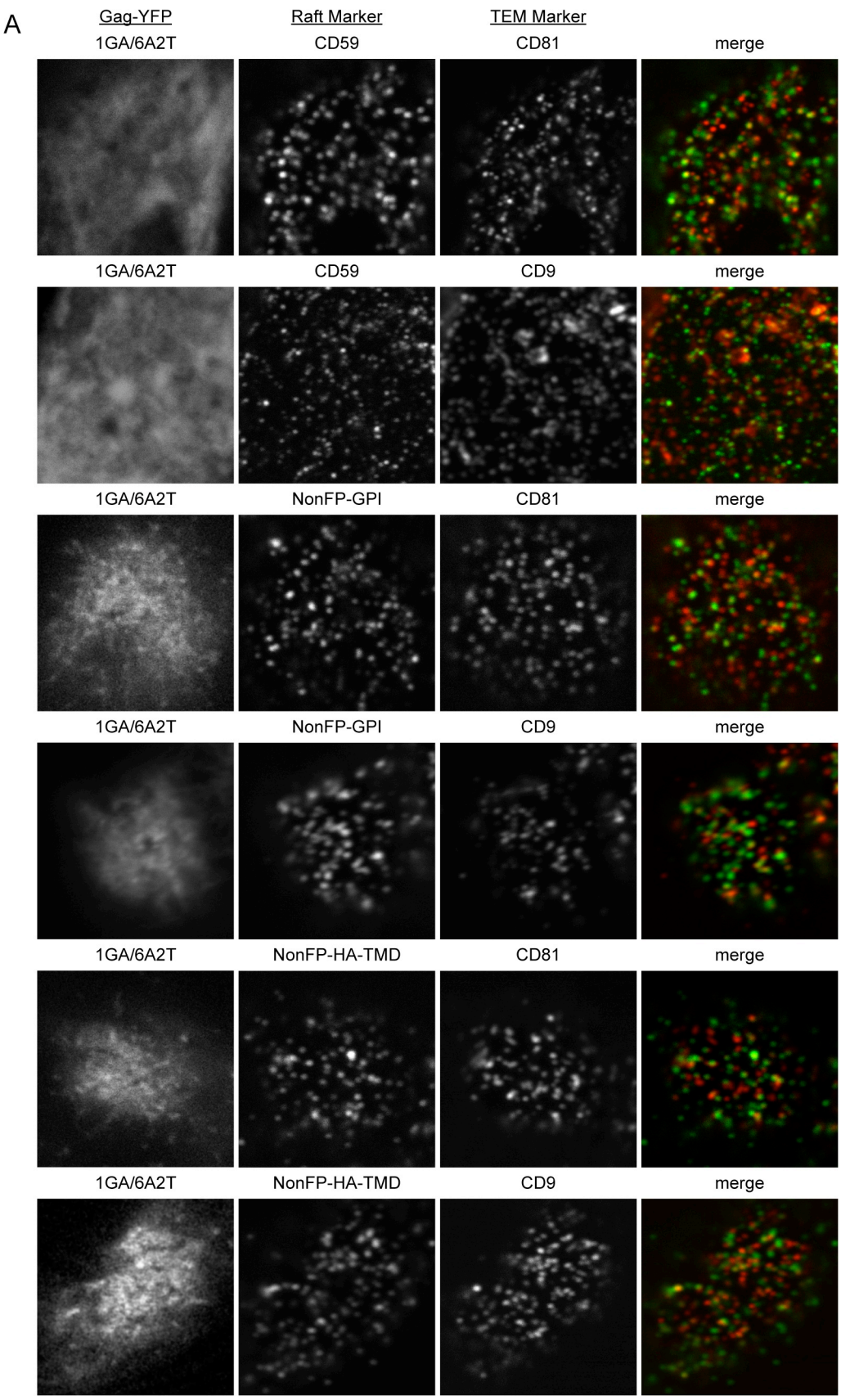
A
Gag-YFP
Raft Marker
TEM Marker
1GA/6A2T
CD59
CD81
merge
1GA/6A2T
CD59
CD9
merge
1GA/6A2T
NonFP-GPI
CD81
merge
1GA/6A2T
NonFP-GPI
CD9
merge
1GA/6A2T
NonFP-HA-TMD
CD81
merge
1GA/6A2T
NonFP-HA-TMD
CD9
merge

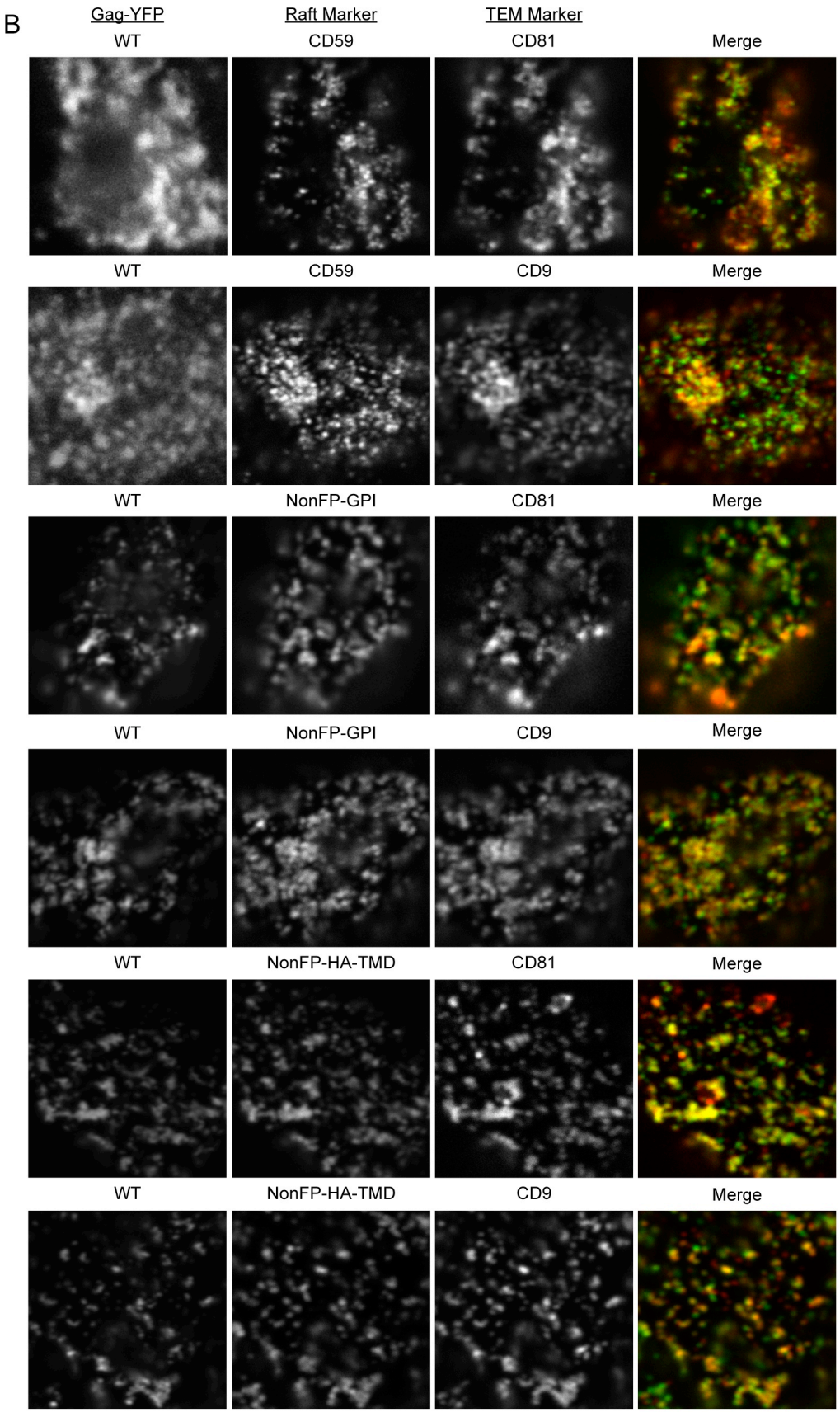
B
Gag-YFP
Raft Marker
TEM Marker
WT
CD59
CD81
Merge
WT
CD59
CD9
Merge
WT
NonFP-GPI
CD81
Merge
WT
NonFP-GPI
CD9
Merge
WT
NonFP-HA-TMD
CD81
Merge
WT
NonFP-HA-TMD
CD9
Merge

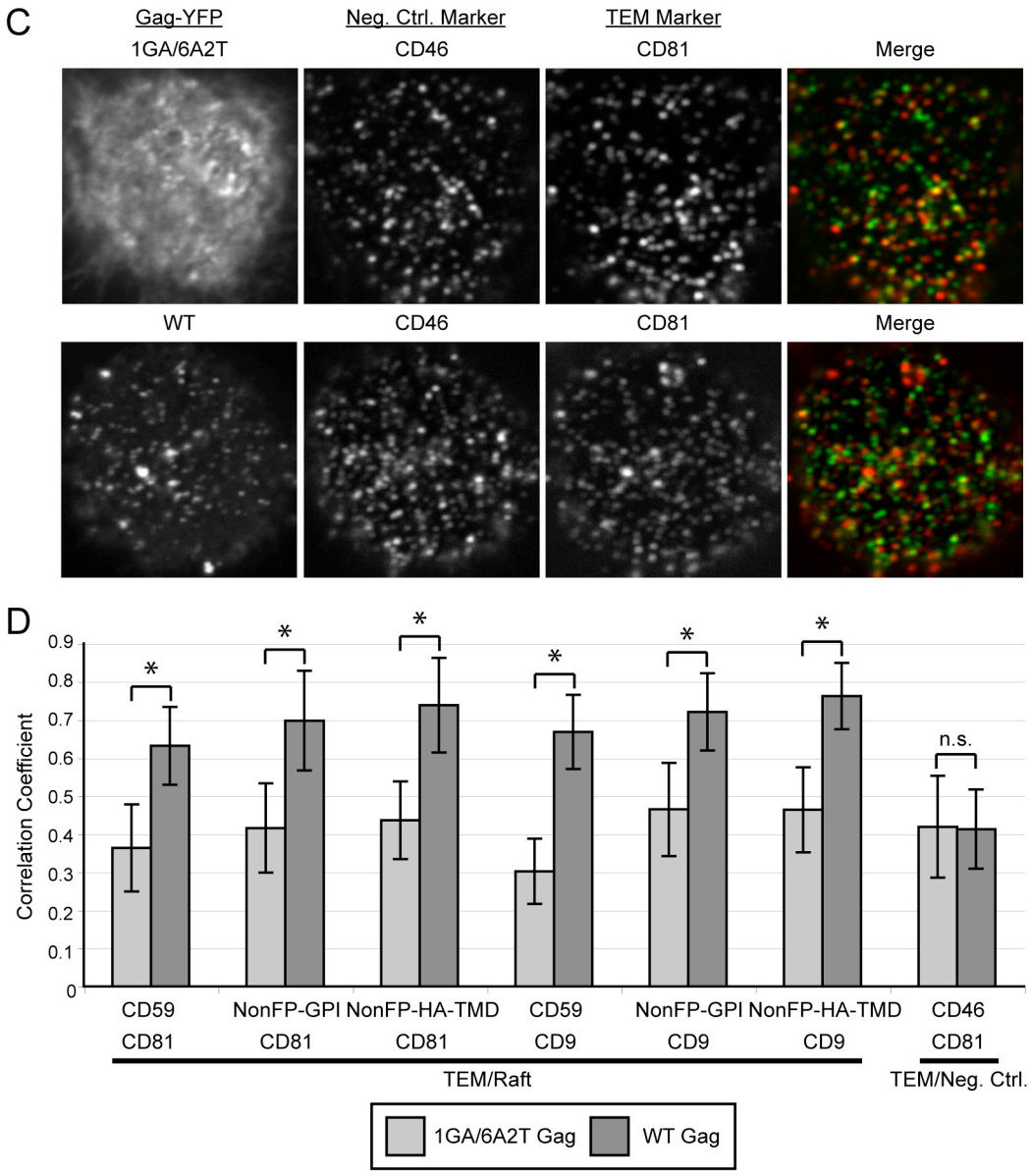

Figure 4.4. Gag induces the coalescence of lipid rafts and TEMs, but non-membrane bound Gag cannot. Cells expressing Gag-YFP derivatives, lipid raft markers, and TEM markers were treated with antibodies to independently induce patching of the microdomain markers (see Table 4.1 for a summary of microdomain markers used). **(A)** In cells expressing a Gag-YFP derivative that is unable to bind membrane (1GA/6A2T), lipid raft and TEM markers segregate. **(B)** In cells expressing WT Gag-YFP, lipid raft and TEM markers coalesce at Gag puncta. **(C)** Neither 1GA/6A2T, nor WT Gag-YFP coalesce a TEM marker with a negative control non-TEM/non-raft marker. Images in panels A, B and C are each 12μm x 12μm. **(D)** The correlation between lipid raft and TEM fluorescence intensities were calculated and averaged from 10-30 cells per condition. Error bars represent ± 1 S.D. *, significantly different ($p < 0.01$).

Figure 4.5. Gag membrane binding motif substitutions have no effect on interaction with microdomains. Cells expressing microdomain markers (see Table 4.1) with Gag-YFP derivatives containing membrane binding motif substitutions were treated with antibodies to independently induce patching of microdomain markers. Fyn(10)fullMA Gag-YFP is acylated and less dependent on $PI(4,5)P_2$. Fyn(10)ΔMA Gag-YFP has a deletion of the entire MA domain, including $PI(4,5)P_2$-binding residues, but is acylated. $PH_{PLC\delta1}$delMA Gag-YFP has a deletion of most of MA, does not contain acylation signals, but contains a $PI(4,5)P_2$-binding domain. **(A)** Lipid raft and TEM markers co-patch at Gag-YFP puncta on the dorsal surface of cells. Each image is 12μm x 12μm. **(B)** The correlation between lipid raft and TEM fluorescence intensities were calculated and averaged from 10-30 cells per condition. Error bars represent ± 1 S.D. *, significantly greater than 1GA/6A2T ($p < 0.01$).

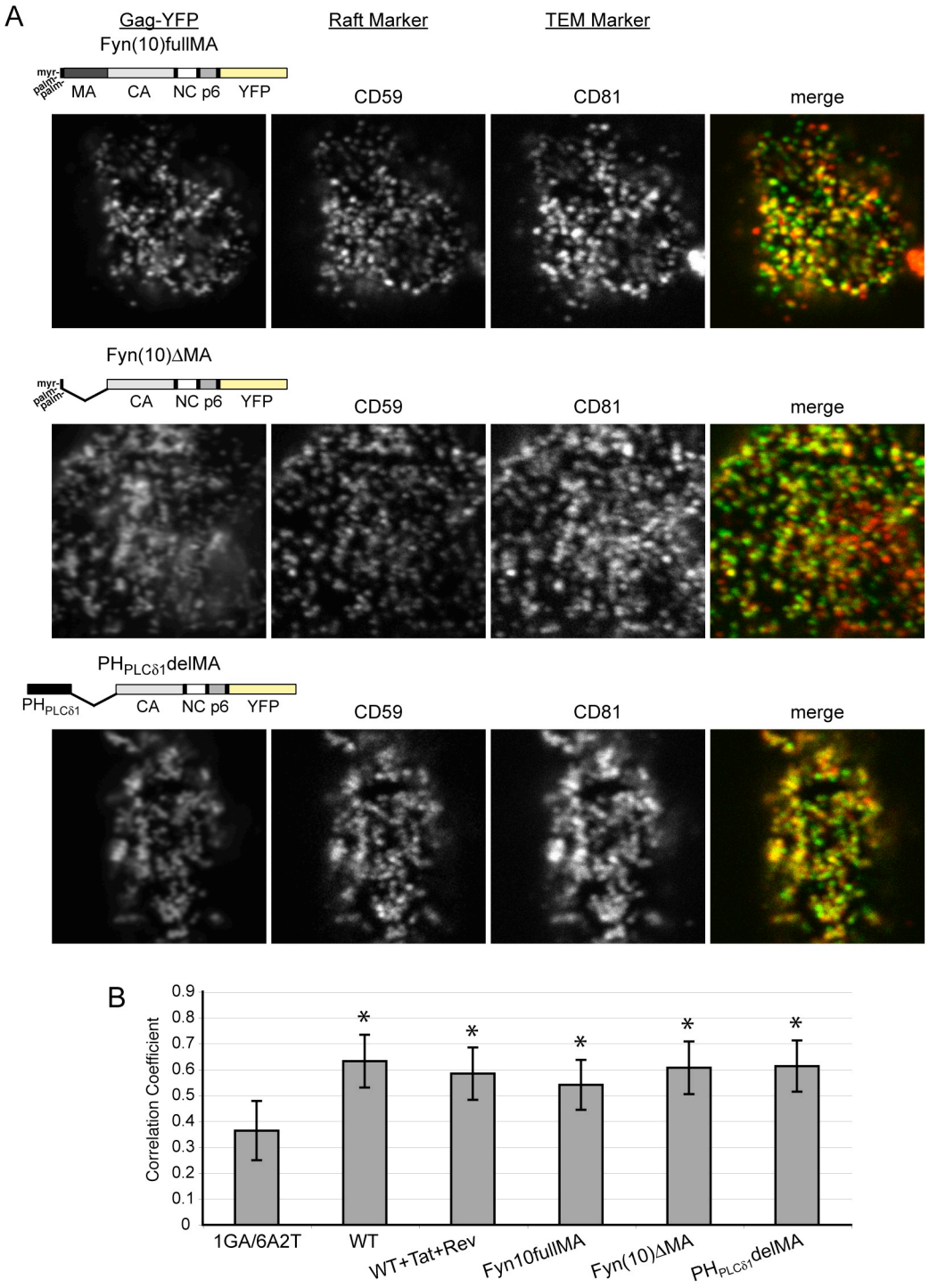

Figure 4.5. Gag membrane binding motif substitutions have no effect on interaction with microdomains.

REFERENCES

1. Coskun, U. and K. Simons, *Membrane rafting: From apical sorting to phase segregation.* FEBS Lett, 2009.

2. Lingwood, D. and K. Simons, *Lipid rafts as a membrane-organizing principle.* Science, 2010. **327**(5961): p. 46-50.

3. Jouvenet, N., et al., *Plasma membrane is the site of productive HIV-1 particle assembly.* PLoS Biol, 2006. **4**(12): p. e435.

4. Gottlinger, H.G., J.G. Sodroski, and W.A. Haseltine, *Role of capsid precursor processing and myristoylation in morphogenesis and infectivity of human immunodeficiency virus type 1.* Proc Natl Acad Sci U S A, 1989. **86**(15): p. 5781-5.

5. Bryant, M. and L. Ratner, *Myristoylation-dependent replication and assembly of human immunodeficiency virus 1.* Proc Natl Acad Sci U S A, 1990. **87**(2): p. 523-7.

6. Zhou, W., et al., *Identification of a membrane-binding domain within the amino-terminal region of human immunodeficiency virus type 1 Gag protein which interacts with acidic phospholipids.* J Virol, 1994. **68**(4): p. 2556-69.

7. Hill, C.P., et al., *Crystal structures of the trimeric human immunodeficiency virus type 1 matrix protein: implications for membrane association and assembly.* Proc Natl Acad Sci U S A, 1996. **93**(7): p. 3099-3104.

8. Saad, J.S., et al., *Structural basis for targeting HIV-1 Gag proteins to the plasma membrane for virus assembly.* Proc Natl Acad Sci U S A, 2006. **103**(30): p. 11364-9.

9. Shkriabai, N., et al., *Interactions of HIV-1 Gag with assembly cofactors.* Biochemistry, 2006. **45**(13): p. 4077-83.

10. Dalton, A.K., et al., *Electrostatic Interactions Drive Membrane Association of the Human Immunodeficiency Virus Type 1 Gag MA Domain.* J Virol, 2007. **81**(12): p. 6434-45.

11. Chukkapalli, V., et al., *Interaction between the human immunodeficiency virus type 1 Gag matrix domain and phosphatidylinositol-(4,5)-bisphosphate is essential for efficient gag membrane binding.* J Virol, 2008. **82**(5): p. 2405-17.

12. Ehrlich, L.S., B.E. Agresta, and C.A. Carter, *Assembly of recombinant human immunodeficiency virus type 1 capsid protein in vitro.* J Virol, 1992. **66**(8): p. 4874-83.

13. Franke, E.K., et al., *Specificity and sequence requirements for interactions between various retroviral Gag proteins.* J Virol, 1994. **68**(8): p. 5300-5.

14. Campbell, S. and V.M. Vogt, *Self-assembly in vitro of purified CA-NC proteins from Rous sarcoma virus and human immunodeficiency virus type 1.* J Virol, 1995. **69**(10): p. 6487-97.

15. Momany, C., et al., *Crystal structure of dimeric HIV-1 capsid protein.* Nat Struct Biol, 1996. **3**(9): p. 763-70.

16. Zhang, W.H., et al., *Gag-Gag interactions in the C-terminal domain of human immunodeficiency virus type 1 p24 capsid antigen are essential for Gag particle assembly.* J Gen Virol, 1996. **77**(4): p. 743-51.

17. Gamble, T.R., et al., *Structure of the carboxyl-terminal dimerization domain of the HIV-1 capsid protein.* Science, 1997. **278**(5339): p. 849-53.

18. Swanstrom, R. and J.W. Wills, *Synthesis, Assembly, and Processing of Viral Proteins*, in *Retroviruses*, J.M. Coffin, S.H. Hughes, and H.E. Varmus, Editors. 1997, Cold Spring Harbor Laboratory Press: New York. p. 263-334.

19. Dawson, L. and X.F. Yu, *The role of nucleocapsid of HIV-1 in virus assembly.* Virology, 1998. **251**(1): p. 141-57.

20. Freed, E.O., *HIV-1 gag proteins: diverse functions in the virus life cycle.* Virology, 1998. **251**(1): p. 1-15.

21. Gross, I., et al., *N-Terminal extension of human immunodeficiency virus capsid protein converts the in vitro assembly phenotype from tubular to spherical particles.* J Virol, 1998. **72**(6): p. 4798-810.

22. Burniston, M.T., et al., *Human immunodeficiency virus type 1 Gag polyprotein multimerization requires the nucleocapsid domain and RNA and is promoted by the capsid-dimer interface and the basic region of matrix protein.* J Virol, 1999. **73**(10): p. 8527-40.

23. Campbell, S. and A. Rein, *In vitro assembly properties of human immunodeficiency virus type 1 Gag protein lacking the p6 domain.* J Virol, 1999. **73**(3): p. 2270-9.

24. Cimarelli, A. and J. Luban, *Human immunodeficiency virus type 1 virion density is not determined by nucleocapsid basic residues.* J Virol, 2000. **74**(15): p. 6734-40.

25. Sandefur, S., et al., *Mapping and characterization of the N-terminal I domain of human immunodeficiency virus type 1 Pr55(Gag).* J Virol, 2000. **74**(16): p. 7238-49.

26. Adamson, C.S. and I.M. Jones, *The molecular basis of HIV capsid assembly--five years of progress.* Rev Med Virol, 2004. **14**(2): p. 107-21.

27. Huseby, D., et al., *Assembly of human immunodeficiency virus precursor gag proteins.* J Biol Chem, 2005. **280**(18): p. 17664-70.

28. Li, H., et al., *Myristoylation is required for human immunodeficiency virus type 1 Gag-Gag multimerization in mammalian cells.* J Virol, 2007. **81**(23): p. 12899-910.

29. Hogue, I.B., A. Hoppe, and A. Ono, *Quantitative fluorescence resonance energy transfer microscopy analysis of the human immunodeficiency virus type 1 Gag-Gag interaction: relative contributions of the CA and NC domains and membrane binding.* J Virol, 2009. **83**(14): p. 7322-36.

30. von Schwedler, U.K., et al., *Functional surfaces of the human immunodeficiency virus type 1 capsid protein.* J Virol, 2003. **77**(9): p. 5439-50.

31. Ono, A., et al., *Association of human immunodeficiency virus type 1 gag with membrane does not require highly basic sequences in the nucleocapsid: use of a novel Gag multimerization assay.* J Virol, 2005. **79**(22): p. 14131-40.

32. Joshi, A., K. Nagashima, and E.O. Freed, *Mutation of dileucine-like motifs in the human immunodeficiency virus type 1 capsid disrupts virus assembly, gag-gag interactions, gag-membrane binding, and virion maturation.* J Virol, 2006. **80**(16): p. 7939-51.

33. Cimarelli, A., et al., *Basic residues in human immunodeficiency virus type 1 nucleocapsid promote virion assembly via interaction with RNA.* J Virol, 2000. **74**(7): p. 3046-57.

34. Muriaux, D., et al., *RNA is a structural element in retrovirus particles.* Proc Natl Acad Sci U S A, 2001. **98**(9): p. 5246-51.

35. Khorchid, A., et al., *Role of RNA in facilitating Gag/Gag-Pol interaction.* J Virol, 2002. **76**(8): p. 4131-7.

36. Chu, H., J.J. Wang, and P. Spearman, *Human immunodeficiency virus type-1 gag and host vesicular trafficking pathways.* Curr Top Microbiol Immunol, 2009. **339**: p. 67-84.

37. Ono, A., *HIV-1 Assembly at the Plasma Membrane: Gag Trafficking and Localization.* Future Virol, 2009. **4**(3): p. 241-257.

38. Thali, M., *The Roles of Tetraspanins in HIV-1 Replication.* Curr Top Microbiol Immunol, 2009. **339**: p. 85-102.

39. Waheed, A.A. and E.O. Freed, *Lipids and membrane microdomains in HIV-1 replication.* Virus Res, 2009. **143**(2): p. 162-76.

40. Aloia, R.C., H. Tian, and F.C. Jensen, *Lipid composition and fluidity of the human immunodeficiency virus envelope and host cell plasma membranes.* Proc Natl Acad Sci U S A, 1993. **90**(11): p. 5181-5.

41. Saifuddin, M., et al., *Role of virion-associated glycosylphosphatidylinositol-linked proteins CD55 and CD59 in complement resistance of cell line-derived and primary isolates of HIV-1.* J Exp Med, 1995. **182**(2): p. 501-9.

42. Nakamura, M., et al., *Quantification of the CD55 and CD59, membrane inhibitors of complement on HIV-1 particles as a function of complement-mediated virolysis.* Microbiol Immunol, 1996. **40**(8): p. 561-7.

43. Graham, D.R., et al., *Cholesterol depletion of human immunodeficiency virus type 1 and simian immunodeficiency virus with beta-cyclodextrin inactivates and permeabilizes the virions: evidence for virion-associated lipid rafts.* J Virol, 2003. **77**(15): p. 8237-48.

44. Brugger, B., et al., *The HIV lipidome: a raft with an unusual composition.* Proc Natl Acad Sci U S A, 2006. **103**(8): p. 2641-6.

45. Chertova, E., et al., *Proteomic and biochemical analysis of purified human immunodeficiency virus type 1 produced from infected monocyte-derived macrophages.* J Virol, 2006. **80**(18): p. 9039-52.

46. Chan, R., et al., *Retroviruses human immunodeficiency virus and murine leukemia virus are enriched in phosphoinositides.* J Virol, 2008. **82**(22): p. 11228-38.

47. Ott, D.E., *Cellular proteins detected in HIV-1.* Rev Med Virol, 2008. **18**(3): p. 159-75.

48. Nguyen, D.H. and J.E. Hildreth, *Evidence for budding of human immunodeficiency virus type 1 selectively from glycolipid-enriched membrane lipid rafts.* J Virol, 2000. **74**(7): p. 3264-72.

49. Holm, K., et al., *Human immunodeficiency virus type 1 assembly and lipid rafts: Pr55(gag) associates with membrane domains that are largely resistant to Brij98 but sensitive to Triton X-100.* J Virol, 2003. **77**(8): p. 4805-17.

50. Ono, A. and E.O. Freed, *Role of lipid rafts in virus replication.* Adv Virus Res, 2005. **64**: p. 311-58.

51. Lindwasser, O.W. and M.D. Resh, *Multimerization of human immunodeficiency virus type 1 Gag promotes its localization to barges, raft-like membrane microdomains.* J Virol, 2001. **75**(17): p. 7913-24.

52. Ono, A. and E.O. Freed, *Plasma membrane rafts play a critical role in HIV-1 assembly and release.* Proc Natl Acad Sci U S A, 2001. **98**(24): p. 13925-30.

53. Lindwasser, O.W. and M.D. Resh, *Myristoylation as a target for inhibiting HIV assembly: unsaturated fatty acids block viral budding.* Proc Natl Acad Sci U S A, 2002. **99**(20): p. 13037-42.

54. Ding, L., et al., *Independent segregation of human immunodeficiency virus type 1 Gag protein complexes and lipid rafts.* J Virol, 2003. **77**(3): p. 1916-26.

55. Halwani, R., et al., *Rapid localization of Gag/GagPol complexes to detergent-resistant membrane during the assembly of human immunodeficiency virus type 1.* J Virol, 2003. **77**(7): p. 3973-84.

56. Bhattacharya, J., A. Repik, and P.R. Clapham, *Gag regulates association of human immunodeficiency virus type 1 envelope with detergent-resistant membranes.* J Virol, 2006. **80**(11): p. 5292-300.

57. Dou, J., et al., *Characterization of a myristoylated, monomeric HIV Gag protein.* Virology, 2009. **387**(2): p. 341-52.

58. Pickl, W.F., F.X. Pimentel-Muinos, and B. Seed, *Lipid rafts and pseudotyping.* J Virol, 2001. **75**(15): p. 7175-83.

59. Gomez, C.Y. and T.J. Hope, *Mobility of human immunodeficiency virus type 1 Pr55Gag in living cells.* J Virol, 2006. **80**(17): p. 8796-806.

60. Ono, A., A.A. Waheed, and E.O. Freed, *Depletion of cellular cholesterol inhibits membrane binding and higher-order multimerization of human immunodeficiency virus type 1 Gag.* Virology, 2007. **360**(1): p. 27-35.

61. Scholz, I., et al., *Analysis of human immunodeficiency virus matrix domain replacements.* Virology, 2008. **371**(2): p. 322-35.

62. Urano, E., et al., *Substitution of the myristoylation signal of human immunodeficiency virus type 1 Pr55Gag with the phospholipase C-delta1 pleckstrin homology domain results in infectious pseudovirion production.* J Gen Virol, 2008. **89**(12): p. 3144-9.

63. Charrin, S., et al., *Lateral organization of membrane proteins: tetraspanins spin their web.* Biochem J, 2009. **420**(2): p. 133-54.

64. Yanez-Mo, M., et al., *Tetraspanin-enriched microdomains: a functional unit in cell plasma membranes.* Trends Cell Biol, 2009. **19**(9): p. 434-46.

65. Meerloo, T., et al., *Modulation of cell surface molecules during HIV-1 infection of H9 cells. An immunoelectron microscopic study.* AIDS, 1992. **6**(10): p. 1105-16.

66. Meerloo, T., et al., *Host cell membrane proteins on human immunodeficiency virus type 1 after in vitro infection of H9 cells and blood mononuclear cells. An immuno-electron microscopic study.* J Gen Virol, 1993. **74**(1): p. 129-35.

67. Orentas, R.J. and J.E. Hildreth, *Association of host cell surface adhesion receptors and other membrane proteins with HIV and SIV.* AIDS Res Hum Retroviruses, 1993. **9**(11): p. 1157-65.

68. Gluschankof, P., et al., *Cell membrane vesicles are a major contaminant of gradient-enriched human immunodeficiency virus type-1 preparations.* Virology, 1997. **230**(1): p. 125-33.

69. Nguyen, D.G., et al., *Evidence that HIV budding in primary macrophages occurs through the exosome release pathway.* J Biol Chem, 2003. **278**(52): p. 52347-52354.

70. Nydegger, S., et al., *HIV-1 egress is gated through late endosomal membranes.* Traffic, 2003. **4**(12): p. 902-10.

71. Pelchen-Matthews, A., B. Kramer, and M. Marsh, *Infectious HIV-1 assembles in late endosomes in primary macrophages.* J Cell Biol, 2003. **162**(3): p. 443-455.

72. Khurana, S., et al., *Human immunodeficiency virus type 1 and influenza virus exit via different membrane microdomains.* J Virol, 2007. **81**(22): p. 12630-40.

73. Sato, K., et al., *Modulation of human immunodeficiency virus type 1 infectivity through incorporation of tetraspanin proteins.* J Virol, 2008. **82**(2): p. 1021-33.

74. Grigorov, B., et al., *A role for CD81 on the late steps of HIV-1 replication in a chronically infected T cell line.* Retrovirology, 2009. **6**: p. 28.

75. Booth, A.M., et al., *Exosomes and HIV Gag bud from endosome-like domains of the T cell plasma membrane.* J Cell Biol, 2006. **172**(6): p. 923-35.

76. Grigorov, B., et al., *Assembly of infectious HIV-1 in human epithelial and T-lymphoblastic cell lines.* J Mol Biol, 2006. **359**(4): p. 848-62.

77. Nydegger, S., et al., *Mapping of tetraspanin-enriched microdomains that can function as gateways for HIV-1.* J Cell Biol, 2006. **173**(5): p. 795-807.

78. Deneka, M., et al., *In macrophages, HIV-1 assembles into an intracellular plasma membrane domain containing the tetraspanins CD81, CD9, and CD53.* J Cell Biol, 2007. **177**(2): p. 329-41.

79. Jolly, C. and Q.J. Sattentau, *Human immunodeficiency virus type 1 assembly, budding, and cell-cell spread in T cells take place in tetraspanin-enriched plasma membrane domains.* J Virol, 2007. **81**(15): p. 7873-84.

80. Welsch, S., et al., *HIV-1 Buds Predominantly at the Plasma Membrane of Primary Human Macrophages.* PLoS Pathog, 2007. **3**(3): p. e36.

81. Garcia, E., D.S. Nikolic, and V. Piguet, *HIV-1 replication in dendritic cells occurs through a tetraspanin-containing compartment enriched in AP-3.* Traffic, 2008. **9**(2): p. 200-14.

82. Turville, S.G., et al., *Resolution of de novo HIV production and trafficking in immature dendritic cells.* Nat Methods, 2008. **5**(1): p. 75-85.

83. Berditchevski, F., et al., *A novel link between integrins, transmembrane-4 superfamily proteins (CD63 and CD81), and phosphatidylinositol 4-kinase.* J Biol Chem, 1997. **272**(5): p. 2595-8.

84. Claas, C., C.S. Stipp, and M.E. Hemler, *Evaluation of prototype transmembrane 4 superfamily protein complexes and their relation to lipid rafts.* J Biol Chem, 2001. **276**(11): p. 7974-84.

85. Charrin, S., et al., *Differential stability of tetraspanin/tetraspanin interactions: role of palmitoylation.* FEBS Lett, 2002. **516**(1-3): p. 139-44.

86. Charrin, S., et al., *EWI-2 is a new component of the tetraspanin web in hepatocytes and lymphoid cells.* Biochem J, 2003. **373**(Pt 2): p. 409-21.

87. Charrin, S., et al., *Multiple levels of interactions within the tetraspanin web.* Biochem Biophys Res Commun, 2003. **304**(1): p. 107-12.

88. Yang, X., et al., *Palmitoylation supports assembly and function of integrin-tetraspanin complexes.* J Cell Biol, 2004. **167**(6): p. 1231-40.

89. Andre, M., et al., *Proteomic analysis of the tetraspanin web using LC-ESI-MS/MS and MALDI-FTICR-MS.* Proteomics, 2006. **6**(5): p. 1437-49.

90. Le Naour, F., et al., *Profiling of the tetraspanin web of human colon cancer cells.* Mol Cell Proteomics, 2006. **5**(5): p. 845-57.

91. Barreiro, O., et al., *Endothelial adhesion receptors are recruited to adherent leukocytes by inclusion in preformed tetraspanin nanoplatforms.* J Cell Biol, 2008. **183**(3): p. 527-42.

92. Espenel, C., et al., *Single-molecule analysis of CD9 dynamics and partitioning reveals multiple modes of interaction in the tetraspanin web.* J Cell Biol, 2008. **182**(4): p. 765-76.

93. Langhorst, M.F., A. Reuter, and C.A. Stuermer, *Scaffolding microdomains and beyond: the function of reggie/flotillin proteins.* Cell Mol Life Sci, 2005. **62**(19-20): p. 2228-40.

94. Cerottini, J.C. and K.T. Brunner, *Localization of mouse isoantigens on the cell surface as revealed by immunofluorescence.* Immunology, 1967. **13**(4): p. 395-403.

95. Taylor, R.B., et al., *Redistribution and pinocytosis of lymphocyte surface immunoglobulin molecules induced by anti-immunoglobulin antibody.* Nat New Biol, 1971. **233**: p. 225-9.

96. Revesz, T. and M. Greaves, *Ligand-induced redistribution of lymphocyte membrane ganglioside GM1.* Nature, 1975. **257**(5522): p. 103-6.

97. Spiegel, S., et al., *Direct visualization of redistribution and capping of fluorescent gangliosides on lymphocytes.* J Cell Biol, 1984. **99**(5): p. 1575-81.

98. Mayor, S., K.G. Rothberg, and F.R. Maxfield, *Sequestration of GPI-anchored proteins in caveolae triggered by cross-linking.* Science, 1994. **264**(5167): p. 1948-51.

99. Harder, T., et al., *Lipid domain structure of the plasma membrane revealed by patching of membrane components.* J Cell Biol, 1998. **141**(4): p. 929-42.

100. Freed, E.O., et al., *Single amino acid changes in the human immunodeficiency virus type 1 matrix protein block virus particle production.* J Virol, 1994. **68**(8): p. 5311-5320.

101. Chukkapalli, V., S.J. Oh, and A. Ono, *Opposing mechanisms involving RNA and lipids regulate HIV-1 Gag membrane binding through the highly basic region of the matrix domain.* Proc Natl Acad Sci U S A, 2010. **107**(4): p. 1600-5.

102. Varnai, P. and T. Balla, *Visualization of phosphoinositides that bind pleckstrin homology domains: calcium- and agonist-induced dynamic changes and relationship to myo-[3H]inositol-labeled phosphoinositide pools.* J Cell Biol, 1998. **143**(2): p. 501-10.

103. Kamen, L.A., et al., *SHIP-1 increases early oxidative burst and regulates phagosome maturation in macrophages.* J Immunol, 2008. **180**(11): p. 7497-505.

104. Ott, M., et al., *Acetylation of the HIV-1 Tat protein by p300 is important for its transcriptional activity.* Curr Biol, 1999. **9**(24): p. 1489-92.

105. Hoppe, A., K. Christensen, and J.A. Swanson, *Fluorescence resonance energy transfer-based stoichiometry in living cells.* Biophys J, 2002. **83**(6): p. 3652-64.

106. Koushik, S.V., et al., *Cerulean, Venus, and VenusY67C FRET reference standards.* Biophys J, 2006. **91**(12): p. L99-L101.

107. Zacharias, D.A., et al., *Partitioning of lipid-modified monomeric GFPs into membrane microdomains of live cells.* Science, 2002. **296**(5569): p. 913-6.

108. Keller, P., et al., *Multicolour imaging of post-Golgi sorting and trafficking in live cells.* Nat Cell Biol, 2001. **3**(2): p. 140-9.

109. Scolari, S., et al., *Lateral distribution of the transmembrane domain of influenza virus hemagglutinin revealed by time-resolved fluorescence imaging.* J Biol Chem, 2009. **284**(23): p. 15708-16.

110. Blott, E.J., et al., *Fas ligand is targeted to secretory lysosomes via a proline-rich domain in its cytoplasmic tail.* J Cell Sci, 2001. **114**(Pt 13): p. 2405-16.

111. Gordon-Alonso, M., et al., *Tetraspanins CD9 and CD81 modulate HIV-1-induced membrane fusion.* J Immunol, 2006. **177**(8): p. 5129-37.

112. Bolte, S. and F.P. Cordelieres, *A guided tour into subcellular colocalization analysis in light microscopy.* J Microsc, 2006. **224**(Pt 3): p. 213-32.

113. Alexander, M., et al., *Human immunodeficiency virus type 1 Nef associates with lipid rafts to downmodulate cell surface CD4 and class I major histocompatibility complex expression and to increase viral infectivity.* J Virol, 2004. **78**(4): p. 1685-96.

114. Nobile, C., et al., *HIV-1 Nef inhibits ruffles, induces filopodia, and modulates migration of infected lymphocytes.* J Virol, 2010. **84**(5): p. 2282-93.

115. Simmons, A., et al., *Nef-mediated lipid raft exclusion of UbcH7 inhibits Cbl activity in T cells to positively regulate signaling.* Immunity, 2005. **23**(6): p. 621-34.

116. Zheng, Y.H., et al., *Nef increases the synthesis of and transports cholesterol to lipid rafts and HIV-1 progeny virions.* Proc Natl Acad Sci U S A, 2003. **100**(14): p. 8460-5.

117. Zheng, Y.H., et al., *Nef increases infectivity of HIV via lipid rafts.* Curr Biol, 2001. **11**(11): p. 875-9.

118. Wong, J., et al., *Liposome-mediated transient transfection reduces cholesterol-dependent coxsackievirus infectivity.* J Virol Methods, 2006. **133**(2): p. 211-8.

119. Kovacs, T., et al., *The density of GM1-enriched lipid rafts correlates inversely with the efficiency of transfection mediated by cationic liposomes.* Cytometry A, 2009. **75**(8): p. 650-7.

120. Leung, K., et al., *HIV-1 assembly: viral glycoproteins segregate quantally to lipid rafts that associate individually with HIV-1 capsids and virions.* Cell Host Microbe, 2008. **3**(5): p. 285-92.

121. Fang, Y., et al., *Higher-order oligomerization targets plasma membrane proteins and HIV gag to exosomes.* PLoS Biol, 2007. **5**(6): p. e158.

122. Gould, S.J., A.M. Booth, and J.E. Hildreth, *The Trojan exosome hypothesis.* Proc Natl Acad Sci U S A, 2003. **100**(19): p. 10592-7.

123. Roux, A., et al., *Role of curvature and phase transition in lipid sorting and fission of membrane tubules.* Embo J, 2005. **24**(8): p. 1537-45.

124. Krementsov, D.N., et al., *Tetraspanins regulate cell-to-cell transmission of HIV-1.* Retrovirology, 2009. **6**: p. 64.

125. Kupzig, S., et al., *Bst-2/HM1.24 is a raft-associated apical membrane protein with an unusual topology.* Traffic, 2003. **4**(10): p. 694-709.

126. Rollason, R., et al., *Clathrin-mediated endocytosis of a lipid-raft-associated protein is mediated through a dual tyrosine motif.* J Cell Sci, 2007. **120**(Pt 21): p. 3850-8.

127. Llewellyn, G.N., et al., *Nucleocapsid-Dependent Localization of HIV-1 Gag to Uropods in Polarized T Cells Facilitates Cell-to-Cell Transmission.* Manuscript in preparation, 2010.

CHAPTER V

Discussion

SUMMARY OF RESULTS

In more than 25 years since its discovery, HIV-1 has become one of the most studied human pathogens. As such, much is known about the molecular biology of HIV-1 assembly, including major host and viral factors, and major molecular mechanisms that drive assembly (reviewed in Chapter I). However, HIV-1 assembly is a complex process involving functionally interdependent molecular mechanisms. The work presented in this dissertation focuses on unraveling the interrelationships between membrane binding, microdomain distribution, and multimerization of Gag that lead to assembly of HIV-1 virus particles.

In Chapter III, I investigated the relative contributions of Gag multimerization motifs and their relationships with membrane binding. Previous studies using reverse genetics, biochemical, and structural biology approaches have identified the major functional motifs within Gag that mediate multimerization: a protein-protein dimerization interface in the C-terminal domain of CA, and basic residues in the NC domain that bind RNA as a scaffold. Similar studies also identified host factors and functional motifs in Gag that mediate membrane binding: N-terminal myristoylation, and basic residues in

MA that bind the phospholipid $PI(4,5)P_2$.

However, because assembly is driven by multiple interrelated mechanisms, experimentally manipulating Gag, or its milieu, has multiple confounding effects. Previous studies that identified Gag functional motifs have largely been unable to distinguish these multiple effects. For example, purified biochemical assays typically measured Gag multimerization in the absence of relevant host factors like cellular membranes. To overcome these limitations, I established a FRET assay for Gag multimerization in cells that, combined with a reverse genetics approach, allowed me to study the interrelated functions of Gag multimerization and membrane binding.

In the context of native MA membrane binding motifs, the CA dimerization interface was necessary to observe Gag multimerization by FRET. I also observed evidence of the formation of a CA "half-interface" predicted by structural and biochemical studies of CA, suggesting that the authentic dimerization interface formed by full-length Gag in cells is the same as that previously observed under non-physiological conditions. In contrast to CA, NC multimerization motifs were partially dispensable.

However, while CA and NC mutations directly affect Gag multimerization, these mutations also affect Gag membrane binding to varying degrees, which, in turn has secondary effects on multimerization. To control for this secondary effect via membrane binding, I altered MA membrane binding motifs to disrupt membrane binding, or make membrane binding constitutive and enhanced. Measuring the ability of these derivatives to multimerize with wild-type Gag by FRET, I showed that the CA dimerization interface is still essential, regardless of membrane binding. However, the phenotype of NC mutants varied with changes in MA membrane binding motifs: with membrane binding disrupted,

NC was essential to detect multimerization; with native membrane binding motifs, NC was partially dispensable; and, with constitutively enhanced membrane binding, NC was completely dispensable. These results are consistent with a model in which NC binding to RNA and MA binding to membrane play mechanistically similar roles, i.e. RNA and membrane may both serve as scaffolds to promote multimerization.

Having demonstrated the importance of membrane binding in Gag multimerization, in Chapter IV, I investigated the relationship between different membrane microdomains during Gag assembly. Previous studies have proposed that either lipid rafts or TEMs are platforms for HIV-1 assembly, although they are thought to be distinct microdomains in the absence of HIV-1. Due to technical limitations that make visualization of small and dynamic microdomains difficult, I took advantage of a well-established antibody-mediated co-patching assay to coalesce and stabilize microdomains into microscopically visible membrane patches. To clarify the relationships between these microdomains during HIV-1 assembly, I measured the degree to which independently antibody-clustered microdomain markers associate with each other in the presence or absence of membrane-bound Gag. Various combinations of lipid raft and TEM markers co-patched to a greater extent in the presence of membrane-bound Gag, suggesting that Gag induces the coalescence of lipid rafts and TEMs. To determine whether the mode of Gag membrane binding plays a role in microdomain association and coalescence, I measured the co-patching of microdomain markers in the presence of Gag derivatives with various membrane binding motif substitutions. While Gag membrane binding is necessary to induce coalescence of lipid rafts and TEMs, either acylation of Gag or ability to bind $PI(4,5)P_2$ are sufficient.

Ongoing efforts aim to establish alternative methods to study Gag microdomain distribution that do not require antibody-mediated patching. These methods include backscattered electron detection of immunogold, or measuring FRET between fluorescent protein-tagged microdomain markers (see Chapter II).

FUTURE DIRECTIONS

Just as Gag membrane binding and multimerization are interrelated functions during HIV-1 assembly, it is likely that microdomain distribution is related to the other functions of Gag during assembly. Future directions include determining the relationships between microdomains and Gag multimerization, membrane curvature/budding, interaction with the host cytoskeleton, inhibition of particle release by the cellular restriction factor tetherin, and cell-to-cell virus transmission. Unraveling the molecular details of these relationships may provide new targets for the development of antiretroviral drugs.

Microdomains and Gag Multimerization

Many proteins that organize membranes for cellular functions, such as reggie/flotillin, tetraspanins, clathrin, and caveolin, do so as oligomeric complexes (1). Similarly, multimerization of Gag may be essential for its interaction with membrane microdomains. Alternatively, microdomain association may promote Gag multimerization by laterally clustering membrane-bound Gag monomers. Further, if small Gag multimers induce specialized membrane microdomains that attract subsequent

Gag monomers, this positive feedback, or cooperativity, may strongly drive Gag multimerization.

The relationship between multimerization and microdomain association is difficult to examine, because, as shown in Chapter III, mutations that disrupt Gag multimerization also reduce overall membrane binding. This membrane-binding defect can be overcome using heterologous membrane binding motifs, but these motifs may themselves alter the microdomain association of Gag. The results presented in Chapter IV suggest this may not be a problem, since Gag derivatives with very different membrane binding motifs were still capable of interacting with and reorganizing microdomains. Therefore, one future direction involves testing Gag derivatives with both membrane binding motif substitutions and multimerization motif mutations, to determine whether multimerization is necessary for microdomain association.

Microdomains and Budding

Biophysical studies of artificial membranes have shown that some mixtures of lipids inherently favor membrane curvature, and that lipid sorting and phase separation can be induced by mechanically applying curvature to membranes (2). It is therefore conceivable that there are relationships between microdomain composition and membrane curvature during virus budding. For example, if Gag recruits or reorganizes microdomains at the site of assembly, the lipid and protein composition at these microdomains may inherently favor membrane curvature, leading to budding. Alternatively, membrane curvature mechanically induced by Gag might favor the recruitment of particular membrane constituents, recruiting microdomains to budding

sites. To determine whether there is a correlation between budding and microdomain association, another future direction involves using polarization TIRF microscopy or the correlative fluorescence/scanning electron microscopy methods, presented in Chapter II, to measure both microdomain association and membrane curvature of assembling virus particles.

Microdomains and Cytoskeleton

HIV-1 Gag associates with the host cytoskeleton, directly or indirectly, during assembly. The cytoskeleton is likely involved in the trafficking and targeting of Gag to the plasma membrane, and cortical actin may play some more direct role in assembly since Gag binds actin and F-actin is packaged into virus particles (3-6). The cytoskeleton is also involved with microdomains; for example, the ERM (ezrin, radixin, and moesin) family of proteins serves as adaptors connecting the cytoskeleton to the plasma membrane. This connection between cytoskeleton and membrane may influence microdomains directly, such as if ERM are themselves microdomain resident proteins, or indirectly, such as if cytoskeleton anchorages function as "picket fence" obstructions limiting free diffusion of microdomain components (7). It is therefore possible that the cytoskeleton plays some role in the microdomain reorganization we have observed in the presence of assembling Gag.

Another possibility is that cytoskeleton effects could be a confounding factor in the copatching assay used in Chapter IV. In one of the original descriptions of the antibody-induced patching phenomenon, Taylor *et al* demonstrated that antibody-mediated patching is separable from antibody-mediated capping (i.e. further clustering of

markers into one large patch at one pole of the cell) (8). The former is governed by diffusion, while the latter is driven by the host cytoskeleton in an energy-dependent manner. Thus, it is possible that the state of the cytoskeleton, particularly cortical actin, may affect the copatching assay. To determine the role of the cytoskeleton in the interactions between Gag and plasma membrane microdomains, and to control for any effects of the cytoskeleton on the copatching assay, it will be useful to repeat the experiments performed in Chapter IV in the presence or absence of drugs that disrupt the cytoskeleton.

Microdomains and the Cellular Restriction Factor Tetherin

The host restriction factor tetherin is thought to inhibit HIV-1 release by incorporating into virus particles, and physically tethering them to the cell surface (9). Tetherin has been shown to inhibit the release of several unrelated enveloped viruses, tetherin homologues from other species can restrict HIV-1, and a completely artificial protein designed to resemble tetherin can inhibit HIV-1 release (10-14). Thus, the association between tetherin and assembling viruses is likely due to some general cellular mechanism commonly used by enveloped viruses. Because several lines of evidence suggest that tetherin associates with lipid rafts (9, 12, 15, 16), and many enveloped viruses are thought to take advantage of lipid rafts during assembly and egress, lipid rafts have been proposed to mediate virus-tetherin association (reviewed in 17). It is tempting to speculate that the reorganization of microdomains we observed in Chapter IV is common to diverse enveloped viruses that assemble on the plasma membrane. This reorganization may underlie the ability of tetherin to restrict the release of HIV-1 and

diverse other viruses. Thus, another future direction is to test the hypothesis that microdomain recruitment or reorganization at assembly sites is required for tetherin incorporation and virus restriction.

Microdomains and Cell-to-Cell Transmission

In vivo, virus transmission by direct cell-to-cell contact is thought to be the most efficient mode of virus spread. This cell-to-cell contact can involve the formation of a virological synapse, which is a contact zone between cells enriched in viral components, virus receptor and co-receptors, cell adhesion molecules, cytoskeleton components, and lipid raft and TEM markers (3, 18-26).

Current work in our laboratory has suggested relationships between cell-to-cell virus transmission and the molecular mechanisms of HIV-1 assembly, including Gag multimerization, microdomain association, and localization of Gag assembly to the protruding uropod of polarized T cells (27) (see Figure 5.1, A). We demonstrated that Gag localizes to a protrusion on polarized T cells, termed the uropod, which is enriched in adhesion molecules and mediates T cell-T cell contacts (28). We showed that higher-order Gag multimerization mediated by NC is necessary for localization of Gag to the uropod, and that disrupting T cell polarization and uropod protrusion reduces cell-to-cell virus transfer in cell culture (27). Interestingly, Gag associates with TEMs both prior to T cell polarization and in polarized T cells (Figure 5.1, B), and another group showed that siRNA knockdown of tetraspanin CD81 prevents polarized localization of Gag within cells (29). Thus, another intriguing future direction involves testing whether microdomain association is necessary for Gag localization to the uropod, establishment of virological

synapses, and cell-to-cell virus spread.

High-Throughput Screening to Develop Antiretroviral Drugs

Because the acquisition of resistance to current antiretroviral drugs is an ongoing threat, there is an ongoing need to develop new drugs and drug targets. Importantly, there are currently no antiretroviral drugs targeting HIV-1 assembly. To date there have been several attempts to identify antiretroviral drugs targeting HIV-1 assembly using high-throughput screening or selection approaches. For example, a peptide inhibitor that blocks the CA dimerization interface was selected by phage display (30), and inhibitors of NC RNA chaperone activity have been identified by high-throughput screening (31). However, the behavior of Gag in vitro may not accurately reflect the assembly of Gag in cells. Thus, it would be useful to develop a cell-based high-throughput assay for HIV-1 assembly. We investigated Bimolecular Fluorescence Complementation as an assay that could be optimized for high-throughput drug screening, but this assay did not work well for Gag assembly, as described in Chapter II. Another interesting future direction would be to optimize the FRET assay used in Chapter III for high-throughput drug screening. It is intriguing to speculate how a cell-based high-throughput assay could identify drugs that inhibit interactions between viral and host factors during assembly, possibly leading to the development of new antiretroviral drugs, or identifying previously unknown virus-host interactions.

In the review of the HIV-1 replication cycle, in the discussions of current issues in the HIV-1 assembly field, and in the specific studies of HIV-1 Gag molecular

mechanisms presented in this dissertation, one major theme stands out: Decades of research have identified the major host and viral factors and their basic functions, yet how these factors and functions interact in a complex system of interdependent molecular mechanisms remains less clear. Thus, to better understand the complexity of HIV-1 replication, there is a great need for ongoing research focusing on unraveling these interrelationships.

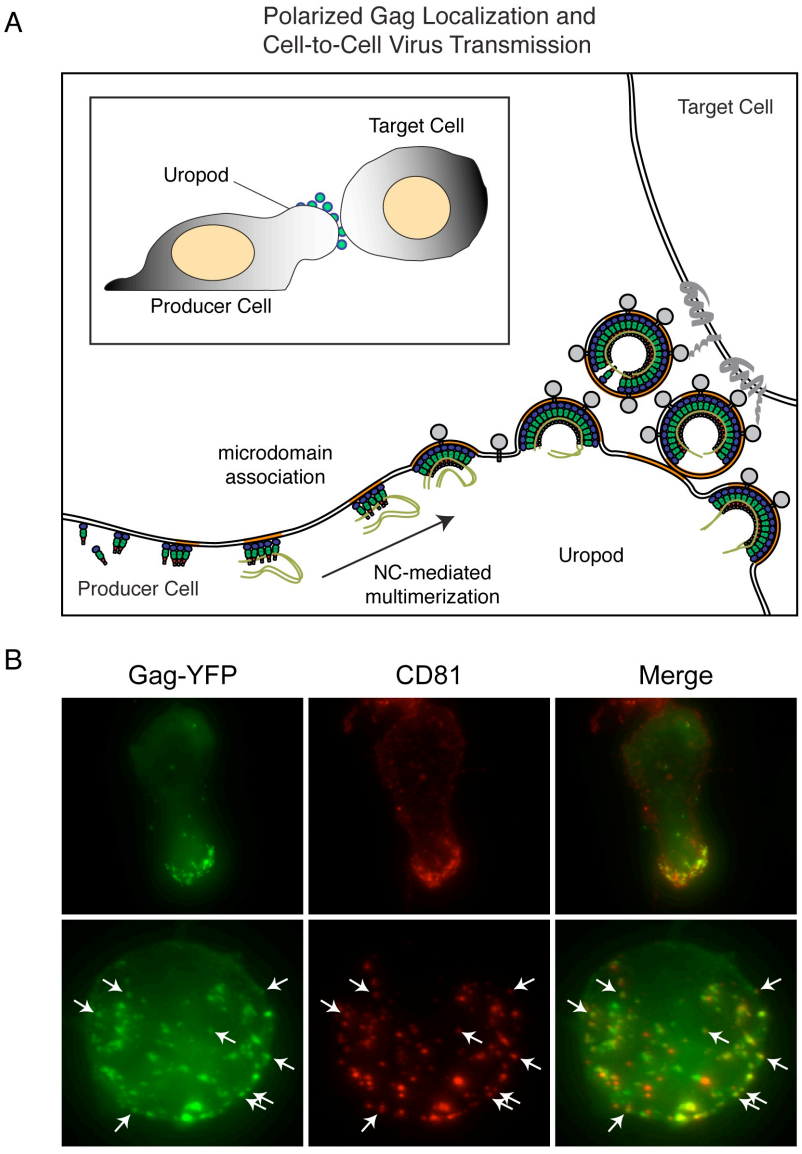

Figure 5.1. Model of assembly at the polarized T cell uropod, and potential role of microdomains. **(A)** Current work indicates that the uropod of polarized T cells is the site of frequent cell-cell contact, and may be the site of virological synapse formation for cell-to-cell virus transmission. NC-mediated higher-order multimerization is necessary for localization of Gag to the T cell uropod, and disrupting uropod protrusion reduces cell-to-cell virus transfer. **(B)** Interestingly, Gag associates with TEM marker CD81 both prior to, and during T cell polarization.

REFERENCES

1. Langhorst, M.F., A. Reuter, and C.A. Stuermer, *Scaffolding microdomains and beyond: the function of reggie/flotillin proteins*. Cell Mol Life Sci, 2005. **62**(19-20): p. 2228-40.

2. Roux, A., et al., *Role of curvature and phase transition in lipid sorting and fission of membrane tubules*. Embo J, 2005. **24**(8): p. 1537-45.

3. Jolly, C., I. Mitar, and Q.J. Sattentau, *Requirement for an intact T-cell actin and tubulin cytoskeleton for efficient assembly and spread of human immunodeficiency virus type 1*. J Virol, 2007. **81**(11): p. 5547-60.

4. Liu, B., et al., *Interaction of the human immunodeficiency virus type 1 nucleocapsid with actin*. J Virol, 1999. **73**(4): p. 2901-8.

5. Ott, D.E., et al., *Cytoskeletal proteins inside human immunodeficiency virus type 1 virions*. J Virol, 1996. **70**(11): p. 7734-43.

6. Wilk, T., B. Gowen, and S.D. Fuller, *Actin associates with the nucleocapsid domain of the human immunodeficiency virus Gag polyprotein*. J Virol, 1999. **73**(3): p. 1931-40.

7. Kusumi, A., I. Koyama-Honda, and K. Suzuki, *Molecular dynamics and interactions for creation of stimulation-induced stabilized rafts from small unstable steady-state rafts*. Traffic, 2004. **5**(4): p. 213-30.

8. Taylor, R.B., et al., *Redistribution and pinocytosis of lymphocyte surface immunoglobulin molecules induced by anti-immunoglobulin antibody*. Nat New Biol, 1971. **233**: p. 225-9.

9. Neil, S.J., T. Zang, and P.D. Bieniasz, *Tetherin inhibits retrovirus release and is antagonized by HIV-1 Vpu*. Nature, 2008. **451**(7177): p. 425-30.

10. Jouvenet, N., et al., *Broad-spectrum inhibition of retroviral and filoviral particle release by tetherin*. J Virol, 2009. **83**(4): p. 1837-44.

11. Kaletsky, R.L., et al., *Tetherin-mediated restriction of filovirus budding is antagonized by the Ebola glycoprotein*. Proc Natl Acad Sci U S A, 2009. **106**(8): p. 2886-91.

12. Perez-Caballero, D., et al., *Tetherin inhibits HIV-1 release by directly tethering virions to cells*. Cell, 2009. **139**(3): p. 499-511.

13. Sakuma, T., et al., *Inhibition of Lassa and Marburg virus production by tetherin*. J Virol, 2009. **83**(5): p. 2382-5.

14. Sato, K., et al., *Comparative study on the effect of human BST-2/Tetherin on HIV-1 release in cells of various species*. Retrovirology, 2009. **6**: p. 53.

15. Kupzig, S., et al., *Bst-2/HM1.24 is a raft-associated apical membrane protein with an unusual topology*. Traffic, 2003. **4**(10): p. 694-709.

16. Waheed, A.A., et al., *Inhibition of human immunodeficiency virus type 1 assembly and release by the cholesterol-binding compound amphotericin B methyl ester: evidence for Vpu dependence*. J Virol, 2008. **82**(19): p. 9776-81.

17. Ono, A., *Relationships between plasma membrane microdomains and HIV-1 assembly*. Biol Cell, 2010. **102**(6): p. 335-50.

18. Arthos, J., et al., *HIV-1 envelope protein binds to and signals through integrin alpha4beta7, the gut mucosal homing receptor for peripheral T cells*. Nat Immunol, 2008. **9**(3): p. 301-9.

19. Igakura, T., et al., *Spread of HTLV-I between lymphocytes by virus-induced polarization of the cytoskeleton*. Science, 2003. **299**(5613): p. 1713-6.

20. Jolly, C., et al., *HIV-1 cell to cell transfer across an Env-induced, actin-dependent synapse*. J Exp Med, 2004. **199**(2): p. 283-93.

21. Jolly, C., I. Mitar, and Q.J. Sattentau, *Adhesion molecule interactions facilitate human immunodeficiency virus type 1-induced virological synapse formation between T cells*. J Virol, 2007. **81**(24): p. 13916-21.

22. Jolly, C. and Q.J. Sattentau, *Human immunodeficiency virus type 1 assembly, budding, and cell-cell spread in T cells take place in tetraspanin-enriched plasma membrane domains*. J Virol, 2007. **81**(15): p. 7873-84.

23. Sol-Foulon, N., et al., *ZAP-70 kinase regulates HIV cell-to-cell spread and virological synapse formation*. Embo J, 2007. **26**(2): p. 516-26.

24. Vasiliver-Shamis, G., et al., *Human immunodeficiency virus type 1 envelope gp120-induced partial T-cell receptor signaling creates an F-actin-depleted zone in the virological synapse*. J Virol, 2009. **83**(21): p. 11341-55.

25. Jolly, C. and Q.J. Sattentau, *Human immunodeficiency virus type 1 virological synapse formation in T cells requires lipid raft integrity*. J Virol, 2005. **79**(18): p. 12088-94.

26. Rudnicka, D., et al., *Simultaneous cell-to-cell transmission of human immunodeficiency virus to multiple targets through polysynapses*. J Virol, 2009. **83**(12): p. 6234-46.

27. Llewellyn, G.N., et al., *Nucleocapsid-Dependent Localization of HIV-1 Gag to Uropods in Polarized T Cells Facilitates Cell-to-Cell Transmission*. Manuscript in preparation, 2010.

28. Sanchez-Madrid, F. and J.M. Serrador, *Bringing up the rear: defining the roles of the uropod*. Nat Rev Mol Cell Biol, 2009. **10**(5): p. 353-9.

29. Grigorov, B., et al., *A role for CD81 on the late steps of HIV-1 replication in a chronically infected T cell line*. Retrovirology, 2009. **6**: p. 28.

30. Sticht, J., et al., *A peptide inhibitor of HIV-1 assembly in vitro*. Nat Struct Mol Biol, 2005. **12**(8): p. 671-7.

31. Shvadchak, V., et al., *Identification by high throughput screening of small compounds inhibiting the nucleic acid destabilization activity of the HIV-1 nucleocapsid protein*. Biochimie, 2009. **91**(7): p. 916-23.

PREFACE TO THE APPENDICES

As our pursuit of science produces increasingly vast bodies of knowledge, new tools will be necessary to cope with the overwhelming complexity of biological systems. The field of systems biology aims to develop tools to combine hypotheses and knowledge of biological systems in order to better understand their complexity. In the following appendices, I present methods to study quantitative models of biological systems, and apply those methods to a model of HIV-1 interacting with host immune system.

The review and development of computational model analysis methods in Appendix A has been previously published:

Marino, S., I. B. Hogue, et al. A methodology for performing global uncertainty and sensitivity analysis in systems biology. Journal of Theoretical Biology, 2008. 254(1): 178-96.

I would like to acknowledge Simeone Marino as the lead author of the introduction, discussion, and section on Partial Rank Correlation, in Appendix A. I was the primary author of the sections on the Extended Fourier Amplitude Sensitivity Test and Agent-Based Models.

The systems biology study using these methods in Appendix B has also previously been published:

Hogue, I. B., et al. The dual role of dendritic cells in the immune response to human immunodeficiency virus type 1 infection. Journal of General Virology, 2008. 89(9): 2228-39.

I would also like to acknowledge the contributions of the Todd Reinhart lab and their collaborators at the University of Pittsburgh who provided the experimental data used in this computational study.

APPENDIX A

Uncertainty and Sensitivity Analysis Methods

ABSTRACT

Accuracy of results from mathematical and computer models of biological systems is often complicated by the presence of uncertainties in experimental data that are used to estimate parameter values. Current mathematical modeling approaches typically use either single-parameter or local sensitivity analyses. However, these methods do not accurately assess uncertainty and sensitivity in the system as, by default they hold all other parameters fixed at baseline values. Using techniques described within we demonstrate how a multi-dimensional parameter space can be studied globally so all uncertainties can be identified. Further, uncertainty and sensitivity analysis techniques can help to identify and ultimately control uncertainties. In this work we develop methods for applying existing analytical tools to perform analyses on a variety of mathematical and computer models. We compare two specific types of global sensitivity analysis indexes that have proven to be among the most robust and efficient. Through familiar and new examples of mathematical and computer models, we provide a complete methodology for performing these analyses, both in deterministic and stochastic settings,

and propose novel techniques to handle problems encountered during this type of analysis.

INTRODUCTION

Systems biology is the study of the interactions between the components of a biological system, and how these interactions give rise to the function and behavior of the system as a whole. The systems biology approach often involves the development of mathematical or computer models, based on reconstruction of a dynamic biological system from the quantitative properties of its elementary building blocks. The need to build mathematical and computational models is necessary to help decipher the massive amount of data experimentalists are uncovering today. The goal of the systems biologist or modeler is to represent, abstract, and ultimately understand the biological world using these mathematical and computational tools. Experimental data that are available for each system should guide, support, and shape the model building process. This can be a daunting task, especially when the components of a system form a very complex and intricate network.

Paraphrasing Albert Einstein, models should be as simple as possible, but not simpler. A parsimonious approach must be followed. Otherwise, if every mechanism and interaction is included, the resulting mathematical model will be comprised of a large number of variables, parameters, and constraints, most of them uncertain because they are difficult to measure experimentally, or are even completely unknown in many cases. Even when a parsimonious approach is followed during model building, available knowledge of phenomena is often incomplete, and experimental measures are lacking,

ambiguous, or contradictory. So the question of how to address uncertainties naturally arises as part of the process. Uncertainty and sensitivity (US) analysis techniques help to assess and control these uncertainties.

Uncertainty analysis (UA) is performed to investigate the uncertainty in the model output that is generated from uncertainty in parameter inputs. Sensitivity analysis (SA) naturally follows UA as it assesses how variations in model outputs can be apportioned, qualitatively or quantitatively, to different input sources (1). In this work we review uncertainty and sensitivity analysis techniques in the context of deterministic dynamical models in biology, and propose a novel procedure to deal with a particular stochastic, discrete type of dynamical model [i.e. an Agent-Based Model (ABM), also called an Individual-Based Model (IBM) in fields like ecology].

By deterministic model, we mean that the output of the model is completely determined by the input parameters and structure of the model. The same input will produce the same output if the model were simulated multiple times. Therefore, the only uncertainty affecting the output is generated by input variation. This type of uncertainty is termed *epistemic* [or subjective, reducible, type B uncertainty] (2). Epistemic uncertainty derives from a lack of knowledge about the adequate value for a parameter/input/quantity that is assumed to be constant throughout model analysis. In contrast, a stochastic model will not produce the same output when repeated with the same inputs because of inherent randomness in the behavior of the system. This type of uncertainty is termed *aleatory* [or stochastic, irreducible, type A] (2). This distinction has been and still is an area of interest and study in the engineering and risk assessment community (3-7).

Many techniques have been developed to address uncertainty and sensitivity analysis: differential analysis, response surface methodology (RSM), Monte Carlo analysis, and variance decomposition methods. See (1, 8) for details on each of these approaches and (9-12) for more general reviews on uncertainty and sensitivity analysis. Here we briefly illustrate the most popular, reliable, and efficient uncertainty analysis techniques and sensitivity analysis indexes. First, we describe two uncertainty analysis techniques: a general Monte Carlo approach and Latin Hypercube Sampling (LHS). Next, we describe two sensitivity analysis indexes: Partial Rank Correlation Coefficient (PRCC) and extended Fourier Amplitude Sensitivity Test (eFAST). PRCC is a sampling-based method, while eFAST is a variance-based method. Next, we perform US analysis on example models, and discuss results. Finally, we present an ABM, where we suggest a method to deal with the aleatory uncertainty that results from the stochasticity embedded in the model structure, to facilitate the use of PRCC and eFAST techniques. We use Matlab (The MathWorks, Inc. version 7.3.0.298 R2006b) to implement most of the US analysis functions described throughout the manuscript (available on our website, http://malthus.micro.med.umich.edu/lab/usanalysis.html).

Uncertainty Analysis

Input factors for most mathematical models consist of parameters and initial conditions for independent and dependent model variables. As mentioned, these are not always known with a sufficient degree of certainty because of natural variation, error in measurements, or simply a lack of current techniques to measure them. The purpose of uncertainty analysis is to quantify the degree of confidence in the existing experimental

data and parameter estimates. In this section we describe the most popular sampling-based approaches used to perform uncertainty analysis, Monte Carlo methods, and their most efficient implementation, namely the LHS technique.

Monte Carlo simulation

Monte Carlo (MC) methods are popular algorithms for solving various kinds of computational problems. They include any technique of statistical sampling employed to approximate solutions to quantitative problems. A MC simulation is based on performing multiple model evaluations using random or pseudo-random numbers to sample from probability distributions of model inputs. The results of these evaluations can be used to both determine the uncertainty in model output and to perform SA. A large body of literature exists on the use of expert review processes to characterize epistemic uncertainty associated with poorly known model parameters (13-16). For each parameter, sampling is guided by the specification of a probability density function (pdf) (i.e. normal, uniform, lognormal, etc.), depending on existing data and *a priori* information. If there are no *a priori* data, a natural choice is a uniform distribution (assigning some hypothetical, but large range with minimum and maximum values for the parameters). If biological knowledge exists suggesting a more frequent or expected value for a parameter, a normal pdf would be the best choice (setting the variance of the distribution as large as needed).

Several sampling strategies can be implemented to perform uncertainty analysis, such as random sampling, importance sampling or LHS (17, 18). To recreate input factor distributions through sampling, a large number of samples are likely required. If too few

iterations are performed, not all values may be represented in the samples or values in the outer ranges may be under-sampled. The LHS algorithm was specifically developed to address this problem and it is by far the most popular sampling scheme for UA (19).

Latin Hypercube Sampling

Latin hypercube sampling (LHS) belongs to the MC class of sampling methods, and was introduced by McKay et al. (18). LHS allows an un-biased estimate of the average model output, with the advantage that it requires fewer samples than simple random sampling to achieve the same accuracy (18). LHS is a so-called *stratified sampling without replacement* technique, where the random parameter distributions are divided into N equal probability intervals, which are then sampled. N represents the sample size. The choice for N should be at least k+1, where k is the number of parameters varied, but usually much larger to ensure accuracy. If the interval of variation for some parameter is very large (several orders of magnitude), the sampling can be performed on a log scale to prevent under-sampling in the outer ranges of the interval where the parameter assumes very small values.

The LHS method assumes that the sampling is performed independently for each parameter, although a procedure to impose correlations on sampled values has also been developed (20, 21). The sampling is done by randomly selecting values from each pdf. Each interval for each parameter is sampled exactly once (without replacement), so that the entire range for each parameter is explored. See Figure A.1 for a hypothetical example of random versus LHS sampling. A matrix is generated (which we call the LHS matrix) that consists of N rows for the number of simulations (sample size) and of k

columns corresponding to the number of varied parameters. *N* model solutions are then simulated, using each combination of parameter values (i.e. each row of the LHS matrix). The model output of interest is collected for each model simulation. Different model outputs can be studied if more than one model output is of interest.

Sensitivity Analysis

Sensitivity analysis (SA) is a method for quantifying uncertainty in any type of complex model. The objective of SA is to identify critical inputs (parameters and initial conditions) of a model and quantifying how input uncertainty impacts model outcome(s). When input factors such as parameters or initial conditions are known with little uncertainty, we can examine the partial derivative of the output function with respect to the input factors. This sensitivity measure can easily be computed numerically by performing multiple simulations varying input factors around a nominal value. This technique is called a local SA because it investigates the impact on model output, based on changes in factors only very close to the nominal values. In biology, input factors are often very uncertain and therefore local SA techniques are not appropriate for a quantitative analysis; instead global SA techniques are needed. These global techniques are usually implemented using Monte Carlo simulations and are, therefore, called sampling-based methods.

Different SA techniques will perform better for specific types of mathematical and computational models. A natural starting point in the analysis with sampling-based methods would be to examine scatter plots. Scatter plots enable graphic detection of nonlinearities, non-monotonicities, and correlations between model inputs and outputs. See (2, 22-26) for a review on the indexes listed in the next paragraph.

For linear trends, linear relationship measures that work well are Pearson correlation coefficient (CC), Partial Correlation Coefficients (PCC) and Standardized Regression Coefficients (SRC). For nonlinear but monotonic relationships between outputs and inputs, measures that work well are based on rank transformations such as Spearman Rank Correlation Coefficient (SRCC), Partial Rank Correlation Coefficient (PRCC) and Standardized Rank Regression Coefficients (SRRC). For nonlinear non-monotonic trends, methods based on decomposition of model output variance are the best choice. Examples of these methods are the Sobol methods (27), the Fourier Amplitude Sensitivity Test (FAST) and its extended version (eFAST). Aside from those listed, there are alternative methods available that are less affected by non-monotonic relationships between the inputs and the output, e.g. common means (CMNs), common distributions or locations (CLs), common medians (CMDs) and statistical independence (SI). These methods are based on gridding (placing grids on a scatter plot) to evaluate any non-randomness in the distribution of points across the grid cells and they are generally less computationally expensive than variance-based methods (such as eFAST).

We will focus and implement only PRCC and eFAST as two examples of SA methods. PRCC and SRRC appear to be, in general, the most efficient and reliable (giving similar results) among the sampling-based indexes (28), while eFAST has proven to be one of the most reliable methods among the variance-based techniques (29), although computationally expensive (30, 31).

It is important to note that PRCCs and variance decompositions obtained with eFAST measure two very different model properties. Specifically, PRCCs provide a measure of monotonicity after the removal of the linear effects of all but one variable. In

contrast, the results obtained with eFAST returns measures of fractional variance accounted for by individual variables and groups of variables. Ideally both indexes should be calculated in order to have a complete and informative US analysis.

We review details for both PRCC and eFAST in the next section. We tested the correctness of our Matlab implementation of LHS\PRCC and eFAST by running similar experiments with the software SaSat (32) and SimLab (33), or comparing with known results for eFAST (1) (data not shown).

METHODS AND RESULTS

Partial Rank Correlation Coefficient

Correlation provides a measure of the strength of a linear association between an input and an output. A correlation coefficient (CC) between x_j and y is calculated as follows:

$$r_{x_j y} = \frac{Cov(x_j, y)}{\sqrt{Var(x_j)Var(y)}} = \frac{\sum_{i=1}^{N}(x_{ij} - \overline{x})(y_i - \overline{y})}{\sqrt{\sum_{i=1}^{N}(x_{ij} - \overline{x})^2 \sum_{i=1}^{N}(y_i - \overline{y})^2}}, \quad j = 1, 2, ..., k,$$

and varies between –1 and +1. $Cov(x_j, y)$ represents the covariance between x_j and y, while $Var(x_j)$ and $Var(y)$ are respectively the variance of x_j and the variance of y ($\overline{x}$ and $\overline{y}$ are the respective sample means). If x_j and y are the raw data, then the coefficient r is called sample or Pearson correlation coefficient.

If the data are rank-transformed, the result is a Spearman or rank correlation coefficient. It is important to note that the process of rank-transforming data assumes that

sampled model inputs are real-valued or can adopt many possible values. If a parameter takes only integer values and the range of possible values it can assume is less than *N*, there is insufficient information to break ties during ranking, resulting in poor correlations.

Partial correlation characterizes the linear relationship between input x_j and output y after the linear effects on y of the remaining inputs are discounted. The PCC between x_j and y is the CC between the residuals of linear regression.

Similarly to PCC, Partial Rank Correlation performs a partial correlation on rank-transformed data: x_j and y are first rank transformed, then linear regression is performed. PRCC is a robust sensitivity measure for nonlinear but monotonic relationships between x_j and y, as long as little to no correlation exists between the inputs (see *Uncertainty and sensitivity functions and implementation* on our website http://malthus.micro.med.umich.edu/lab/usanalysis.html for the use of scatter plot functions to enable graphic detection of non-monotonicities). By combining the uncertainty analyses with PRCC, we are able to reasonably assess the sensitivity of our outcome variable to parameter variation (29, 34).

Extended Fourier Amplitude Sensitivity Test

Extended FAST (eFAST), developed by Saltelli et al. (1, 29, 35, 36), is based on the original Fourier Amplitude Sensitivity Test (FAST) developed by Cukier et al. (37-39). eFAST is a variance decomposition method (analogous to ANOVA): input parameters are varied, causing variation in model output. This variation is quantified

using the statistical notion of variance: $s^2 = \frac{\sum_{i=1}^{N} (y_i - \overline{y})^2}{N-1}$ where N=sample size (or equivalently, total number of model runs), y_i=i^{th} model output, $\overline{y}$=sample mean. The algorithm then partitions the output variance, determining what fraction of the variance can be explained by variation in each input parameter (i.e. partial variance). Partitioning of variance in eFAST works by varying different parameters at different frequencies, encoding the identity of parameters in the frequency of their variation. Fourier analysis then measures the strength of each parameter's frequency in the model output. Thus, how strongly a parameter's frequency propagates from input, through the model, to the output serves as a measure of the model's sensitivity to the parameter.

The sampling procedure implemented in eFAST defines a sinusoidal function of a particular frequency for each input parameter (i.e. a *search curve*), $x = f(j),\ j = 1, 2, ..., N_S$, that assigns a value to x based on the sample number 1 through the total number of samples per search curve, N_s. The choice of sinusoidal function depends on the distribution of parameter values desired (e.g. uniform, normal, etc.). The frequency of each sinusoidal function f is critical, as this frequency is used as a parameter identifier to partition variance in later algorithm steps.

Frequencies (and their first few harmonics) must be less than the Nyquist critical frequency to avoid aliasing effects. The Nyquist-Shannon sampling theorem defines the Nyquist critical frequency of any discretely sampled signal is equal to 1/2 the sampling frequency. Any frequency component in the signal that exceeds the Nyquist critical frequency is incorrectly aliased to a lower frequency during Fourier analysis. Frequencies must additionally be linearly independent to avoid interference. The collection of one-

dimensional sinusoidal functions, one for each input parameter, defines a multi-dimensional search curve that explores many different parameter combinations.

The minimum recommended value for N_S is 65 (1). Due to the symmetry properties of trigonometric functions, the sinusoidal function will eventually repeat the same samples. A *resampling* scheme is implemented to avoid this inefficiency (36): eFAST algorithm is repeated N_R (the resampling size) times with different search curves specified by introducing a random phase shift into each sinusoidal function. So, the total number of model simulations, N, is given by $N = N_S \, x \, k \, x \, N_R$, where k is the number of parameters analyzed.

As an example, in Figure A.2, we illustrate the steps within the eFAST algorithm applied to the classic Lotka-Volterra predator-prey model, an ordinary differential equation (ODE) model of population dynamics. The model equations are given by: $\dot{Q} = \alpha Q(t) - \beta Q(t)P(t), \quad Q(0) = 10(\#\text{prey})$; $\dot{P} = -\sigma P(t) + \delta Q(t)P(t), \quad P(0) = 5(\#\text{predator})$. It has two state variables (Q, P) and several parameters. Q represents the density of prey, P represents the density of predators, α is the intrinsic rate of prey population increase, β is the predation rate coefficient, σ is the predator mortality rate, and δ is the reproduction rate of predators per prey consumed. As an example, we assume that these four parameters follow normal pdfs with means±std of α = 1.5±0.01, β = 1±0.2, σ = 3±0.2, δ = 1±0.01. We use 257 samples per search curve with no resampling (i.e. N_S =257, N_R=1). Parameter σ is taken as the parameter of interest. The algorithm assigns parameter σ a frequency of 31, and parameter β a frequency of 2. For simplicity, parameters α (frequency = 1) and δ (frequency = 3) are not illustrated. Each sampled parameter combination is then used to solve the model (Figure A.2).

The primary advantage of the eFAST method over the original FAST is the ability to estimate the total-order sensitivity index of each input parameter. The original FAST method assigns a unique frequency to each input parameter, and thus calculates the unique contribution of each parameter in determining the model output. This unique contribution is the first-order sensitivity index, S_i (Figure A.2, white pie-slice). First, variance (s_i^2) is calculated from the Fourier coefficients at the frequency of interest, j,

$s_i^2 = 2(A_j^2 + B_j^2)$, where $A_j = \frac{1}{\pi}\int_{-\pi}^{\pi} f(x)\cos(jx)dx$, $B_j = \frac{1}{\pi}\int_{-\pi}^{\pi} f(x)\sin(jx)dx$

then, the first-order S_i is calculated as a fraction of total variance:

$$S_i = s_i^2 / s_{total}^2$$

This index represents the fraction of model output variance explained by the input variation of a given parameter. To calculate the total-order sensitivity index of a given parameter i, the eFAST method instead varies i at a unique, high frequency, but all other parameters at low, not-necessarily unique frequencies. Both FAST and eFAST calculate the first-order S_i of parameter i by Fourier analysis, using its unique high frequency. In contrast to FAST, eFAST then calculates the summed sensitivity index of the entire complementary set of parameters (all parameters except i; Figure A.2, black pie-slice). Thus, while FAST partitions variance to each parameter, eFAST partitions variance into two categories: variance due to the parameter of interest i, and variance due to all other parameters (the complementary set to i).

Any variance that remains unaccounted for is assumed to be due to non-linear interaction between the parameter of interest and other parameters. The total-order

sensitivity index, S_{Ti} is then calculated as the remaining variance after the contribution of the complementary set, S_{ci}, is removed (Figure A.2, gray pie-slice):

$$S_{Ti} = 1 - S_{ci}$$

This includes higher-order, nonlinear interactions between the parameter of interest and the complementary set of parameters.

Statistical inference on eFAST using a dummy parameter

Because there does not currently exist a statistical inference test for variance-based sensitivity indexes, we propose a novel method based on dummy parameters for determining the significance of eFAST first- and total-order indexes. The use of dummy parameters is a standard practice in screening methods (1), although, to our knowledge, it has never been applied in the context of eFAST with the purpose of testing the significance of first and total-order sensitivity coefficients.

The eFAST method implements random resampling (N_R) of search curves for more efficient parameter sampling. Because different search curves will produce different combinations of parameter values, different search curves will lead to slightly different sensitivity measures. We take advantage of these repeated measures to perform statistical tests comparing eFAST sensitivity indexes. The algorithm already performs these repeated measures, thus the statistical tests entail no additional computationally intensive model simulations.

The eFAST method artifactually produces small but non-zero sensitivity indexes for parameters to which the model is completely independent. This is also true for the PRCC method. To illustrate this point, we run an example sensitivity analysis where we

include a negative-control "dummy" parameter. This dummy parameter does not appear in the model equations and thus does not affect the model in any other way, so should ideally be assigned a sensitivity index of zero. Figure A.3 shows eFAST and PRCC SA results with the use of a dummy parameter on the Lotka-Volterra model.

The eFAST algorithm assigns this dummy parameter a small but non-zero first-order sensitivity index (S_{dummy}= 0.003), and total-order sensitivity index (S_{Tdummy}) of approximately 0.11 (Figure A.3). The non-zero first-order index, S_{dummy}, likely derives from aliasing and interference effects. The assignment of a larger artifactual value to the total-order index, S_{Tdummy}, is more complicated. eFAST estimates the total-order index from the variance unaccounted for after partitioning variance to the parameter of interest and the complementary set of parameters. The remaining variance is assumed to be higher-order interactions between the parameter of interest, i, and other parameters. However, this assumption is imprecise, as interaction between other parameters, but not with the parameter of interest, is included in this remaining variance. For example, given a model with parameters i, j, and k, the total-order sensitivity index of parameter i, S_{Ti}, is given by: $S_{Ti} = S_i + S_{ij} + S_{ik} + S_{ijk}$. The higher-order terms, $S_{ij} + S_{ik} + S_{ijk}$, are approximated by the remaining variance after first-order partitioning. However, this remaining variance includes the interaction between parameters j and k, S_{jk}. Therefore, by approximating the higher-order interactions of i using the remaining variance, the interaction effect S_{jk} is inappropriately included in the total-order index.

Since we cannot test if those artifactual values are significantly different from zero, by taking a dummy parameter as the parameter of interest, we propose a way to quantify these artifacts and test for significance. Parameters with a total-order sensitivity

index less than or equal to that of the dummy parameter should be considered not significantly different from zero.

We propose using a *two-sample t-test* on data generated by resampling the eFAST search curve to determine whether the sensitivity indexes of a parameter of interest are significantly different from the indexes calculated for the dummy parameter. The t-test compares two distributions, the S_i^j or $S_{T_i}^j$ $\left(j = 1, 2, ..., N_R\right)$ with the S_{dummy}^j or $S_{T_{dummy}}^j$ $\left(j = 1, 2, ..., N_R\right)$.

Since N_R is usually small (for ease of computation), the adequacy of this t-test procedure is limited, considering that the normality assumption of the t-test is unlikely to hold for the first and total order sensitivity indexes. However, it can indicate on whether a small total-order sensitivity index should be considered an artifact of eFAST total-order estimation. The two-sample t-test might also be used to determine whether the indexes of multiple parameters of interest are significantly different from each other, allowing qualitative comparisons of effect size. Figure A.3 illustrates the use of resampling and statistical significance testing. The LHS/PRCC algorithm (Figure A.3) assigns a PRCC value to the dummy parameter that is not significantly different from zero (0.04054, p-value>0.05). Although not relevant for our examples, multiple test corrections should be considered if a large number of tests are performed in the US analysis.

Uncertainty and Sensitivity Analysis in Agent-Based Models

Agent-Based Models (ABMs, also called "individual-based models", IBMs) are a formalism evolved from early research in cellular automata and artificial life. The defining feature of ABMs is that elements of the system are represented as discrete agents

that move and interact according to defined rules, in an explicitly defined spatial environment. Stochasticity enters the model as some decision-making rules can be based on random chance, such as a random walk movement of cells. In an ABM, the individual, possibly stochastic, interactions between agents give rise to global, system-wide dynamics and patterns. Thus, ABMs are ideal for studying complex systems in which stochasticity, and spatial and temporal heterogeneity are important, such as biological systems.

Stochastic models, such as the ABM we consider here, pose unique challenges to uncertainty and sensitivity analysis. Most uncertainty and sensitivity analysis techniques have been developed for use with deterministic models, such as those presented in previous sections of this work. To our knowledge, very few researchers have attempted extensive and systematic uncertainty and sensitivity analysis on ABMs (40-42).

To perform uncertainty and sensitivity analysis on an ABM, it is critical to keep in mind the distinction between aleatory and epistemic uncertainty during model building. In this analysis, epistemic uncertainty is handled by holding a parameter to a fixed value during a particular model simulation, but allowing probabilistic variation between model simulations to reflect uncertainty. In contrast, stochastic components vary randomly from moment to moment within a single ABM simulation. Some studies have applied a stochastic component to otherwise deterministic models by sampling a random sequence of values prior to running a model simulation (43-45). However, this approach cannot be easily applied to ABMs as presented here: stochastic decisions made by each agent at each time step are based on conditional probabilities that depend on both random chance and the state of other interacting agents. Therefore it is impossible to correctly

specify a random sequence of agent decisions prior to running the simulation. When performing uncertainty analysis on an ABM, epistemic uncertainty and aleatory uncertainty become conflated in the model output. It is difficult to know whether variability in model outcome is due to experimentally introduced variation in input parameters (epistemic uncertainty) or to the inherent stochastic components of the model (aleatory uncertainty). Therefore, it is difficult to apportion variability to input parameters during sensitivity analysis. In this section, we perform uncertainty and sensitivity analysis on an ABM, identify the strengths and weaknesses of the PRCC and eFAST techniques in dealing with aleatory uncertainty, and propose an averaging method to reduce the influence of aleatory uncertainty.

An agent-based model example

As an example, we present a published ABM describing granuloma formation during *Mycobacterium tuberculosis* infection (41). This was the first ABM to use a modification of a US analysis using PRCC. In this model, the spatial environment represents a 2mm square section of lung tissue. This area is subdivided into a 100x100 lattice of 20μm square micro-compartments. Agents (cells) populate this environment, representing resident or infiltrating macrophages and T-cells. Bacteria and chemokines also exist in the model, but are treated as a continuous quantity rather than discrete agents. Each micro-compartment can contain at most one macrophage and one T-cell agent (and a quantity of bacteria/chemokines, as these are assumed to have negligible size). Some micro-compartments are designated as vascular source compartments, through which new macrophage and T-cell agents arrive from the blood.

A simulation is initiated by distributing an initial population of resting macrophages randomly on the lattice and an initial load of extracellular bacteria in the center of the lattice. The simulation evolves by a series of discrete time steps, during which rules are evaluated governing the diffusion of chemokines, infection and replication of bacteria, and arrival, movement, interaction, and change in phenotype of immune cells. Parameters that we will analyze by US methods control initial conditions and rates or probabilities used to evaluate rules. The range of values sampled for simulations are as follows:

- Chemokine diffusion constant (λ): 0.4 - 0.8
- Chemokine degradation constant (δ): 2.8811×10^{-4} - 0.0011
- Intracellular growth rate (α_{BI}): 0.002 - 0.006
- Probability of T cell recruitment (T_{recr}): 0.10 - 0.40
- Probability of T cell movement (T_{move}): 0.01 - 0.20
- Probability of T cell activating macrophage (T_{actm}): 0.05 - 0.20
- Initial number of macrophages (M_{init}): 40 - 400
- Probability of macrophage recruitment (M_{recr}): 0.20 – 0.70
- Activated macrophage speed (M_{asp}): 200-8000
- Number of T cells needed to activate macrophage (N_{tact}): 1-6
- Probability of bacteria killed by resting macrophage (p_k): 0.01-0.1
- Probability that T cell kills a macrophage (p_{Tk}): 0.01-0.1

See (41) for a more detailed description of the model.

Aleatory Uncertainty

It is impossible to entirely separate model output variability due to either aleatory or epistemic uncertainty. However, it is useful to crudely quantify aleatory uncertainty in the absence of variability due to epistemic uncertainty by repeatedly solving the model, holding all parameters constant. Figure A.4 represents two typical scenarios: containment of infection and dissemination. The baseline set of parameter values differs between the two scenarios [see (41) for definitions of these scenarios and baseline parameters]. The variability around each scenario is determined by aleatory uncertainty, while epistemic uncertainty causes the emergence of this bimodal outcome. We find that the containment scenario produces a moderate level of aleatory uncertainty. To roughly quantify aleatory uncertainty, we calculate the coefficient of variation of 10 replicates, holding all parameters constant at their average values. For this model, coefficients of variation of the output for the containment scenario (extracellular bacterial load) are 3.5% at day 500 and 62.4% at day 30. The coefficient of variation at day 30 is much larger than at day 500, meaning that aleatory uncertainty at this early time point will more strongly mask any variability due to epistemic uncertainty introduced in subsequent analysis steps. We will focus our analysis on day 30, as this time point is analyzed in (41), providing a reference point to compare our results to, and because aleatory effects should be most problematic at this time point due to the high coefficient of variation.

Replication and averaging scheme for Agent-Based Models

To study aleatory uncertainty, we propose a replication and averaging scheme that can be applied with either PRCC or eFAST. First, parameter combinations are created

using the LHS or eFAST internal sampling algorithm. Next, multiple model simulations are repeatedly run for each parameter combination (replication step). Note that when using a pseudorandom number generator in the algorithm, we reinitialize the random seed for each model simulation. Finally, the sensitivity coefficients are calculated using the average of model outputs across replicates. By comparing these results with the sensitivity coefficients obtained from each replicate individually, we can assess whether US analysis is robust at a specific sample size. One caveat to this approach is that using the average to characterize the distribution of output values over aleatory uncertainty is reliable only if the output values are clustered around a central value (i.e. unimodal). We apply the replication and averaging scheme to the Segovia-Juarez ABM.

Results of LHS/PRCC on an Agent-Based Model

When aleatory uncertainty is moderate, as is in this example, LHS/PRCC produces consistent results at large LHS sample size: in the original analysis of this model, Segovia-Juarez *et al* use an LHS sample size of 1000. As sample size is reduced to less than approximately 200-300, two effects occur: first, PRCC becomes less reliable due to the influence of aleatory uncertainty; second, statistical power for PRCC significance is reduced due to the smaller sample size; therefore weakly correlated parameters are not found to be significant.

Next, we explore whether averaging replicates can reduce effects of aleatory uncertainty, allowing fewer computationally intensive model simulations. We find that averaging replicates has two beneficial effects. First, PRCC becomes reliable at smaller sample sizes due to the removal of some of the variability induced by aleatory

uncertainty. Specifically, by using replicates (4 replicates in this case), a similar set of parameters with significant PRCC is achieved with a smaller number of samples (at least 50) compared to the standard scheme without replicates (at least 300 samples). Second, parameter values and model output becomes more tightly correlated due to the removal of some confounding aleatory noise, resulting in PRCC of greater magnitude (see Figure A.5). This increase in PRCC magnitude that occurs by averaging is apparent even when PRCC is already reliable due to large sample size, e.g. 1000 samples (not shown). These benefits come at a cost, however: if the total number of model simulations is held constant, performing replicates reduces the number of samples available for statistical tests (e.g. 300 parameter samples simulated once, versus 100 parameter samples replicated 3 times, then averaged, yielding 100 sample averages). In Figure A.5, we show that there are some situations where the gain in PRCC magnitude due to averaging is favorable despite the loss in statistical power. In the original analysis of this model, using a sample size of 1000 with no replication, Segovia-Juarez et al (41) find 9 significant parameters, including parameters α_{BI} and λ. Reducing sample size to 300 with no replication (Figure A.5, black bars), for a total of 300 model simulations, parameters α_{BI} and λ are not significantly different from zero. Using 100 samples and averaging 3 replicates (Figure A.5, gray bars), for a total of 300 model simulations, however, successfully identifies α_{BI} and λ as significant, yielding performance similar to that of 1000 samples used by Segovia-Juarez *et al*. Therefore, for this ABM we suggest that performing replicate simulations of each parameter sample and averaging these replicates is a useful strategy that can provide better performance with fewer computationally intensive model simulations.

Results of eFAST on an Agent-Based Model

To our knowledge, eFAST has been used to analyze an ABM once before (40), but details of the methodology used are lacking. To explore the suitability of the eFAST method in analysis of stochastic models, we analyze the Segovia-Juarez model, described above, taking advantage of the replication and averaging scheme (described in the previous section) and of the use of a dummy parameter. Extended FAST is performed using 257 samples per search curve (i.e., N_S=257), a resampling size of 4 (i.e., N_R=4), and 4 replicates for averaging. By allowing eFAST to partition variance to a dummy parameter, we find that the first-order index is relatively unaffected (Figure A.6). However, eFAST severely mishandles the variability induced by aleatory uncertainty by incorrectly partitioning it to the total-order sensitivity index, resulting in a large artifactual S_{Ti}=24.3% (Figure A.6, dummy parameter, black bar). Thus, use of a dummy parameter to quantify this artifact reveals that parameters with a total-order S_{Ti} in the range of ~20-30% are likely artifactual. Using replication and averaging to limit variability induced by aleatory uncertainty successfully reduces this artifact by more than half (Figure A.6, dummy parameter, gray bar): this allows 7 of the 8 significant parameters identified by LHS/PRCC to exceed the dummy parameter background value for S_i (Figure A.6). Increasing N_S and N_R, as well as performing averaging with additional replicates will likely further improve the limit of detection. Performing significance testing in combination with replication and averaging, we find that 8 of the 9 parameters identified as significant by LHS/PRCC are also identified by eFAST first-order S_i (Figure A.6), while the S_{Ti} coefficients are significantly different from the dummy only for 4 of

the 8 parameters listed by LHS/PRCC (Figure A.6). Note that eFAST result come at a much higher computational cost: 53456 total model simulations using eFAST, as opposed to 300 total model simulations with LHS/PRCC.

Summary of Sensitivity Analyses of an Agent-Based Model

This specific ABM example shows how LHS/PRCC and eFAST are typically in agreement, identifying a similar set of important parameters. However, these two methods have different relative strengths and weaknesses. eFAST requires many more model simulations, which is a particular problem as ABMs are often more computationally intensive than deterministic models. Also, when analyzing stochastic models, eFAST produces an artifact whereby aleatory variance is inappropriately partitioned to the total-order sensitivity index. Therefore, this example suggests how LHS/PRCC method (with the modifications presented here) can perform better than eFAST for a specific time point, reaching the same conclusions with much less computational cost.

The eFAST method has the strength of identifying non-monotonic sensitivities, however. Though we see no evidence of this strength in the ABM we analyze here, there is no *a priori* way of knowing if non-monotonic sensitivities are present in a model. Therefore, if computational cost is not prohibitive, use of eFAST on stochastic models can complement LHS/PRCC results. In this case, one should take steps to reduce the artifact of eFAST mishandling aleatory variance in the total-order sensitivity index, or one should rely solely on the first-order index, as it is unaffected by the artifact.

DISCUSSION AND CONCLUSION

Uncertainty and sensitivity analyses offer a way to assess the adequacy of models and establish what factors affect model outputs. We reviewed and compared two specific types of global sensitivity analysis indexes that have proven to be among the most reliable and efficient, namely a sampling-based method (Partial Rank Correlation Coefficient – PRCC) and a variance-based method (extended Fourier Amplitude Sensitivity Test – eFAST). All functions used throughout the paper are available on our website (http://malthus.micro.med.umich.edu/lab/usanalysis.html).

PRCC provides answers to questions such as how the output is affected if we increase or decrease a specific parameter (linearly discounting the effects of the uncertainty over the rest of the parameters). Thus PRCC can be informative on what parameters to target if we want to achieve specific goals (e.g., control or regulatory mechanisms). For example, the most significant set of parameters can be used to determine how to efficiently reduce viral load or increase immune response (by both timing and magnitude). eFAST, and all variance-based methods in general, indicate which parameter uncertainty has the greatest impact on output variability. In other words, our predictions will be strengthened if we can reduce uncertainty and get better estimates on specific parameters of the model (i.e., the ones with highest S_i and S_{Ti} sensitivity coefficients). This will also enhance any additional PRCC or sampling-based analysis, because any regulatory or control strategy will be more reliable.

One critical point is the selection of adequate pdfs and the choice of parameter ranges used for sampling. The selection of probability distributions for the uncertain

parameters depends in part on whether the intent of the analysis is an exploration of variable effects (i.e., a sensitivity analysis) or a propagation of uncertainty to assess the uncertainty in the outcomes of interest (i.e., an uncertainty analysis). For meaningful uncertainty analyses, the selected distributions are chosen based on the degree of our understanding of biology with respect to the appropriate values of model parameters. In contrast, the distributions might be selected simply to fully explore potential variable effects in a sensitivity analysis.

The choice of parameter range should also be guided by the available knowledge of the biological problem. If a parameter range is completely outside the biological realm, the practical relevance of the US analysis is lost. Unfortunately, exact or even hypothetical biological ranges are many times unknown. Unless the choice of very small ranges for certain parameters is guided by some *a priori* knowledge, the sampling should be performed within the whole range of plausible values, since US analysis results can be quite different. Moreover, if the range of variation for some parameter spans several orders of magnitude and we want to avoid under-sampling in the outer ranges of parameter space, the implementation of a logarithmic sampling scheme (for example, a log-uniform in place of a uniform pdf) would achieve the goal, but the final results will be affected.

Our examples showed how eFAST is more general than PRCC (it deals with any type of relationship between inputs and outputs of a model) with one major drawback: its computational cost, especially for computing S_{Ti}. Our examples highlight how a large number of iterations are needed to achieve a recommended degree of accuracy in eFAST.

We designed a new method (together with an heuristic for its accuracy) to check for significant eFAST S_i and S_{Ti}. This new method is based on a two-sample t-test approach and uses a re-sampling scheme to compare each sensitivity index with that of a dummy parameter. The use of dummy parameters is a standard practice in screening methods (1), although, to our knowledge, it has never been applied in the context of eFAST.

We built several functions to display scatter plots of sampled parameters versus the output under study (given on our website: http://malthus.micro.med.umich.edu/lab/usanalysis.html). They can be extremely useful to detect non-monotonicities and non-linearities and possibly explain why PRCC and eFAST results are different.

In the context of ABM, we also implemented a new averaging strategy to efficiently and reliably perform US analysis within the context of this particular class of stochastic models. By running the ABM multiple times with the same set of parameters and then averaging the output, we are able to attenuate the effect of aleatory uncertainty, obtaining more reliable results both for PRCC and eFAST.

Throughout our examples, we found that the set of significant first order S_i and total order S_{Ti} sensitivity indexes returned by eFAST is consistent and with the same ranking. eFAST generally returns smaller sets of parameter with significant S_i and S_{Ti}, compared to the set of parameters with significant PRCC. Also, eFAST often returns S_i and S_{Ti} for parameters that are not listed as significant by PRCC and, when a similar set of parameters is returned, the order of importance is frequently different between the two methods.

Based on the examples shown, we conclude that PRCC and eFAST S_i and S_{Ti} should both be computed, keeping in mind that they measure different things, and that eFAST is generally computationally more expensive. If the computational cost is too high (i.e. cpu time per one model run), more efficient methods are available (e.g. methods that are less affected by non-monotonicities). A lower computational cost can be achieved by reducing N_S and N_R, (i.e. the total number of runs) but the accuracy of the results might be adversely affected. To increase the accuracy of eFAST results, in general, it is better to increase N_S first, and then eventually increase N_R (to improve the accuracy of inference on the indexes). We found that values and significances of first-order S_i are affected by increasing N_S: the values of the not significant S_i get smaller, as does the dummy parameter S_{dummy}, making the t-test more reliable. Increasing N_S does not affect S_{Ti} values, although the t-test becomes more precise.

In general, the computational execution time of the model is the major concern when performing US analysis. Models with several parameters and many complex nonlinear mechanisms likely result in high computational costs. Screening methods are available to address this problem. Within the class of screening methods, Morris (or elementary effects) is the most popular (46): it is global, computationally efficient and should be implemented as a first preliminary US analysis when the execution time of the model is prohibitive (several hours or days).

In summary, characterizing uncertainty in parameter values and initial conditions in mathematical models in biology is attainable and is dependent on the type of system under study. For the math biology community to continue to gain a foothold and have an impact in important biology problems, it is clear that identifying uncertainty in our

models is of key importance. By the very act of classifying this uncertainty, we can simultaneously identify the parameters (i.e. biological mechanisms) that are driving system outputs. These mechanisms can then be posed to the experimental community to test. This close interaction between theorists and experimentalists provides the greatest opportunity for the use of mathematical models.

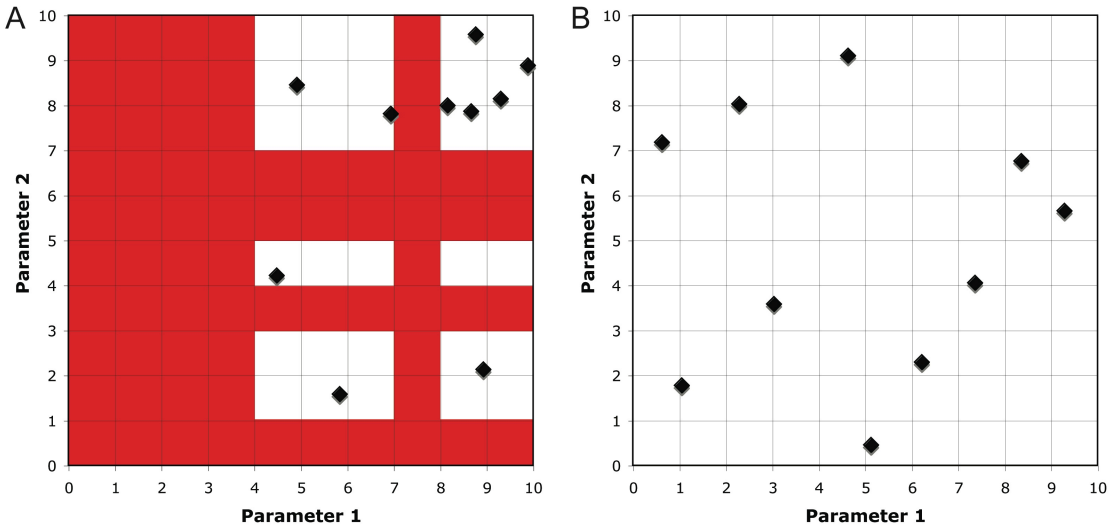

Figure A.1. Random versus Latin Hypercube Sampling (LHS). In this example, two parameters are sampled over a 0-10 range using a uniform probability density. **(A)** Using simple random sampling, large regions of each parameter's range is not sampled (red areas). **(B)** LHS sampling divides each parameter's range into equal-probability binds. Each bin is sampled, ensuring parameter space is explored as efficiently as possible.

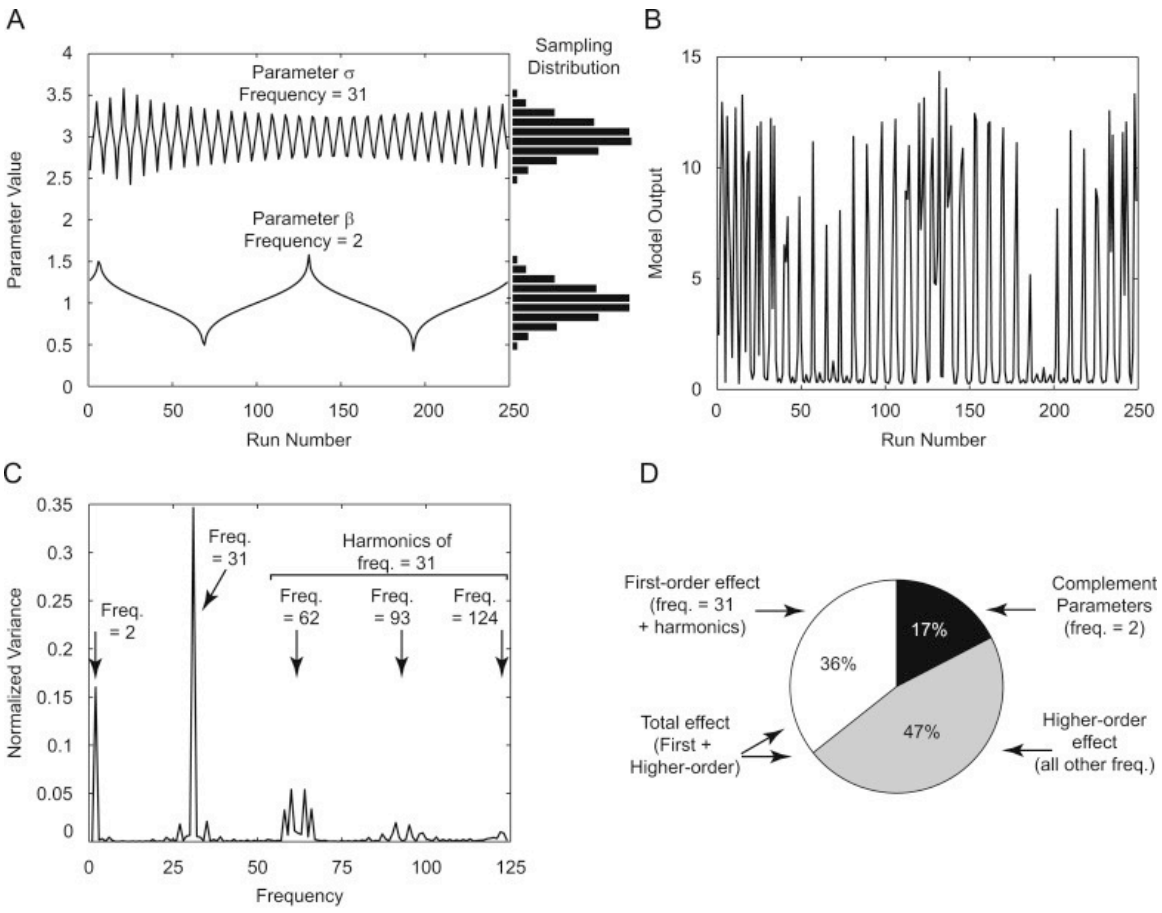

Figure A.2. Example of eFAST performed on the classic Lotka-Volterra predator-prey model. **(A)** Input Parameter Sampling: Parameters are varied according to a sinusoidal function based on model run number. Note that the shapes of these search curves result in normal distribution of parameter values when sampled (horizontal histograms). σ is assigned a frequency of 31, and β is assigned a frequency of 2. α and δ are sampled at frequencies 1 and 3, respectively (not shown). These frequencies are chosen automatically to meet the criteria described in the text. **(B)** Model Output: The model is solved for each parameter combination from (A). The number of prey at t=9 is taken as the model output. Note that both high- and low-frequency components are evident by inspection. **(C)** Fourier analysis and Variance Spectrum: The variance at each frequency is calculated from the model ouput (see text) and normalized to total variance. The variance at frequency 2, 31, and higher harmonics of frequency 31 are indicated (arrows). **(D)** Sensitivity Indexes: Taking parameter σ (varied at frequency 31) as our parameter of interest, first-order sensitivity index (S_i) is calculated by the sum of variance at frequency 31 and higher harmonics, normalized to total variance (white pie slice). The sensitivity of the complementary set of parameters is calculated similarly (black pie slice). The remaining variance is assumed to be the result of non-linear higher-order interaction between parameters (gray pie slice). The total-order sensitivity index (S_{Ti}) is calculated by the sum of S_i and higher-order effects (white + gray pie slices).

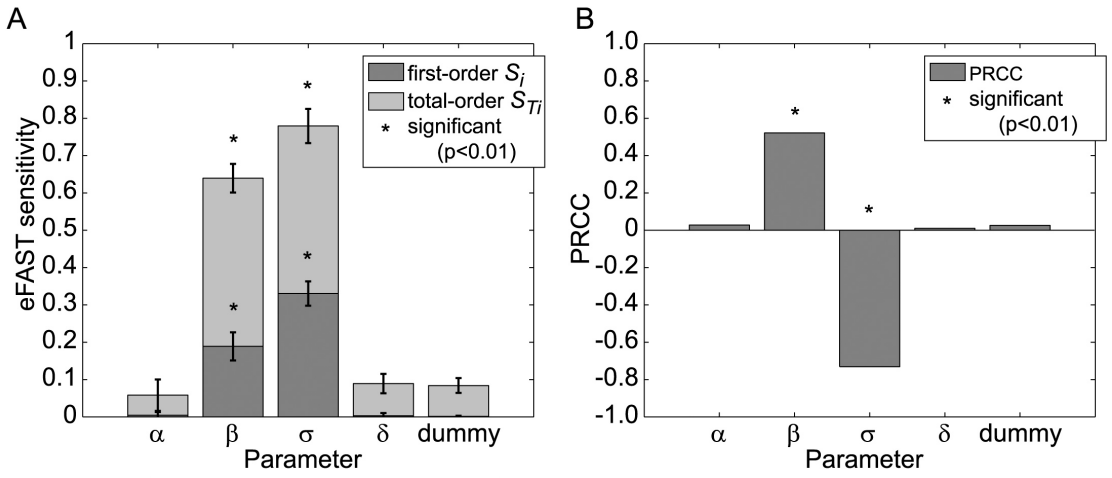

Figure A.3. Statistical inference using a dummy parameter in eFAST, compared to PRCC. Model equations and parameters are as described in the text. The reference output is Q(t)-prey, at t=9. **(A)** eFAST results with resampling and significance testing. Search curves were resampled 5 times (N_R=5), for a total of 1285 model evaluations (N_S=257). First-order S_i and total-order S_{Ti} are shown for each parameter, including a dummy parameter, as described in the text. Error bars indicate ± 2 std on mean of resamples. Parameters with first- or total-order indexes significantly different ($p<0.01$) from those of the dummy parameter are indicated with asterisks (*). **(B)** PRCC results. Sample size N=1000. (*) denotes PRCCs that are significantly different from zero.

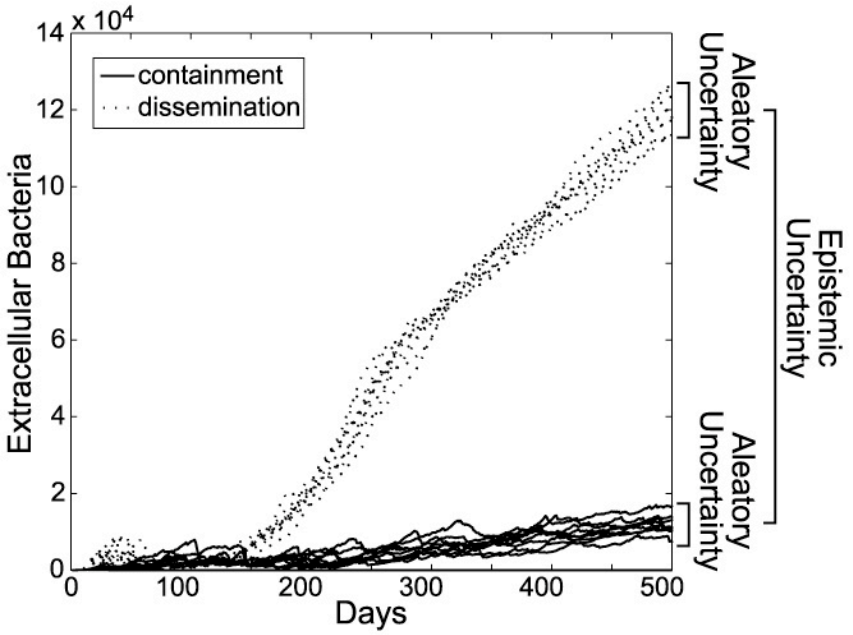

Figure A.4. Variation in ABM output due to epistemic uncertainty and aleatory uncertainty. Differences in parameter values lead to either containment of extracellular bacterial load (solid lines), or dissemination of bacteria (dotted lines), as described previously in (41). Within each parameter combination, inherent stochasticity within the model causes aleatory uncertainty. At time points earlier than approximately day 150, aleatory uncertainty masks the epistemic difference that USA methodologies seek to measure.

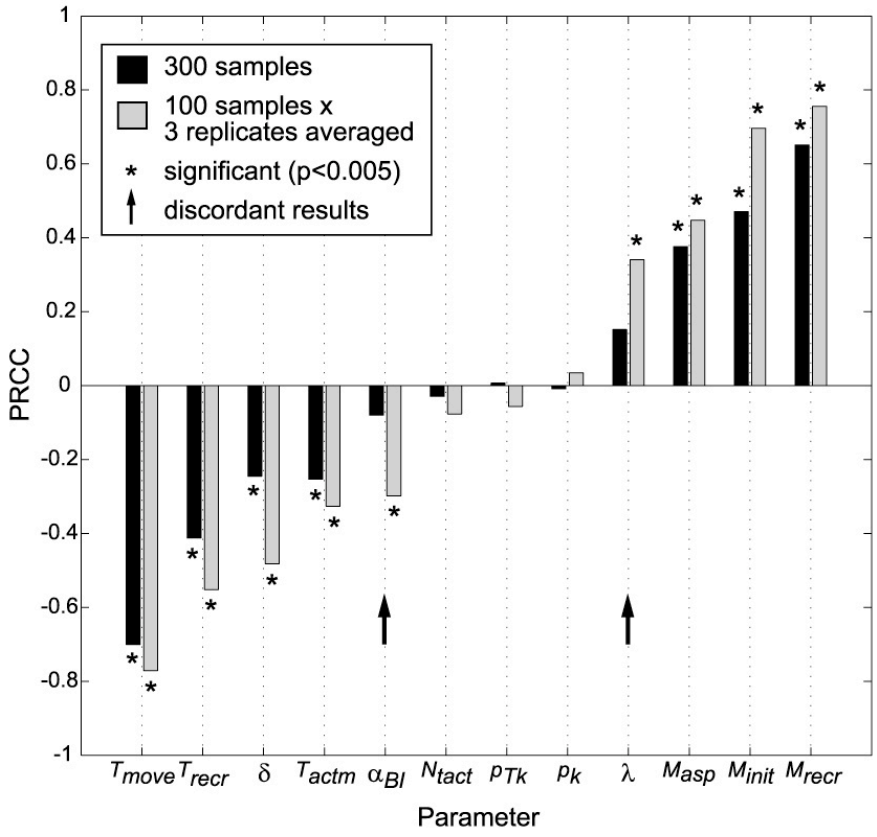

Figure A.5. Effect of aleatory uncertainty on LHS/PRCC and the benefit of averaging replicates. Model parameters were sampled 300 (black bars) or 100 times (gray bars). For the 100 sample condition, the 3 replicate model simulations were performed for each sample and averaged. Parameters with a PRCC significantly ($p<0.005$) different from zero are indicated with (*). Parameters with discordant statistical significance between the two experimental conditions are indicated (arrow).

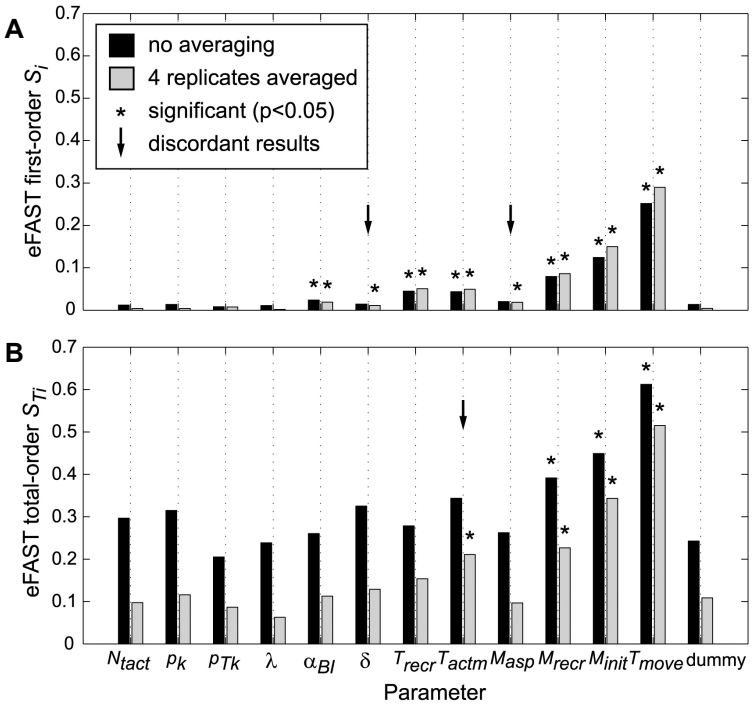

Figure A.6. Performance of eFAST on a stochastic agent-based model. **(A)** eFAST first-order sensitivity index S_i. Replication and averaging (gray bars) has a small effect on S_i, allowing additional parameters (indicated by arrow) to be identified as statistically significant (*). **(B)** eFAST total-order sensitivity index S_{Ti}. eFAST artifactually assigns aleatory variance to the total-order index, resulting in a high dummy parameter background value (dummy parameter, black bar). Replication and averaging (gray bars) partially reduces this artifact, allowing an additional parameter (indicated by arrow) to be found significant (*).

REFERENCES

1. Saltelli, A., K. Chan, and E.M. Scott, *Sensitivity analysis*. Wiley series in probability and statistics. 2000, Chichester ; New York: Wiley. xv, 475 p.

2. Helton, J.C., et al., *Survey of sampling-based methods for uncertainty and sensitivity analysis.* Reliability Engineering & System Safety, 2006. **91**(10-11): p. 1175-1209.

3. Apostolakis, G., *The Concept of Probability in Safety Assessments of Technological Systems.* Science, 1990. **250**(4986): p. 1359-1364.

4. Helton, J.C., *Uncertainty and sensitivity analysis in the presence of stochastic and subjective uncertainty.* Journal of Statistical Computation and Simulation, 1997. **57**(1-4): p. 3-76.

5. Parry, G.W. and P.W. Winter, *Characterization and Evaluation of Uncertainty in Probabilistic Risk Analysis.* Nuclear Safety, 1981. **22**(1): p. 28-42.

6. Pate'-Cornell, M.E., *Uncertainties in Risk Analysis: Six Levels of Treatment.* Reliability Engineeering and System Safety, 1996. **54**(2-3): p. 95-111.

7. Helton, J.C., et al., *A sampling-based computational of epistemic uncertainty in model strategy for the representation predictions with evidence theory.* Computer Methods in Applied Mechanics and Engineering, 2007. **196**(37-40): p. 3980-3998.

8. Iman, R.L. and J.C. Helton, *An investigation of uncertainty and sensitivity analysis techniques for computer models.* Risk Anal, 1988. **8**(1): p. 71-90.

9. Cacuci, D.G. and M. Ionescu-Bujor, *A comparative review of sensitivity and uncertainty analysis of large-scale systems - II: Statistical methods.* Nuclear Science and Engineering, 2004. **147**(3): p. 204-217.

10. Draper, D., *Assessment and Propagation of Model Uncertainty.* Journal of the Royal Statistical Society Series B-Methodological, 1995. **57**(1): p. 45-97.

11. Helton, J.C., *Uncertainty and Sensitivity Analysis Techniques for Use in Performance Assessment for Radioactive-Waste Disposal.* Reliability Engineering & System Safety, 1993. **42**(2-3): p. 327-367.

12. Saltelli, A., et al., *Sensitivity analysis for chemical models.* Chemical Reviews, 2005. **105**(7): p. 2811-2827.

13. Cooke, R., *Experts in uncertainty : opinion and subjective probability in science*. Environmental ethics and science policy. 1991, New York: Oxford University Press. xii, 321.

14. Evans, J.S., et al., *Use of Probabilistic Expert Judgment in Uncertainty Analysis of Carcinogenic Potency.* Regulatory Toxicology and Pharmacology, 1994. **20**(1): p. 15-36.

15. Hora, S.C. and R.L. Iman, *Expert Opinion in Risk Analysis - the Nureg-1150 Methodology.* Nuclear Science and Engineering, 1989. **102**(4): p. 323-331.

16. McKay, M. and M. Meyer, *Critique of and limitations on the use of expert judgements in accident consequence uncertainty analysis.* Radiation Protection Dosimetry, 2000. **90**(3): p. 325-330.

17. Helton, J.C. and F.J. Davis, *Latin hypercube sampling and the propagation of uncertainty in analyses of complex systems.* Reliability Engineering & System Safety, 2003. **81**(1): p. 23-69.

18. Mckay, M.D., R.J. Beckman, and W.J. Conover, *Comparison of 3 Methods for Selecting Values of Input Variables in the Analysis of Output from a Computer Code.* Technometrics, 1979. **21**(2): p. 239-245.

19. Morris, M.D., *Three Technometrics experimental design classics.* Technometrics, 2000. **42**(1): p. 26-27.

20. Iman, R.L. and W.J. Conover, *A Distribution-Free Approach to Inducing Rank Correlation among Input Variables.* Communications in Statistics Part B-Simulation and Computation, 1982. **11**(3): p. 311-334.

21. Iman, R.L. and J.M. Davenport, *Rank Correlation Plots for Use with Correlated Input Variables.* Communications in Statistics Part B-Simulation and Computation, 1982. **11**(3): p. 335-360.

22. Hora, S.C. and J.C. Helton, *A distribution-free test for the relationship between model input and output when using Latin hypercube sampling.* Reliability Engineering & System Safety, 2003. **79**(3): p. 333-339.

23. Kleijnen, J.P.C. and J.C. Helton, *Statistical analyses of scatterplots to identify important factors in large-scale simulations, 2: robustness of techniques.* Reliability Engineering & System Safety, 1999. **65**(2): p. 187-197.

24. Storlie, C.B. and J.C. Helton, *Multiple predictor smoothing methods for sensitivity analysis: Description of techniques.* Reliability Engineering & System Safety, 2008. **93**(1): p. 28-54.

25. Storlie, C.B. and J.C. Helton, *Multiple predictor smoothing methods for sensitivity analysis: Example results.* Reliability Engineering & System Safety, 2008. **93**(1): p. 55-77.

26. Helton, J.C. and F.J. Davis, *Illustration of sampling-based methods for uncertainty and sensitivity analysis.* Risk Anal, 2002. **22**(3): p. 591-622.

27. Saltelli, A., *Making best use of model evaluations to compute sensitivity indices.* Computer Physics Communications, 2002. **145**(2): p. 280-297.

28. Saltelli, A. and J. Marivoet, *Nonparametric Statistics in Sensitivity Analysis for Model Output - a Comparison of Selected Techniques.* Reliability Engineering & System Safety, 1990. **28**(2): p. 229-253.

29. Saltelli, A., *Sensitivity analysis in practice : a guide to assessing scientific models*. 2004, Hoboken, NJ: Wiley. xi, 219 p.

30. Ratto, M., A. Pagano, and P. Young, *State dependent parameter metamodelling and sensitivity analysis.* Computer Physics Communications, 2007. **177**(11): p. 863-876.

31. Tarantola, S., D. Gatelli, and T.A. Mara, *Random balance designs for the estimation of first order global sensitivity indices.* Reliability Engineering & System Safety, 2006. **91**(6): p. 717-727.

32. Hoare, A., D.G. Regan, and D.P. Wilson, *Sampling and Sensitivity Analyses Tools (SaSat) for Computational Modeling.* Theoretical Biology and Medical Modelling (open access at http://www.tbiomed.com/content/5/1/4.), 2008. **5**: p. 4.

33. SimLab, *http://simlab.jrc.ec.europa.eu/.* distributed under the SimLab Software License, Version 1.0, 2006.

34. Blower, S.M. and H. Dowlatabadi, *Sensitivity and Uncertainty Analysis of Complex-Models of Disease Transmission - an Hiv Model, as an Example.* International Statistical Review, 1994. **62**(2): p. 229-243.

35. Saltelli, A. and R. Bolado, *An alternative way to compute Fourier amplitude sensitivity test (FAST).* Computational Statistics & Data Analysis, 1998. **26**(4): p. 445-460.

36. Saltelli, A., S. Tarantola, and K.P.S. Chan, *A quantitative model-independent method for global sensitivity analysis of model output.* Technometrics, 1999. **41**(1): p. 39-56.

37. Collins, D.C. and R. Avissar, *An Evaluation with the Fourier Amplitude Sensitivity Test (Fast) of Which Land-Surface Parameters Are of Greatest Importance in Atmospheric Modeling.* Journal of Climate, 1994. **7**(5): p. 681-703.

38. Cukier, R.I., et al., *Study of Sensitivity of Coupled Reaction Systems to Uncertainties in Rate Coefficients .1. Theory.* Journal of Chemical Physics, 1973. **59**(8): p. 3873-3878.

39. Schaibly, J.H. and K.E. Shuler, *Study of Sensitivity of Coupled Reaction Systems to Uncertainties in Rate Coefficients .2. Applications.* Journal of Chemical Physics, 1973. **59**(8): p. 3879-3888.

40. Lempert, R., S. Popper, and S. Bankes, *Confronting surprise.* Social Science Computer Review, 2002. **20**(4): p. 420-440.

41. Segovia-Juarez, J.L., S. Ganguli, and D. Kirschner, *Identifying control mechanisms of granuloma formation during M. tuberculosis infection using an agent-based model.* J Theor Biol, 2004. **231**(3): p. 357-76.

42. Riggs, T., et al., *A comparison of random vs. chemotaxis-driven contacts of T cells with dendritic cells during repertoire scanning.* J Theor Biol, 2008. **250**(4): p. 732-51.

43. Helton, J.C., *Uncertainty and sensitivity analysis in performance assessment for the Waste Isolation Pilot Plant.* Computer Physics Communications, 1999. **117**(1-2): p. 156-180.

44. Helton, J.C. and R.J. Breeding, *Calculation of Reactor Accident Safety Goals.* Reliability Engineering & System Safety, 1993. **39**(2): p. 129-158.

45. Helton, J.C., et al., *Uncertainty and Sensitivity Analysis of Early Exposure Results with the Maccs Reactor Accident Consequence Model.* Reliability Engineering & System Safety, 1995. **48**(2): p. 91-127.

46. Morris, M.D., *Factorial Sampling Plans for Preliminary Computational Experiments.* Technometrics, 1991. **33**(2): p. 161-174.

APPENDIX B

The Dual Role of Dendritic Cells in the Immune Response to HIV-1 Infection

ABSTRACT

Many aspects of the complex interaction between HIV-1 and the human immune system remain elusive. Our objective is to study these interactions, focusing on the specific roles of dendritic cells (DCs). DCs enhance HIV-1 infection processes as well as promote an anti-viral immune response. We explore the implications of these dual roles. We present and analyze a mathematical model describing the dynamics of HIV-1, CD4+ and CD8+ T-cells, and DCs interacting in a human lymph node. We validate the behavior of our model against non-human primate SIV experimental data and published human HIV-1 data. Our model qualitatively and quantitatively recapitulates clinical HIV-1 infection dynamics. We perform sensitivity analyses on the model to determine which mechanisms strongly affect infection dynamics. Sensitivity analysis identifies system interactions that contribute to infection progression, including DC-related mechanisms. We compare DC-dependent and DC-independent routes of CD4+ T-cell infection. The model predicts that simultaneous priming and infection of T cells by DCs is critical during early infection stages when activated T-helper cell numbers are low. Further, our model predicts that, while direct failure of DC function and an indirect failure due to loss of CD4+ T-cell help

are both significant contributors to infection dynamics, our results support the hypothesis that the former has a more significant impact on HIV-1 immunopathogenesis.

INTRODUCTION

Despite enormous advances in our understanding of HIV-1 and the human immune response in the last 25 years, much of this complex interaction remains elusive. CD4+ T-cells are crucial to host-viral dynamics: these cells are not only targets of HIV-1, but are also of key importance for the establishment and maintenance of an adaptive immune response (1). CD8+ T-cells are the primary effector cells in HIV-1 infection, as they produce non-lytic anti-viral factors and are essential for killing infected cells. In lymph nodes (LNs), myeloid dendritic cells (DCs) serve as antigen presenting cells, activating both CD4+ and CD8+ T-cells (2). DCs are also of particular importance because HIV-1 exploits DCs to enhance infection (3). Thus DCs serve as a critical link between virus, CD4+ T-cells, and CD8+ T-cells (Figure B.1). Elucidating the mechanisms behind DC-virus interactions is crucial in uncovering more details about host-virus dynamics during HIV-1 infection. Toward this goal, we develop a mathematical model of HIV-1 dynamics within a human LN, as it is the major site of viral replication and generation of the anti-viral immune response.

Role of DCs in Adaptive Immunity

DCs play a key role during the adaptive immune response by presenting antigen to resting T-cells within lymphoid tissue (2), particularly during HIV-1 infection (4).

Immature DCs in peripheral tissue are often the first immune cells to encounter antigen. These DCs undergo maturation by decreasing antigen uptake and processing, increasing antigen presentation on MHC Class I and II, and up-regulating co-stimulatory molecules such as CD80 and CD86 (2). DCs mature and migrate from the periphery to draining lymphoid tissue carrying antigen. Additionally, a population of immature myeloid DCs resides within lymphoid tissue (5). It is thought that these immature DCs within lymphoid tissue can become functionally mature after encountering antigen that is either brought by other DCs or enters through lymphatics (6, 7). Mature DCs present antigen on MHC Class II molecules and co-stimulate naïve CD4+ T-cells to become effector helper T cells, a process termed priming. Additionally, DCs cross-present exogenous antigens on MHC Class I to prime CD8+ T-cells. Primed CD8+ T-cells differentiate into effector cytotoxic T-lymphocytes (CTLs). This induction of cell-based immunity is essential for fighting intracellular pathogens such as HIV-1 (8, 9).

There is currently much debate over the detailed requirements for CD8+ T-cell priming, in particular, the requirement for CD4+ T-cell help. In some experimental models, T-cell help is necessary for a robust primary CTL response (10-12), whereas others suggest that help is only required for a subsequent memory response (13, 14). One possible mechanism to deliver T-cell help relies on DCs becoming "licensed" through interactions with effector helper T-cells, such as signaling by CD40 ligation (15, 16). Once licensed, DCs up-regulate expression of MHC Class I and co-stimulatory molecules (17), making them capable of priming a strong and sustained CTL response. Here we define licensed DCs as those DCs competent to prime CD8+ T-cells.

Dual Role of DCs in HIV Infection

In the context of HIV-1 infection, DCs play a dual role of promoting immunity while also facilitating infection. It has been shown that diverse C-type lectin receptors expressed on the surface of DCs, such as DC-SIGN (CD209), langerin (CD207), and mannose receptor (CD206), can bind HIV-1 envelope gp120 (18). DCs can then internalize and protect virus within intracellular compartments, extending the typically short infectious half-life of virus to several days (19) (though the situation is complicated, as it has recently been shown that some interactions between HIV-1 gp120 and C-type lectin receptors facilitate destruction of the virus instead (20)). Alternatively, because DCs express CD4 and CCR5/CXCR4, the receptor and co-receptors of HIV-1 respectively, productive infection of DCs is possible and has been observed (21). In both of these situations, HIV-1 associates with DCs to travel to lymphoid tissue, where 98% of T-cells reside (22, 23). During antigen presentation to CD4+ T-cells, DC-associated infectious virus, CD4 receptor, and HIV-1 co-receptors co-localize at the site of cell contact. This "infectious synapse" allows DCs to facilitate infection of CD4+ T-cells (24, 25). It is also recently suggested that infectious virus may associate with exosomal vesicles released by DCs, which could enhance infection of CD4+ T-cells (26). Taken together, these interactions suggest that DC dynamics are particularly important through the entire course of HIV-1 infection, as DC activities govern both the spread of infection and the induction of an HIV-specific CTL response.

Typical Course of HIV-1 Infection

After an initial acute phase of infection and immune response, characterized by

high viral loads and high immune system activity that lasts on the order of weeks, the viral-host system stabilizes to a long-term chronic infection (i.e. clinical latency) that lasts on the order of years. This chronic state of infection is characterized by a lower, stable, "set-point" viral load (27). Eventually, due to unknown mechanisms, this stable state is broken, leading to low CD4+ T-cell counts and high viral load characteristic of AIDS. At this point in disease progression, the architecture of lymph nodes is destroyed (28), making further quantification of CD4+ T-cells technically unfeasible (29).

SIV Non-human Primate Model of HIV-1 Infection

It is difficult to obtain data on the entire time course of HIV-1 disease in human subjects, as patients are typically not diagnosed until well after establishment of infection and therapeutic agents mask the underlying host-pathogen interactions. It is also difficult to obtain data on the lymphoid compartment in humans, due to the invasiveness of LN biopsy. Therefore, SIV infection of non-human primates (NHP) is an important experimental model for human HIV-1 infection. SIV infection of NHPs begins with an acute period of high viremia that lasts approximately 3 weeks (30), in agreement with the human course of HIV-1 infection. In contrast, however, chronic infection lasts on the order of months to a year, rather than years. This accelerated progression is similar to progression in human pediatric AIDS (31). As with AIDS in humans, simian AIDS is characterized by high viremia and depletion of CD4+ T-cells (32). Though the causes of this accelerated progression to AIDS are unknown, SIV infection of NHPs is currently the best experimental model of HIV-1 infection in humans.

Role of DCs in Progression to AIDS

Several mechanisms have been proposed to trigger progression from the chronic phase of infection to AIDS. Many have suggested that failure to control the virus results from adaptation of the virus during the course of infection, such as enhanced infection or replication capacities (33, 34), or acquisition of mutations allowing escape from immune control (35). Instead of an adaptive change in virus, others have hypothesized that progressive alteration of the immune system results in the transition to AIDS (36-38). Dysfunction of DCs is central to many of these hypotheses. During progressive HIV-1 infection, DCs either fail to prime T-cells and/or induce immunosuppressive regulatory T-cells (36, 37), resulting in failure of immune control; however, the mechanisms of this dysfunction are unknown. Are DCs directly affected by HIV-1? Or, does virus alter CD4+ T-cells, indirectly causing DC dysfunction due to lack of T-cell help (38)? Since DCs are central to the establishment and maintenance of an anti-viral immunity, DCs likely play a key role in progression to AIDS. Because components of the immune system are highly interactive, progressive HIV-1 infection to AIDS is likely a multi-factorial and multi-step process.

To study the roles of DCs during HIV-1 infection, we present a deterministic mathematical model of human HIV-1 infection and accompanying immune response. In previous work (39), we explored the interactions of naïve and activated classes of T-cells, DCs, and HIV-1. Here we develop a next-generation model to focused on the dynamics solely occurring within a LN, include recent findings regarding the roles of DCs in the immune response, and address current questions regarding the role of DCs in HIV-1 infection. We validate our model by comparison to data generated within a non-human

NHP SIV infection model, in addition to published human HIV-1 clinical data. As the equations that constitute our mathematical model describe specific interactions between cell types and virus, our analysis allows us to address the importance of DC mechanisms in acute and chronic phases of infection, as well as their role in triggering progression to AIDS. Our model predicts that DC functions are crucial to the outcome of host-viral interactions. We explore how T-cell infection is enhanced by DCs, showing that the relative importance of this effect changes with respect to infection state. We predict that many virus-host interactions are important in determining infection state. In particular, our model predicts which mechanisms of DC dysfunction are most significant in leading to a transition to AIDS.

MATERIALS and METHODS

NHP SIV Infection Model

The studies involving animals, from which lymphoid tissues were examined, were performed under the guidance and approval of the University of Pittsburgh Institutional Animal Care and Use Committee. Adult cynomolgus macaques (*Macaca fascicularis*) were infected intrarectally with a characterized stock of the SIV/DeltaB670 isolate (40) and sacrificed at 2 wk post-infection, or upon development of AIDS, defined by reduced CD4 T-lymphocyte counts, progressive weight loss and other clinical symptoms such as loss of appetite and/or intractable diarrhea. Axillary and hilar LN Tissues were processed by immersion fixation in 4% paraformaldehyde/PBS, cryoprotection, and snap-freezing as described (41, 42).

Immunofluorescence Microscopy and Immunohistochemistry

To detect Ki67 and CD3 in macaque axillary LN paracortex, we performed multi-color immunofluorescence staining using antibodies specific for Ki67 (Novocastra, clone MM1; 1:100) and CD3 (Novocastra, clone CD3-12; 1:100). Tissue sections (14um) were pretreated by microwaving in 0.01M citrate buffer (pH 6.0), cooled to room temp. for 30min, then incubated with primary antibodies at room temp. in a humid chamber for 1hr. After washing in 1XPBS, the secondary antibodies FITC-conjugated goat anti-mouse IgG1 (Jackson ImmunoResearch; 1:100) and biotinylated goat anti-rabbit Ig (Zymed; 1:100) were incubated at room temp in a humid chamber for 30min., and washed with 1XPBS. Tissue sections were then incubated with AF488-conjugated rabbit anti-Fluorescein (Molecular Probes; 1:80) and streptavidin-AF647 (Molecular Probes; 1:100) at room temp in a humid chamber in the dark for 30min., washed with 1XPBS, immersed in 70% ethanol for 5min., incubated at room temp with Autofluorescence Eliminator (Chemicon) for 15min., immersed in 70% ETOH three times for 1min. each, and washed in 1XPBS. To label all nuclei we used Sytox Orange (Invitrogen; 1:30,000) and immersed the slides for 1min. at room temp followed by washing in 1XPBS. The slides were then mounted using Prolong Gold Antifade (Invitrogen) and stored at room temp overnight. Images were captured on an Olympus Fluoview 500 laser scanning confocal microscope using a 40X objective. Captured images were analyzed using multiple processing and measuring functions in the MetaMorph software package (Universal Imaging) to count total, CD3+, Ki67+, and combined CD3+/Ki67+ cells.

We stain tissue sections for the cell cycle-associated nuclear antigen Ki67 (43). In

the Rhesus macaque, Ki67 expression in T-cells indicates cells that have divided within the past 3-4 days (44). It is possible that some of these Ki67+ T-cells are naïve cells that are proliferating due to a homeostatic response to lymphopenia. However, in the context of HIV-1 infection of humans, researchers have shown that CD4+Ki67+ T-cells have an effector phenotype (45), and that T-cell division during HIV-1 infection is primarily due to antigen-driven immune activation, rather than an antigen-independent homeostatic response (46, 47). Thus, we consider Ki67 to be a marker for active, effector T-cells.

Immunohistochemical staining (IHC) was performed to detect DC-SIGN+ cells in hilar LN paracortex tissue from SIV-infected and uninfected macaques as described (41, 42) by using an anti-CD209/DC-SIGN monoclonal antibody (BD Pharmingen, clone DCN46) using the SuperPicture kit (Zymed). The number of CD209/DC-SIGN$^+$ cells was determined by counting stained cells in five different sites in paracortex at a magnification of 600X. DC-SIGN is expressed by multiple DC populations, as well as some subpopulations of macrophages. Although this is not a completely specific marker for DCs, we note that there is no single marker that serves this purpose and that the dendritic morphology of most of the stained cells in the paracortical regions of LNs provided confidence that DCs were being stained and counted.

IHC for CD3$^+$ cells was performed in the same way and counted in five random microscopic fields at 1,000X under oil, and the mean number of positive cells per mm^2 of tissue was calculated.

In all cases, cell counts per volume of tissue are calculated by multiplying the cell count per mm^2 of tissue by the thickness of the tissue section (14um) and scaling to appropriate units (per ml).

In Situ Hybridization

In situ hybridization was performed as previously described (41, 42), using autoradiographic exposure times of 7 days. The numbers of SIV vRNA+ cells in 10-20 random 400X microscopic fields per region were manually counted and the mean number of productively infected cells was converted to cells per mm^2.

Mathematical Model

We developed a mathematical model representing the temporal dynamics of cells and virus, interacting in the paracortical region of a human LN. Our model describes cell-cell and virus-cell interactions within a LN using a system of nine non-linear ordinary differential equations. These equations describe the rates of flow as cells arrive into a single LN: they interact, change phenotype, and exit or undergo apoptosis. Figure B.1 shows a schematic outlining key features of the model. A detailed mathematical description of the model is given in online supplemental material (http://dx.doi.org/10.1099/vir.0.83600-0), but here we outline some of the major interactions that we have included.

CD4+ T-cell Dynamics

We consider three phenotypic classes of CD4+ T-cells: resting, activated effector, and infected. Resting CD4+ T-cells that are naïve (i.e. CD45RA+/CD62L+) arrive in the LN due to infection-independent homeostatic mechanisms, maintaining the resting pool in the absence of infection. During infection, additional resting T-cells (either

CD45RA+/CD62L+ naïve or CD45RO+/CD62L- memory) are recruited to the LN by DC-produced chemokines (48-50), by up-regulation of homing receptors due to non-productive contact with DC-associated virus in the periphery (51, 52), and by LN-homing central memory cells (53). Once in LNs, resting CD4+ T-cells can encounter virus. In most cases, contact between host cells and virus does not result in productive infection. Most of these abortively-infected cells undergo apoptosis (54). However, some abortively-infected naïve cells can be stimulated to become productively infected, a phenomenon thought to occur in the milieu of lymphoid tissue (55, 56). It has been shown that these resting cells are less commonly infected than active T-helper cells (55, 57).

DCs are potent antigen presenting cells. Upon encountering mature or licensed DCs, a fraction of resting CD4+ T-cells that are antigen-specific are primed to become effector T-helper cells (8). As DCs sequester infectious virus and facilitate infection of T-cells, a fraction of CD4+ T-cells become infected during priming (3). Otherwise, effector T-helper cells undergo clonal expansion. T-helper cells can encounter virus, or re-encounter virus-loaded DCs, leading to productive infection. Infection is inhibited by CTLs as they produce chemokines, such as CCL3 (MIP-1α), CCL4 (MIP-1β), and CCL5 (RANTES), that compete with HIV-1 for CCR5 co-receptor binding (58). Once infected, CD4+ T-cells can be killed by CTLs through perforin/granzyme and Fas/Fas-ligand mechanisms. Resting, activated, or infected CD4+ T-cells can exit via efferent lymphatics or undergo apoptosis.

HIV-1 Dynamics

Virus is produced by infected CD4+ T-cells. This production is inhibited by the action of CTLs producing CAF, α-defensins, and interferon, non-lytic anti-viral factors (58-60). HIV-1 particles exit the system, as virions are labile. However, the vast majority of virus is associated with follicular dendritic cells (23). The half-life of follicular dendritic cell-associated HIV-1 RNA is 1.7 days (61), and infectious virus is detectable for up to 9 months (62). Follicular dendritic cells are not explicitly considered in this model, though we account for their effect on virus half-life.

CD8+ T-cell Dynamics

We consider two phenotypic classes of CD8+ T-cells: resting, and activated effector. Naïve resting CD8+ T-cells arrive in the LN due to infection-independent homeostatic mechanisms. It has been shown that this continuous recruitment of naïve CD8+ T-cells is particularly important during chronic infections (63). During infection, additional resting CD8+ T-cells are recruited to the LN by DC-produced chemokines (48-50) and by LN-homing central memory cells (53). DCs cross-present exogenous antigens on MHC class I molecules to CD8+ T-cells. Some investigators have reported that CD8+ T-cells require more or different co-stimulatory signals to become fully activated effector CTLs (64). Licensed DCs have been shown to up-regulate co-stimulatory molecules that promote development of CTLs, such as CD86 (15) and 4-1BBL (17, 65). In our model, CD8+ T-cells are primed only by licensed DCs. Once primed, CTLs undergo clonal expansion. Either resting CD8+ T-cells or effector CTLs can exit via efferent lymphatics or undergo apoptosis.

Dendritic Cell Dynamics

The prototypical "Langerhans cell paradigm" behavior of DCs is that, after encountering antigen in the periphery, DCs mature and travel to the LN (66). Thus, in our model, mature DCs arrive from the periphery during HIV-1 infection. In contrast to this paradigm, however, there is evidence that there are resident immature DCs in the LN, and that immature DCs spontaneously migrate from the periphery to the LN without having encountered antigen (5). Thus, we assume immature DCs arrive to the LN independently of infection. Once in the LN, immature DCs can encounter antigen and undergo maturation. This source of antigen can be soluble antigen carried by lymphatic fluid (6), opsonized virus particles (67), HIV-1 protein released by live or apoptotic infected cells (68-71), entire MHC-peptide complexes acquired from dead cells (72, 73), or antigen released from migratory DCs (7). Mature DCs can become licensed though interactions with activated helper T-cells, such as by CD40-CD40L signaling (15). Because mature and licensed DCs present antigen on MHC-I, they are susceptible to being killed by CTLs (74, 75), though some findings suggest that DCs might be partially protected from CTL killing while in the LN (75). As DCs have a finite life span, any of these DC phenotypes can undergo cell death, though mature and licensed DCs are short-lived compared to immature DCs (76).

Parameter Estimation

Parameters that govern the rates of interaction described above (such as rate constants) are estimated based on published biological data from a variety of sources.

Because there exists biological variability between animal models (77), and systematic error between any experimental systems, all parameter estimates have an associated degree of uncertainty. We address this uncertainty in a systematic manner during uncertainty and sensitivity analysis (see "Uncertainty and Sensitivity Analysis" section below). For full details of parameter estimation, see online supplemental material (http://dx.doi.org/10.1099/vir.0.83600-0).

Initialization of the Simulation

Prior to infection, the LN is assumed to contain only resting CD4+ and CD8+ T-cells, and immature DCs. We determine the initial values of total T-cells and DCs from immunohistochemistry counts derived from uninfected NHPs herein. We also determine initial CD4+ and CD8+ T-cell counts by scaling the total T-cell counts by published human CD4:CD8 T-cell ratios (78). In the presence of HIV-1 infection, dynamics begin with the arrival to the LN of a single mature DC at day 0. As mature DCs arriving from the periphery can present both viral antigen and infectious virus, both infection and immune dynamics are initiated. We also initiated infection dynamics by the arrival of free virus particles, with similar results (not shown).

Solving the Model System

The system of ordinary differential equations is solved using the ode15s numerical solver in the software package MATLAB (The MathWorks, Inc.) (79). The solution of the system at any given time point yields the average number of each type of cells (or virions) within a prototypical LN. It is important to note that differential

equation models, like this one, do not consider stochastic processes - such as one cell encountering another by chance. Rather, the models capture the average rate of interaction within the system, dependent on the number of interacting cells (or virions) and the parameters governing the interaction. We solve our system over a time course representing years in order to capture known temporal dynamics of cell and viral populations from initial through late stages of infection in humans.

Validation with NHP Data

To validate the behavior of our model, we compare data derived from our model simulations to NHP SIV-infection data. Comparing our model simulation with experimental data presents a unique challenge: our model simulates paracortical LN tissue over a longitudinal time course, however, the invasiveness of LN biopsy makes a longitudinal NHP study difficult. Thus, our experimental data are cross-sectional and categorized by disease state. Due to inherent variability in the kinetics of infection between non-isogenic animals, categorization by time post infection is not completely reliable. For example, an animal might be in *bona fide* clinical latency at 4 months post-infection but at that same duration of infection, another animal might be developing AIDS. Instead, we categorize infection state not only by time post infection but also by plasma viral load, blood CD4+ T-cell counts, and clinical symptoms such as progressive weight loss, loss of appetite, or intractable diarrhea. We map our experimental animal study categories to ranges of time in our model simulation, for the purpose of comparison. We align the uninfected experimental category with pre-infection negative time points in our model simulation. Similarly, we align the chronic infection (clinical

latency) experimental category with the chronic steady state of our model simulation. Because the acute phase of infection is consistently within weeks 1 to 3 post-infection in multiple NHP models of AIDS, we align the acute infection *macaque* categorical data to days 7 through 21 of our mathematical model simulation. To illustrate the robustness of our model simulations to uncertainty in parameter estimation, we perform uncertainty analysis (described below), simultaneously varying all model parameters +/- 2-fold, with the exception of proliferation and death/exit to efferent lymph parameters, which are varied according to the sampling ranges shown in supplemental Table 1 (online supplemental material: http://dx.doi.org/10.1099/vir.0.83600-0).

Validation with Published Human Data

We additionally validate the behavior of our model by comparing our model simulations to published human HIV-1 infection data. For purposes of comparison, we scale human total-body cell count estimates by 1/700 to represent one ml of lymphoid tissue. This conversion assumes a typical human body weight is 70 kg, 1% of body weight is lymphoid tissue (23), and tissue density is approximately 1 g/ml.

Uncertainty and Sensitivity Analysis

We perform uncertainty and sensitivity analysis since we cannot perfectly estimate the values of parameters, all parameters exhibit biological variability, and we wish to determine which parameters are most important in governing the state of the system. Sensitivity and uncertainty analysis is performed using Latin Hypercube Sampling and Partial Rank Correlation (LHS/PRC) (80), and the Extended Fourier

Amplitude Sensitivity Test (eFAST). LHS/PRC is performed using 1000 model simulations, and eFAST is performed using 697 simulations per parameter and 6X parameter resampling for a total of 175,644 model simulations. Briefly, both algorithms sample input parameters over a range (see supplemental Table 1 of supplemental material online: http://dx.doi.org/10.1099/vir.0.83600-0), repetitively run model simulations with each parameter combination, and then measure the sensitivity of the system to changes in each parameter. Like ANOVA, the eFAST method decomposes variance in model output to determine how much each parameter contributes. The eFAST algorithm reports the fraction of variance in model output explained by each input parameter. The eFAST total-order sensitivity index, which we report here, takes into account higher-order interactions between multiple parameters. We determine the limit of detection by allowing the eFAST algorithm to partition variance to a dummy parameter that does not affect model output. To determine statistical significance and compare between parameters, we perform two-sample Student's t-test on eFAST values from parameter resampling (81). LHS/PRC reports sensitivity as a coefficient of correlation between input parameter and model output. To prevent false positives due to multiple testing, statistical significance of these correlations is determined by Student's t-test with Bonferroni correction (82). Statistical comparison between these correlation coefficients is performed using Fisher's z transformation (83). For a more detailed discussion of these methods of uncertainty and sensitivity analysis, see (84).

In Silico Interventions

To explore the role of particular interactions or mechanisms, we perform *in silico*

interventions by changing rate constants and other parameters during the course of a simulation. *In silico* intervention is analogous to disrupting or enhancing particular interactions *in vivo* using pharmacological treatments or conditional gene knockdown. The flexibility of our *in silico* system, however, allows us to perform an intervention even if there is no analogous experimental system. It is important to note that, because we restrict our scope to the LN, we necessarily assume our intervention occurs only in the LN. Thus our *in silico* intervention experiments are analogous to local administration of a pharmaceutical or a tissue-specific conditional gene knockdown, not full-body treatment or genetic knockout.

In addition, we use *in silico* intervention to induce an *in silico* depletion of cell types. For depletion of a particular cell type, we block mechanisms involving arrival to the LN, maturation, and proliferation, so that no new cells enter the population. Mechanisms leading to differentiation into other phenotypes or exit from a LN are left in place. Thus cells are gradually depleted from a LN as they exit but are not replenished. This *in silico* cell depletion is analogous to *in vivo* antibody-mediated neutralization of cells. Several groups performed experiments in which monoclonal antibodies are used to deplete CD8+ T-cells from blood and lymphoid tissue of simian immunodeficiency virus (SIV) or chimeric simian/human immunodeficiency virus (SHIV) infected *Rhesus macaques*. These groups demonstrate that CD8+ T-cell experimental depletion during infection causes a dramatic rise in viral load, 1-3 orders of magnitude over pre-depletion levels, depletion of CD4+ T-cells, and disease progression. However, as *in vivo* depletion is temporary, CD8+ T-cell counts rebound, and viral loads accordingly drop to pre-depletion levels (85-87). As a positive control, we deplete CD8+ T-cells *in silico*. For the

purpose of our model analysis, we define an "AIDS-like state" based on this immunity-impaired positive control.

RESULTS

To explore the role of DCs during HIV-1 infection in the LN, we first capture the homeostatic mechanisms of a healthy LN in the absence of virus. Next, we introduce virus to simulate an acute phase and chronic state of infection, and validate our model by comparing our simulations to SIV-infected NHP data and published human clinical data. Finally, we analyze our model using uncertainty and sensitivity analysis techniques to identify mechanisms involved in HIV-1 infection and pathogenesis.

Simulation of a healthy lymph node

As a negative control, we simulate a healthy lymph node in the absence of virus. By construction, all cell types remain constant in number, reflecting an assumption of homeostasis in the absence of antigen (88). Resting CD4+ T-cells are maintained at approximately 3.5×10^8 cells per ml, resting CD8+ T-cells are maintained at approximately 1.2×10^8 cells per ml, and LN resident immature DCs are maintained at 1.17×10^8 cells per ml of paracortical LN tissue. These levels observed in our simulation agree with NHP infection data derived herein and also with published human clinical data (23) (Table B.1).

Simulation of acute phase and chronic steady state match human and NHP infection data

We initiate virus-induced dynamics in the lymph node by the arrival of a single mature DC carrying HIV-1, at day 0. Solving the model simulates the populations of each cell/virus type over time (Figure B.2). From our model, we calculate experimentally relevant variables for comparison to our NHP experimental data (Figure B.3). We find that our model quantitatively recapitulates the depletion of DCs and T-cells (Figure B.3, A-B), and the increase in infected and activated T-cell populations (Figure B.3, C-D) in the paracortical regions of a LN during uninfected, acute and chronic infection.

Other studies have shown that mature DCs are short-lived (76). As a result, it has been observed that labeled mature DC counts are depleted after only 2 days post-immunization (89), that stimulation with bacterial lipopolysaccharide causes the accumulation of apoptotic DCs (90), and that DCs are depleted during simian AIDS (91). Similarly, we find that total dendritic cells become depleted during SIV infection, both in our experimental animal studies and our model simulations (Figure B.3, A). The model simulation predicts that DC depletion occurs gradually after infection peaks (Figure B.3, compare panels A and C).

Because our model distinguishes CD4+ from CD8+ T-cells, but our experimental data only measures total CD3+ T-cells, we additionally validate the model simulation CD4:CD8 ratio by comparison to published HIV-1-infected human lymph node data (78). Typically in the blood, the CD4:CD8 ratio inverts from 2:1 to 1:2 over the course of infection (92). However, our model recapitulates the 4:1 to 1:2 inversion of the CD4:CD8 ratio that occurs in human lymphoid tissue during chronic HIV-1 infection (Figure B.3,

E). Although it is currently not experimentally tractable, our model predicts what the abrupt dynamics of the inversion may look like (Figure B.3, E).

To ensure relevance to human disease, we additionally validate our model simulation by comparison to published human HIV-1 infection data (Table B.1). Our model agrees with human estimated lymphoid tissue cell counts.

Determination of parameters that drive viral load

Sensitivity and uncertainty analysis reveals how variation in model parameters affects the entire system. First, we analyze parameters related to CD4+ T-cells and virus during chronic state infection by LHS/PRC (see supplemental material online: http://dx.doi.org/10.1099/vir.0.83600-0). We do not express viral production in terms of a single rate constant (virus produced per infected cell per day) because this parameter would be difficult to estimate experimentally. Rather we express this rate as the product of two separate parameters: one represents the viral "burst size", the average number of virions produced per infected cell lifetime (N); the other is the death rate constant of infected cells per day (μ_I), which determines the average length of a cell lifetime. We find that increasing either of these parameters (μ_I, N) increases viral load. We also find that infection of active T-helper cells by free virus (k_V), has a significant positive correlation with viral load. We find that the destruction rate of virions (μ_V), has a significant negative correlation with viral load. Thus, our model suggests that any mechanism that reduces the destruction of virions, such as a defect in clearance by phagocytes or protective sequestration of virus, should increase viral load. Finally, we find that the parameter controlling the rate of abortive infection/bystander killing of resting CD4+ T-cells (k_{ab}) has a significant negative correlation with viral load. Although abortive infection and

bystander killing is implicated in loss of CD4+ T-cells in progressive HIV-1 disease, we find that this mechanism decreases viral load by removing host cells that might have otherwise had a chance of becoming productively infected.

Next we analyze parameters related to CD8+ T-cells during chronic state infection by LHS/PRC (see supplemental material online: http://dx.doi.org/10.1099/vir.0.83600-0). As expected, since CD8+ T-cells are precursors to antiviral effector CTLs, many CD8+ T-cell related parameters are significantly correlated with viral load. The parameters that control recruitment of additional CD8+ T-cells due to DC chemokines (ϕ_8, f_{11}) are significantly correlated with viral load: increasing ϕ_8 or decreasing f_{11} allows greater CD8+ T-cell recruitment, decreasing viral load. The parameter that controls the rate of proliferation of primed CTLs (p_C) has a significant negative correlation with viral load. In contrast, mechanisms that remove CD8+ T-cells (μ_8, μ_C) increase viral load. The importance of these parameters highlight the idea that controlled migration of cells through lymphoid tissue is critical during HIV-1 infection (63). Dysfunction that prevents proper recruitment of CD8+ T-cells, or disruption of cell migration within the LN that causes these cells to exit faster would lead to increased viral load.

The model also predicts that parameters involved in CTL effector functions are significantly correlated with viral load. Parameters that control non-lytic anti-viral functions of CTLs are significant. Specifically, CTL-produced anti-viral factors inhibiting infection of T-helpers by mature DC-associated virus (c_2), and inhibiting viral production by infected cells (c_4) each correlate with viral load. Because these parameters appear in the denominator of the equations (see online supplemental material:

http://dx.doi.org/10.1099/vir.0.83600-0), increasing these parameters decreases the strength of the CTL non-lytic viral inhibition. Thus these parameters are positively correlated with viral load. The lytic killing of infected cells and licensed DCs (κ_I and κ_L, respectively) also correlate with viral load. By killing infected cells, CTLs decrease viral load. CTL killing of DCs is hypothesized to serve as a negative feedback, to shutdown an immune response that has successfully run its course (74). While this might be advantageous to prevent excess tissue damage once an acute pathogen is cleared, our result shows that this dampening of immune response during a chronic HIV-1 infection leads to an increase in viral load.

Many of the significant parameters identified by this analysis are DC-related (Table B.2). These DC-related mechanisms are either positively or negatively correlated with viral load by LHS/PRC, indicating the dual role of DCs in promoting both infection and immunity. We find that the parameter governing the immigration of mature DCs that have encountered antigen in the periphery (ϕ_{DM}) has a negative correlation with viral load. Although additional mature DCs promotes infection, their net effect is to promote immunity, reducing steady state viral load. The parameters that control licensing of DCs by T-helper cells (λ) and priming of CTLs by licensed DCs (r_{8L}) are both negatively correlated with viral load as these mechanisms promote immunity. In contrast, parameters that control priming and subsequent infection of T-helper cells by DC-associated virus (r_{DM} and k_{DM}, respectively) are correlated with increased viral load.

Importance of DC-facilitated infection varies during the course of HIV-1 infection

Our model captures four mechanisms leading to productive infection of CD4+ T-

cells (Figure B.4, A). By all four routes, resting CD4+ T-cells can become infected cells. In the first case, virus infects resting T-cells directly without a need for priming. Of these cells, a small fraction can be stimulated to become productively infected, and the rest remain abortively infected and undergo apoptosis. This is the only route of infection described that is completely independent of DCs. In the second case, CD4+ T-cells are *concurrently* primed and infected by DCs. Cases 3 and 4 depend on mature or licensed DCs to first prime CD4+ T-cells. In the third case, virus infects activated T-helper cells independently of DCs. In the fourth case, DC-associated virus infects primed T-helper cells. To gauge the relative importance of each of these infection mechanisms, we perform local sensitivity analysis on these nine parameters during both establishment of infection/early acute phase (days 2-6) and chronic state (day 300) of infection. During the acute phase of infection, four parameters are significantly correlated with viral load (see asterisks, Figure B.4, B): abortive infection of T-cells (κ_{ab}), which are then stimulated to become productively infected (α), priming of T-helper cells by mature DCs (r_{DM}), and concurrent priming and infection by mature DCs (b_M) are significantly correlated with viral load. During the earliest establishment of infection, there has not been sufficient time to prime many T-helper cells. Thus, mechanisms that require activated T-helper host cells cannot contribute significantly to infection levels. Comparing the relative strength of each these four infection mechanisms, we find that priming of T-helper cells and concurrent priming and infection by mature DCs have a significantly greater correlation with viral load than the other infection mechanisms (see daggers, Figure B.4, B). Our model predicts that the ability of DCs to concurrently prime and infect resting CD4+ T-cells is crucial to the establishment of the acute phase of infection.

In contrast, during the chronic state of infection (Figure B.4, C), abortive infection of resting T-cells becomes negatively correlated, and concurrent priming and infection of T-cells by DCs becomes insignificant. Instead, infection mechanisms 3 and 4, priming followed by infection, are significantly correlated to chronic state viral loads (see asterisks, Figure B.4, C). Comparing the relative significance of each of these mechanisms, we find that infection of activated T-helper cells by DC-associated virus has a significantly greater correlation, revealing the importance of DCs enhancing infection (see dagger, Figure B.4, C).

Positive control model of transition to AIDS

As a positive control, we deplete CTLs *in silico* (Figure B.5). In the absence of immune effector functions, the system establishes a new steady state characterized by a high viral load set-point (Figure B.5, A-D, bold solid line) and further depletion of CD4+ T-cells (not shown). In subsequent model analysis, we compare the effects of other *in silico* interventions to this positive control "AIDS-like state".

Many mechanisms can cause progression to an AIDS-like state

Parameters we found to be significant in our sensitivity analysis (Table B.2) are important in determining viral load. Thus, mechanisms controlled by these parameters are likely involved, singly or in combination, in the transition to AIDS. Specific parameters identified by both LHS/PRC and eFAST methods have a very significant effect on viral load. However, the relative strengths and weaknesses of these algorithms cause them to identify different subsets of marginally sensitive parameters. These parameters, though

significant, have a relatively small effect on viral load. These significant but weak mechanisms might therefore work in combination with each other, or the more significant mechanisms, causing a multi-factorial progression to AIDS. To test which mechanisms could be involved in progression to an AIDS-like state, we perform *in silico* intervention by varying the mechanisms we identified in the sensitivity analysis (Figure B.5). We find that parameters that are able to cause an AIDS-like state fall into three functional categories: first, mechanisms related to death or exit of CD8+ T-cells or virus (Figure B.5, A); second, mechanisms related to infection and viral replication (Figure B.5, B); third, mechanisms related to maintenance or effector functions of immune response (Figure B.5, C).

The first functional group identified, parameters related to death or exit of CD8+ T-cells or virus, represents mechanisms related to lymphoid tissue architecture and regulated traffic of cells though LNs. Studies have shown that labeled T-cells injected i.v. can be detected in efferent lymph in as few as 6 hours (93, 94). Increasing the rate at which CD8+ T-cells circulate out of the LN to correspond to a half-life of one hour causes an AIDS-like increase in viral load. Immunologically, this could correspond to a infection-induced alteration of LN architecture, signaling, or adhesion molecules, causing quicker exit to efferent lymph (95). Indeed, other investigators have found that lymph node topology dictates T-cell migration (96). This finding is not surprising given that alterations in T-cell migration and lymph node architecture are hallmarks of HIV-1 infection, other chronic infections, and immunodeficiency in general (95). Based on this theoretical result, we suggest that FTY720 (fingolimod), an experimental drug that blocks egress of lymphocytes from LN (97), could be used to experimentally address the role of

abnormal traffic of lymphocytes in HIV-1 pathogenesis. We also find that reducing the rate of virus destruction increases viral load. Other studies have shown that infectious virus can persist when associated with the follicular dendritic cell network for up to 9 months (62). We calculate that this corresponds to maximal viral half-life of approximately 11.5 days, or a rate of 0.06 per day. When we reduce the rate of virus destruction to this minimal rate, we see an increase in viral load indicating transition to an AIDS-like state, revealing the importance of mechanisms that preserve infectious virus.

The second functional group of parameters identified are those related to mechanisms of infection and viral replication. Increasing parameters controlling viral infection or replication can induce a transition to an AIDS-like state. This supports the hypothesis that a progressive adaptation of virus could result in progression to AIDS. Adaptation of virus has been suggested by others: mechanisms include changes in co-receptor usage or affinity (98, 99), or increases in replication number (34). Alternatively, it has been shown that the HIV-1 protein Nef causes up-regulation of DC-SIGN in infected DCs, possibly increasing DC-enhanced infection (100).

The third functional group of parameters controls maintenance or effector functions of immune response. Three of these mechanisms form a causal pathway: first, DCs become licensed by T-cell help; next, licensed DCs prime CTLs; finally; CTLs kill infected T-cells. We find that reducing any of these mechanisms results in a failure of the immune response to control infection, leading to an AIDS-like state. This finding lends support to the hypothesis that an impairment of immune response results in an inability to control viral load. Immunologically, reduction in CTL priming or CTL killing of infected cells could result from acquisition of CTL epitope mutations (35). Alternatively, as DCs

are central to the generation of CTL response, alterations in licensed DC function could impair immunity.

We, however, found that weakly correlated parameters were unable to independently induce an AIDS-like viral load. To test whether these weakly correlated parameters in combination could lead to multi-factorial progression to an AIDS-like state, we varied them simultaneously. We find that these parameters in combination can lead to an increase in viral load approximately equal to acute phase viremia (Figure B.5, D).

DC dysfunction in progression to AIDS

There exist two main hypotheses for the role of DC dysfunction in progression to AIDS (Figure B.6, A). The first hypothesis suggests that, as helper T cells become depleted during the course in infection they are present in insufficient numbers to license DCs, which in turn reduces the ability of DCs to prime CD8+ T cells. As CTLs are the key to anti-viral immunity, in their absence, progression to AIDS follows. The second hypothesis suggests that DC dysfunction is the result of a direct viral effect on DC intracellular processes (38, 101). Likely, both mechanisms are at play during infection; however, our model analysis tests if one hypothesis is more significant in AIDS progression. To this end, we vary parameters controlling DC licensing by T-cell help (λ) and licensed DC priming of CTLs (r_{8L}). First, we wish to test how these mechanisms affect the system when all other confounding factors are held constant at their default parameter values (see supplemental Table 1 in online supplemental material: http://dx.doi.org/10.1099/vir.0.83600-0). Interestingly, we find that these two mechanisms can trade-off. For example, increasing efficiency of DC licensing can compensate for inefficiency in priming CTLs, and *vice versa*, leading to the same viral

loads (Supplemental Figure 2 in online supplemental material: http://dx.doi.org/10.1099/vir.0.83600-0). Decreasing either or both of these mechanisms can cause an AIDS-like viral load. This finding supports both of the hypotheses, as both have an effect on progression to AIDS. Examining further however, we use global sensitivity analysis using the eFAST method to perform thousands of *in silico* experiments varying all model parameters simultaneously. This analysis identifies overall sensitivities that are apparent despite uncertainty or variability in other mechanisms. We find that licensed DC priming of CTLs (r_{8L}) is a significantly more sensitive ($p<0.01$) control point than DC licensing by T-cell help (λ). This result indicates that, given biological variability in many other mechanisms affecting both DCs and CTLs, a direct failure of licensed DCs more likely contributes to HIV-1 immunopathogenesis than an indirect failure of CD4+ T-cell help to license DCs. Additionally, this finding suggests that therapies targeting DCs function will be more successful than therapies targeting a failure of CD4+ T-cell help, as this is a stronger control point of the system.

DISCUSSION

The immune response to infectious disease is complex: the individual cells of the immune system are highly interactive, and the overall function of the system is a product of this multitude of non-linear interactions. The interplay between HIV-1 and the immune system is particularly complicated, as HIV-1 directly interacts with many immune cells, altering their functions, ultimately subverting the system at its core. Because of this complexity, the immune response and its interaction with HIV-1 are naturally suited to a

mathematical modeling approach. Building on previous work (39, 102), we present, to our knowledge, the first mechanistic model of the specific roles of DCs during HIV-1 infection. Here we focus on the dynamics within a lymph node and the role of different classes of DCs in HIV-1 dynamics, incorporating recent findings regarding the diverse roles of DCs. We move beyond the classic "Langerhan's cell paradigm" of DC function by including LN-resident immature DCs and multiple maturation/activation states. We focus on the dynamics within a lymph node, as it is the nexus of viral replication and generation of the anti-viral immune response, and is historically under-studied due to difficulties in observing human lymphoid tissue. Further, the lymph node has been consistently under-appreciated in mathematical models studying overall HIV-1 infection and immune system dynamics.

Sensitivity and uncertainty analysis reveals which parameters and, by extension, which interactions are most important in determining the overall function of the virus-host system. Our analysis shows that many of the most important parameters that determine viral load levels relate to DCs. This finding illustrates the role of DCs as a central hub of interaction and information exchange during HIV-1 infection.

Others have suggested that the immune system has evolutionarily optimized "bow-tie" or "hour-glass" structural motifs, in which diverse and redundant input signals converge on a single control point. The signals are integrated and produce diverse and redundant output signals to the rest of the system. They suggest that CD4+ T-cells serve as one control point, and propose that the severity of AIDS results from HIV-1 compromising this vulnerable control point (103). Similarly, DCs serve as a control point, integrating signals from the pathogen and the innate immune system, then

signaling other cells by way of MHC molecules, co-stimulation, and cytokines.

Given the central position of DCs in immune system interactions, it is not surprising that HIV-1 has adapted to exploit them to enhance infection. We showed that this enhancement is important in maintaining chronic infection viral load levels, and that increasing this effect can induce progression to an AIDS-like state. Others have suggested that the ability of HIV to infect resting CD4+ T-cells is critical to the earliest stage of infection, as resting T-cells predominate in the peripheral tissue where HIV is first encountered (104). Importantly, we find a similar phenomenon when HIV arrives in a lymph node: in the early stages, when activated T-helper host cells are limited, concurrent priming and infection by DCs is crucial in driving acute viremia.

We also explored the opposing anti-viral immunogenic role of DCs. We showed that T-cell help for DC licensing, priming of CTLs by licensed DCs, and CTL killing of infected cells are all critical steps in controlling chronic infection. Impairing any of these steps can cause an AIDS-like state. In particular, our model analysis suggests that the system as a whole is more sensitive to the direct failure of DCs to prime CTLs, rather than by the indirect route of failure of T-cell help to DCs. This finding has implications for the design of therapeutic vaccines and adjuvants: modulation of DC numbers, phenotype, and function could improve the outcome of infection, even if other immunological defects cannot be treated.

One limitation of this kind of model is that differential equations consider average rates of interaction between populations. When populations are small, stochastic events predominate, which our model does not capture. In addition, this kind of model does not take into account spatial effects, such as the microanatomic structure of lymphoid tissue.

Current work includes an agent-based model of immune response in a lymph node that will address these issues (105).

Clearly experimental science has made vast advances in our study of the immune response and, in particular, HIV-1 infection dynamics. The systems biology approach presented here lends an additional tool to guide our understanding of the complexities of this and other biological systems. An integrative approach can be most useful for identifying factors that are crucial to infection outcomes, and here we have presented multiple predictions that can now be further explored in an experimental setting. The close ties between experimental and theoretical science has the strong potential to push science forward.

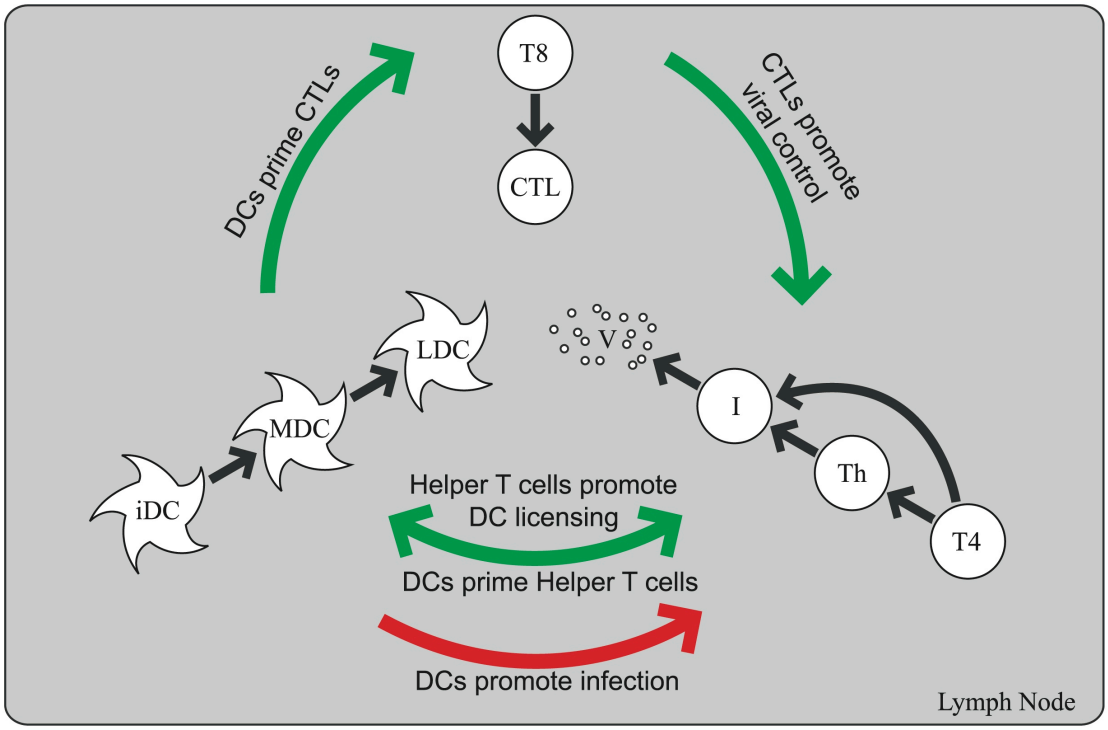

Figure B.1. Summary of interactions captured in the lymph node model. Resting CD4+ T-cells (T4) become active helper T-cells (Th) via DC antigen presentation. T4 and Th cells become infected (I) and produce virus (V). Viral and infected cell antigen, and T-helper cells promote DC function (bottom green arrow). Immature dendritic cells (iDC) become matured (MDC) by viral antigen, and licensed (LDC) by T-helper cells. LDC promote immunity (top left green arrow) by priming naïve CD8+ T-cells to become cytotoxic T-lymphocytes (CTL). CTL promote viral control (top right green arrow) by killing infected cells (I), and preventing infection and viral production via non-lytic factors. This immunogenic cycle (green arrows) is disrupted by the dual role of dendritic cells promoting infection (bottom red arrow).

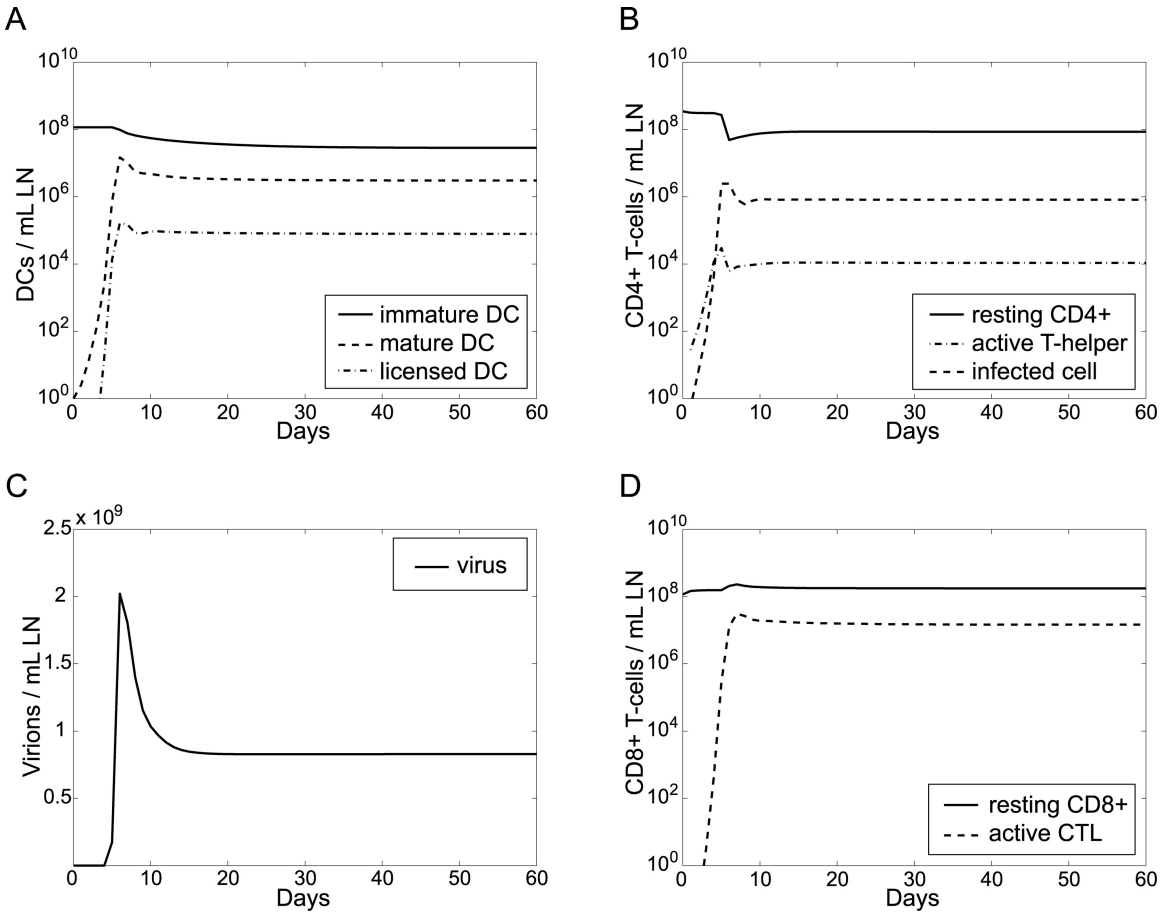

Figure B.2. Model simulation, beginning with a single HIV-1-bearing mature DC on day 0. Simulations show acute infection settling into chronic by day 20. Shown are time courses for all cell types and virus as follows: **(A)** Immature, mature, and licensed dendritic cells. **(B)** Resting CD4+ T-cells, active helper T-cells, and infected cells. **(C)** Viral load. **(D)** Resting CD8+ T-cells and active cytotoxic T lymphocytes.

Figure B.3. Comparison of model output to experimental non-human primate lymph node paracortical cell counts (generated herein) and published human lymph node data from (78). Model simulation values are derived from Figure B.2. Dotted lines indicate +/- 1 S.D. on the median of uncertainty analysis model simulations. Error bars on experimental data represent 1 S.D. on the mean. **(A)** Model simulation of total dendritic cell counts compared to experimental NHP data. **(B)** Model simulation of total T-cell counts compared to NHP data. **(C)** Model simulation of infected cell counts compared to NHP data. **(D)** Model simulation of percent activated T-cells compared to NHP data. **(E)** Model simulation of CD4:CD8 T-cell ratio compared to human clinical data from (78).

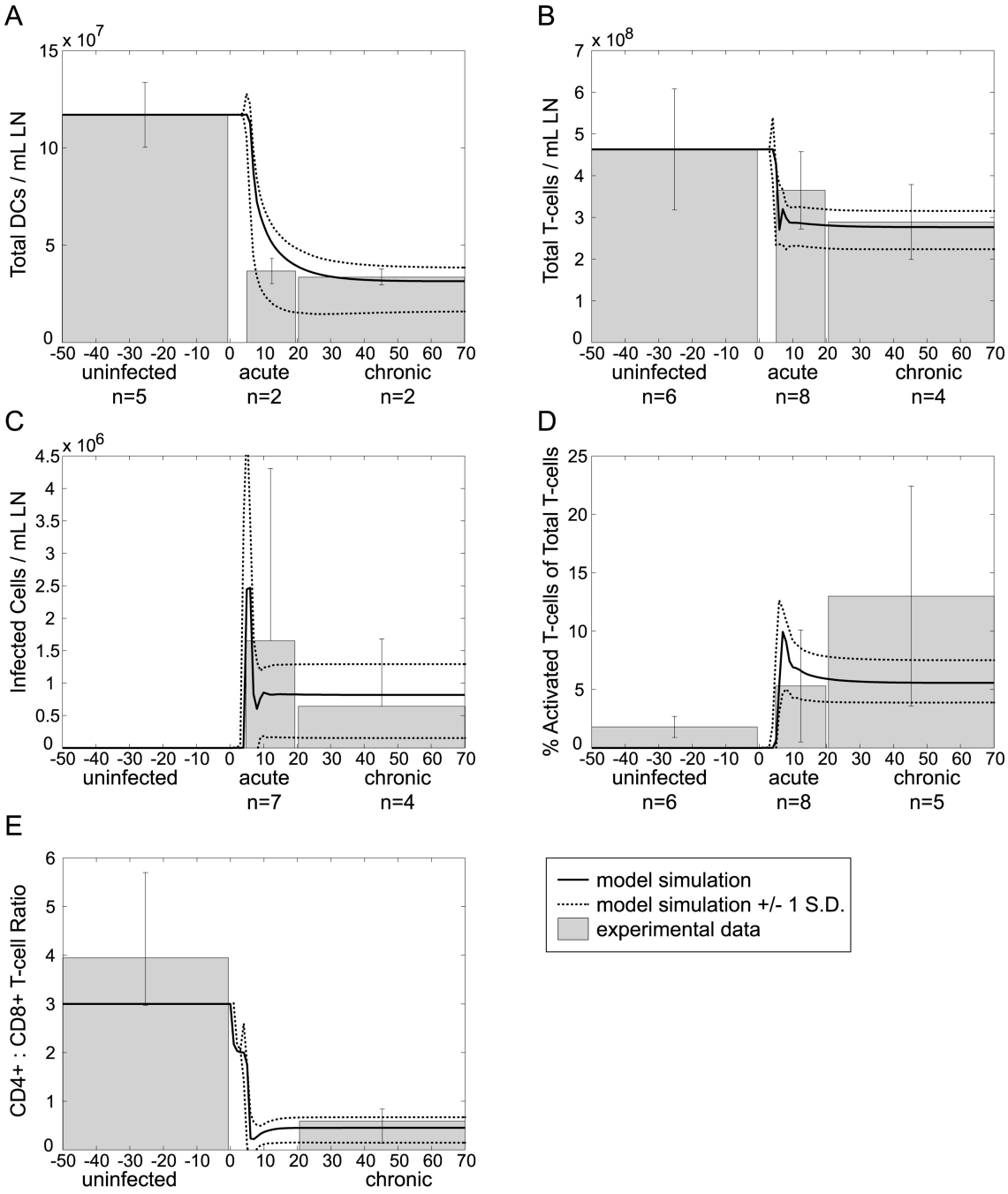

Figure B.3. Comparison of model output to experimental non-human primate lymph node paracortical cell counts (generated herein) and published human lymph node data from (78).

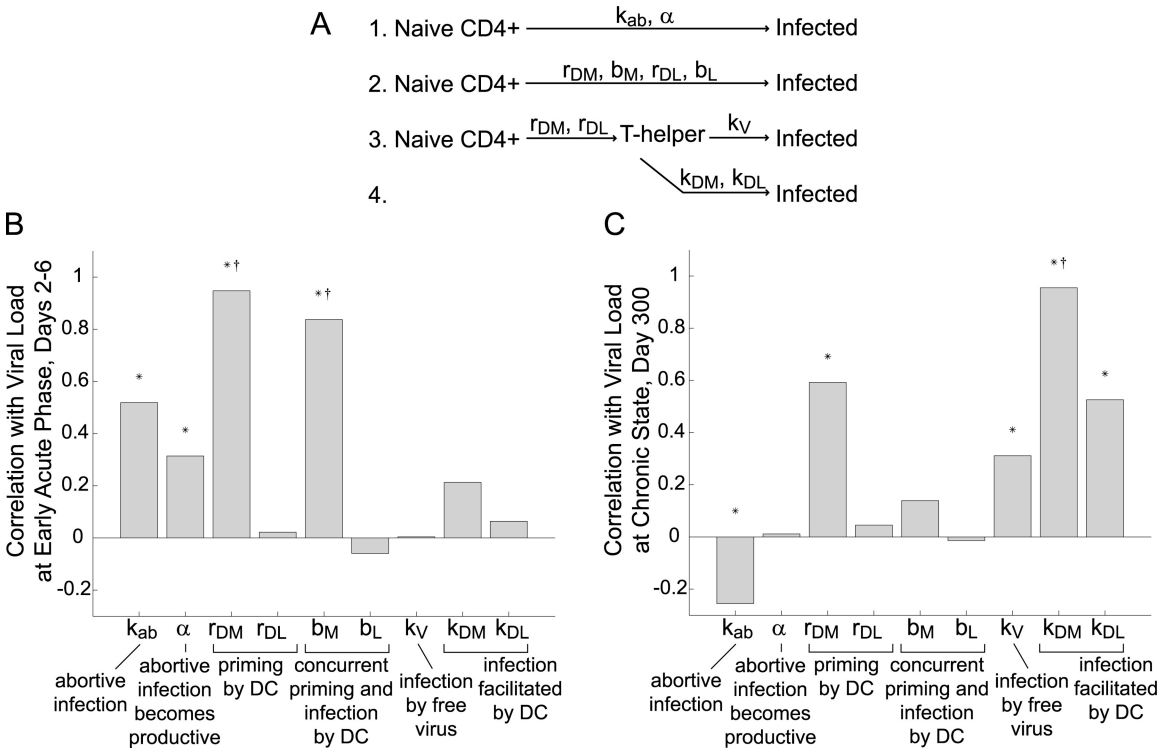

Figure B.4. Sensitivity analysis of parameters controlling different routes of infection. **(A)** Four mechanisms of infection that are captured by the model. **(B)** Correlation between parameter value and early acute phase viral load (days 2-6). **(C)** Correlation between parameter value and chronic state viral load (day 300). Note that partial rank correlations coefficients shown can range from –1 to 1. Those shown with an asterisk (*) are significant to the p-value of < 0.0011. Those shown with a dagger (†) are significantly different from all other parameters to a p-value of 0.0003.

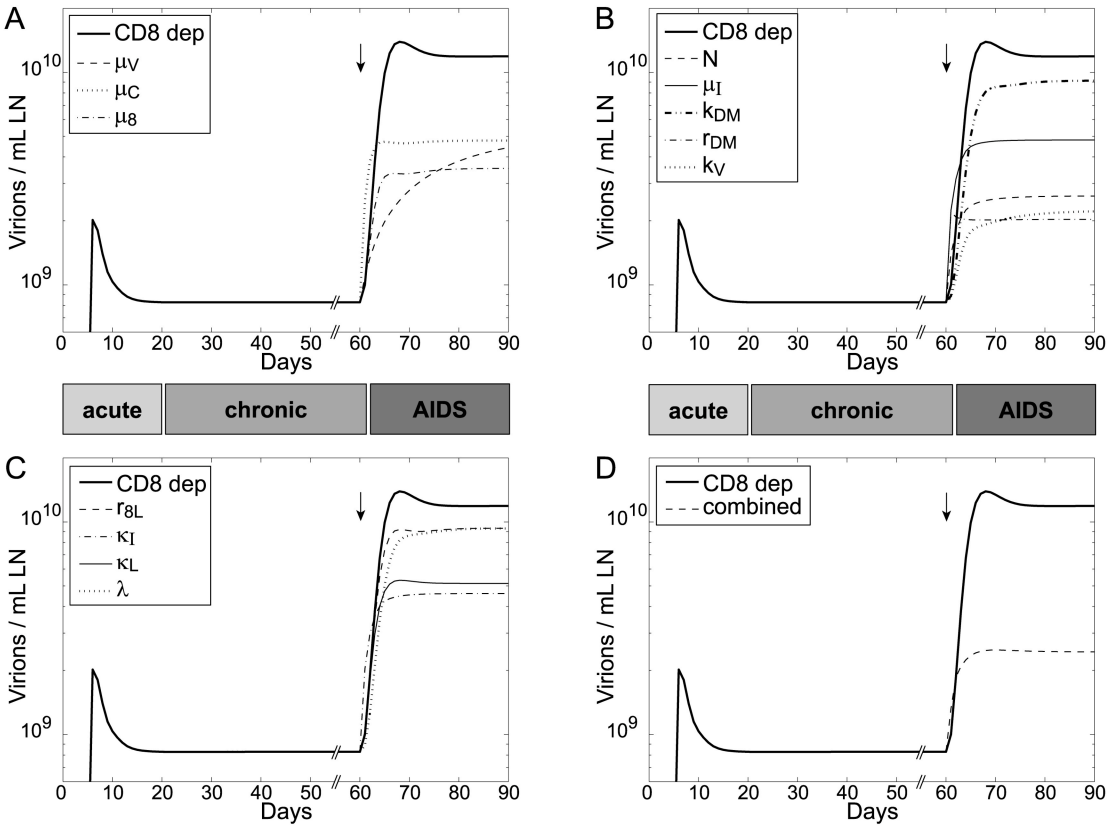

Figure B.5. Parameters that can induce an AIDS-like increase in viral load. In each panel, an AIDS-like state is induced by CD8+ T-cell depletion, as a positive control for comparison. In each case, *in silico* depletion or intervention is performed at day 60, as indicated by an arrow. **(A)** Parameters related to LN architecture. **(B)** Parameters related to infection and viral production. **(C)** Parameters related to immune maintenance and effector functions. Table B.2 accompanies this figure and presents all the parameters and their definitions.

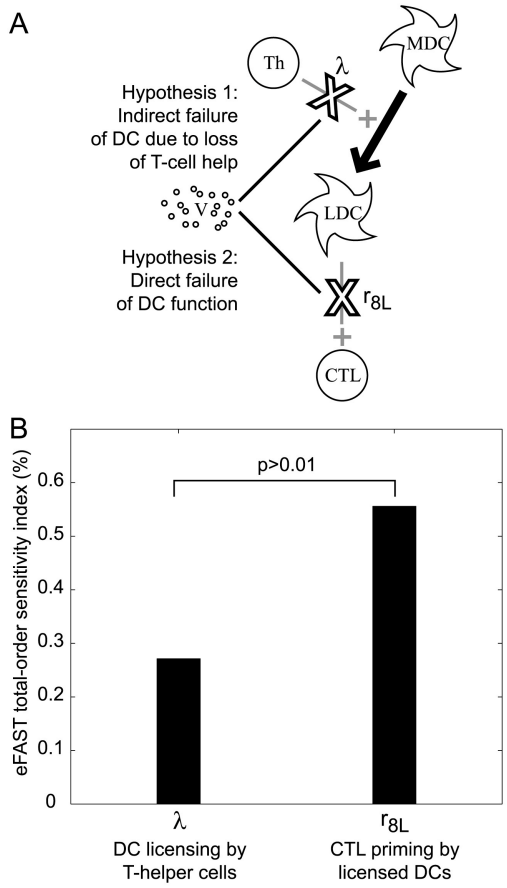

Figure B.6. Direct failure of licensed DCs more likely contributes to HIV-1 immunopathogenesis than an indirect failure of CD4+ T-cell help to license DCs. **(A)** Two hypotheses can explain DC dysfunction during HIV-1 infection: Loss of CD4+ T-cell help could indirectly cause DC failure to prime CTLs (Hypothesis 1). This is represented in the model by decrease in parameter λ. Alternatively, the virus could directly impair DC function, preventing CTL priming (Hypothesis 2). This is represented in the model by decrease in parameter r_{8L}. **(B)** Global sensitivity analysis using the eFAST method shows that CTL priming by licensed DCs (r_{8L}) is a significantly more sensitive control point of the host-virus system, favoring Hypothesis 2.

Table B.1. Model simulation values compared to non-human primate experimental data and published human clinical data in lymph node

Infection state / Model timepoint	**Count**	**Model simulation**	**Non-human Primate**	**Human clinical data** (23)
no infection / day 0	total CD4+ T-cell	3.5×10^8	3.7×10^8 *	2.9×10^8
chronic / day 300	total CD4+ T-cell	8.6×10^7	10.7×10^7 *	6.7×10^7
acute / day 6	infected cell	2.5×10^6	1.7×10^6	7.1×10^5
chronic / day 300	infected cell	8.2×10^5	6.4×10^5	5.7×10^4
acute / day 6	virus	2.0×10^9		$> 10^8$
chronic / day 300	virus	8.3×10^8		$> 10^8$

* = this value was calculated from total T-cell count and the CD4:CD8 ratio from (76)

Table B.2. Sensitivity and uncertainty analysis identifies parameters that drive viral load of DC parameters during chronic state

Parameter Definition	Symbol	Sensitivity
Sensitivity of DC parameters during chronic state		
Recruitment		
Max. immigration rate of mat. DC due to antigen	ϕ_{DM}	↓
Licensing		
Licensing rate of mat. DCs by T-helper	λ	↓
Priming		
Priming rate of naïve CD4+ by mat. DC	r_{DM}	↑
Priming rate of naïve CD8+ by lic. DC	r_{8L}	↓
Enhancement of CD4+ T-cell Infection		
Infection rate of T-helper by mat. DC-associated virus	k_{DM}	↑
Global sensitivity analysis identifies mechanisms that can cause progression to AIDS-like state		
Source and Recruitment		
Max. recruitment rate of naïve CD4+ by DC	ϕ_4	*
Max. recruitment rate of naïve CD8+ by DC	ϕ_8	↓ *
Max. immigration rate of mat. DC due antigen	ϕ_{DM}	*
Death / Exit to Efferent Lymph		
Death/Exit rate of infected cells	μ_I	↑
Destruction rate of virus particles	μ_V	↓ *
Death/Exit rate of naïve CD8+	μ_8	↑
Death/Exit rate of CTL	μ_C	↑
Proliferation / Clonal Expansion		
Proliferation rate of CTL	p_C	↓
Priming		
Priming rate of naïve CD4+ by mat. DC	r_{DM}	↑ *
Priming rate of naïve CD8+ by lic. DC	r_{8L}	↓ *
Infection		
Abortive infection and bystander effects of naïve CD4+	k_{ab}	↓ *
Infection rate of T-helper by virus	k_V	↑
Infection rate of T-helper by mat. DC-associated virus	k_{DM}	↑
Virus Properties		
Average number of virus produced by an infected cell	N	↑ *
CTL Effector Functions		
Inhibition of mat. DC-associated virus infection by CTL	c_2	↑
Inhibition of infected cell virus production by CTL	c_4	↑
Killing rate of infected cells by CTL	κ_I	↓ *
Killing rate of lic. DC by CTL	κ_L	↑
DC Maturation and Licensing		
Licensing rate of mat. DCs by T-helper	λ	↓ *

↑ = statistically significant positive correlation by LHS/PRC ($p < 5.9 \times 10^{-4}$).
↓ = statistically significant negative correlation by LHS/PRC ($p < 5.9 \times 10^{-4}$).
* = statistically significant total-order sensitivity index by eFAST ($p < 0.01$).

REFERENCES

1. Poli, G., G. Pantaleo, and A.S. Fauci, *Immunopathogenesis of human immunodeficiency virus infection.* Clin Infect Dis, 1993. **17 Suppl 1**: p. S224-9.

2. Steinman, R.M., *The dendritic cell system and its role in immunogenicity.* Annu Rev Immunol, 1991. **9**: p. 271-96.

3. Lekkerkerker, A.N., Y. van Kooyk, and T.B. Geijtenbeek, *Viral piracy: HIV-1 targets dendritic cells for transmission.* Curr HIV Res, 2006. **4**(2): p. 169-76.

4. Bottomly, K., *T cells and dendritic cells get intimate.* Science, 1999. **283**(5405): p. 1124-5.

5. Lutz, M.B. and G. Schuler, *Immature, semi-mature and fully mature dendritic cells: which signals induce tolerance or immunity?* Trends Immunol, 2002. **23**(9): p. 445-9.

6. Sixt, M., et al., *The conduit system transports soluble antigens from the afferent lymph to resident dendritic cells in the T cell area of the lymph node.* Immunity, 2005. **22**(1): p. 19-29.

7. Carbone, F.R., G.T. Belz, and W.R. Heath, *Transfer of antigen between migrating and lymph node-resident DCs in peripheral T-cell tolerance and immunity.* Trends Immunol, 2004. **25**(12): p. 655-8.

8. Janeway, C., *Immunobiology : the immune system in health and disease*. 6th ed. 2005, New York: Garland Science.

9. Mellman, I. and R.M. Steinman, *Dendritic cells: specialized and regulated antigen processing machines.* Cell, 2001. **106**(3): p. 255-8.

10. Wang, J.C. and A.M. Livingstone, *Cutting edge: CD4+ T cell help can be essential for primary CD8+ T cell responses in vivo.* J Immunol, 2003. **171**(12): p. 6339-43.

11. Smith, C.M., et al., *Cognate CD4(+) T cell licensing of dendritic cells in CD8(+) T cell immunity.* Nat Immunol, 2004. **5**(11): p. 1143-8.

12. Serre, K., et al., *CD4 T cell help is required for primary CD8 T cell responses to vesicular antigen delivered to dendritic cells in vivo.* Eur J Immunol, 2006. **36**(6): p. 1386-97.

13. Janssen, E.M., et al., *CD4+ T cells are required for secondary expansion and memory in CD8+ T lymphocytes.* Nature, 2003. **421**(6925): p. 852-6.

14. Shedlock, D.J. and H. Shen, *Requirement for CD4 T cell help in generating functional CD8 T cell memory.* Science, 2003. **300**(5617): p. 337-9.

15. Ridge, J.P., F. Di Rosa, and P. Matzinger, *A conditioned dendritic cell can be a temporal bridge between a CD4+ T-helper and a T-killer cell.* Nature, 1998. **393**(6684): p. 474-8.

16. Schoenberger, S.P., et al., *T-cell help for cytotoxic T lymphocytes is mediated by CD40-CD40L interactions.* Nature, 1998. **393**(6684): p. 480-3.

17. Bukczynski, J., et al., *Enhancement of HIV-specific CD8 T cell responses by dual costimulation with CD80 and CD137L.* J Immunol, 2005. **175**(10): p. 6378-89.

18. Turville, S.G., et al., *Diversity of receptors binding HIV on dendritic cell subsets.* Nat Immunol, 2002. **3**(10): p. 975-83.

19. Kwon, D.S., et al., *DC-SIGN-mediated internalization of HIV is required for trans-enhancement of T cell infection.* Immunity, 2002. **16**(1): p. 135-44.

20. de Witte, L., et al., *Langerin is a natural barrier to HIV-1 transmission by Langerhans cells.* Nat Med, 2007. **13**(3): p. 367-71.

21. Blauvelt, A., et al., *Productive infection of dendritic cells by HIV-1 and their ability to capture virus are mediated through separate pathways.* J Clin Invest, 1997. **100**(8): p. 2043-53.

22. Trepel, F., *Number and distribution of lymphocytes in man. A critical analysis.* Klin Wochenschr, 1974. **52**(11): p. 511-5.

23. Haase, A.T., *Population biology of HIV-1 infection: viral and CD4+ T cell demographics and dynamics in lymphatic tissues.* Annu Rev Immunol, 1999. **17**: p. 625-56.

24. McDonald, D., et al., *Recruitment of HIV and its receptors to dendritic cell-T cell junctions.* Science, 2003. **300**(5623): p. 1295-7.

25. Arrighi, J.F., et al., *DC-SIGN-mediated infectious synapse formation enhances X4 HIV-1 transmission from dendritic cells to T cells.* J Exp Med, 2004. **200**(10): p. 1279-88.

26. Wiley, R.D. and S. Gummuluru, *Immature dendritic cell-derived exosomes can mediate HIV-1 trans infection.* Proc Natl Acad Sci U S A, 2006. **103**(3): p. 738-43.

27. Ho, D.D., *Viral counts count in HIV infection.* Science, 1996. **272**(5265): p. 1124-5.

28. Pantaleo, G., et al., *Role of lymphoid organs in the pathogenesis of human immunodeficiency virus (HIV) infection.* Immunol Rev, 1994. **140**: p. 105-30.

29. McCune, J.M., *The dynamics of CD4+ T-cell depletion in HIV disease.* Nature, 2001. **410**(6831): p. 974-9.

30. Reimann, K.A., et al., *Pathogenicity of simian-human immunodeficiency virus SHIV-89.6P and SIVmac is attenuated in cynomolgus macaques and associated with early T-lymphocyte responses.* J Virol, 2005. **79**(14): p. 8878-85.

31. Meyers, A., et al., *Thymic size on chest radiograph and rapid disease progression in human immunodeficiency virus 1-infected children.* Pediatr Infect Dis J, 2001. **20**(12): p. 1112-8.

32. Dioszeghy, V., et al., *Changes in soluble factor-mediated CD8+ cell-derived antiviral activity in cynomolgus macaques infected with simian immunodeficiency virus SIVmac251: relationship to biological markers of progression.* J Virol, 2006. **80**(1): p. 236-45.

33. Connor, R.I. and D.D. Ho, *Human immunodeficiency virus type 1 variants with increased replicative capacity develop during the asymptomatic stage before disease progression.* J Virol, 1994. **68**(7): p. 4400-8.

34. Stilianakis, N.I., K. Dietz, and D. Schenzle, *Analysis of a model for the pathogenesis of AIDS.* Math Biosci, 1997. **145**(1): p. 27-46.

35. Wodarz, D. and M.A. Nowak, *Mathematical models of HIV pathogenesis and treatment.* Bioessays, 2002. **24**(12): p. 1178-87.

36. Granelli-Piperno, A., et al., *HIV-1-infected monocyte-derived dendritic cells do not undergo maturation but can elicit IL-10 production and T cell regulation.* Proc Natl Acad Sci U S A, 2004. **101**(20): p. 7669-74.

37. Krathwohl, M.D., T.W. Schacker, and J.L. Anderson, *Abnormal presence of semimature dendritic cells that induce regulatory T cells in HIV-infected subjects.* J Infect Dis, 2006. **193**(4): p. 494-504.

38. Chougnet, C. and S. Gessani, *Role of gp120 in dendritic cell dysfunction in HIV infection.* J Leukoc Biol, 2006.

39. Bajaria, S.H. and D. Kirschner, *CTL action during HIV-1 is determined via interactions with multiple cell types*, in *Deterministic and Stochastic Models for AIDS Epidemics and HIV Infection with Interventions*, W.Y. Tan and H. Wu, Editors. 2005, World Scientific: River Edge, New Jersey. p. 219-254.

40. Murphey-Corb, M., et al., *Isolation of an HTLV-III-related retrovirus from macaques with simian AIDS and its possible origin in asymptomatic mangabeys.* Nature, 1986. **321**(6068): p. 435-7.

41. Fallert, B.A. and T.A. Reinhart, *Improved detection of simian immunodeficiency virus RNA by in situ hybridization in fixed tissue sections: combined effects of temperatures for tissue fixation and probe hybridization.* J Virol Methods, 2002. **99**(1-2): p. 23-32.

42. Reinhart, T.A., et al., *Increased expression of the inflammatory chemokine CXC chemokine ligand 9/monokine induced by interferon-gamma in lymphoid tissues of rhesus macaques during simian immunodeficiency virus infection and acquired immunodeficiency syndrome.* Blood, 2002. **99**(9): p. 3119-28.

43. Gerdes, J., et al., *Cell cycle analysis of a cell proliferation-associated human nuclear antigen defined by the monoclonal antibody Ki-67.* J Immunol, 1984. **133**(4): p. 1710-5.

44. Pitcher, C.J., et al., *Development and homeostasis of T cell memory in rhesus macaque.* J Immunol, 2002. **168**(1): p. 29-43.

45. Combadiere, B., et al., *CD4+Ki67+ lymphocytes in HIV-infected patients are effector T cells accumulated in the G1 phase of the cell cycle.* Eur J Immunol, 2000. **30**(12): p. 3598-603.

46. Cohen Stuart, J.W., et al., *The dominant source of CD4+ and CD8+ T-cell activation in HIV infection is antigenic stimulation.* J Acquir Immune Defic Syndr, 2000. **25**(3): p. 203-11.

47. Hazenberg, M.D., et al., *T-cell division in human immunodeficiency virus (HIV)-1 infection is mainly due to immune activation: a longitudinal analysis in patients before and during highly active antiretroviral therapy (HAART).* Blood, 2000. **95**(1): p. 249-55.

48. Izmailova, E., et al., *HIV-1 Tat reprograms immature dendritic cells to express chemoattractants for activated T cells and macrophages.* Nat Med, 2003. **9**(2): p. 191-7.

49. Foley, J.F., et al., *Roles for CXC chemokine ligands 10 and 11 in recruiting CD4+ T cells to HIV-1-infected monocyte-derived macrophages, dendritic cells, and lymph nodes.* J Immunol, 2005. **174**(8): p. 4892-900.

50. Reinhart, T.A., *Chemokine induction by HIV-1: recruitment to the cause.* Trends Immunol, 2003. **24**(7): p. 351-3.

51. Kirschner, D., G.F. Webb, and M. Cloyd, *Model of HIV-1 disease progression based on virus-induced lymph node homing and homing-induced apoptosis of CD4+ lymphocytes.* J Acquir Immune Defic Syndr, 2000. **24**(4): p. 352-62.

52. Cloyd, M.W., et al., *How does HIV cause depletion of CD4 lymphocytes? A mechanism involving virus signaling through its cellular receptors.* Curr Mol Med, 2001. **1**(5): p. 545-50.

53. Sallusto, F., et al., *Two subsets of memory T lymphocytes with distinct homing potentials and effector functions.* Nature, 1999. **401**(6754): p. 708-12.

54. Jekle, A., et al., *In vivo evolution of human immunodeficiency virus type 1 toward increased pathogenicity through CXCR4-mediated killing of uninfected CD4 T cells.* J Virol, 2003. **77**(10): p. 5846-54.

55. Eckstein, D.A., et al., *HIV-1 actively replicates in naive CD4(+) T cells residing within human lymphoid tissues.* Immunity, 2001. **15**(4): p. 671-82.

56. Unutmaz, D., et al., *Cytokine signals are sufficient for HIV-1 infection of resting human T lymphocytes.* J Exp Med, 1999. **189**(11): p. 1735-46.

57. Ostrowski, M.A., et al., *Both memory and CD45RA+/CD62L+ naive CD4(+) T cells are infected in human immunodeficiency virus type 1-infected individuals.* J Virol, 1999. **73**(8): p. 6430-5.

58. Geiben-Lynn, R., *Anti-human immunodeficiency virus noncytolytic CD8+ T-cell response: a review.* AIDS Patient Care STDS, 2002. **16**(10): p. 471-7.

59. Levy, J.A., *The search for the CD8+ cell anti-HIV factor (CAF).* Trends Immunol, 2003. **24**(12): p. 628-32.

60. Kedzierska, K. and S.M. Crowe, *Cytokines and HIV-1: interactions and clinical implications.* Antivir Chem Chemother, 2001. **12**(3): p. 133-50.

61. Cavert, W., et al., *Kinetics of response in lymphoid tissues to antiretroviral therapy of HIV-1 infection.* Science, 1997. **276**(5314): p. 960-4.

62. Smith, B.A., et al., *Persistence of infectious HIV on follicular dendritic cells.* J Immunol, 2001. **166**(1): p. 690-6.

63. Vezys, V., et al., *Continuous recruitment of naive T cells contributes to heterogeneity of antiviral CD8 T cells during persistent infection.* J Exp Med, 2006.

64. Whitmire, J.K. and R. Ahmed, *Costimulation in antiviral immunity: differential requirements for CD4(+) and CD8(+) T cell responses.* Curr Opin Immunol, 2000. **12**(4): p. 448-55.

65. Futagawa, T., et al., *Expression and function of 4-1BB and 4-1BB ligand on murine dendritic cells.* Int Immunol, 2002. **14**(3): p. 275-86.

66. Wilson, N.S. and J.A. Villadangos, *Lymphoid organ dendritic cells: beyond the Langerhans cells paradigm.* Immunol Cell Biol, 2004. **82**(1): p. 91-8.

67. Larsson, M., *HIV-1 and the hijacking of dendritic cells: a tug of war.* Springer Semin Immunopathol, 2005. **26**(3): p. 309-28.

68. Larsson, M., et al., *Activation of HIV-1 specific CD4 and CD8 T cells by human dendritic cells: roles for cross-presentation and non-infectious HIV-1 virus.* Aids, 2002. **16**(10): p. 1319-29.

69. Maranon, C., et al., *Dendritic cells cross-present HIV antigens from live as well as apoptotic infected CD4+ T lymphocytes.* Proc Natl Acad Sci U S A, 2004. **101**(16): p. 6092-7.

70. Zhao, X.Q., et al., *Induction of anti-human immunodeficiency virus type 1 (HIV-1) CD8(+) and CD4(+) T-cell reactivity by dendritic cells loaded with HIV-1 X4-infected apoptotic cells.* J Virol, 2002. **76**(6): p. 3007-14.

71. Blachere, N.E., R.B. Darnell, and M.L. Albert, *Apoptotic cells deliver processed antigen to dendritic cells for cross-presentation.* PLoS Biol, 2005. **3**(6): p. e185.

72. Dolan, B.P., K.D. Gibbs, Jr., and S. Ostrand-Rosenberg, *Dendritic cells cross-dressed with peptide MHC class I complexes prime CD8+ T cells.* J Immunol, 2006. **177**(9): p. 6018-24.

73. Dolan, B.P., K.D. Gibbs, Jr., and S. Ostrand-Rosenberg, *Tumor-specific CD4+ T cells are activated by "cross-dressed" dendritic cells presenting peptide-MHC class II complexes acquired from cell-based cancer vaccines.* J Immunol, 2006. **176**(3): p. 1447-55.

74. Ronchese, F. and I.F. Hermans, *Killing of dendritic cells: a life cut short or a purposeful death?* J Exp Med, 2001. **194**(5): p. F23-6.

75. Yang, J., et al., *Perforin-dependent elimination of dendritic cells regulates the expansion of antigen-specific CD8+ T cells in vivo.* Proc Natl Acad Sci U S A, 2006. **103**(1): p. 147-52.

76. Ruedl, C., et al., *Anatomical origin of dendritic cells determines their life span in peripheral lymph nodes.* J Immunol, 2000. **165**(9): p. 4910-6.

77. Savage, V.M., et al., *Scaling of number, size, and metabolic rate of cells with body size in mammals.* Proc Natl Acad Sci U S A, 2007. **104**(11): p. 4718-23.

78. Biancotto, A., et al., *Abnormal activation and cytokine spectra in lymph nodes of persons chronically infected with HIV-1.* Blood, 2007.

79. Shampine, L.F. and M.W. Reichelt, *The MATLAB ODE Suite.* SIAM Journal on Scientific Computing, 1997. **18**: p. 1-22.

80. Blower, S.M. and H. Dowlatabadi, *Sensitivity and Uncertainty Analysis of Complex Models of Disease Transmission: an HIV Model, as an Example.* International Statistical Review, 1994. **62**(2): p. 229-243.

81. Saltelli, A., S. Tarantola, and K.P.-S. Chan, *A Quantitative Model-Independent Method for Global Sensitivity Analysis of Model Output.* Technometrics, 1999. **41**(1): p. 39-56.

82. Curran-Everett, D., *Multiple comparisons: philosophies and illustrations.* Am J Physiol Regul Integr Comp Physiol, 2000. **279**(1): p. R1-8.

83. Meng, X., R. Rosenthal, and D.B. Rubin, *Comparing Correlated Correlation Coefficients.* Psychological Bulletin, 1992. **111**(1): p. 172-175.

84. Marino, S., et al., *A methodology for performing global uncertainty and sensitivity analysis in systems biology.* J Theor Biol, 2008. **254**(1): p. 178-96.

85. Jin, X., et al., *Dramatic rise in plasma viremia after CD8(+) T cell depletion in simian immunodeficiency virus-infected macaques.* J Exp Med, 1999. **189**(6): p. 991-8.

86. Schmitz, J.E., et al., *Control of viremia in simian immunodeficiency virus infection by CD8+ lymphocytes.* Science, 1999. **283**(5403): p. 857-60.

87. Matano, T., et al., *Administration of an anti-CD8 monoclonal antibody interferes with the clearance of chimeric simian/human immunodeficiency virus during primary infections of rhesus macaques.* J Virol, 1998. **72**(1): p. 164-9.

88. Doherty, P.C. and J.P. Christensen, *Accessing complexity: the dynamics of virus-specific T cell responses.* Annu Rev Immunol, 2000. **18**: p. 561-92.

89. Ingulli, E., et al., *In vivo detection of dendritic cell antigen presentation to CD4(+) T cells.* J Exp Med, 1997. **185**(12): p. 2133-41.

90. De Smedt, T., et al., *Antigen-specific T lymphocytes regulate lipopolysaccharide-induced apoptosis of dendritic cells in vivo.* J Immunol, 1998. **161**(9): p. 4476-9.

91. Brown, K.N., A. Trichel, and S.M. Barratt-Boyes, *Parallel loss of myeloid and plasmacytoid dendritic cells from blood and lymphoid tissue in simian AIDS.* J Immunol, 2007. **178**(11): p. 6958-67.

92. Margolick, J.B., et al., *Impact of inversion of the CD4/CD8 ratio on the natural history of HIV-1 infection.* J Acquir Immune Defic Syndr, 2006. **42**(5): p. 620-6.

93. Westermann, J., Z. Puskas, and R. Pabst, *Blood transit and recirculation kinetics of lymphocyte subsets in normal rats.* Scand J Immunol, 1988. **28**(2): p. 203-10.

94. Westermann, J., et al., *IFN-gamma influences the migration of thoracic duct B and T lymphocyte subsets in vivo. Random increase in disappearance from the blood and differential decrease in reappearance in the lymph.* J Immunol, 1993. **150**(9): p. 3843-52.

95. von Andrian, U.H. and T.R. Mempel, *Homing and cellular traffic in lymph nodes.* Nat Rev Immunol, 2003. **3**(11): p. 867-78.

96. Beltman, J.B., et al., *Lymph node topology dictates T cell migration behavior.* J Exp Med, 2007. **204**(4): p. 771-80.

97. Chiba, K., et al., *Role of sphingosine 1-phosphate receptor type 1 in lymphocyte egress from secondary lymphoid tissues and thymus.* Cell Mol Immunol, 2006. **3**(1): p. 11-9.

98. Gorry, P.R., et al., *The role of viral coreceptors and enhanced macrophage tropism in human immunodeficiency virus type 1 disease progression.* Sex Health, 2004. **1**(1): p. 23-34.

99. Xiao, L., et al., *Adaptation to promiscuous usage of CC and CXC-chemokine coreceptors in vivo correlates with HIV-1 disease progression.* Aids, 1998. **12**(13): p. F137-43.

100. Sol-Foulon, N., et al., *HIV-1 Nef-induced upregulation of DC-SIGN in dendritic cells promotes lymphocyte clustering and viral spread.* Immunity, 2002. **16**(1): p. 145-55.

101. Cohen, S.S., et al., *Pronounced acute immunosuppression in vivo mediated by HIV Tat challenge.* Proc Natl Acad Sci U S A, 1999. **96**(19): p. 10842-7.

102. Bajaria, S.H., et al., *Dynamics of naive and memory CD4+ T lymphocytes in HIV-1 disease progression.* J Acquir Immune Defic Syndr, 2002. **30**(1): p. 41-58.

103. Kitano, H. and K. Oda, *Robustness trade-offs and host-microbial symbiosis in the immune system.* Mol Syst Biol, 2006. **2**: p. 2006 0022.

104. Zhang, Z.Q., et al., *Roles of substrate availability and infection of resting and activated CD4+ T cells in transmission and acute simian immunodeficiency virus infection.* Proc Natl Acad Sci U S A, 2004. **101**(15): p. 5640-5.

105. Riggs, T., et al., *A comparison of random vs. chemotaxis-driven contacts of T cells with dendritic cells during repertoire scanning.* J Theor Biol, 2008. **250**(4): p. 732-51.